CHARACTERIZATION AND CONTROL OF A CHEMICAL VAPOUR DEPOSITION REACTOR

by

© Marlene G. Lenarduzzi

A thesis submitted to the School of Graduate Studies and Research

in partial fulfillment of the requirements for the

degree of

MASTER OF APPLIED SCIENCE

in the Department of Chemical Engineering

University of Ottawa

December 1997

0-612-28439-5

ABSTRACT

Much work has been done on developing mechanistic models of Chemical Vapour Deposition (CVD) reactors, however the use of these models is often cumbersome and computer intensive. Equipment specific empirical models are simpler to use and develop yet provide good representation of the process behaviour. In this work, empirical models were developed to characterize film thickness of an industrial CVD reactor used in the semiconductor industry to deposit polycrystalline silicon films on silicon wafers.

The goals were to reduce variability in film thickness over time and space by appropriately choosing operating conditions and implementing more effective process monitoring and control. Spacial variability in film thickness is measured across a wafer (within-wafer) and along the length of the reactor (cross-load). From these measurements, film thickness variance is calculated. The predictor variables for the model were the controllable reactor inputs: centre temperature (T_c), temperature difference between the front and centre of the reactor (R_1), temperature difference between end and centre of the reactor (R_2), pressure (P), silane flow rate (F_{SiH_4}), and deposition time (t_{dep}). A central composite experimental design was used to generate the data for the models. Transformation of the response variables was required for the cross-load variance and within-wafer variance models to overcome model inadequacy. Optimization of the predictor variables to keep film thickness on target and reduce within-wafer and cross-load variances was achieved using a multi-objective optimization routine.

Batch-to-batch variability was reduced by more than 50% through a proposed change in the operation of the reactor. Statistical Process Control (SPC) charts for mean thickness of a batch, within-wafer variance and cross-load variance were developed to monitor the process.

RÉSUMÉ

Beaucoup de travail a été fait dans le développement des modèles mécaniques pour les réacteurs de dépôt à vapeur chimique (DVC). Cependant ces modèles sont souvent lourds à manier et très informatisés. Les modèles empiriques exigent un équipement spécifique et sont en revanche plus facile à utiliser et à développer mais, néanmoins, nous démontrent de façon assez précise le procédé original. Dans cette recherche. les modèles empiriques sont développés pour étudier l'épaisseur du dépôt d'un DVC industriel utilisé dans !'industrie du semiconducteur, le dépôt des films silicon polycrystalline silicon wafers fait de silicon.

Les buts de la recherche sont la réduction de la variabilité de l'épaisseur du film avec le temps et l'emplacement dans le réacteur, par le choix approprié de conditions opérationnelles et par l'éxécution d'un mécanisme de surveillance et de contrôle plus efficace. La variabilité de l'épaisseur du film, à cause de la position dans le réacteur. est mesuré à travers du wafer (*within-wafer*) et sur la longueur du réacteur (*cross-load*). Avec ces mesures, la variation de l'épaisseur du film est calculé. Les prédictions variables pour les modèles sont les conditions du réacteur que l'on peut contrôler: la température au centre (T_c), la différence de températures entre le devant et le centre du réacteur (R_1), la différence de températures entre les extrémités et le centre du réacteur (R_2). la pression (P). l'écoulement du silane (F_{SiH_4}), et la durée du dépôt (Tdep). Un dessin expérimental *central composite* a été utilisé afin de générer les données les modèles. La transformation des variables des réponses a été nécessaire pour les modèles de variation cross-load et within-wafer afin de compenser pour l'insuffisance des modèles. L'optimisation des modèles pour obtenir l'épaisseur de film désiré et pour la réduction de variabilité cross-load et within-wafer est réalisé en utilisant une méthode d'optimisation à objectifs multiples.

La variabilité de quantités est réduite par plus de 50%, dû à un changement proposé à l'opération du réacteur. Des diagrammes sont inclus pour surveiller l'épaisseur moyenne du film dans une quantité, la variabilité du within-wafer et du cross-load.

ACKNOWLEDGEMENTS

I wish to express my gratitude to my two supervisors, Dr. David McLean and Mr. Jim Fraser, for their support and guidance throughout this project.

I would like to thank Nortel for providing financial and technical support and the use of the wafer fabrication facility that made this research possible.

I would also like to thank the Department of Chemical Engineering at the University of Ottawa's for providing Teaching Assistantships which added financial support to this research.

Finally I wish to thank my husband, Bruce Watson, and my mother, Elda Lenarduzzi for their constant love, support and encouragement.

TABLE OF CONTENTS

LIST OF TABLES

LIST OF FIGURES

ACRONYMS

ACF	Autocorrelation Function
ARL	Average Run Length
C1	Centre 1
C1DR	C1 Deposition Rate
C1TH	C1 Thickness
C1WWV	C1 Within-Wafer Variance
C2	Centre 2
C2DR	Centre 2 Deposition Rate
C2TH	Centre 2 Thickness
C2WWV	Centre 2 Within-Wafer Variance
CL	Centre Line
CLS	Cross-Load Standard Deviation
CLV	Cross-Load Variance
CUSUM	Cumulative Sum
CVD	Chemical Vapour Deposition
DR	Deposition Rate
EWMA	Exponentially Weighted Moving Average
IID	Identically Independently Distributed
LCL	Lower Control Limit
LDR	Load Deposition Rate
LOF	Lack of Fit
LPCVD	Low Pressure Chemical Vapour Deposition
LTH	Load Thickness
LWWV	Load Within-Wafer Variance
MCUSUM	Multivariate Cumulative Sum
MEWMA	Multivariate Exponentially Weighted Moving Average
MOS	Metal Oxide Semiconductor
PCA	Principal Component Analysis
PDR	Pump Deposition Rate
PECVD	Plasma Enhanced Chemical Vapour Deposition
PM	Preventative Maintenance
poly-Si	Polycrystalline Silicon
PQV	Product Quality Variable
PTH	Pump Thickness
PWWV	Pump Within-Wafer Variance
SPC	Statistical Process Control
std. dev.	standard deviation
STP	Standard Temperature and Pressure
TC	Thermocouple
TH	Thickness
UCL	Upper Control Limit
WWS	Within-Wafer Standard Deviation
WWV	Within-Wafer Variance

NOMENCLATURE

C_n, h, k, s_n	parameters of the MCUSUM procedure
e_i	i^{th} residual
F_{SiH_4}	silane flowrate
h_4, r_j	parameters of the MEWMA procedure
m, n	parameters of the Hotelling's T^2 procedure
n	number of observations in the data set
N_p	multivariate Normal distribution with p variates
P	pressure
p	number of variates in the data set
P_{min}	minimum pressure
$\mathbf{R}$	sample correlation matrix
R_1	Ramp 1
R_2	Ramp 2
R^2	Coefficient of Determination
r_{ik}	sample correlation coefficient
s	sample standard deviation
$\mathbf{S}$	sample covariance matrix
S_i	CUSUM statistic
t	time
T^2	Hotelling's T^2 statistic
T_c	centre temperature
t_{dep}	deposition time
T_i^2	MEWMA statistic
x_{ij}	observation from a multivariate data set - i^{th} variate, j^{th} batch
$\bar{\mathbf{x}}$	vector of sample means - no sub-groups
$\bar{\bar{\mathbf{x}}}$	vector of sample means - with sub-groups
$\mathbf{X}_{nxp}$	multivariate data set with p variates and n observations
X1,X2,X3, X4,X5,X6	coded input variables representing T_c, R_1, R_2, P, F_{SiH_4} and t_{dep} respectively
y	observed value of the PQV
y_i	i^{th} observation of a univariate data set
$\hat{y}_i$	predicted value of the PQV
Y_i	i^{th} Principal Component
z_i	standardized observation
z_t	observation at time t in a time series
$\mathbf{Z}_i$	vector used in the computation of the MEWMA statistic
α	axial points or star in a central composite design
β	model parameters
δ	factor used in Phase I to determine allowable pressure for a given flowrate of silane gas
λ_i, $\mathbf{e}_i$	eigenvalue-eigenvector pair of the covariance matrix

λ, L_1, L_2, σ_z^2	Parameters of the EWMA procedure
μ	population mean
$\boldsymbol{\mu}$	vector of population means
ν	degrees of freedom associated with estimate of pure error variance
$\hat{\sigma}_p^2$	estimate of pure error variance
σ^2	population variance
Σ	population variance-covariance matrix
Σ_{Z_i}	variance-covariance matrix of $\mathbf{Z}_i$
τ	target value for mean

Chapter One

Introduction

As the semiconductor industry races to reduce the size of integrated circuits, engineers and scientists involved with each step in the overall process are challenged to make their processes more precise by reducing process variability. Variability is the enemy of manufacturing. The identification and elimination of non-random sources of error is essential for continuous quality improvement.

Chemical Vapour Deposition (CVD) reactors are used extensively in the semiconductor industry to deposit thin films on silicon wafers as an intermediate step in the fabrication of integrated circuits. Chemical vapour deposition is a crucial process used in most, if not all, integrated circuit fabrication centres. Low-pressure CVD (LPCVD) of polycrystalline silicon is currently the process of choice for manufacturers of integrated circuits since it offers both high throughput of product with acceptable film thickness variations within wafers and from wafer to wafer. However, it is the minimization of variations in film thickness that will better able process engineers to produce high quality products.

This study is focused on the low-pressure CVD of poly-Si onto silicon wafers using a production reactor at Nortel's integrated circuit fabrication facility in Nepean, Ontario. The reactor used was a Tylan/Tytan LPCVD reactor and is referred to as 415TYLAN. Although this study focused on the deposition of poly-Si, the techniques presented here could be applied to CVD reactors depositing or growing other films such as Si_3N_4, SiO_2, amorphous silicon, etc.

The thickness of the poly-Si film deposited in 415TYLAN was monitored using Shewart charts for the mean and the standard deviation of the thickness measurements. Process engineers typically made changes to the process input variables when at least one of these control charts signaled an out-of-control situation. There was no standard

This led to the motivation of this work. Clearly, there was a need for a more definitive approach to monitoring and controlling this reactor.

The objectives of this work were to:

i. gain a better understanding of process behaviour through the development of an empirical model

ii. reduce process variability

iii. implement an improved control scheme.

Once it became clear that a reduction in process variability was possible, tests were conducted to determine if feedback control was appropriate for this process. This was determined by examining past control action and by plotting the first-order autocorrelations of the thickness data. Next, relationships between the process operating variables and the output or response variables were built in the form of empirical models using data generated from a central composite design. These models were then used to determine an optimal set of operating conditions for the 415TYLAN. Finally, various charting methods for monitoring the process were explored including multivariate control charts, and clear control guidelines were proposed.

Following this introductory chapter, details about each of the steps taken to achieve the objectives are provided. Chapter Two describes the graphical and computational tools that were used to identify whether the use of automatic process control (APC) or statistical process control (SPC) or both were appropriate for this process and thus suggest an approach to problem solving. Also included are background details of the process. Chapter Three describes the central composite design that was used to generate data used to build empirical models of the process. The model building process is described along with the accepted models. Chapter Four presents the results of simultaneously optimizing the accepted models. The optimum found is tested to determine its accuracy. Chapter Five proposes a control scheme for monitoring the process.

Conclusions and recommendations are found in Chapter Six, as well as recommendations for future work. The references and appendices, including data, results and supplementary information, follow Chapter Six.

Chapter Two

Preliminary Work

This chapter discusses some key background issues pertaining to this research. First, chemical vapour deposition (CVD) is described. This is followed by details of the low pressure CVD reactor used in this research for the deposition of polycrystalline silicon (poly-Si). The next section, exploratory data analysis, is a guide through the statistical tools that led to some early conclusions that directed the research. Finally, a screening experiment, used to learn more specific details about reactor performance, is described.

2.1 Chemical Vapour Deposition

Chemical vapour deposition is a process where one or more gaseous species react on a solid surface and one of the reaction products is a solid phase. CVD reactors are used in the semiconductor industry to deposit thin films on silicon. Typically, the film is either silicon dioxide (SiO_2), silicon nitride (Si_3N_4) or polycrystalline silicon (poly-Si). There are two basic CVD reactor configurations, low pressure CVD and atmospheric CVD. A third type is Plasma Enhanced CVD (PECVD). The advantages and disadvantages of each, along with their respective applications, are listed in Table 2.1.

Low pressure CVD reactors are the most commonly used reactors in the semiconductor industry because costs due to capital, labour, and reactant gas are significantly lower on a per wafer basis than in atmospheric CVD systems. These costs are reduced due to significantly higher wafer throughput in low pressure CVD systems than in atmospheric pressure CVD systems. In atmospheric pressure CVD systems, the reactions are mass-transport limited; therefore the wafers must be spaced sufficiently (horizontally) to provide adequate and uniform accessibility of the wafer surfaces to the reactant gas or gases. Low pressure CVD systems are surface-reaction limited; therefore wafers can be loaded vertically and close together allowing for more wafers to be processed per batch (Bowman, 1990). For these reasons and because the CVD reactor studied was a low pressure CVD system, only low pressure CVD systems will be discussed in detail.

Table 2.1: Characteristics and Applications of CVD Reactors

Atmospheric Pressure CVD - low temperature	Simple reactor, high deposition rate, low temperature	Poor step coverage[1], particle contamination	Low temperature oxides, both doped and undoped[2]
Low Pressure CVD	Minimum contamination, excellent uniformity, conformal step coverage, large wafer capacity	High temperature, low deposition rate	High temperature oxides, both doped and undoped, Si_3N_4, poly-Si, W, WSi_2
Plasma Enhanced CVD	Low temperature, high deposition rate, good step coverage	Chemical (e.g. H_2) and particulate contamination	Insulators deposited at low temperature over metals, passivation[3] (Si_3N_4)

1. Step coverage is a measure of how well a film maintains its nominal thickness. It is expressed by the ratio of the minimum thickness of a film as it crosses a step, t_s, to the nominal thickness of the film on horizontal regions, t_n (Wolf, 1990).
2. Doping involves introduction of *n*-type dopant sources such as PH_3 or AsH_3 or p-type dopant sources such as B_2H_6 to the deposition process to modify the electrical properties of the film. It is used in the formation of high-value resistors (Bowman, 1990; Kamins, 1988).
3. Passivation - a layer of material put over a wafer to stabilize and protect the surface (Bowman, 1990).

In order for a CVD reaction to occur, the following volatility criteria must be met:

1. Reactants must have sufficiently high vapour pressure at the deposition temperature so that reasonable rates of introduction into the reaction chamber can be met.
2. The reaction products must be volatile except for the material to be deposited.
3. The chemical reaction must take place at the substrate surface to form the film.
4. The gaseous by-products of the chemical reaction must be desorbed and removed from the chamber (Sherman, 1987).

2.1.1 Deposition of Poly-Si

The pyrolysis of silane (SiH_4) occurs by the reaction

$$SiH_4 \xrightarrow{HEAT} Si^{*} + 2H_2 \uparrow .$$

When a silane molecule strikes a hot surface it can be reflected or adsorbed. If adsorbed and the temperature is high enough to promote silane decomposition, it may decompose solid silicon and hydrogen gas. The solid silicon deposits on the surface of the wafers and everywhere inside the reactor whereas hydrogen desorbs and enters the gas phase.

2.1.2 Importance of the Polycrystalline Silicon Layer

The primary use of polycrystalline silicon (poly-Si) is for gate formation in silicon-gate metal-oxide-semiconductor (MOS) devices. A MOS device is a transistor that is controlled by voltage rather than current. Poly-Si is the substance of choice for such devices because of the ability of poly-Si to be oxidized and its compatibility with further high-temperature processing. These properties have allowed development of more complex device structures, such as capacitors, employing several layers of poly-Si. Moreover, poly-Si can be used to interconnect devices allowing for a flexible layout. Poly-Si can also be used for high-value resistors, further reducing chip area (Kamins, 1988).

2.2 Process Description

There are two variations of the LPCVD processes commonly used to deposit polycrystalline silicon. One uses 100% silane at 0.2 to 1.0 Torr total pressure, while the other uses the same total pressure but 20 to 30 percent silane diluted in nitrogen. Diluting silane with nitrogen carrier gas reduces the partial pressure of silane in the gas phase thus decreasing the deposition rate of poly-Si and resulting in more uniform film thicknesses across a wafer. The process used in this research operates with 100% silane and no carrier gas because the benefits of a carrier gas did not outweigh the added costs. The deposition temperature can range from 600°C to 650°C. Typical deposition rates range from 80 to 150 Å/min. At fixed reactor conditions, film thickness varies between 3433 Å and 3567 Å representing a 95% confidence interval. Temperature, pressure and silane concentration are important process variables. Wafer spacing and load size have only minor effects (Bowman, 1990).

In this study, low pressure chemical vapour deposition of poly-Si was conducted in a Tylan/Tytan furnace similar to the one depicted in Figure 2.1. The reactor operates as a semi-batch system. Silicon wafers (which have gone through pre-processing) are loaded vertically in quartz wafer "boats" with each boat holding twenty-five wafers. Each batch must contain exactly four boats for a total of 100 wafers processed per batch. To monitor the deposition in the 415 Tylan/Tytan LPCVD reactor, a test wafer is inserted in the centre of each boat.

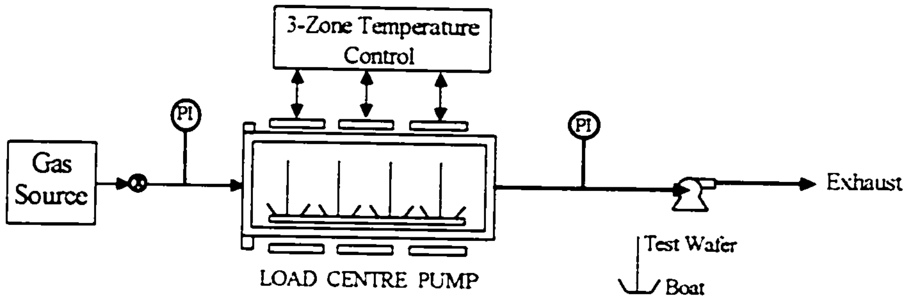

Figure 2.1: Schematic of a Low Pressure CVD Reactor

The test wafer positions are denoted as Load, C1, C2 (for Centre 1 and Centre 2) and Pump. Immediately following deposition, the thickness of the deposited poly-Si layer is measured on all four test wafers in the five locations depicted in Figure 2.2. This yields a total of 20 thickness measurements per batch. The thickness of the deposited polycrystalline silicon film was measured using a Nanometrics spectrophotometer. This instrument requires some calibration with standard samples. Over a period of eighty days, a 95% confidence interval for the mean thickness of the standard was 3580 ± 5Å. The repeatability data along with a description of the data analysis is found in Appendix I.

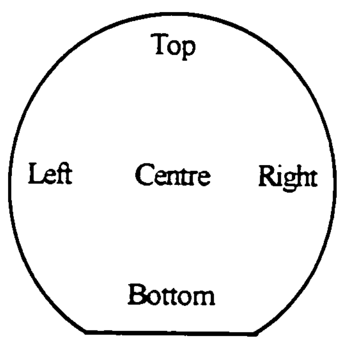

Figure 2.2: Thickness Measurement Locations for Test Wafers

From these thickness measurements the following response variables are derived:

- batch mean thickness - the mean thickness of all 20 thickness measurements taken from the four test wafers
- individual wafer mean thickness - the mean thickness of the thickness measurements of the test wafers (i.e. Load wafer mean thickness, C1 wafer mean thickness, C2 wafer mean thickness and Pump wafer mean thickness)
- batch mean deposition rate - batch mean thickness divided by the deposition time for that batch
- batch standard deviation - standard deviation of the twenty thickness measurements for a batch
- individual wafer standard deviation - the standard deviation of the thickness measurements of the individual test wafers (i.e. load wafer standard deviation, C1 wafer standard deviation, C2 wafer standard deviation and pump standard deviation).

The batch mean thickness, mean deposition rate and standard deviation of the thickness measurements were historically monitored using Shewart charts with Western Electric runs rules (Western Electric Company, 1956). Runs rules are used to increase the sensitivity of Shewart charts to changes in the process. The individual wafer means and standard deviations were recorded in log books along with special information regarding the batch such as the batch type (test or production), the name of the operator who started the batch and whether changes were made to the process input variables prior to the batch. This information was referenced when the control charts signaled an out-of-control situation.

The controllable process input variables are temperature in three zones (load, centre and pump), pressure, silane flowrate and deposition time. Under standard operating policy, only the load and pump zone temperatures and deposition time were adjusted from batch to batch while the other variables were strictly held constant. The position of the test wafers and thermocouples are shown in Figure 2.3.

2.3 Exploratory Data Analysis

The first step of this project was to collect and analyze historical data. This was done to uncover information in the data, such as trends and correlations, that were not immediately recognizable. The historical data included batch thickness measurements along with load zone temperature, pump zone temperature and deposition time for each batch. These data, found in Appendix II, were gathered from August 6, 1993 to January 27, 1994 and represent 243 batches.

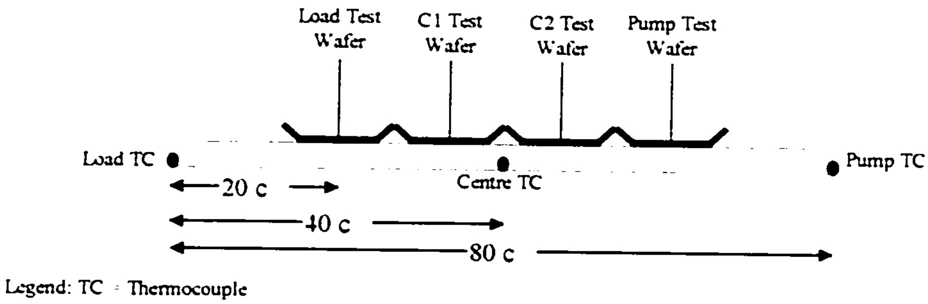

Figure 2.3: Test Wafer and Thermocouple Positions

2.3.1 Calculations Involved in Exploratory Data Analysis

A description of three of the more complicated exploratory data analysis techniques used to gain greater insight into the behaviour of the LPCVD poly-Si process follows. These techniques are: Components of Variance Analysis, Autocorrelation Plots, and Two-Level Factorial Designs.

Components of Variance Analysis

The objective of a components of variance analysis is to deduce relative contributions of the various sources of variability making up the overall observed variability in some process characteristic. For example, the variability in thickness of a deposited layer of polycrystalline silicon on a wafer is a combination of the variability due to the different test locations on the wafer (within-wafer), the variability due to the different test wafer locations along the reactor (cross-load) and variability from batch to batch. The following procedure for separating the total variation into components has been described by Box et al. (1978).

The following model is proposed to explain the generation of the observations,

$$y = \eta + \varepsilon \tag{2.1}$$

where y is the observed value, η is the long-term process mean, and ε is the overall error or deviation of the observation from the long-term mean. In this case the overall error contains three separate error components:

$$\varepsilon = \varepsilon_w + \varepsilon_c + \varepsilon_b \tag{2.2}$$

where ε_w is the within-wafer error, ε_c is the cross-load error, and ε_b is the batch-to-batch error. The model assumes that ε_w, ε_c and ε_b are independently distributed normally with mean zero and variances σ^2_W, σ^2_C and σ^2_B, respectively.

Estimating σ^2_W, σ^2_C σ^2_B using V_W, V_C and V_B

For the general case, where there are W observations from one sample, y_{bc1}, y_{bc2}, y_{bc3}... y_{bcW} are the W observations from the c^{th} wafer (or sample) of the b^{th} batch. From these observations individual wafer (sample) averages ($\bar{y}_{bc}$) can be calculated for each wafer or sample based on W observations. Within-wafer variance, σ^2_W, was estimated using V_W which represents the pooled variances of the $B \times C$ wafers or samples. There are BC(W-1) degrees of freedom associated with this estimate.

$$V_w = \frac{\sum_{b=1}^{B}\sum_{c=1}^{C}\sum_{w=1}^{W}(y_{bcw} - \bar{y}_{bc})^2}{BC(W-1)} \tag{2.3}$$

In general, there are C wafer (sample) averages per batch. From these results the batch average, $\bar{y}_b$, and the within-batch variance $\left[\sum_{c}^{C}(\bar{y}_{bc} - \bar{y}_b)^2\right]\Big/(C-1)$, which has C-1 degrees of freedom, can be calculated. Pooling the within-batch variances over all B batches results in,

$$V_c = \frac{\sum_{b=1}^{B}\sum_{c=1}^{C}(\bar{y}_{bc} - \bar{y}_b)^2}{B(C-1)} \tag{2.4}$$

which has $B(C$-1) degrees of freedom. V_C is not an estimate of σ^2_C alone because each wafer or sample is represented by an average of W measurements within a wafer. Thus, going back to an earlier assumption that the within-wafer and cross-load errors are independently distributed, V_C provides an estimate of $\sigma^2_C + (\sigma^2_W/W)$.

Finally, consider the general case of the B batch averages, $\bar{y}_1, \bar{y}_2, \ldots, \bar{y}_B$. Each is an average over C wafers or samples and CW thickness measurements. Thus, the quantity

$$V_B = \frac{\sum_{b=1}^{B} (\bar{y}_b - \bar{\bar{y}})^2}{B-1} \tag{2.5}$$

where $\bar{\bar{y}}$ is the grand average, is an estimate of $\sigma^2_B + (\sigma^2_C/C) + (\sigma^2_W/CW)$. Sample calculations can be found in Appendix III.

Autocorrelation Plots

Autocorrelation plots reveal how the correlation between any two values of a series changes as their separation changes. If serial correlation were found to be significant, this would indicate that the process, if left alone, would tend to drift from the process target or mean. Tucker et al. (1993) report that in many cases the root cause of process drift can be complex and not easily understood. In cases in which the root cause of drifting is known (for example raw-material variations), removal of the root cause may not be feasible. In such cases a stochastic or time-series model incorporating autocorrelation can be used to describe the drift. This model could then be incorporated into a feedback control scheme. If serial correlation is not significant, a statistical process control (SPC) approach would be more suitable. It has been shown by Deming (1986) that applying feedback control to a process that is not serially correlated inflates the process variance.

The following equation defines autocorrelation at lag k:

$$\rho_k = \frac{E[(z_t - \mu)(z_{t-k} - \mu)]}{\sqrt{E[(z_t - \mu)^2]E[(z_{t-k} - \mu)^2]}} \tag{2.6}$$

where E is the expectation operator. The numerator of Equation 2.6 represents the covariance between z_t, the observation at time t, and z_{t-k}, the observation k time intervals ahead of z_t. The denominator is the variance of the observations in the time series. Thus, Equation 2.5 can be rewritten as,

$$\rho_k = \frac{\mathrm{cov}[z_t, z_{t-k}]}{\sigma_z^2} \tag{2.7}$$

The autocorrelations up to lag K are then plotted. Box and Jenkins (1976) suggested selecting $K \leq N/4$, where N is the total number of observations in the data set. Autocorrelations plotted for the historical data are shown and discussed in Section 2.3.2.

Two-Level Factorial Designs

Two-level factorial designs are often used as screening designs. They are used to determine which input variables significantly effect the output variables. Each factor is examined at two levels; for k factors, 2^k runs are required. Two-level factorial designs provide information regarding terms in a first-order model with interactions of the form,

$$\begin{aligned} E(Y) &= \beta_0 + \beta_1 X_1 + \cdots + \beta_k X_k \\ &+ \beta_{12} X_1 X_2 + \cdots + \beta_{k-1,k} X_{k-1} X_k \\ &+ \beta_{123} X_1 X_2 X_3 + \cdots + \beta_{12\ldots k} X_1 X_2 \cdots X_k \end{aligned} \tag{2.8}$$

where E(Y) is the expected value of the response or output variable Y, the X_i are suitably coded factors or input variables, and the β_i are model parameters or effects. Considering a model with up to third-order interaction effects, the β_i terms are referred to as the main effects, the β_{ij} terms are known as the two-factor interaction effects, and the β_{ijl} terms are known as three-factor interaction effects.

These parameters can be estimated using the least-squares criterion, yielding

$$\hat{\beta} = \left(\mathbf{X}^T\mathbf{X}\right)^{-1}\mathbf{X}^T\mathbf{Y} \tag{2.9}$$

where $\hat{\beta} = \begin{bmatrix} \hat{\beta}_0 \\ \hat{\beta}_1 \\ \vdots \\ \hat{\beta}_{12} \\ \vdots \\ \hat{\beta}_{k-1,k} \end{bmatrix}$; $\mathbf{X} = \begin{bmatrix} 1 & x_{11} & x_{12} & \cdots & x_{1k} \\ 1 & x_{21} & x_{22} & \cdots & x_{2k} \\ & & \vdots & & \\ 1 & x_{n1} & x_{n2} & \cdots & x_{nk} \end{bmatrix}$ and $\mathbf{Y} = \begin{bmatrix} y_1 \\ y_2 \\ \vdots \\ y_n \end{bmatrix}$.

The "^" or "hat" is used to indicate that the parameter is an estimated value. The X's are coded such that their lower value is coded as -1 and their upper value is coded as +1. Coding in this manner yields parameter estimates that are uncorrelated. The general form of the coding equation for any variable v is

$$X = \frac{v - \left(\frac{v_u + v_l}{2}\right)}{\frac{v_u - v_l}{2}}. \tag{2.10}$$

Two-level factorial designs are used extensively in both research and industry. According to Box et al. (1978), the popularity of factorial designs is due to the following characteristics:

i. They require few runs per factor studied.
ii. They can be easily augmented to form composite designs if needed.
iii. Two-level factorial designs form the basis of fractional factorial designs.
iv. Interpretation of the results can be accomplished using simple arithmetic.

Fractional Factorial Designs

As the number of factors increases, a full factorial design will quickly lead to a large number of experiments. Also, a full factorial design will give information about high-order interactions, which are not likely to be significant. A fractional factorial design attempts to obtain all the pertinent information available from a full factorial design using only a fraction of the runs. This is accomplished by confounding higher-order interactions with main effects and other lower-order interactions.

Fractional factorial designs are categorized in terms of resolution to ease interpretation. For example, a fractional factorial design with 6 factors executed as a 2^{6-2} design would require a minimum of 16 different runs. One possible confounding pattern for factors 5 and 6 could be 5 = 124 and 6 = 234. The defining relation for such an experiment would be I = 1245 = 2346 = 1356. In the defining relation, 1245, 2346 and 1356 are called *words*. The resolution, *R*, of a design is determined by the shortest word in the defining relation. For this example, the resolution is four and is written as 2_{IV}^{6-2}.

A design of resolution *R* is one in which no *p*-factor effect is confounded with any other effect containing less than *R-p* factors. For the example given, this translates to no main effects are confounded with other main effects or two-factor interaction, however, two-factor interactions are confounded with other two-factor interactions. Factor 1 is confounded with the combined effect of 245 and with 356. The two-factor interaction term 12 is confounded with 45, 13 is confounded with 56, 14 is confounded with 25, and so on. No information solely regarding the 12 interaction can be determined. Further experimentation would be required to determine its significance.

2.3.2 Exploratory Data Analysis for the Tylan/Tytan LPCVD poly-Si Process

Once a representative data sample was collected, a number of graphical methods were used to obtain visual representations of the data to ease interpretation. Only the most informative analyses are reported here.

Figure 2.4 is a serial plot of the batch mean thickness measurements. Preventative maintenance shut-downs (PM's) are indicated by the triangles. During the deposition process, silicon is deposited on all internal surfaces of the reactor. When preventative maintenance shut-downs are conducted, the reactor's internal quartzware is removed and stripped of the deposited silicon coating. Preventative maintenance shut-downs occur approximately every 55 runs. Figure 2.4 was meant to uncover any time trends and trends from one PM to the next.

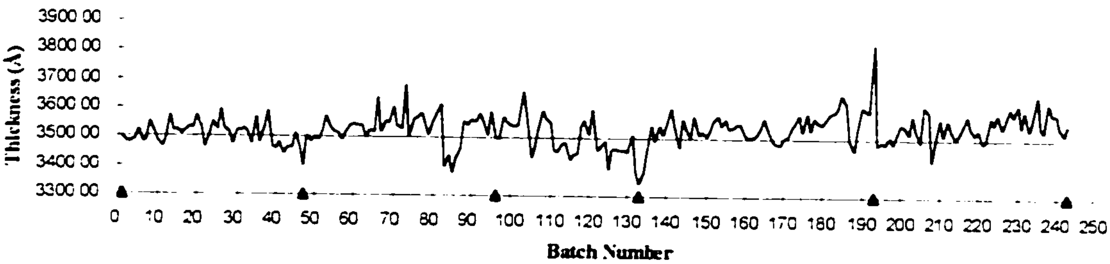

Figure 2.4: Serial Plot of Batch Mean Thickness and PM

Figure 2.4 shows that over this period of 243 batches the mean is stable. Although some process engineers felt that there were significant differences in reactor performance from one PM to the next, Figure 2.4 shows no significant PM to PM effect.

Figure 2.5 is a histogram of the batch mean thickness measurements. Subsequent analyses of the process, specifically experimental design and components of variances, require that data from the process studied are distributed normally. This histogram shows that the data are approximately normally distributed and thus data analysis techniques that can only be applied to normally distributed data can be used to analyze this process.

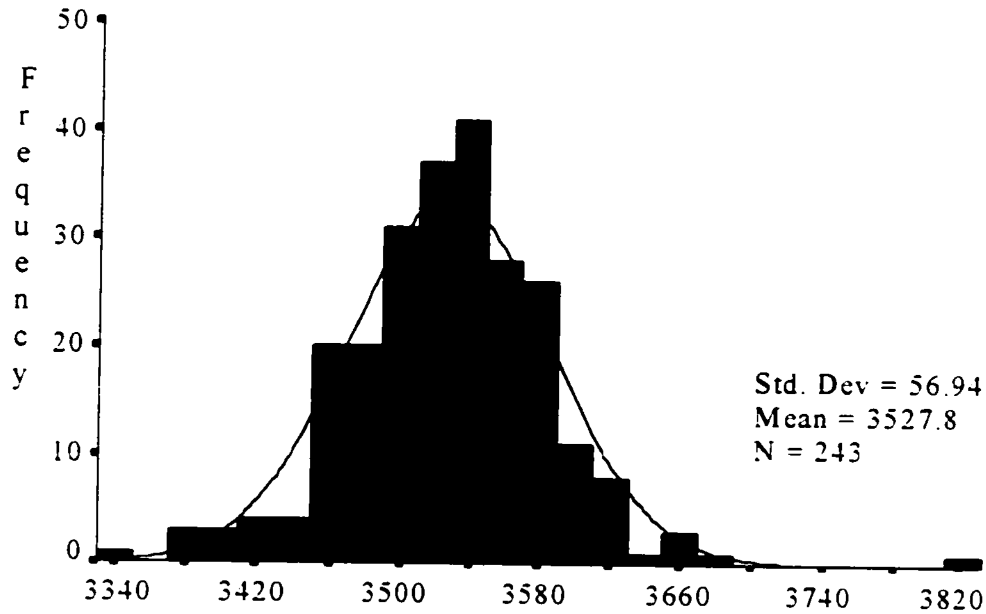

Figure 2.5: Histogram of Batch Mean Thickness

Next, components of variance analysis was conducted to decompose process variability into three categories: 1) batch-to-batch variance, 2) cross-load variance and 3) within-wafer variance. This was done to determine if any one of the components of variance was more significant than the others. The procedure reported by Box et al. (1978) was followed to determine the contribution that each of the categories made to the total process variability. The results of the components of variance analysis are listed in Table 2.2. This table lists the source of variation with its respective standard deviation and percent contribution to the total variance.

The largest contributors to the process variability were batch-to-batch variability and within-wafer variability. The large batch-to-batch variability suggests that using the measurements at the end of each batch to make adjustments to the process input variables for the next batch might reduce process variability. However, it will be shown that such feedback control is not appropriate.

Table 2.2: Components of Variance Analysis for Historical Data Set

[illegible]	[illegible]	[illegible]
Batch-to-Batch	48.1	42.8 %
Cross-Load	28.4	14.9 %
Within-Wafer	47.9	42.3 %
Total	73.6	100%

Within-wafer variability also greatly contributed to the process variability. This suggests that the reactant gas may not be equally distributed over wafers or that the wafers are not uniformly heated. Sherman (1987) showed that within-wafer variability decreases as pressure is decreased due to better distribution of reactant gas over the surface of the wafer. Thus an adjustment to the process pressure may be required to decrease within-wafer variability. The deposition rate of poly-Si is greatly dependent on temperature. Near a deposition temperature of 625°C, Kamins (1988) reported an approximate change in deposition rate (and therefore a change in film thickness) of 2 to 2.5% for every degree change in temperature. Thus improving wafer temperature uniformity during the deposition process may reduce within-wafer variability. A non-uniform temperature gradient could be the result of "hot-spots" in the heating coil surrounding the reactor or the result of a misalignment of the cantilever arm on which the wafers sit during the deposition process. These results suggest that a reduction in within-wafer variability can be achieved by either adjusting the process pressure or by adjusting the process equipment.

The relatively small contribution of cross-load variability to the overall process variability suggests that the reactor conditions, specifically front-end and back-end temperatures, were suitably set to compensate for depletion of silane along the reactor. Greater gains in the reduction of the overall process variability can be expected by reducing either batch-to-batch or within-wafer variability rather than reducing cross-load variability, because these sources contibute much more to the overall process variability.

Autocorrelations were calculated and plotted, with the aid of Statgraphics Statistical Graphics System, to determine if there was significant serial correlation (Statgraphics, 1991). Figure 2.6 is a plot of the autocorrelations with respect to lag. A 95% confidence interval is indicated by the dashed lines. At low lags, the autocorrelations extend beyond the 95% confidence interval indicating that there is significant serial correlation at low lags.

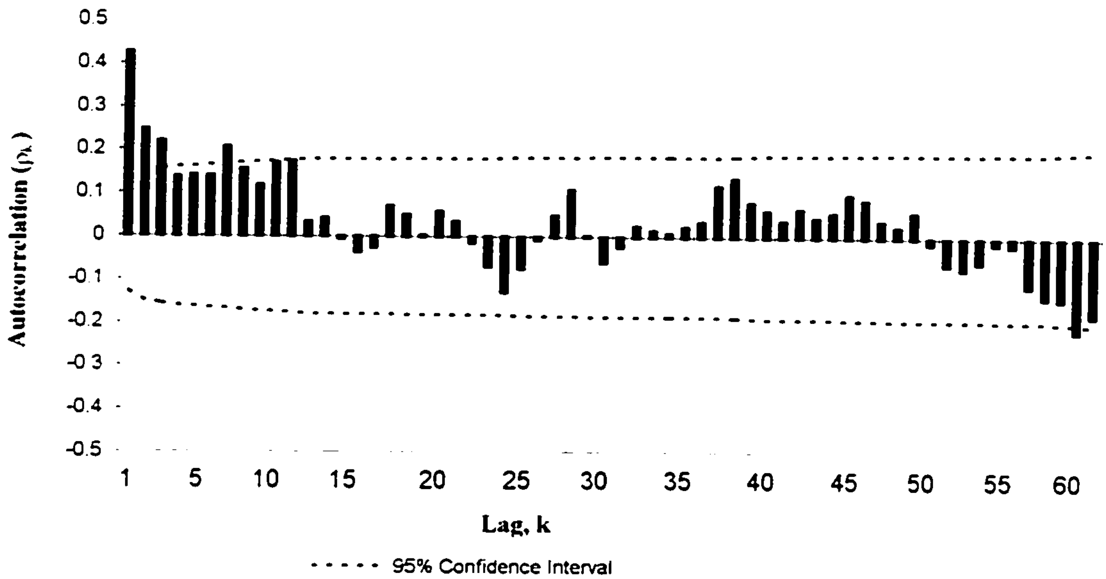

Figure 2.6: Autocorrelations of batch-mean thickness observations for the historical data set

Before deciding to incorporate an automatic process control APC approach to controlling 415 Tylan/Tytan, possible sources of the autocorrelation were explored. To do so, the adjustments that were made to the process input variables from batch to batch were examined. Two things were discovered. First, the adjustments made to the process input variables were not standardized and in some cases the wrong control action was taken. Such "tweaking" leads to inflated variability. Second, a series of 41 data points was discovered in the historical data set in which no adjustments to the process input variables had been made. The autocorrelations for this data, shown in Figure 2.7, show no sign of serial correlation. In fact, a components of variance analysis for this time period, shown in Table 2.3, showed that the batch-to-batch standard deviation was reduced by 52%. This finding also suggests that the observed autocorrelation found over the entire data set was induced by the seemingly unnecessary tweaking.

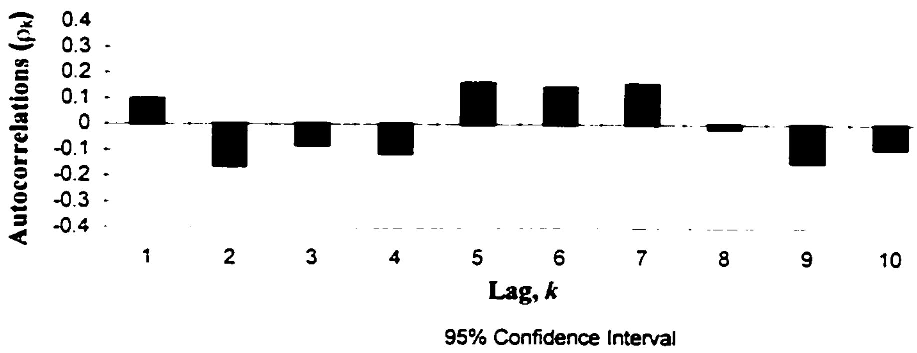

Figure 2.7: Autocorrelations of batch-mean thickness observations for the tweak-free data set

Table 2.3: Components of Variance Analysis of the Tweak-Free Batch Mean Thickness Data

[illegible]	[illegible]	[illegible]
Batch-to-Batch	23.1	10.5 %
Cross-Load	51.9	53.4%
Within-Wafer	42.7	36.1%
Total	71.1	100%

The cross-load standard deviation for this data set was significantly higher than for the historical data set while the within wafer standard deviation displayed no statistically significant change. The cause of the increase in cross-load standard deviation is likely to be an incorrect temperature ramp along the reactor. Front-end and back-end temperatures used for this period are shown in batches 1 to 41 of Table AII.1 of Appendix II. The front-end and back-end temperatures used in the period of time that the "tweak-free" data were collected were 617°C and 626°C, respectively. The portion of the historical data that does not contain the "tweak-free" is shown in batches 42 to 243 of Table AII.1. The mean front-end and back-end temperature for this "tweaked" portion of the data were 616.2°C and 623.6°C, respectively. Although there is little difference between the front-end temperatures for the "tweak-free" and "tweaked" data sets, the back-end temperature used in the "tweak-free" data is substantially larger than that used in the rest of the dataset. This too corroborates the need for a standard operating procedure.

The results of the analysis of the historical data showed evidence that the batch mean thickness data were not serially correlated. This result led to an early recommendation that changes should not be made to the process input variables from batch to batch. To further substantiate this recommendation, data collected over a two-month period (60 batches worth of data) after the recommendation was made, were collected and analyzed. These results, shown in Figure 2.8, show very slight serial correlation (0.31 at lag 1 and 0.34 at lag 5). Although these autocorrelations are significant at the 95% level, they are just barely outside the 95% confidence interval and are not large enough to merit dismissing the previous hypothesis. The components of variance analysis, the results of which are listed in Table 2.4, continues to show a significant reduction in batch-to-batch variability. A significant reduction in process variability was also achieved as indicated by the decrease in total standard deviation from 73.6 to 60.5.

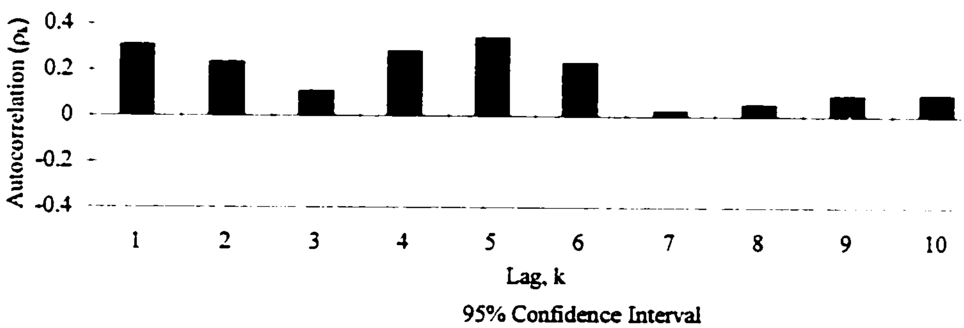

Figure 2.8: Autocorrelations of batch mean thickness observations for data collected after the recommendation

Table 2.4: Components of Variance Analysis - After Recommendation

Batch to Batch	33.0	30.6 %
Cross-Load	39.1	27.0 %
Within-Wafer	39.4	42.4 %
TOTAL	60.5	100 %

Experimental Design

This section outlines the design and the results from the first stage of experiments conducted on the Tylan/Tytan LPCVD reactor for the deposition of poly-Si. The objectives of this experiment were to determine a feasible operating region and to screen out any factors that do not affect the response variables.

The experiment was set up as a 2^{6-2}_{IV} design with the following generators: 5=124 and 6=234 yielding the defining relation I = 1245 = 2346 = 1356. Confounding was chosen in this manner in order to obtain unconfounded estimates of the main effects. The levels of the input variables were chosen based on the physical limits of the reactor, product quality limits (Sherman, 1987) and from discussions with process engineers. The constraints and range of operation for each of the factors considered in the experiment are shown in Table 2.5.

Table 2.5: Factor Constraints and Ranges for Phase I

Factor	[illegible]	Range Chosen
Centre Temperature (T_c)	Reactor Maximum: 650°C Below 550°C the film is no longer polycrystalline but amorphous	595°C to 625°C
Front Ramp ($R_1=T_{Centre}-T_{Load}$)	Must be greater than or equal to 0°C	5°C to 15°C
Back Ramp ($R_2=T_{Pump}-T_{Centre}$)	Must be greater than or equal to 0°C	5°C to 15°C
Pressure (P)	P < 200 mTorr - good within-wafer uniformity - low deposition rate P > 275 mTorr - gas phase nucleation The minimum attainable pressure is dependent on silane flowrate	185 mTorr to 260 mTorr
Silane Flowrate (F_{SiH_4})	Low flowrates - good within-wafer uniformity - low deposition rate High flowrates - poor within-wafer uniformity	150 cm^3/min to 250 cm^3/min at STP
Deposition Time (t_{dep})		37.5 to 42.5 min

The minimum attainable pressure in the reactor was found to be dependent on the flow rate of silane. This meant that some of the required combinations of pressure and silane flowrate were not achievable, namely those which had a high silane flowrate and a low pressure. To account for this, an experiment was done whereby the minimum attainable pressure was recorded for various flowrates of silane gas. This was conducted at different levels of temperature using a flat temperature profile. For the region in question, the relationship between minimum attainable pressure and silane flowrate was described by the following linear model,

$$P_{min} = 0.45F_{SiH_4} + 85 \qquad (2.11)$$

where P_{min} is the minimum attainable pressure in milliTorr and F_{SiH_4} is silane flowrate in cm^3/min. Instead of using pressure as a variable in the experimental design, a new factor, δ, was introduced. This factor, δ, changes the slope of Equation 2.11. Furthermore, a

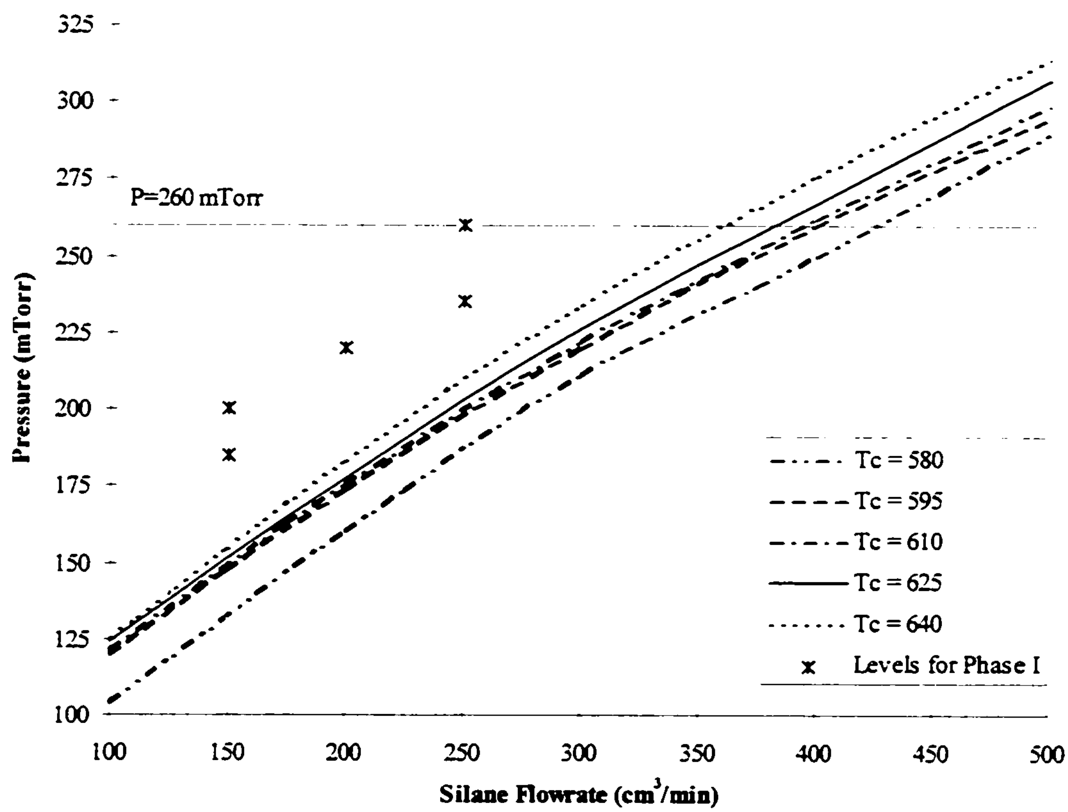

Figure 2.9: Minimum Attainable Pressure vs. Silane Flowrate

safety factor of 25 mTorr was added to Equation 2.11 to ensure that the desired pressure could be achieved. Thus, Equation 2.11 becomes

$$P_{min} = (0.45 + \delta)F_{SiH_4} + 110 \qquad (2.12)$$

and δ becomes the factor that is changed in the experimental design. The upper and lower levels of δ were set at 0.15 and 0.05, respectively. The results of the pump experiment are shown graphically in Figure 2.9.

While this research was conducted, the internal control system of the reactor was updated to a SEMY control system. This was implemented by the manufacturing facility and was applied to all oxidation and diffusion furnaces in the wafer fabrication facility. The new system promised better temperature control throughout a batch and the ability to continuously monitor process variables such as temperature, pressure and gas flowrate during a batch. It also provided for easier data collection and plotting, better recipe management and reactor specific recipe adjustments. The latter is significant due to reactor to reactor variability.

The 2^{6-2} design was executed in blocks of eight runs such that each block contained a half fraction of the 2^{6-2} design. This resulted in a 2^{6-3}_{III} design. The blocking variable was B = 134. The first block was executed prior to the change in the temperature control system and the second after the control system upgrade. The block effect was used to determine the validity of applying results from before the change in control system to the process after the change. Including the block effect, the defining relation becomes I = 1245 = 2346 = 134B = 1356 = 235B = 126B = 456B. The raw data generated from this experiment is given in Appendix IV. The estimated factorial effects from the 2^{6-2} experiment along with confidence intervals for the estimated effects are given in Table 2.6. Non-significant terms are indicated by shading.

The block effect was not found to be significant for the thickness and deposition rate models but was significant for the within-wafer and cross-load wafer models. These results do not strongly indicate that the exploratory data analysis results should not be used to describe the reactor. The suggestion is made that the exploratory data analysis should be repeated in the future.

It was found that all main effects were significant for the cross-load and within-wafer variance models. All main effects, with exception of the back-end ramp (β_3), were significant in the thickness model and the deposition rate models. Due to confounding, it was difficult to determine which two-factor interaction terms were significant.

Table 2.6: Results from the 2^{6-2} Design

Effect	Estimate of Effect and 95% Confidence Interval for Effect			
	Thickness	**Deposition Rate**	**Within-Wafer Std. Deviation**	**Cross-Load Std. Deviation**
average (β_0)	2995.81 ± 13.61	74.87 ± 0.33	39.30 ± 1.74	284.81 ± 7.80
Centre T (β_1)	950.61 ± 15.42	23.77 ± 0.39	-17.49 ± 2.04	-29.28 ± 9.14
Front Ramp (β_2)	20.13 ± 15.42	0.40 ± 0.39	2.24 ± 2.04	38.31 ± 9.14
Back Ramp (β_3)	[redacted]	[redacted]	-25.96 ± 2.04	67.60 ± 9.14
Pressure (β_4)	51.07 ± 15.42	1.21 ± 0.39	-22.90 ± 2.04	-34.93 ± 9.14
Silane Flowrate (β_5)	447.98 ± 15.42	11.20 ± 0.39	4.66 ± 2.04	-48.15 ± 9.14
Deposition time (β_6)	208.98 ± 15.42	0.50 ± 0.39	2.08 ± 2.04	29.89 ± 9.14
$\beta_{12}+\beta_{45}$	[redacted]	[redacted]	[redacted]	64.60 ± 9.14
$\beta_{13}+\beta_{56}$	25.79 ± 15.42	[redacted]	26.45 ± 2.04	11.86 ± 9.14
$\beta_{14}+\beta_{25}$	[redacted]	[redacted]	27.79 ± 2.04	48.85 ± 9.14
$\beta_{15}+\beta_{24}+\beta_{36}$	73.95 ± 15.42	1.84 ± 0.39	[redacted]	129.49 ± 9.14
$\beta_{16}+\beta_{35}$	57.90 ± 15.42	[redacted]	[redacted]	[redacted]
$\beta_{23}+\beta_{46}$	45.88 ± 15.42	1.07 ± 0.39	[redacted]	-78.21 ± 9.14
$\beta_{26}+\beta_{34}$	66.12 ± 15.42	1.63 ± 0.39	26.51 ± 2.04	-65.27 ± 9.14
β_{123}	-45.69 ± 15.42	1.17 ± 0.39	[redacted]	71.98 ± 9.14
β_{134} (blocking)	[redacted]	[redacted]	16.59± 2.04	29.77 ± 9.14

It was believed that deposition rate was independent of deposition time. These results show that over the operating range chosen in this experiment, deposition rate is moderately dependent on deposition time. Prior to conducting this experiment, the effects of deposition time on within-wafer and cross-load variance were not known. This experiment shows that both within-wafer and cross-load variance increase as deposition time increases.

The design region was tested to determine if the region showed signs of curvature. Box and Draper (1987) reported the average response of the centre-point replicates is equal to the response at X1 = X2 = X3 = X4 = X5 = X6 = 0 given by β_0 when the response surface is planar. The average of the centre point replicates and β_0 along with a 95% confidence interval for each are shown in Table 2.7 for the batch-mean thickness, deposition rate, within-wafer standard deviation and cross-load standard deviation data. If the confidence intervals for the average of the centre-point replicates overlaps the confidence interval for β_0, it can be concluded that there is no significant evidence of a difference between the values, and hence no indication of curvature in the response surface. Conversely, if the confidence intervals do not overlap, this would inidcate evidence that the values are significantly different, and hence there is evidence of curvature over the response surface.

Table 2.7: A Comparison of the Average Response of the Centre-Point Replicates and the Response at X1=X2=X3=X4=X5=X6 given β_0

Response	Average of Centre-Point Replicates	$\hat{\beta}_0$
Batch-Mean Thickness	2913.1 ± 57.2	2995.8 ± 13.6
Deposition Rate	72.8 ± 1.4	74.9 ± 0.3
Within-Wafer Std. Dev.	20.4 ± 3.2	39.3 ± 1.7
Cross-Load Std. Dev.	235.5 ± 40.8	284.8 ± 7.8

For all four responses, the confidence intervals for the average of the centre-point replicates do not overlap with the confidence intervals for β_0. This is an indication that there is significant curvature over the response surface for all four responses. Such curvature can typically be represented by a second-order model. Additional experimentation is required to fit the data generated in Phase I to a second order model.

Since the observed values of the response variables stretched beyond the range of normal operation, it was decided to start a new experiment rather than execute additional batches to eliminate confounding. In summation, it was found that all the factors are significant, and the behaviour of the reactor at the limits was unacceptable. Table 2.8 shows the batch mean thickness results from the 2^{6-2} design. The results for the other response variables, as well as the raw data, can be found in Appendix IV.

Table 2.8: Experimental Operating Conditions and Resultant Batch Mean Thickness

Batch Number	Centre Temperature (°C)	Front Ramp (°C)	Back Ramp (°C)	Pressure (mTorr)	Silane Flowrate (cm^3/min)	Deposition Time (min)	[redacted]
2	595	5	5	260	150	37.5	[redacted]
cp	610	10	10	220	200	40	[redacted]
cp	610	10	10	220	200	40	[redacted]
cp	610	10	10	220	200	40	[redacted]
3	625	15	15	185	150	37.5	[redacted]
5	625	15	5	260	250	37.5	[redacted]
7	595	15	15	235	250	42.5	[redacted]
9	625	5	15	235	250	42.5	[redacted]
11	625	5	5	200	150	42.5	[redacted]
13	595	15	5	235	250	42.5	[redacted]
15	595	5	15	260	250	37.5	[redacted]
1	625	15	15	260	250	42.5	[redacted]
4	595	5	5	260	250	42.5	[redacted]
cp	610	10	10	220	200	40	[redacted]
cp	610	10	10	220	200	40	[redacted]
cp	610	10	10	220	200	40	[redacted]
6	595	5	15	185	150	42.5	[redacted]
8	625	5	5	235	250	37.5	[redacted]
10	625	5	15	200	150	37.5	[redacted]
12	625	15	5	185	150	42.5	[redacted]
14	595	15	15	235	250	37.5	[redacted]
16	595	15	5	200	150	37.5	[redacted]

2.4 Preliminary Conclusions and Recommendations

Analysis of historical data showed that:

- The largest contributor to the process variability is batch-to-batch variability which contributes 42.8% of the total process variability.
- The batch-mean thickness data are not significantly autocorrelated when the reactor is operated in "tweak-free" mode (without changing the input settings from batch to batch). This result led to the recommendation that the changes should not be made to the process input variables from batch to batch.
- Adjustments to the process input variables were not standardized and in some cases the wrong control action was taken. Such "tweaking" of the process input variables leads to inflated variability.

Data collected and analyzed after the recommendation was followed also showed that the batch mean thickness data were not significantly autocorrelated. Significant reductions in overall process variability and batch-to-batch variability were achieved by operating the reactor in "tweak-free" mode as indicated by decrease in total standard deviation and batch-to-batch standard deviation. Total standard deviation was reduced from 73.6 Å to 60.5 Å, and batch-to-batch standard deviation was reduced from 48.1 Å to 33.1 Å.

The results of the screening experiment indicated the need for a smaller design region. Also, the design region showed signs of curvature indicating that axial or star points would be needed so that a second-order model could be fitted to the data. The design of the experiment and model building process are described in detail in Chapter Three.

Chapter Three

Modeling the LPCVD Reactor Performance

In the previous chapter the early recommendation was made not to adjust the level of the process input variables from batch to batch and to follow an SPC approach to controlling the LPCVD Poly-Si process. The next step towards achieving the objectives set forth in Chapter One was to determine a set of operating conditions that meet the manufacturing objectives. The manufacturing objectives are:

i. keep the mean thickness on target

ii. maximize the batch deposition rate

iii. minimize both within-wafer and cross-load variability.

A model is needed to determine the relationship between the input and output variables so that optimal operating conditions can be determined. These models were built using data generated from a central composite design. In this chapter, empirical model building for describing the behaviour of the LPCVD Poly-Si process is described.

3.1 Background - Central Composite Design

Central composite designs are often used when the response over the design region in question is thought to be quadratic. A central composite design contains three components. The first two components are a factorial or fractional factorial design and centre point replicates which were described in detail in Chapter Two. The third component augments the factorial design with axial points. The level of the axial points is denoted as α. These axial points provide a third level of analysis so that a second-order model for the form,

$$E(y) = \beta_o + \sum_{i=1}^{k} \beta_i X_i + \sum_{i=1}^{k} \sum_{j \geq i}^{k} \beta_{ij} X_i X_j \qquad (3.1)$$

may be fitted to the data, where β_i and β_{ij} are the model parameters and y is the response variable.

3.1.1 Experimental Design and the LPCVD Reactor - Phase II

In this section, the application of a central composite design to learn about the behaviour of the LPCVD reactor is described. The design was comprised of a 2^{6-1} fractional factorial augmented with axial points set at $\alpha = 0.75$ and ten centre-point replicates. This resulted in a total of 32+12+10 = 54 experimental batches.

The factors used in phase II were the same as those in phase I, since phase I showed that all factors were significant. These factors were: (1) centre temperature (T_c), (2) front temperature ramp (R_1), (3) back temperature ramp (R_2), (4) pressure (P), (5) silane flow rate (F_{SiH_4}), and (6) deposition time (t_{dep}). Centre temperature was denoted as 1, front temperature ramp was denoted as 2, back temperature ramp was denoted as 3, pressure was denoted as 4, silane flow rate was denoted as 5, and deposition time was denoted as 6.

Table 3. 1: Range of Factors for Phase II

Factor	Lower Value	Centre Point Value	Upper Value
T_c	614°C	620°C	626°C
R_1	3°C	5°C	7°C
R_2	3°C	5°C	7°C
P	200 mTorr	220 mTorr	240 mTorr
F_{SiH_4}	175 cm^3/min	200 cm^3/min	225 cm^3/min
t_{dep}	38 min	40 min	42 min

The initial experiment determined that the design region was too large as evidenced by the large number of responses located outside the normal region of operation. Thus, it was decided to reduce the design region for the second phase of experimentation. The choice of the new design region was decided upon through discussions with Nortel engineers and by examining the results obtained in Phase I. Also taken into consideration was the fact that since the reactor had been in operation for quite some time, it was considered likely that the optimum operating region was in the area of the current operating conditions. The resultant levels are listed in Table 3.1.

As in Chapter Two, the factors were transformed or coded to obtain parameter estimates that are uncorrelated. Applying Equation 2.10 resulted in the following transformations:

$$X_1 = \frac{T_c - 620}{6} \tag{3.2}$$

$$X_2 = \frac{m_1 - 5}{2} \tag{3.3}$$

$$X_3 = \frac{m_2 - 5}{2} \tag{3.4}$$

$$X_4 = \frac{P - 220}{20} \tag{3.5}$$

$$X_5 = \frac{F_{SiH_4} - 200}{25} \tag{3.6}$$

$$X_6 = \frac{t_{dep} - 40}{2} \tag{3.7}$$

The response variables were chosen based upon what was typically measured in production. Table 3.2 lists the definition, nomenclature and a brief description of each response variable.

Using a full 2^6 factorial design as part of the composite design would have contributed 64 runs, an unacceptable and unnecessarily large number. The number of runs was reduced to 32 from 64 by using a 2_V^{6-1} fractional factorial design. The 2_V^{6-1} design still provided unconfounded estimates of the main effects and any two-factor interactions despite the large reduction in experimental effort. The 2^{6-1} design was achieved by confounding the sixth factor, deposition time, with the combined effect of R_1, R_2, P, and F_{SiH_4}. In experimental design notation this is expressed as 6=2345. The confounding pattern was chosen such that the combined effect of T_c, R_1, R_2 (123) would not be confounded with main effects or two factor interactions, since this three-factor interaction was expected to be significant since it was found to be significant in Phase I.

Table 3. 2 Response Variables

1	Batch Mean Thickness	TH	$TH = \frac{1}{20}\sum_{i=1}^{20} TH_i$ TH represents the mean of all 20 thickness measurements and is also called the overall mean.
2,3,4,5	Mean Thickness in Zones: Load, C1, C2, Pump	LTH C1TH C2TH PTH	$TH_{Zone} = \frac{1}{5}\sum_{i=1}^{5} TH_{Zone,i}$ TH_{Zone} represents the mean thickness of the wafer measurements in a particular zone (i.e., Load, C1, C2, Pump).
6	Batch Mean Deposition Rate	DR	$DR = \frac{TH}{t_{dep}} = \frac{1}{20}\sum_{i=1}^{20} DR_i$ DR represents the mean deposition rate of all 20 points measured in a batch.
7, 8, 9, 10	Deposition Rate in Zones: Load, C1, C2, Pump	LDR, C1DR, C2DR, PDR	$DR_{Zone} = \frac{TH_{Zone}}{t_{dep}} = \frac{1}{t_{dep}}\sum_{i=1}^{5} \frac{TH_{Zone,i}}{5}$ DR_{Zone} represents the mean deposition rate in a particular zone.
11	Batch Within-Wafer Variance	WWV	$WWV = \frac{4}{16}\sum_{i=1}^{4} s_i^2 = \frac{1}{4}\sum_{i=1}^{4} s_i^2$ WWV represents the pooled within-wafer variance of the thickness measurements over the four test wafers.
12, 13, 14, 15	Within-Wafer Variance in Zones: Load, C1, C2, Pump	LWWV, C1WWV, C2WWV, PWWV	$Var(TH_{Zone,i})$ Represents the variance of the thickness measurements in a particular zone.
16	Cross-load Variance	CLV	$CLV = Var(TH_{Load}, TH_{C1}, TH_{C2}, TH_{Pump}) - WWV/5$ CLV represents the variance due to wafer position in the reactor and is computed using the components of variance equations discussed in Chapter Two. It is essentially the variance of the wafer means minus the contribution of the variance within a wafer (WWV/5).

The fractional factorial portion of the design was executed in four blocks of eight runs. Blocking was achieved by confounding the first blocking variable, denoted as B1, with the 1234 effect, and confounding the second blocking variable, denoted as B2, with the 1345 effect. The experimental runs were then sorted into 4 blocks. The first block consisted of all runs such that (B1, B2) = (-1, -1), the second block, (B1, B2)= (-1, +1), the third block, (B1, B2) = (+1, -1), and the fourth block, (B1, B2) = (+1, +1). The overall defining relation for the design was therefore I = 23456 = $1234B_1$ = $1345B_2$ = $156B_1$ = $126B_2$ = $25B_1B_2$ = $346B_1B_2$.

The order of execution of runs within each block was chosen at random. It was decided to run two centre point replicates per block so that the effect of time could be monitored from one preventative maintenance shut down (PM) to the next.

In Phase I, it was determined that the design region showed signs of quadratic behaviour. A contrast of the average response of the centre points with the average response at X1=X2=X3=X4=X5=X6=0 given by the β_0 term indicated curvature over the design region. Further evidence of curvature was indicated by the large two-factor interaction terms. This indicated that although the design region for Phase II was smaller, the response surface could possibly be quadratic. Without prior knowledge of the nature of the design region (planar or non-planar), one should execute the fractional factorial component of the design; analyze the results, check the need for quadratic terms in the model, then execute the axial points if they are needed. In Phase II the axial points were executed without first analyzing the results of the fractional factorial section because prior knowledge (Phase I results) indicated curvature over the design region and production constrainsts did not allow time for analysis.

The value for locating the axial points, α, was chosen based on the relative variances in the predicted response and in the precision of the parameter estimates that would arise from choosing a particular level of α. Several values were tested. Table 3.3 lists the variance of the predicted response, the variance of the parameter estimates, and the correlation between parameter estimates for different levels of α. Values of α >1 were not considered because that would lead to experimental results in areas which were deemed unacceptable in Phase I. Based on these results in Table 3.3, it was decided to use $\alpha = 1$.

After analyzing the results from the first two blocks of the fractional factorial design, it was decided that α should be lowered to 0.75. This was because the factor levels of +1 and -1 covered a range of responses which was outside the region of normal operation. Thus, lowering the level of α to 0.75 provided adequate coverage of the design region and greatly reduced the risk of unsuccessful batches. Sample calculations are found in Appendix V.

Due to production constraints, it was not possible for all 54 runs to be completed in one PM cycle. It was therefore decided to perform the first three blocks, plus 2 centre points for each and the axial points in the first PM cycle. The last block plus two additional centre points were conducted in the second PM cycle. These two additional centre points were added so that a more sensitive comparison of the two PM cycles could be accomplished. A summary of the run conditions as well as the experimental results are presented in Appendix V.

Table 3. 3: Relative Variances of Predicted Response and of Parameter Estimates at Various Levels of α

Levels of α	(Variance of $\hat{y}_k$)/σ^2		(Variance of $\hat{\beta}$)/ σ^2			
	factorial	axial	β_0	β_1 to β_6	β_{12} to β_{56}	β_{11} to β_{66}
$\alpha = 1.0$	0.676	0.484	0.055	0.029	0.031	0.421
$\alpha = 0.8$	0.680	0.477	0.051	0.030	0.031	1.021
$\alpha = 0.75$	0.681	0.475	0.050	0.030	0.031	1.321
$\alpha = 0.6$	0.683	0.471	0.049	0.031	0.031	3.219
$\alpha = 0.5$	0.685	0.468	0.048	0.031	0.031	6.670

The runs were executed according to block. After the first block had been completed, the results were examined to determine if the chosen operating region was suitable. When all blocks were completed, the results were analyzed. Analysis involved fitting a model of the form,

$$E(y) = \beta_0 + \sum_{i=1}^{6} \beta_i X_i + \sum_{i=1}^{6} \beta_{ii} X_i^2 + \sum_{i=1}^{6} \sum_{j>i}^{6} \beta_{ij} X_i X_j + \beta_{123} X_1 X_2 X_3 \qquad (3.8)$$

to the data. Techniques used to test for model adequacy and refine the models are described in the next section.

3.2 Background - Model Building

This section describes the methods used to develop empirical models characterizing the LPCVD reactor. These models will be used to develop a mathematical relationship between the input variables and the output variables and to optimize the reactor conditions. Full second-order models were fitted to data generated from a central composite design. The models were simplified by omitting terms which were not significantly different from zero at the 5% level. The optimum operating conditions for the simplified models were then determined. The models also played a key role in establishing a control scheme designed to reduce batch-to-batch variability. These models were also used to make process adjustments in the event of an out-of-control situation, thereby allowing production to continue while the engineering staff searched for the cause of the situation.

3.2.1 Tests for Determining Model Adequacy

There are many methods for determining model adequacy. Quantitative methods are based on comparing a statistic to a known distribution and drawing inferences. Qualitative methods rely on graphics such as residual plots. The quantitative methods used to assess the models were the coefficient of determination, R^2, and a lack of fit test (Draper and Smith, 1981). The qualitative methods employed were based on examining various residual plots for signs of trends and non-normality.

Fraction of Variation Explained, R^2. The R^2 statistic is the ratio of the sum of squares due to regression and the sum of squares about the mean. It measures the portion of total variation about the mean, μ, explained by the regression. R^2 is the correlation between y and $\hat{y}$ and is usually called the multiple correlation coefficient. It is desirable that this number be close to unity. The R^2 statistic should not be used alone to determine model adequacy since it gives no information regarding the fit. Furthermore, it is not known how close to unity is desirable (Draper and Smith, 1981).

$$R^2 = \frac{\sum_{i=1}^{n}(\hat{Y}_i - \bar{Y})^2}{\sum_{i=1}^{n}(Y_i - \bar{Y})^2} \qquad (3.9)$$

Lack of Fit Test. When testing a model for lack of fit the lack of fit statistic, LOF is compared to an F-distribution with the same degrees of freedom at a significance level α. If the lack of fit statistic is larger than the upper α per cent value of F_{ν_1,ν_2}, then the fitted model is said to display lack of fit. It is common to choose α equal to 5%. The lack of fit statistic is calculated by the following equation,

$$\mathrm{LOF} = \left[\frac{\mathbf{e}^{T}\mathbf{e} - \nu_p \hat{\sigma}_p^2}{(n-p) - \nu_p}\right] \Big/ \hat{\sigma}_p^2 \tag{3.10}$$

where $\mathbf{e}$ is the nx1 vector of the residuals, $\mathbf{y} - \hat{\mathbf{y}}$, $\hat{\sigma}_p^2$ is the estimate of pure error variance obtained from replicates, ν_p is the degrees of freedom associated with the estimate of pure error variance, n is the number of residuals, and p is the number of estimated parameters in the fitted model (Draper and Smith, 1981).

3.2.2 Transforming Variables

For cases where the model does not adequately describe the data, a transformation of variables may improve the fit. Transformations are typically used in order to achieve a linear model, to achieve constant error variance, and to achieve an approximate normal distribution of the residuals. Box and Cox (1964) suggested a series of power transformations aimed at achieving these goals. The equations involved in the transformation are,

$$y^{(\lambda)} = \begin{cases} \dfrac{y^{\lambda} - 1}{\lambda} & \lambda \neq 0 \\ \ln y & \lambda = 0 \end{cases} \tag{3.11}$$

where λ is the transformation variable. The maximum likelihood estimates of λ are given by the values for which the following likelihood is maximized.

$$l(\lambda) = -\frac{n}{2}\ln\left[\frac{1}{n}\sum_{j=1}^{n}(y_j^{(\lambda)} - \overline{y^{(\lambda)}})^2\right] + (\lambda - 1)\sum_{j=1}^{n}\ln y_j \tag{3.12}$$

where,

$$\overline{y^{(\lambda)}} = \frac{1}{n}\sum_{j=1}^{n} y_j^{(\lambda)} = \frac{1}{n}\sum_{j=1}^{n}\left(\frac{y_j^{\lambda}-1}{\lambda}\right) \tag{3.13}$$

The maximum of $l(\lambda)$ can be found graphically by plotting $l(\lambda)$ versus λ for various values of λ. Graphs of $l(\lambda)$ versus λ are used rather than a more rigorous approach so that the behaviour of λ near the maximum value $\hat{\lambda}$ may be studied. For example, if either $\lambda = 0$ (log transformation) or $\lambda = ½$ (square root transformation) is near $\hat{\lambda}$, one of these may be preferred because of simplicity. Typically, λ ranges from -2 to +2.

Transformation of the predictor variables, **X**, may be necessary when 1) there is theoretical or empirical evidence suggesting that model simplification may occur as a result, 2) transformation of some sort is clearly called for but the error structure is satisfactory in the original response metric. Transformation of the predictor variables involves fitting the following nonlinear equation with *k* predictor variables,

$$\begin{aligned} Y_u &= \beta_o + \beta_1 X_1^{\alpha_1} + \beta_2 X_2^{\alpha_2} + \cdots + \beta_k X_k^{\alpha_k} \\ &+ \beta_{12} X_1^{\alpha_1} X_2^{\alpha_2} + \cdots + \beta_{k-1,k} X_{k-1}^{\alpha_{k-1}} X_k^{\alpha_k} + \cdots \; etc. \end{aligned} \tag{3.14}$$

The solution to this nonlinear equation may be found using a non-linear regression routine.

Occasionally, transformation of both response and predictor variables may be necessary. In these cases, it is necessary to study all possible combinations of X and Y transformed and then assess which combination of transformations gives the best results. For example, apply all the standard power transformations (λ = -1, -½, 0, 1, ½). For each of these cases, transform the X's and then assess the results.

3.2.3 Strategies for Examining Residuals

The above quantitative tests alone are not sufficient for testing model adequacy. While R^2 measures the fraction of variability explained by the model, it does not provide information specifically regarding any non-random distribution of the residuals. Also, the sensitivity of the lack of fit test decreases with the number of degrees of freedom ν_p associated with σ^2_p. Thus, for designs with few replicates, only gross lack of fit will be detected by this method (Draper and Smith , 1981).

Examination of plots of the residuals provides a means to check the fundamental assumptions of least squares (i.e., that the residuals are identically, independently, normally distributed with mean $\mu=0$ and constant variance, σ^2). If the fitted models adequately describe the variation in the data then the residuals will show only random or normal variation. A number of plotting techniques exist to check residuals. The methods used in this thesis are:

i) Histograms - used to check the normality assumption and the $\mu=0$ assumption.
ii) Normal probability plot - checks the normality assumption.
iii) Residuals versus fitted values and versus input variables - checks for constant variance and for $\mu=0$.
iv) Residual versus run number - checks for time trends. The residuals should be scattered randomly around the zero value on the y-axis.
v) Lag plots (e_{u+1} versus e_u and e_{u+2} versus e_u) - checks for autocorrelation between the residuals. If the residuals are independently distributed then these plots should not show any trends.

3.3 The Model Building Procedure

Once a second-order model was fitted to the data, the models were analyzed and refined. Figure 3.1 shows the algorithm used for the model building process. An example of how this flowsheet was used for the overall thickness model follows.

A model of the form given in Equation 3.14 was fitted to the batch mean thickness data using RS/1 Statistical Software. Estimates of the parameters and associated statistics are listed in Table 3.4. The lack of fit tests performed on the resultant model yielded LOF ratio of 1.89 with degrees of freedom associated with the numerator and denominator, $\nu_1=38$ and $\nu_2=10$, respectively. The value of an F-distribution with the same degrees of freedom at a significance level of 0.05 is 2.67. Since the LOF ratio is less than $F_{0.05,38,10}$, it can be concluded that there is no evidence of significant lack of fit. The R^2 value, 0.98, is close to unity and, a transformation of the variables was not necessary.

Next, the model terms with a t-value significance of greater than 0.05 were removed. The simplified results are listed in Table 3.5. This reduced model showed no significant lack of fit, and the new R^2 value was 0.9714. Since the R^2 value was close to unity and all the remaining terms were significant, it was possible to move on to the next step - plotting the residuals. This is one of the last steps in the model building process before the model is accepted. These steps were followed for all models, the results of which can be found in Appendix VI.

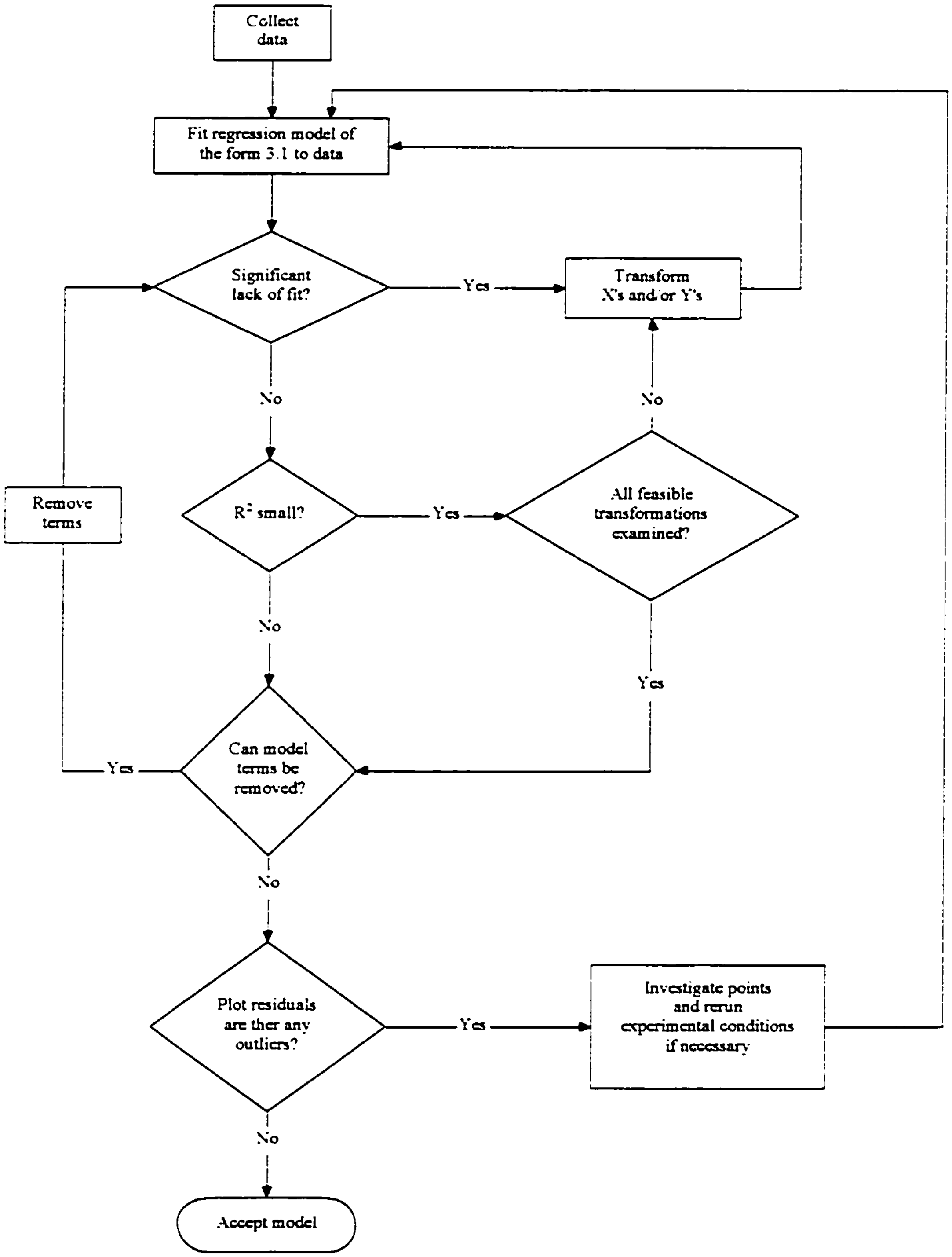

Figure 3. 1: Flowsheet of Model Building Process

Table 3. 4: Parameter Estimates from Thickness Model

Effect	Estimate of Effect	t-value	Significance of t-value
β_o	3581.67	213.33	0.0001
β_1	414.67	31.99	0.0001
β_2	1.65	0.13	0.8994
β_3	-7.53	-0.58	0.5651
β_4	95.09	7.28	0.0001
β_5	155.65	12.11	0.0001
β_6	196.27	15.10	0.0001
β_{12}	3.60	0.27	0.7864
β_{13}	-8.35	-0.64	0.5307
β_{14}	17.71	1.35	0.1893
β_{15}	33.90	2.65	0.0131
β_{16}	20.23	1.54	0.1356
β_{23}	-2.87	-0.22	0.8290
β_{24}	-23.98	-1.82	0.0793
β_{25}	-0.04	-0.00	0.9976
β_{26}	-11.36	-0.86	0.3953
β_{34}	11.93	0.91	0.3724
β_{35}	1.66	0.13	0.9003
β_{36}	15.13	1.15	0.2602
β_{45}	20.12	1.53	0.1377
β_{46}	28.05	2.06	0.0496
β_{56}	10.22	0.78	0.4439
β_{11}	19.00	0.22	0.8273
β_{22}	34.20	0.40	0.6949
β_{33}	- 73.66	-0.85	0.4006
β_{44}	37.18	0.43	0.6699
β_{55}	-27.53	-0.32	0.7521
β_{66}	-17.62	-0.20	0.8397
β_{123}			

Table 3.5: Significant Parameters for the Thickness Model

Effect	Estimate of Effect	t-value	Significance of t-value
β_o	3581.67	369.18	0.0001
β_1	414.67	33.64	0.0001
β_4	95.09	7.71	0.0001
β_5	155.65	12.63	0.0001
β_6	196.27	15.92	0.0001
β_{15}	33.90	2.70	0.0094
β_{46}	28.05	2.24	0.0299

3.4 Results and Discussion

This section gives details of the results obtained from fitting the overall models. Of the possible 16 models, only the thickness (overall), deposition rate (overall) within-wafer variance (overall) and cross-load variance are described here, since they are the four that will be used to determine the optimal operating conditions. Models based on individual wafers are discussed in Appendix VII. The individual wafer models were used to gain a better understanding of the process at the wafer level.

The four overall accepted models are assessed in detail in this section. Each of these models was tested for lack of fit using standard lack of fit tests. The number in parentheses appearing below the model is the significance of the F-value associated with the lack of fit test. A value less than 0.05 indicates significant lack of fit; also indicated are the R^2 values.

Various plots of the residuals were used to determine each model's ability to fit the data. Plots of observed versus predicted values of the response were used to assess the model's prediction capabilities. Histograms and normal probability plots of the residuals were used to assess the normality assumption. Residuals were plotted versus the predicted values, and the experiment factors were used to uncover any trends with respect to these variables. To determine if trends with respect to batch number were significant, the residuals were plotted versus batch number, *i*, the ith residual was plotted against the *i*-1 residual, and the residual *i*th was plotted against the *i*-2 residual.

3.4.1 Batch Mean Thickness (TH)

$$\begin{aligned} TH = &\ 3581.67 + 414.68X1 + 95.09X4 + 155.65X5 + 196.27X6 \\ &+ 33.90X1X5 + 28.05X4X6 \end{aligned} \tag{3. 15}$$

No significant lack of fit (0.14)
$R^2 = 0.97$
The residual plots show no sign of trends.

Interesting aspects of this model include the absence of quadratic terms and the strong dependency on X1, X5 and X6. The absence of quadratic terms means that the behaviour of the reactor with respect to the model parameters is linear within the design region. A strong dependency on X1, the coded centre temperature, was expected since X1 dictates the level of temperature in the reactor. The rate of reaction for the pyrolysis of silane is strongly dependent on temperature. Thus, it is not surprising that temperature featured prominently in the model.

Equation 3.15 shows that thickness increases as X5, the coded silane flow rate, increases. It has been shown by Kamins (1988), that at very low flowrates (below 50 cm^3/min) the effect of silane flowrate on poly-Si thickness was not linear. This phenomenon is not represented by equation (3.15) since this experiment did not cover very low silane flowrates.

X6, the coded deposition time, determines the length of time the reactant gas flows across the wafers. The longer the time the thicker the film and so it was not surprising to learn that deposition time has a strong effect on film thickness.

X4, coded pressure, also appears as an important factor but to a lesser degree. The influence of pressure on batch mean thickness is positive, that is, an increase in pressure will result in thicker films of polycrystalline silicon. This result agrees with the result reported by Azzaro et al. (1992). LPCVD reactors operate in a reaction-limited regime. The adsorption of silane to the wafer surface and its subsequent decomposition to solid silicon and hydrogen gas is dependent on the partial pressure of silane at the surface of the wafer. As the partial pressure of silane increases, the number of silane molecules available at the surface for reaction increase resulting in thicker films (Sherman, 1987).

The temperature ramps, X2 and X3 were not significant at the 95% level. The temperature ramps affect the thickness in a particular zone. Since the batch mean thickness is an average of the thickness measurements from all regions of the reactor, it is likely that the effects of X2 and X3 are lost in the averaging process.

Residual plots are depicted in Figures 3.2 to 3.11. Figure 3.2 shows that the thickness model adequately fits the data with only minor deviations from the experimental values.

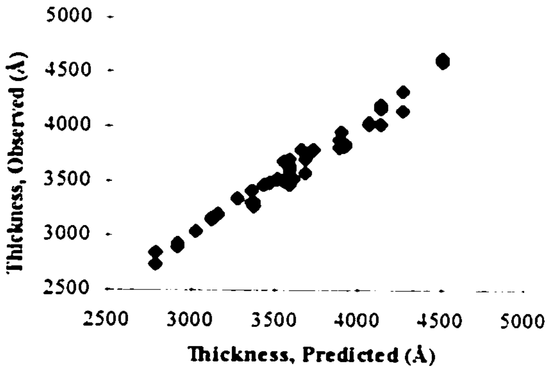

Figure 3.2: Observed versus Predicted for Thickness Model

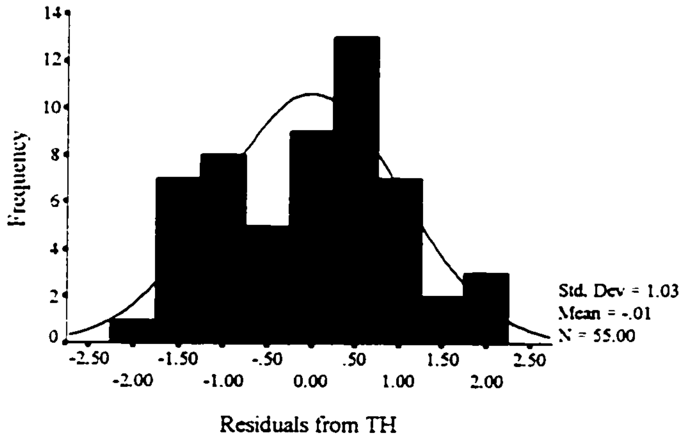

Figure 3.3: Histogram of Residuals from Thickness Model

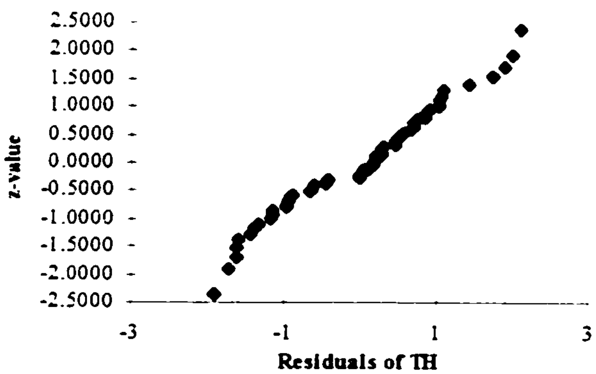

Figure 3.4: Normal Probability Plot of Residuals from Thickness Model

Judging by the histogram of the residuals (Figure 3.3) and the normal probability plot of residuals (Figure 3.4), the residuals are approximately normally distributed.

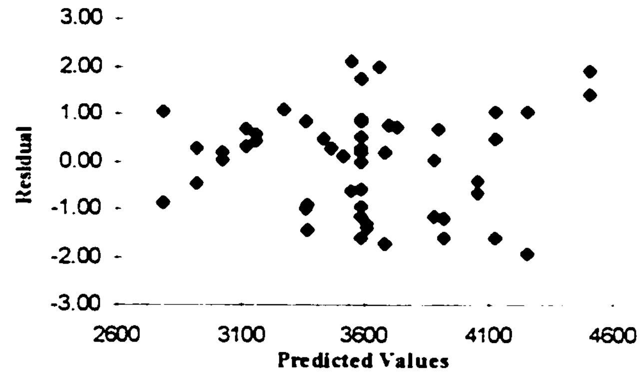

Figure 3.5: Residuals vs. Predicted Values for Thickness Model

Figure 3.5 depicts the residuals from the thickness model plotted versus predicted values. This plot shows no sign of trends, indicating that the variance is approximately constant and that the model is adequate.

In the next four figures, the residuals are plotted versus the experimental factors, X1, X2, X3, X4, X5, X6. Figure 3.6 shows that at lower X1 values (i.e., lower centre temperature) the variance of the residuals is slightly lower. However, it is not large enough to merit a weighted least-squares approach. Residual plots versus X2, X3, X4, X5, X6 show no sign of trends.

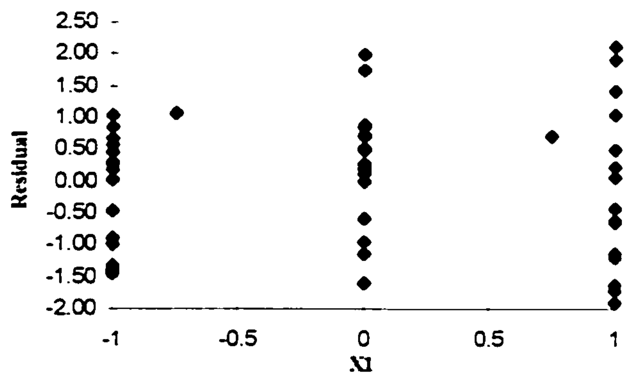

Figure 3.6: Residuals vs. X1 for Thickness Model

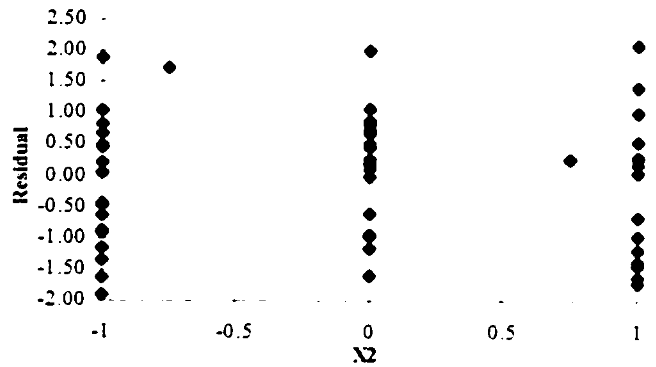

Figure 3.7: Residuals vs. X2 for Thickness Model

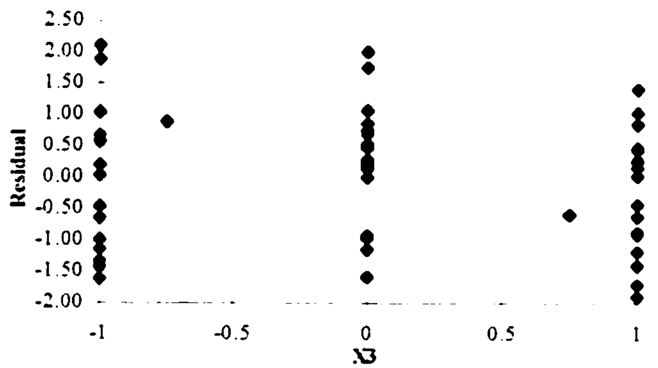

Figure 3.8: Residuals vs. X3 for Thickness Model

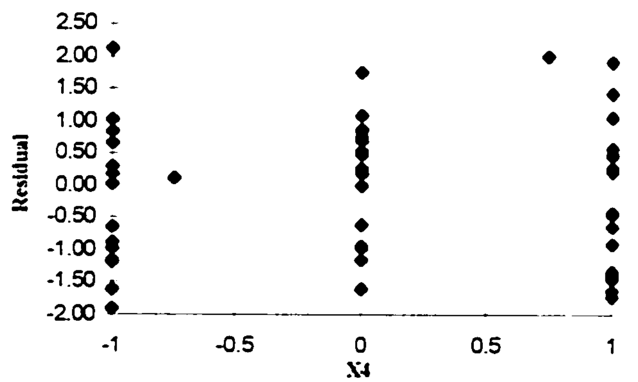

Figure 3.9: Residuals vs. X4 for Thickness Model

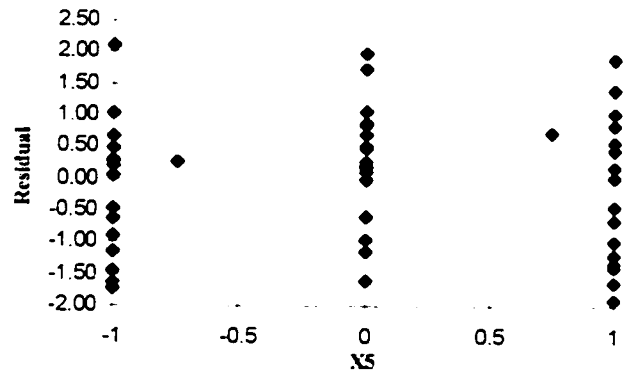

Figure 3.10: Residuals vs. X5 for Thickness Model

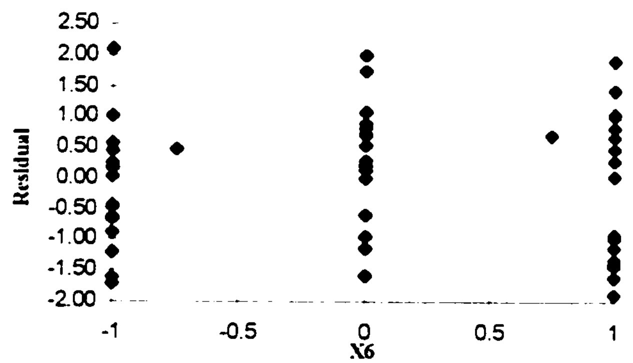

Figure 3.11: Residuals vs. X6 for Thickness Model

The following three plots are meant to uncover any time trends. Figure 3.12 is a serial plot of the residuals. This plot shows a possible shift at batch number 30. Investigation of these points indicates that no changes in operation occurred around this time. The PM change occurred at batch number 43, which does not correspond to the phenomenon seen in Figure 3.12. Lag-1 and lag-2 serial plots indicate no significant serial correlation.

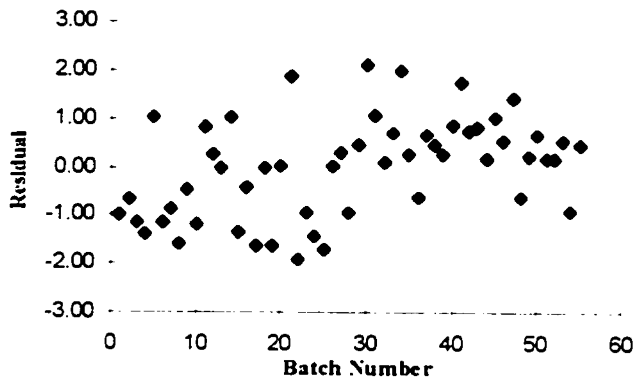

Figure 3.12: Serial Plot of Residuals from Thickness Model

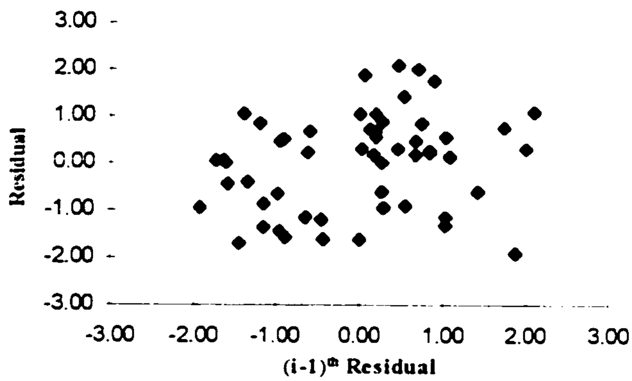

Figure 3.13: Lag 1 Plot of Residuals from Thickness Model

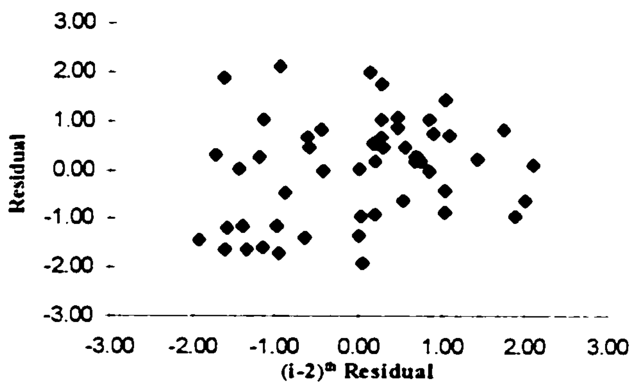

Figure 3.14: Lag 2 Plot of Residuals from Thickness Model

3.4.2 Batch Mean Deposition Rate (DR)

$$DR = 89.53 + 10.37X1 + 2.35X4 + 3.89X5 + 0.82X1X5 - 0.63X2X4 \quad (3.16)$$

No significant lack of fit (0.18)
$R^2 = 0.97$
The residual plots showed no sign of trends.

Just as was the case with the thickness model, none of the quadratic effects has a significant effect on the overall deposition rate. As expected, deposition rate is not a function of deposition time (X6). It follows then that the deposition rate is constant throughout a run.

The deposition rate model is very similar to the thickness model. In fact, the $\hat{\beta}_0$, $\hat{\beta}_1$ $\hat{\beta}_4$, $\hat{\beta}_5$, $\hat{\beta}_{15}$ terms for the deposition rate model differ from the corresponding $\hat{\beta}_i$'s in the thickness model by a factor of 1/40. This is interesting because the mean deposition time is 40 min. Thus the deposition rate model is equal to thickness model minus the X6 term divided by the mean deposition time (40 min). The DR model also contains the X2X4 term. The significance of the t-value for this term is 0.042, which means that it is only marginally significant and could be removed for the purpose of simplification. Residual plots follow in Figures 3.16 to 3.24.

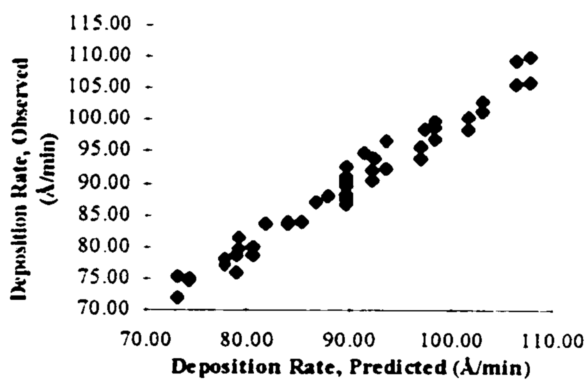

Figure 3.15: Observed vs. Predicted for Deposition Rate Model

Figures 3.15 shows that the thickness model adequately fits the data with only minor deviations from the experimental values.

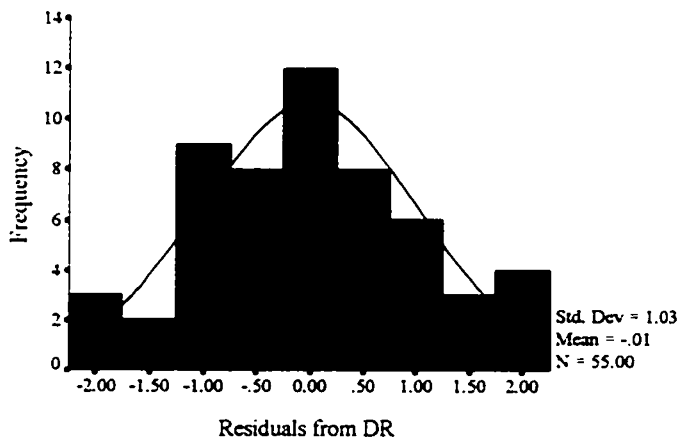

Figure 3.16: Histogram of Residuals for Deposition Rate Model

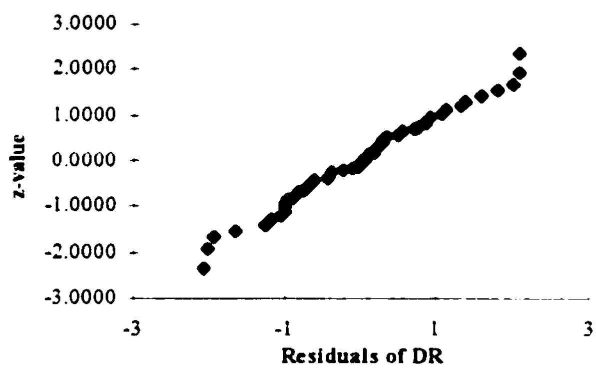

Figure 3.17: Normal Probability Plot of Residuals from Deposition Rate Model

From the histogram of residuals and the normal probability plot, it can be concluded that the residuals are approximately normally distributed.

The residuals were plotted versus the predicted values in Figure 3.18. This plot shows that the variance is approximately constant.

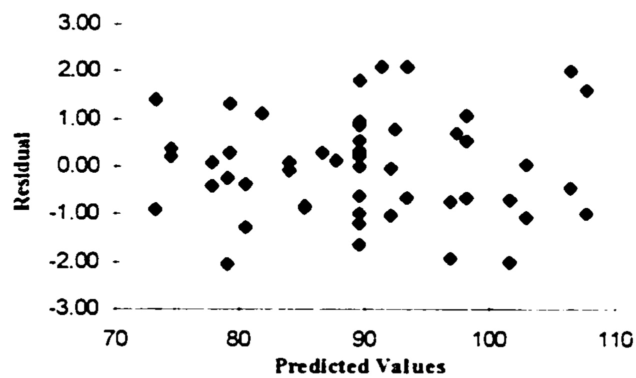

Figure 3.18: Residuals vs. Predicted Values for Deposition Rate Model

The next six figures are plots of the residuals versus the factors X1, X2, X3, X4, X5 and X6. These plots show that the variance is approximately constant over these parameters and that the model accounts for them.

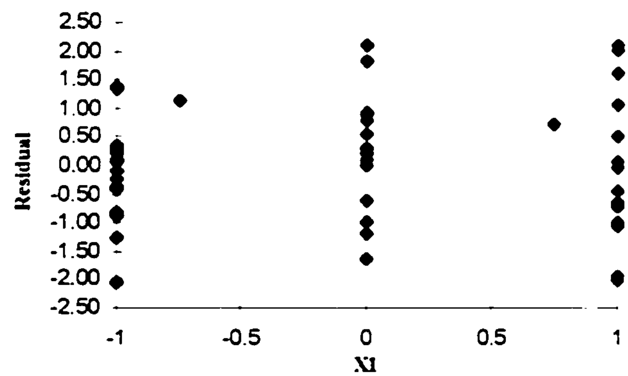

Figure 3.19: Residuals vs. X1 for Deposition Rate Model

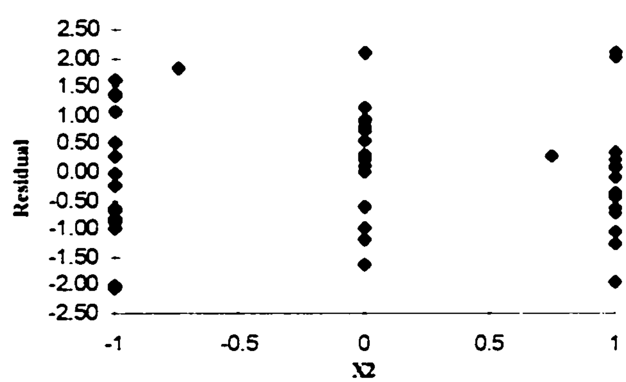

Figure 3.20: Residuals vs. X2 for Deposition Rate Model

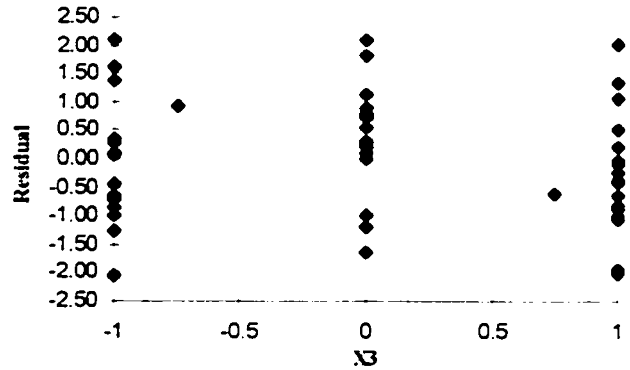

Figure 3.21: Residuals vs. X3 for Deposition Rate Model

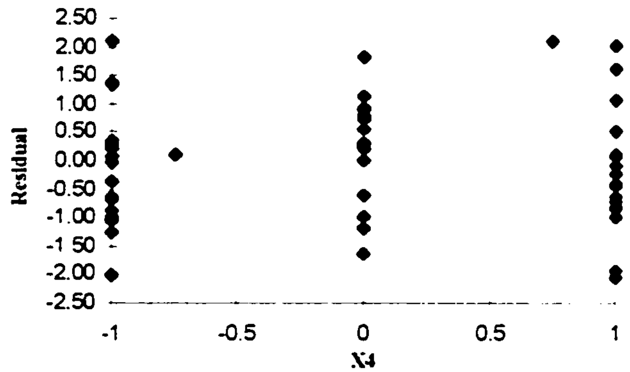

Figure 3.22: Residuals vs. X4 for Deposition Rate Model

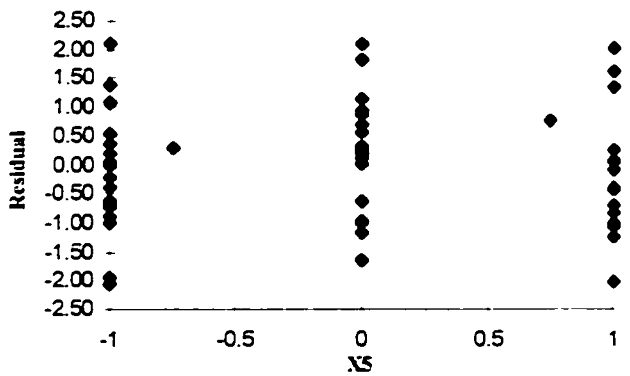

Figure 3.23: Residuals vs. X5 for Deposition Rate Model

The plot of the residuals versus batch number (Figure 3.25) shows the same shift in the residuals at around batch number 30 that was seen in the plot of the residuals from the thickness model. It is not surprising that both thickness and deposition rate models showed the same trend, since deposition rate is derived from the batch mean thickness. Neither the lag-1 nor the lag-2 residual plots showed signs of serial correlation.

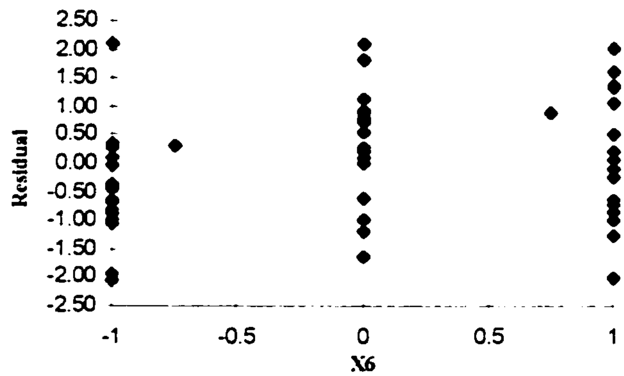

Figure 3.24: Residuals vs. X6 for Deposition Rate Model

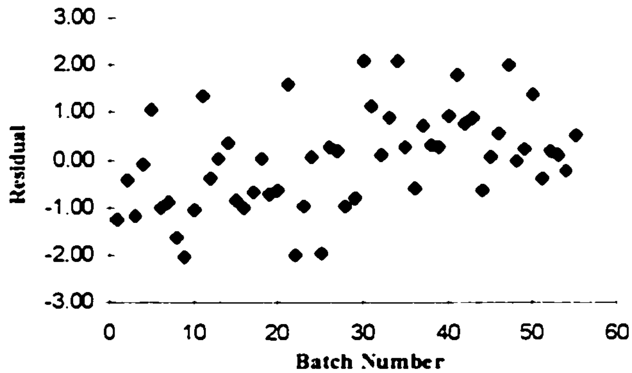

Figure 3.25: Residuals vs. Batch Number for Deposition Rate Model

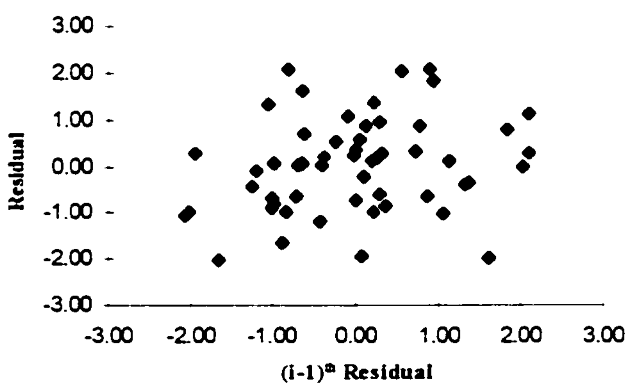

Figure 3.26: Lag 1 Plot of Residuals for Deposition Rate Model

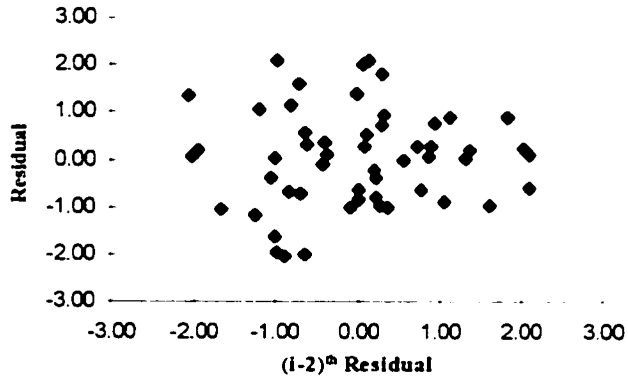

Figure 3.27: Lag 2 Plot of Residuals for Deposition Rate Model

3.4.3 Within-Wafer Variance - Overall (WWV)

$$WWV' = (0.0464 - 0.0058X1 + 0.0034X2X3 + 0.0034X1X6)^{-2} \qquad (3.17)$$

No significant lack of fit (0.83)
R^2=0.33
Residual plots showed no strong indication of lack of fit.

When linear regression was applied to the within-wafer variance data, it was found that there would be a significant improvement in the fit if the response variable was transformed to (within-wafer variance)$^{-1/2}$. The fit was then performed on the transformed data. Although this model did not show any significant lack of fit, the R^2 value, 0.33, was quite low. This indicates that there are factors affecting the within-wafer variance which were not taken into account in this study. This result is not surprising, since variance within a wafer results from reactor design factors, such as the position of the cantilever post PM and to a lesser degree from operating conditions.

The three terms dealing with temperature, X1, X2 and X3, feature prominently in this model. X1, centre temperature, is present on its own and combined with X6, deposition time. Looking solely at the X1 terms, minimum within-wafer variance is achieved at low temperatures. The X1X6 interaction term, indicates that if X1 is low then X6 should be low in order to minimize the within-wafer variance. At low temperatures, the silane gas has a better chance of diffusing between the wafers before adsorbing to the surface and reacting. This yields a more uniform thickness profile across the wafer. Residual plots are depicted in Figures 3.28 to 3.34.

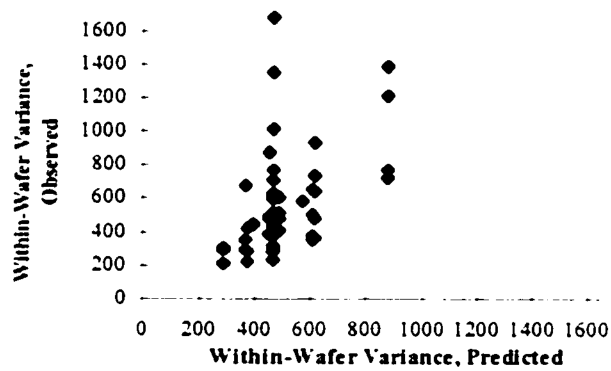

Figure 3.28: Observed vs. Predicted for Within-Wafer Variance Model

The within-wafer variance models generally compare well with the experimental data. However, there are some discrepancies in the within-wafer variance model corresponding to batches 2, 18, 21, 30, 33 and 34. The model seems to have difficulty predicting values that are extreme. However, the reactor would not normally operate with such large within-wafer variances.

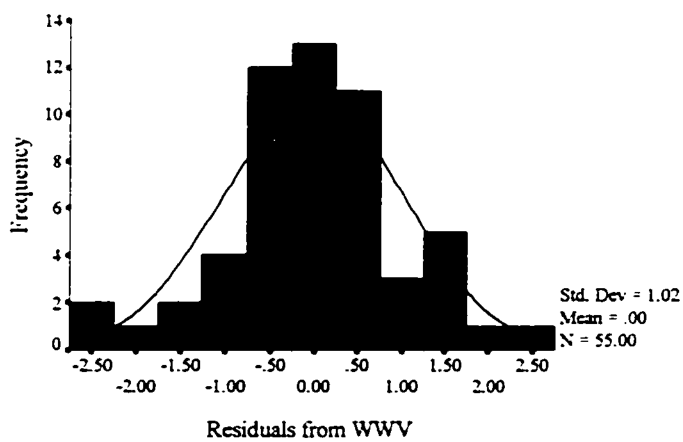

Figure 3.29: Histogram of Residuals from Within-Wafer Variance Model

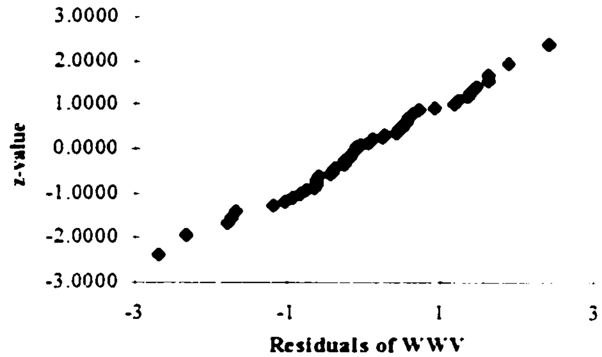

Figure 3.30: Normal Probability Plot of Residuals from Within-Wafer Variance Model

The histogram and normal probability plot for the residuals of the within-wafer variance model given in Figures 3.29 and 3.30 show the residuals approximately follow a normal distribution.

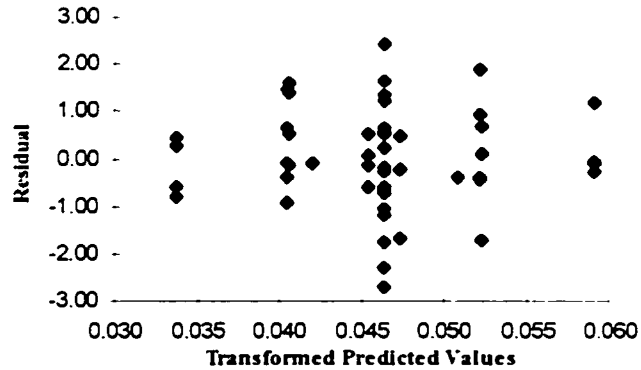

Figure 3.31: Residuals versus Predicted Values for Within-Wafer Variance Model

In Figure 3.31 the residuals are plotted versus the predicted values. Although there is an apparent increase in variance when the transformed predicted value is 0.047, it may be due to the larger amount of data at this point relative to that at the ends of the plot.

The next six figures are plots of the residuals versus the factors X1, X2, X3, X4, X5 and X6. These plots show that the variance is approximately constant over these parameters and there is no evidence of lack of fit.

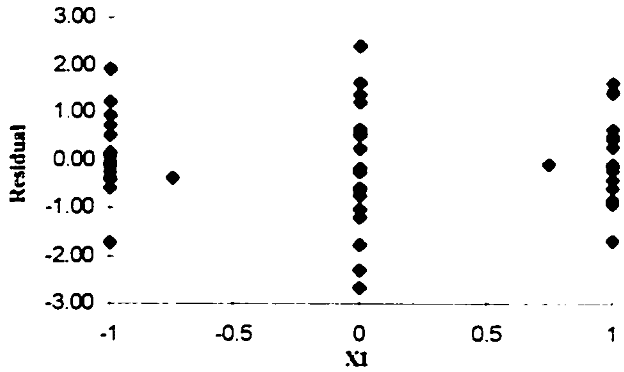

Figure 3.32 : Residuals versus X1 for Within-Wafer Variance Model

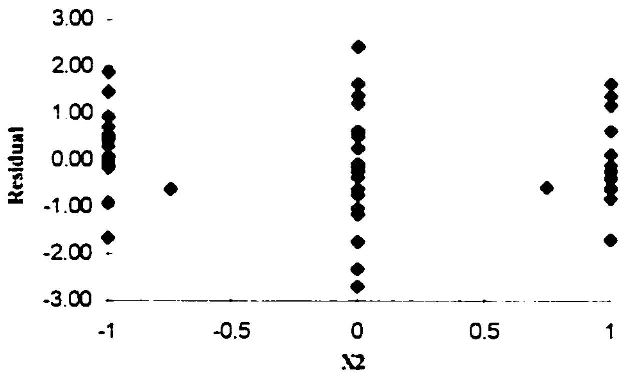

Figure 3.33: Residuals versus X2 for Within-wafer Variance Model

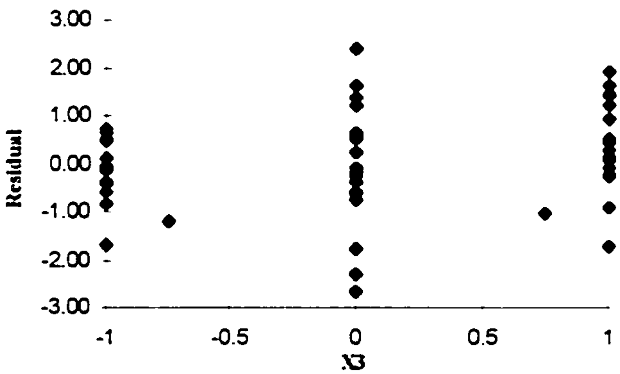

Figure 3.34: Residuals versus X3 for Within-wafer Variance Model

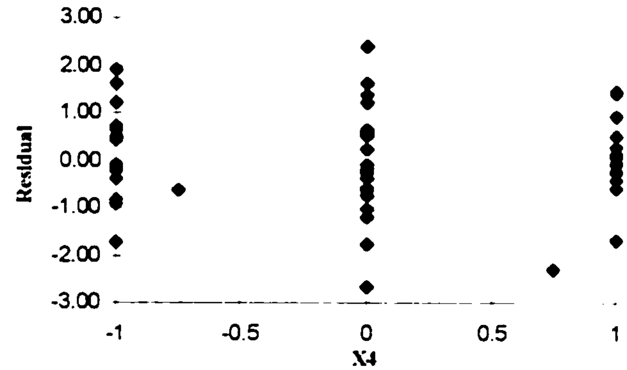

Figure 3.35: Residuals versus X4 for Within-wafer Variance Model

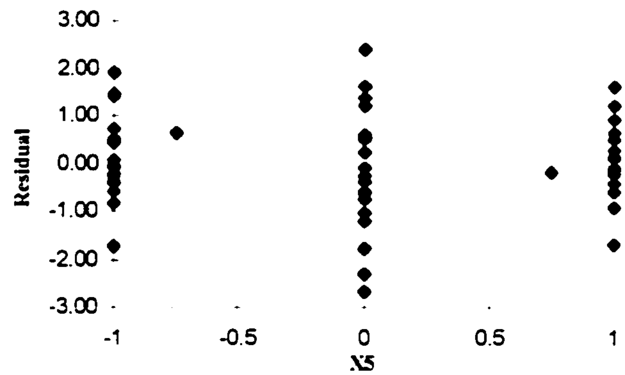

Figure 3.36: Residuals versus X5 for Within-wafer Variance Model

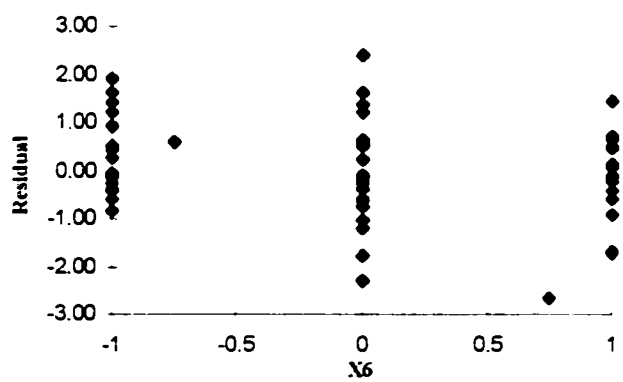

Figure 3.37: Residuals versus X6 for Within-wafer Variance Model

The next three plots, meant to uncover autocorrelation and time trends, show that there is no significant correlation between the residuals and time. It is also interesting to note that the phenomenon show in Figures 3.12 and 3.25 is not manifested in Figure 3.38. Lag-1 and lag-2 serial plots shown in Figures 3.34 and 3.35 show no sign of significant serial correlation.

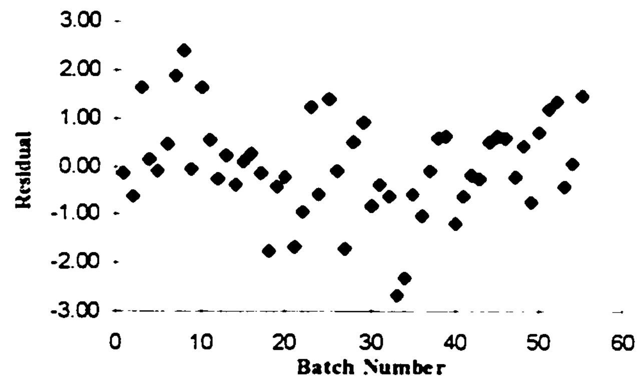

Figure 3.38: Serial Plot of Residuals from Within-wafer Variance Model

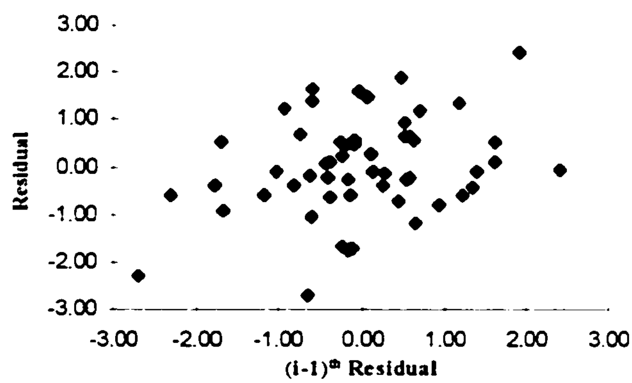

Figure 3.39: Lag 1 Plot of Residuals from Within-wafer Variance Model

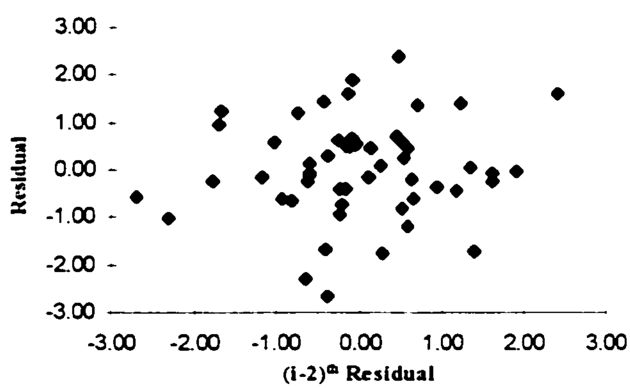

Figure 3.40: Lag 2 Plot of Residuals from Within-wafer Variance Model

3.4.4 Cross-Load Variance (CLV)

$$\begin{aligned} CLV' = (55.39 + 36.00X1 - 10.16X2 - 20.01X3 \\ -30.42X1X2 - 13.42X1X3 - 11.39X1X5 \\ +15.38X2X3 + 5.91X3X5 + 7.75X4X5 + 37.65X1^2)^2 \end{aligned} \quad (3.\ 18)$$

No significant lack of fit (0.06)
$R^2 = 0.93$
The residuals showed no sign of trends.

As expected, the temperature ramps, X2 and X3, have a significant effect on the cross-load variance. The variable that has the largest effect, however, is the centre temperature, X1. It is present on its own, in quadratic form and in combination with other effects. This agrees with the literature since the depletion rate or rate of reaction depends greatly upon temperature (Kamins, 1988). At higher temperatures, the reactant depletes very quickly moving outwards from the inlet to the reactor leaving a lower concentration of reactant towards the outlet. This causes the wafers at the front end of the reactor to be thicker than those at the back end. Also, at higher temperatures, a steeper temperature ramp is required than at lower temperatures in order to keep the thickness profile along the reactor flat. This is why the interaction terms between X1 and X2, and X1 and X3 figure prominently in the model. Also notice that the interaction terms X1X2 and X1X3 are both negative meaning that cross-load variance is reduced when X1 = X2 = X3.

Silane flowrate, X5, also influences the cross-load variance but to a lesser degree than the temperature terms. According to Kamins (1988), cross-load variance decreases as silane flowrate increases. This occurs because as silane flow increases, roughly the same amount of reactant is used at the upstream end of the reactor. However, the *fraction* of gas consumed is less; therefore there is more silane available to travel to the pump end of the reactor allowing for a more uniform thickness profile. It is important to note that in the example from Kamins (1988), a flat temperature profile was used and no information was available concerning interactions between temperature ramps and silane flowrate.

According to Equation 3.18, when X1, centre temperature, is high X5, silane flowrate, should also be high so as to reduce cross-load variance. Also, cross-load variance is reduced when both X1 and X5 are low. This result agrees with Kamins (1988), since at high temperatures silane will react quickly upon entering the reactor. This necessitates a larger flowrate so that there will be sufficient silane available for reaction at the pump end of the reactor. At low temperatures, silane reacts slowly, allowing for the concentration of reactant at the pump end of the reactor to be higher than it would be at higher temperatures. As a result, a higher silane flowrate is not required.

X5 flowrate also has a combined effect with X3, the back-end temperature ramp. When X3 is high, X5 should be small in order to reduce the cross-load variance. This is because the increase in temperature ramp compensates for the depletion of silane; therefore additional silane would serve to over-compensate for the depletion effect. When X3 is small, a large X5 is needed in order to compensate for the depletion effect.

When the results were first analyzed, an outlier was detected at batch number 5. This was flagged when the studentized (normalized) residual for batch #5 was greater than 3.0. Examination of the tube plot for the reactor conditions during the batch showed no abnormalities. The recipe for this batch was also found to be correct. Thus, it was decided to repeat the run twice to ascertain if the phenomenon was part of the true behaviour of the system. Both batches were very different from the original reading. The model, fitted with the replicated batches, showed no lack of fit and no outliers. Accordingly, the original batch was deemed an outlier and was discarded.

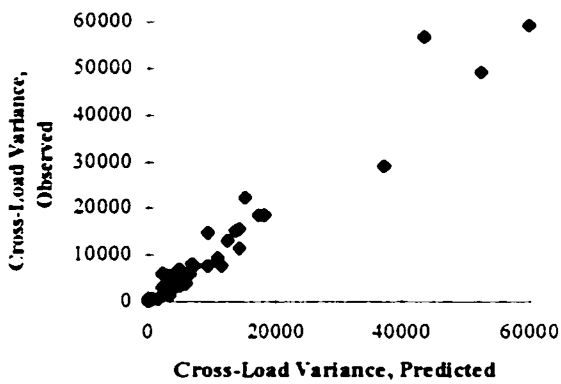

Figure 3.41: Observed versus Predicted for Cross-Load Variance Model

The cross-load variance model results compared well with the experimental data. However, there are some discrepancies in cross-load variance corresponding to batches 16, 17 and 21. In each of these three cases, the cross-load variance is much larger than would what would be acceptable for manufacturing integrated circuits. This indicates that the model is not able to adequately predict cross-load variance when the reactor conditions are such that the cross-load variance is large. Since the reactor would not normally operate at conditions with yeilded such large cross-load variances these descrepancies do not merit discarding the model.

The histogram and normal probability plot of the residuals for the cross-load variance model are given in Figures 3.36 and 3.37. Both these plots indicate that the residuals are approximately normally distributed.

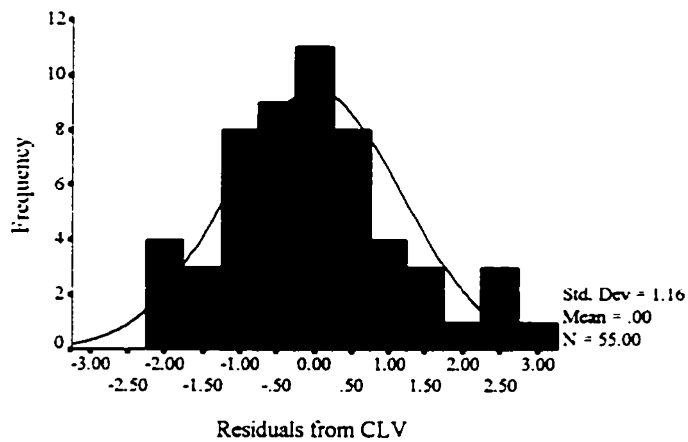

Figure 3.42: Histogram of Residuals for Cross-Load Variance Model

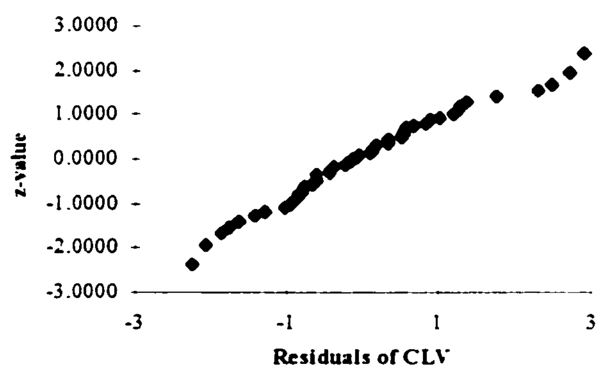

Figure 3.43: Normal Probability Plot of Residuals from Cross-Load Variance Model

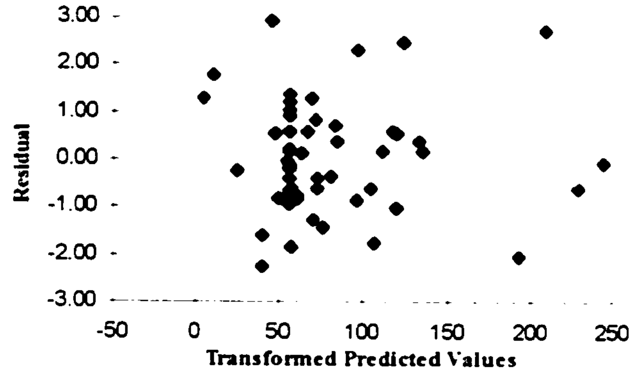

Figure 3.44: Residuals vs. Predicted Values for Cross-Load Variance Model

Figure 3.44, where the residuals versus fitted values are plotted, shows that the variance of the residuals is approximately constant over the range of fitted values.

The following six figures are plots of the residuals from the cross-load variance model versus the model parameters, X1, X2, X3, X4, X5 and X6. These plots indicate that there are no significant trends between the residuals and the factor levels.

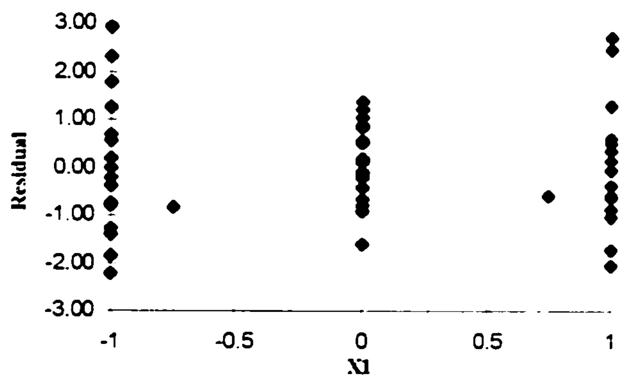

Figure 3.45: Residuals versus X1 for Cross-Load Variance Model

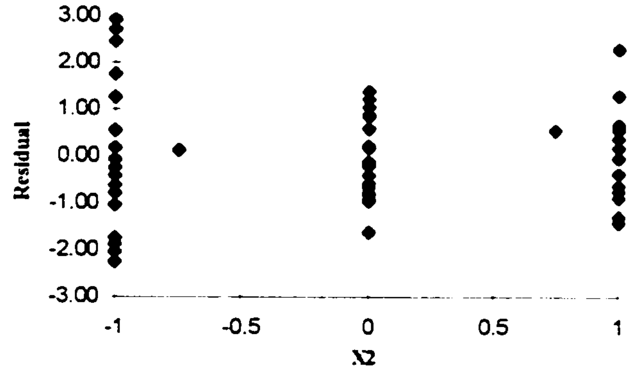

Figure 3.46: Residuals versus X2 for Cross-Load Variance Model

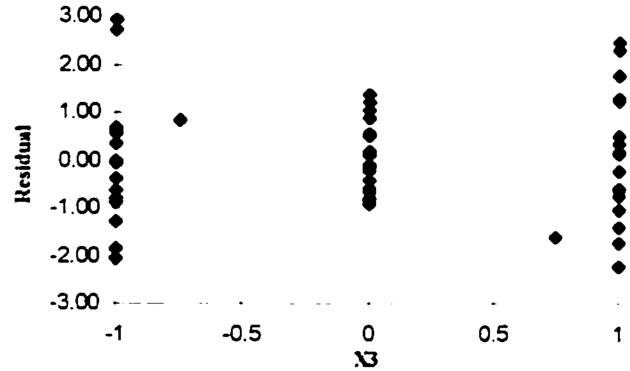

Figure 3.47: Residuals versus X3 for Cross-Load Variance Model

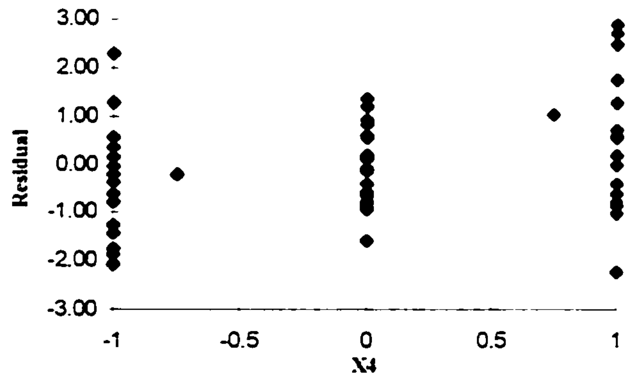

Figure 3.48: Residuals versus X4 for Cross-Load Variance Model

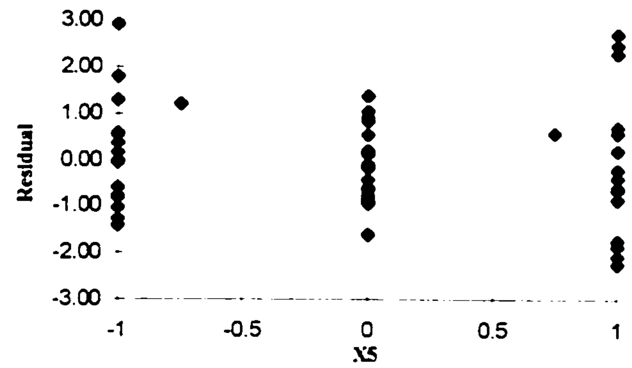

Figure 3.49: Residuals versus X5 for Cross-Load Variance Model

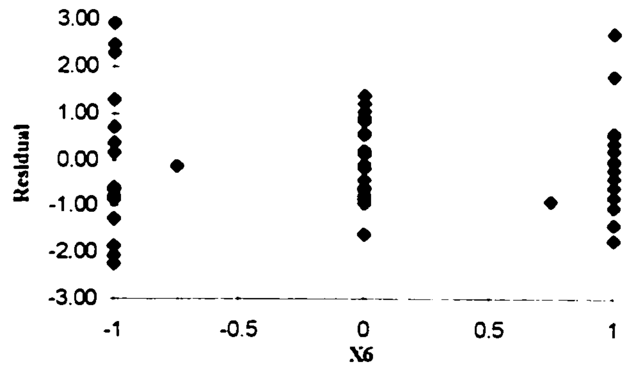

Figure 3.50: Residuals versus X6 for Cross-Load Variance Model

The next figures seek to uncover correlation in the residuals with respect to time. Figure 3.44 is a serial plot of the residuals, and this plot shows no significant time trends. Similarly, lag-1 and lag-2 plots, given in Figures 3.45 and 3.46, show no significant serial correlation at either lag-1 or lag-2.

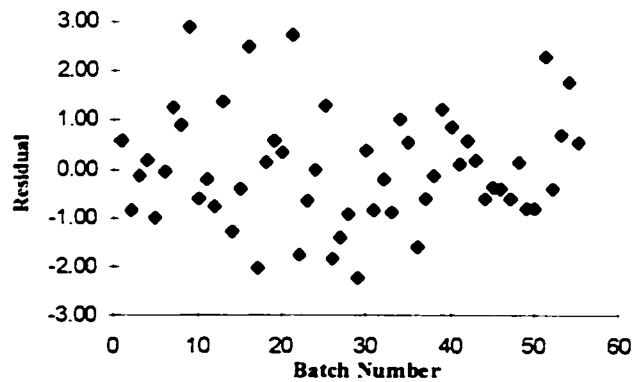

Figure 3.51: Serial Plot of Residuals from Cross-Load Variance Model

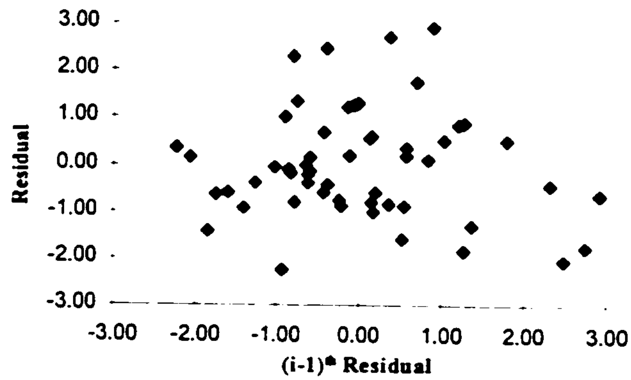

Figure 3.52: Lag 1 Plot of Residuals from Cross-Load Variance Model

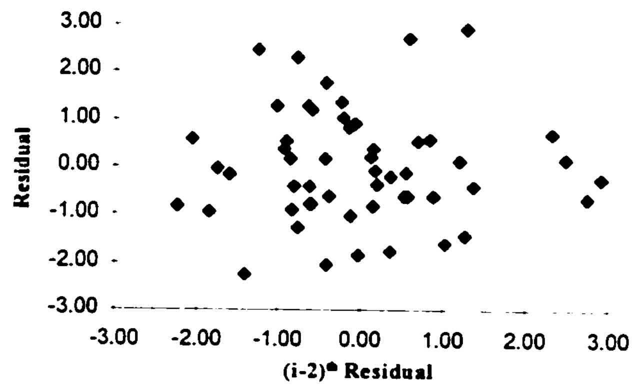

Figure 3.53: Lag 2 Plot of Residuals from Cross-Load Variance Model

3.5 Conclusions

It was found that a central composite design provided information that helped provide a better understanding of how operating variables affect the process. Specifically, the centre temperature (X1), which dictates the temperature level in the reactor, has a strong effect on the overall batch mean thickness, the overall deposition rate, the overall within-wafer variance and the cross-load variance.

It was also discovered that mean thickness and mean deposition rate are closely connected to the method of calculating deposition rate. Thus, an explanation of the effects of the process operating variables on the thickness and deposition rate models is the same. The only exception is X6, deposition time. Deposition time has a direct effect on film thickness but no effect on deposition rate. Next to X1, X5, silane flowrate has the largest effect on thickness and deposition rate. Both the thickness and deposition rate models are independent of the temperature ramps X2 and X3.

Obtaining a useful model for within-wafer variance proved to be difficult since the R^2 value (R^2=0.33) was quite low. This is an indication that there are factors affecting within-wafer variance which were not studied in the experiment. LPCVD reactors are operated in a reaction-limited regime in order to obtain deposited films of uniform thickness across a wafer (low within-wafer variance). Further improvements in within-wafer variance are unlikely. This is supported by the modeling results. Only 33% of the variation in the data is explained by the model, indicating that there is little that the model parameters can do to reduce within-wafer variance.

Cross-load variance is highly dependent on the three process operating variables associated with temperature (X1, X2 and X3). This demonstrates that proper manipulation of these factors will be key in reducing the cross-load variance. It was also learned that deposition time, X6, has no effect on cross-load variance.

These results confirm in a concrete manner the experience of engineers working on this process. In the past, maintaining the target thickness while achieving a flat thickness profile along the reactor was difficult. The four models described in this chapter have the potential to alleviate this problem. Conditions that achieve the target thickness at a reasonable deposition rate can be found using the overall batch mean thickness and deposition rate models. Optimizing these two models will set the centre temperature, X1, pressure, X4, silane flowrate, X5, and deposition time, X6. Reducing the cross-load variance can be achieved by adjusting the temperature ramp terms (X2 and X3) in the cross-load variance model. The results of this process are outlined in Chapter Four: Optimization.

Chapter Four

Optimization

In this chapter, the techniques involved in the determination of optimal operating conditions are described. The optimal operating condition is one in which: (i) the target thickness of 3500Å is achieved, (ii) the deposition rate is maximized, and (iii) the cross-load and within-wafer variances are minimized. It was hoped that improvements could be made over the operating conditions from the historical data set which were:

thickness = 3527.80 Å

deposition rate = 88.3 Å/min

cross-load standard deviation = 40.88 Å

within-wafer standard deviation = 41.38 Å

4.1 Background: Tools Used in Optimization

The optimization of the accepted models was conducted in two ways. First, the individual model was optimized using the constrained optimization routine, *constr*, in the mathematical programming package, MATLAB. Second, the four main models (Overall Thickness, Overall Deposition Rate, Overall Within-Wafer Variance and Cross-Load Variance) were simultaneously optimized using the multi-objective optimization routine, *attgoal*, also in MATLAB. The optimization was conducted in two different ways for the sake of comparison.

Confidence intervals were determined for the value of the response at the optimum. This is described in detail in Appendix VIII. In order to obtain a visual image of the surface, contour plots were used.

4.1.1 Constrained Optimization of Individual Models

The minimum or maximum of the individual models was determined using a constrained optimization technique. The optimization was constrained to the limits of the operating region used in the experimental design (-1,1) for all X1, X2, X3, X4, X5 and X6. MATLAB's constrained optimization routine, *constr*, uses a Sequential Quadratic Programming method. A complete description of the algorithm can be found in the MATLAB *Optimization Toolbox User's Guide.*

4.1.2 Multi-Objective Optimization

Optimization of the overall models was achieved using the goal attainment routine in MATLAB, *attgoal*. This function allows for multi-objective constrained optimization. Thus, a set of objective functions can be minimized (or maximized) simultaneously subject to constraints on the input variables. This program also allows constraints to be placed on the objective functions. In the case of the thickness model, it was desired that the optimum be found such that the value of the thickness model was equal to the target value of 3500Å. *attgoal* has provisions for such a case. A set of GOALS was set for each function. The user then specifies whether the GOAL should be exceeded (maximization problem) or attained exactly (equality problem). As for *constr, attgoal* uses a modified Sequential Quadratic Programming Method to solve the optimization problem. For further details see the *Optimization Toolbox User's Guide* for MATLAB.

4.2 Optimization Results

The accepted models for batch mean thickness, batch mean deposition rate, within-wafer variance and cross-load variance were individually and simultaneously optimized. The results were compared in order to obtain a better understanding of the optimal operating conditions. The results from the simultaneous optimization of the overall models were used to determine the predictions from the individual wafer models. Comparisons were made between the predicted values and the values obtained by operating the reactor at the optimal operating conditions. This provided a measure of the accuracy of the prediction. Finally, the overall models were compared to the individual wafer models in order to determine if the four overall models adequately described the reactor system.

4.2.1 Overall Models: Results and Discussion

The following four models were individually and simultaneously optimized using MATLAB's constrained optimization and goal attainment routines:

$$TH = 3581.67 + 414.68X1 + 95.09X4 + 155.65X5 + 196.27X6 + 33.90X1X5 + 28.05X4X6 \quad (4.1)$$

$$DR = 89.53 + 10.37X1 + 2.35X4 + 3.89X5 + 0.82X1X5 - 0.63X2X4 \quad (4.2)$$

$$WWS = (0.0464 - 0.0058X1 + 0.0034X2X3 + 0.0034X1X6)^{-1} \quad (4.3)$$

$$CLS = 55.39 + 36.00X1 - 10.16X2 - 20.01X3 - 30.42X1X2 - 13.42X1X3 - 11.39X1X5 + 15.38X2X3 + 5.91X3X5 + 7.75X4X5 + 37.65X1^2 \quad (4.4)$$

Individual optimization results of the four overall models are listed in Table 4.1. The optimum for Equation (4.1) is the target value of 3500 Å, which does not lead to a unique solution but rather a set of solutions. The optimum batch mean thickness is given by Equation (4.5).

$$-81.67 = 414.68X1 + 95.09X4 + 155.65X5 + 196.27X6 + 33.90X1X5 + 28.05X4X5 \quad (4.5)$$

Table 4. 1: Individual Optimization Results of Equations (4.1) to (4.4)

Response Variable	Desired Action	Value of Operating Variables X1	X2	X3	X4	X5	X6	Response Value
DR	Maximize	+1	-1	n/a	+1	+1	n/a	108 Å/min
WWS	Minimize	-1	+1	+1	n/a	n/a	-1	16.9 Å
		-1	-1	-1	n/a	n/a	-1	16.9 Å
CLS	Minimize	-0.86	-1	+1	+1	-1	n/a	-11.5 Å

n/a = term not applicable to model

The literature (Wolf, 1990; Kamins, 1988; Sherman, 1987) reports that the deposition rate increases as a function of increased centre temperature, pressure and silane flowrate; thus the results shown in Table 4.1 for deposition rate were expected.

For optimization of the within-wafer variance model, again, it was learned from the literature (Wolf, 1990; Kamins, 1988; Sherman, 1987) that within-wafer variance decreases as reactor temperature decreases. Thus the result X1=-1 agrees with the literature. The effects of temperature ramps or deposition time on within-wafer variance were not discussed in the literature, and so there was no expectation for the optimal settings of X2, X3 and X6.

There has been much discussion in the literature on the factors affecting the cross-load variance (Wolf, 1990; Kamins, 1988; Sherman, 1987). According to Kamins (1988), better cross-load thickness uniformity can be achieved at low temperatures, high pressure and high silane flowrate. According to Wolf (1990), a larger back-end temperature ramp is necessary to offset the effects of reactant depletion. The results of the optimization compare very well to what was reported in the literature except for the optimal value of silane flowrate (X5=-1). However, the reports in the literature discuss the effects of temperature, pressure and silane flowrate individually with little mention of interaction effects. Also, literature discussions of the effects of the operating variables on the thickness of the deposited film assume a flat or constant temperature profile along the reactor. Because of these factors, it is difficult to make a fair comparison between the literature and the findings in this study.

The *GOAL*'s set for the simultaneous optimization of Equations (4.1) to (4.4) were: TH = 3500 Å; DR > 90 Å/min; WWS < 40 Å and CLS < 40 Å. The goals for the thickness and deposition rate models were set according to conditions required for production. The goals for the within-wafer and cross-load variance models were set to so that the optimization would look for solutions that would yield a reduction in within-wafer and cross-load variance over the historic values. Simultaneous optimization of Equations (4.1) to (4.4) yielded an optimum at the following conditions:

X1 = -0.24	X4 = 1.00
X2 = -1.00	X5 = 1.00
X3 = 1.00	X6 = -1.00

In terms of the original variables,

$T_c = 619°C$	$P = 239$ mTorr
$R_1 = 3°C$	$F_{SiH_4} = 223\ cm^3/min$
$R_2 = 7°C$	$t_{dep} = 38$ min

Operating the reactor under these conditions should yield the following results based on model predictions:

Mean Batch Thickness	3500 Å
Mean Batch Deposition Rate	93.1 Å/min
Within-Wafer Standard Deviation	20.6 Å
Cross-Load Standard Deviation	36.1 Å

The optimal centre temperature is close to the historical level of centre temperature (620°C). Examination of the models shows X1, out of all the process operating variables, has the largest effect on the responses. Thus, it is encouraging that the historic operating level of X1 is very close to the optimal operating conditions.

Deviations from the standard operating conditions were found in pressure, silane flow rate and deposition time. The optimal values of X4, X5 and X6 were found at the design boundary 1, 1, -1 respectively, indicating that the design region may be too narrow. However, an earlier experiment with a broader design region found that operation outside of the design region specified in the Phase II experiment led to results which were far from the target region of operation. For this reason, operation outside the design region established in Phase II was not recommended.

Two test runs were conducted at the optimal conditions. Table 4.2 below lists the model predictions along with a 95% confidence interval for the prediction and the results of the two runs. For comparison, the historical conditions are also reported in Table 4.2. Sample calculations for the 95% confidence interval are given in Appendix VII.

Table 4.2: Predictions and Test Results for Overall Models

Response	Prediction	95% Confidence Interval	Test #1	Test #2	Historical Conditions
Thickness - Mean	3500	(3346, 3654)	3514.40	3544.05	3527.80
Deposition Rate	93.10	(89.50, 96.70)	92.48	93.26	88.30
Cross-Load Std. Dev.	36.0	(4.22, 67.78)	24.20	41.41	40.88
Within-Wafer Std. Dev.	20.6	(15.84, 36.82)	27.93	22.83	41.38

At the optimal operating conditions the predicted batch mean thickness is equal to the target thickness, 3500 Å. The 95% confidence interval is quite broad indicating the inherent noisiness of the data. However, it is encouraging the two test batches performed at the optimum conditions fall not only within the 95% confidence interval but also quite close to the target.

The predicted batch mean deposition rate is 93.1 at the optimum. Both test batches fall within the 95% confidence interval for this prediction; however, the deposition rate for the historical conditions does not. Thus, a 5% increase in deposition rate can be expected at the optimal operating conditions.

The predicted cross-load variance is 36 Å at the optimum. This result was verified by two test runs, the results of which fall within a 95% confidence interval for the predicted cross-load variance. Because the historical conditions also fall within the 95% confidence interval, there is no evidence that a significant improvement in cross-load standard deviation can be expected by operating at the optimal conditions. The two factors appearing repeatedly in the cross-load standard deviation model are the temperature ramp terms, X2 and X3. At the optimum, these values are -1 and +1, respectively, which represents a design region boundary. Perhaps the reason for the lack of improvement over the historical conditions is that the operating range for X2 and X3 is too narrow.

The predicted within-wafer standard deviation is 20.6 at the optimal operating conditions. Two test runs performed at the optimum fall within the 95% confidence interval which helps to validate the model. Since the historical conditions do not fall within the 95% confidence interval, we can conclude that a significant reduction (50%) in within-wafer standard deviation can be expected at the optimum.

Comparing the results of the individual optimization of model, equations (4.1) to (4.4), to the simultaneous optimization of the models shows some interesting compromises. Both the within-wafer and cross-load standard deviation models were minimized when X1 was small (X1 equal to -1 and -0.86, respectively). However, deposition rate is maximized when X1 = +1. When the models were simultaneously optimized, the 'best' solution was found when X1 was closer to zero (X1 = -0.24).

The optimal settings for X2 and X3 were dictated by the cross-load standard deviation model, since these terms figure most prominently in this model. Although minimal within-wafer standard deviation could be achieved when X2 = X3, it will be shown in the next section that for the optimal values of X1 and X6 all combinations of X2 and X3, including (X2, X3) = (-1,+1), offered improved within-wafer standard deviations.

For both the deposition rate and cross-load variance models, the optimal level of X4 is +1. As expected, X4 = +1, was the optimal level of X4 found in the simultaneous optimization of the overall models.

The optimal level of X5, found by the simultaneous optimization of the overall models, was +1. This result agrees with the level for X5 which maximization of Equation (4.2) but disagrees with the value of X5 which minimizes Equation (4.4). When the optimization was conducted, more weight was placed upon maximizing deposition rate rather than minimizing cross-load variance based on the needs of the manufacturer. For production reasons, the engineers at Nortel require a poly-Si deposition rate of 90 Å/min or greater from the LPCVD reactor. If the emphasis on maximizing deposition rate were relaxed, a reduction in cross-load variance would be expected.

Table 4.3: Sensitivity Analysis

[illegible]	[illegible]	[illegible]	[illegible]	[illegible]	[illegible]
1.0	-1.00	93.12	36.08	3500.00	22.13
0.8	-0.88	92.51	32.81	3500.00	22.18
0.6	-0.75	91.90	29.54	3500.00	22.24
0.4	-0.61	91.28	26.26	3500.00	22.29
0.2	-0.48	90.67	22.99	3500.00	22.34
0.0	-0.35	90.05	19.72	3500.00	22.39
-0.2	-0.22	89.44	16.45	3500.00	22.45
-0.4	-0.09	88.83	13.18	3500.00	22.50
-0.6	0.04	88.21	9.91	3500.00	22.55
-0.8	0.18	87.60	6.64	3500.00	22.61
-1.0	0.31	86.98	3.36	3500.00	22.66

X1=-0.24; X2=-1; X3=+1; X4=+1

The results of a sensitivity analysis on response variables at X1, X2, X3, and X4 set to the optimal levels are presented in Table 4.3. In order to continue to target the thickness at the desired level (3500 Å), deposition time had to be altered. This was accomplished by simply solving Equation (4.5) for X6 at given levels of X1, X2, X3, and X4. Table 4.3 shows that if deposition rate were allowed to drop to its historic value (88 Å/min), then cross-load variance can be expected to decrease to 9.9 Å. This reduction in cross-load standard deviation could be achieved while continuing to target the batch mean thickness, and without substantially increasing within-wafer standard deviation.

Deposition time, X6, appears in the within-wafer standard deviation model (Equation (4.4)), which was minimized, and in the thickness target constraint (Equation (4.5)). The level of X6 determined in the simultaneous optimization routine (X6 = -1) agrees perfectly with the level of X6 found to minimize within-wafer standard deviation.

4.2.2 Visual Representation of the Optimum

Contour plots were used to obtain a clearer picture of the region about the optimum. The total number of contour plots required to examine the effects of all the factors on all the response variables is 25. In the interest of simplification, effect of the X2 and X3 on cross load and within wafer variance were examined, while holding the other factors constant at their optimal values. To further simplify, the X2X4 term was removed from the deposition rate model. This term is significant at the 95% level but not at the 99% level. Thus, it was concluded that little information would be lost by removing the X2X4 term. Contour plots with respect to X2 and X3 were created using the cross-load and within-wafer standard deviation models with the values of X1, X4, X5 and X6 set to the optimal settings. It was decided to concentrate on the X2 and X3 factors since these are the factors that engineers tend to adjust to compensate for poor results in cross-load and within-wafer variance. Although the recommendation had been made not to adjust the process input variables from batch to batch, engineers may be required to make adjustments to the temperature ramps after a preventative maintenance shut-down in order to qualify the reactor for production. Contour plots with respect to X2 and X3 were neither created for the thickness model, nor created for the deposition rate model because the temperature ramp terms were not present in these models. These results are shown in Figures 4.1 and 4.2.

According to the cross-load standard deviation model, cross-load standard deviation is minimized at X2 = -1, X3 = +1. This agrees well with literature findings that the effects of reactant depletion are greater towards the pump zone of the reactor; thereby necessitating a higher pump zone temperature (Wolf, 1990).

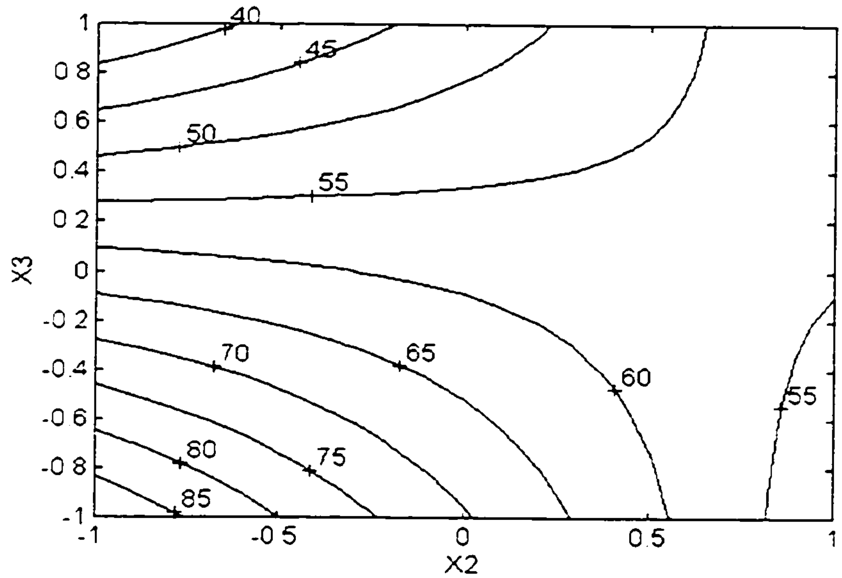

Figure 4. 1: Contour Plot of X2 vs. X3 for Cross-Load Standard Deviation

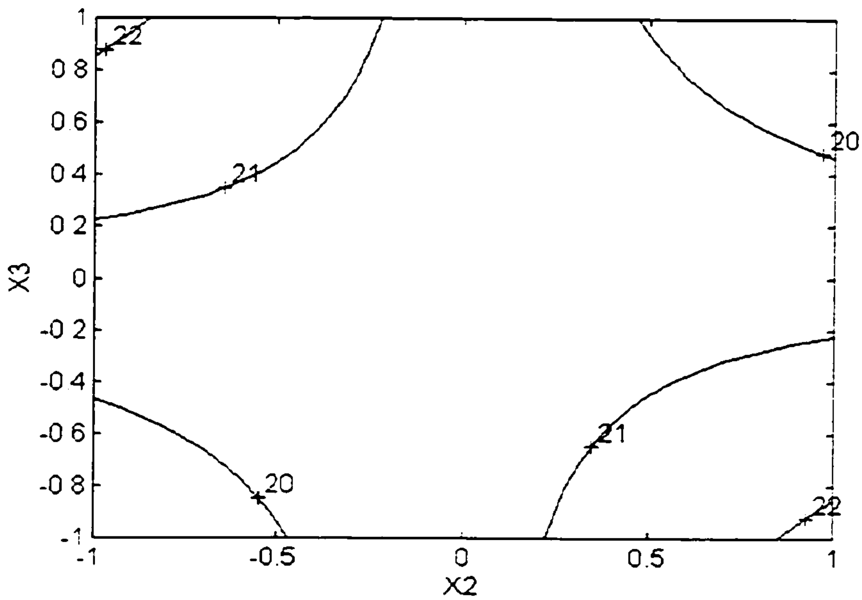

Figure 4. 2: Contour Plot of X2 versus X3 for Within-Wafer Standard Deviation Model

The within-wafer variance contour plot appears to be the centre of a very large saddle shaped surface with minimum within-wafer variance occurring at X2 = -1, X3 = -1 and X2 = +1, X3 = +1. However, for all X2 and X3 in the design space, the within-wafer variance is lower than the currently obtained within-wafer variance. This indicates that the within-wafer variance will be reduced at any combination of X2 and X3 and the optimal values of X1, X4, X5, X6.

4.2.3 Individual Wafer Models: Results and Discussion

In the following section the model predictions for thickness, deposition rate, cross-load variance and within-wafer variance were found for each of the four wafer positions. Details of the development of these models are found in Appendix IV. The operating conditions used were those found in the simultaneous optimization of the four overall models.

Thickness Models

Listed below are models that describe the film thickness in each of the four wafer positions. The optimum is not a minimum or maximum in these cases as the goal was to target the thickness of 3500Å. Thus the optimum is defined by an equation.

$$\begin{aligned} LTH = (&0.000278 - 0.000038X1 + 0.000005X2 + 0.000002X3 \\ &-0.000007X4 - 0.00001X5 - 0.000015X6 \\ &+0.000003X1X6 + 0.000007X4^2)^{-1} \end{aligned} \tag{4.6}$$

$$\begin{aligned} C1TH = &3631.72 + 442.72X1 - 28.66X3 + 96.58X4 + 151.49X5 \\ &+194.62X6 + 36.71X1X5 - 26.87X2X4 \\ &+26.47X4X6 \end{aligned} \tag{4.7}$$

$$\begin{aligned} C2TH = &3593.11 + 389.63X1 + 29.35X2 + 92.91X4 \\ &+164.20X5 + 196.39X6 + 32.98X1X5 + 28.89X4X6 \end{aligned} \tag{4.8}$$

$$\begin{aligned} PTH = &3500.66 + 336.47X1 + 39.19X2 + 36.56X3 + 87.32X4 \\ &+174.27X5 + 198.09X6 + 30.90X1X5 + 29.58X4X6 \end{aligned} \tag{4.9}$$

The model predictions for the individual wafer thickness models are listed in Table 4.4 along with the results of test runs carried out at the optimal conditions: X1 = -.24, X2 = -1, X3 = +1, X4 = +1, X5 = +1 and, X6 = -1.

Table 4. 4: Predictions and Test Run Results for Thickness Models

Response	Prediction	95 % Confidence Interval	Test #1	Test #2
Load Thickness	3461.6	(3342.4, 3589.6)	3510.2	3520.4
C1 Thickness	3541.7	(3375.7, 3707.7)	3476.4	3506.4
C2 Thickness	3492.5	(3322.3, 3662.7)	3504.6	3546.4
Pump Thickness	3440.0	(3270.2, 3609.8)	3566.4	3603.0

The test results fall within the 95% confidence interval for future measured values of thickness. The confidence intervals are quite broad as a result of the large pure error variances. It is encouraging however, to note that the test batches fall reasonably close to the target value of 3500 Å. The mean value of the predictions using the predictions from equations (4.6) to (4.9) is 3484.0 which is not significantly different from the prediction of 3500 ± 154 Å obtained from equation (4.1).

Deposition Rate Models

The following models describe the deposition rate of poly-Si at the four wafer positions: Load, C1, C2, Pump.

$$LDR = 90.02 + 12.26X1 - 1.62X2 - 0.73X3 + 2.57X4 + 3.30X5 + 0.85X1X5 - 0.68X2X4 + 0.60X4X5 \tag{4.10}$$

$$C1DR = 90.74 + 11.09X1 - 0.72X3 + 2.40X4 + 3.76X5 + 0.87X1X5 - 0.69X2X4 \tag{4.11}$$

$$C2DR = 89.81 + 9.76X1 + 0.73X2 + 2.31X4 + 4.08X5 + 0.77X1X5 \tag{4.12}$$

$$PDR = 88.33 + 8.44X1 + 0.96X2 + 0.92X3 + 2.19X4 + 4.33X5 + 0.71X1X5 - 1.20X5^2 \tag{4.13}$$

Table 4. 5: Predictions and Test Run Results for Deposition Rate Models

Responses	Predictions	95% Confidence Interval	Test #1	Test #2
Load Deposition Rate	91.32	(87.74, 94.90)	92.37	92.64
C1 Deposition Rate	93.99	(90.00, 97.98)	91.48	92.27
C2 Deposition Rate	92.88	(88.96, 96.80)	92.23	93.33
Pump Deposition Rate	91.46	(87.25, 95.67)	93.85	94.82

Both test runs fell within the 95% confidence interval of the predicted responses. Averaging the predictions for the four zones should yield the batch-mean deposition rate. Using the four predictions in Table 4.5 the batch-mean deposition rate is predicted to be 92.4. The batch-mean deposition rate was predicted to be 93.1 ±3.6 using Equation (4.2). Since the 95% confidence interval for the prediction using Equation (4.2) includes the prediction resulting from averaging the predictions in Table 4.5, there is no significant difference between the two methods of predicting the batch-mean deposition rate.

Within-Wafer Variance Models

The following models represent the within-wafer variance of the individual wafers.

$$LWWV = \exp(4.67 + 0.39X1 - 0.52X5X6 + 1.86X4^2 - 1.87X5^2) \quad (4.14)$$

$$C1WWV = (0.046 - 0.0076X1 + 0.0040X1X6 + 0.0038X2X3 - 0.020X4^2 + 0.022X5^2)^{-1} \quad (4.15)$$

$$C2WWV = (0.035 - 0.0046X1 + 0.0026X2X3)^{-1} \quad (4.16)$$

$$PWWV = (0.0460 - 0.0053X1 + 0.0036X1X6 + 0.0050X2X3 + 0.0045X2X5 - 0.0040X3X6)^{-1} \quad (4.17)$$

The model predictions for the individual wafer variance models are listed in Table 4.6 along with the test run results.

Table 4. 6: Predictions and Test Run Results for Within-Wafer Variance Models

Responses	Predictions	95% Confidence Interval	Test #1	Test #2
Load Variance	228.32	(33.6, 1549.7)	457.53	332.33
C1 Variance	520.89	(248.8, 1702.8)	526.24	212.28
C2 Variance	880.96	(473.4, 2179.3)	1141.09	953.57
Pump Variance	549.38	(253.7, 1967.9)	994.77	586.61

The test run results fall within the confidence intervals of the predicted responses. The 95% confidence intervals are quite broad due to the large pure error variances. Pooling the within-wafer variances predicted using Equations (4.9) to (4.12) yields an overall within-wafer standard deviation of 23.3. The predicted within-wafer variance using Equation (4.3) is 20.6, the 95% confidence interval is (15.84, 36.82), which includes 23.3.

4.3 Conclusions

The optimal operating conditions for the LPCVD reactor were found using the four overall models developed in Chapter Three along with optimization routines in MATLAB. In terms of the untransformed variables, these conditions were: T_c = 619°C, R_1 = 3°C, R_2 = 7°C, P = 239 mTorr, F_{SiH_4} = 223 cm^3/min and t_{dep} = 38 min. The predicted values of the response variables were: batch-mean thickness = 3500 Å, batch-mean deposition rate = 93.1 Å/min, within-wafer standard deviation = 20.6, and cross-load standard deviation = 36.1.

It was expected that the optimal operating conditions would be near the standard operating condition since the reactor had been in operation for quite some time and some experimentation with reactor conditions had been done in the past. The standard operating conditions were: T_c = 620°C, R_1 varied between 1°C and 5°C, R_2 varied between 6°C and 2°C, P = 220 mTorr, F_{SiH_4} = 200 cm^3/min and t_{dep} varied between 38.66 min and 40.66 min. The standard centre temperature and front-end temperature ramp compared well with optimal centre temperature and front-end ramp, however, the optimal back-end temperature ramp, pressure and silane flowrate are significantly larger than the standard operating conditions, while the optimal deposition time is shorter than the standard deposition time. These results show that there was room for improvement in reactor performance over the reactor performance at the standard operating conditions.

Test batches carried out at the optimal operating conditions fell within 95% confidence interval for the predicted optimal values of the response variables for both overall and individual wafer models. Moreover, predictions of overall values using individual wafer models fell within the 95% confidence intervals for the overall models, indicating that the four overall models adequately describe the system.

Chapter Five

Monitoring and Control

In this chapter a monitoring and control scheme are proposed with the intent of reducing batch to batch variability over time. The procedure discussed here was not tested as it is partially dependent on the models built in Chapter Three. Due to fundamental changes in the reactor, these models may no longer be characteristic of the process. However, the proposed procedure could be applied to the system after reformulating the models to compensate for the changes made to the reactor. This procedure was also meant as a general guideline for the monitoring and control of LPCVD reactors.

5.1 Monitoring Scheme

A process that is in a state of statistical process control (SPC) displays only stable, inherent, random variations in its output. This type of variation is referred to as "common cause" variation and is considered a normal part of the process operation. The purpose of a monitoring scheme is to detect significant detrimental change in the process or to identify changes that lead to process improvement. Typical monitoring schemes consist of one or more on-line control charts.

Before an appropriate monitoring scheme can be chosen, it is necessary to determine if the underlying assumptions of SPC charts are valid with respect to the process in question. The assumptions are that the data are independently and identically distributed (iid) as a normal distribution with mean μ and variance σ^2. This is commonly expressed as iid $N(\mu, \sigma^2)$.

In Chapter Two, it was established that the data are iid normal. A histogram of the batch mean thickness data showed that the data are approximately normally distributed. A plot of the autocorrelations showed that the control data were not significantly autocorrelated. The control data (referred to as 'tweak-free' data in Chapter Two) consist of a set of 41 data points in which no changes to the process operating variables were made. The charts presented in this chapter are based upon this data set.

The thickness data collected from the reactor may be treated as multivariate data since each batch gives thickness measurements in twenty different locations. Each of these locations can be treated as separate Product Quality Variables (PQV). If the data are to be treated in this manner, then multivariate control can be used to monitor the process. The underlying assumption of multivariate control charts is that the data are distributed multivariate normal, $N_p(\mu, \Sigma)$, where p is the number of PQV. The symbol μ represents the vector of true but unknown mean value of each of the p variates. The symbol Σ represents a p x p matrix of variances and covariances of the p characteristics.

According to Johnson and Wichern (1992), a process that is distributed multivariate normal is defined by a vector of means or target values of the PQV and by their variance-covariance matrix of the PQV. Characteristics of a random vector $\mathbf{x}$ having a multivariate normal distribution include:

1. The marginal distributions from a multivariate normal process will be distributed normal.
2. Linear combinations of the components of $\mathbf{x}$ are normally distributed.
3. When n and n-p are greater than 25 or 30, the squared distances, d_i^2, should behave like a chi-square random variable. The squared distances d_i^2 are given by,

   $$d_i^2 = (\mathbf{x}_i - \bar{\mathbf{x}})'\mathbf{S}^{-1}(\mathbf{x}_i - \bar{\mathbf{x}}),\ i = 1, 2, \ldots, n \qquad (5.1)$$

   where $\mathbf{x}_1, \mathbf{x}_2, \ldots, \mathbf{x}_n$ are sample observations or subgroup averages, and $\bar{\mathbf{x}}$ is the sample mean of the p variates used to estimate μ. A chi-square plot of the ordered squared distances should resemble a straight line.

   The ordered squared distances for the 41 "control" batches are plotted in Figure 5.1. The number of data points, n, was 41 and p = 20. Although n is greater than 30, the data requirement for this test is not satisfied since n-p is less than 25. Figure 5.1 shows some deviations from the multivariate normal distribution, however, the deviations are not large enough to deem the process non-normal. A histogram of the batch mean thickness data (a linear combination of the marginal distributions), depicted in Figure 5.2, appears to be roughly normally distributed, and shows some deviation from a normal distribution at low batch-mean thickness values .

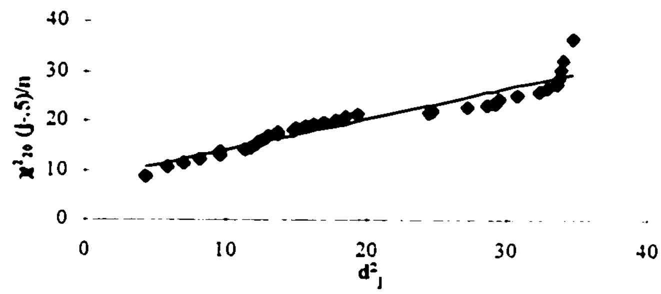

Figure 5.1: Chi-Square Plot of the Ordered Square Distances (Control Data)

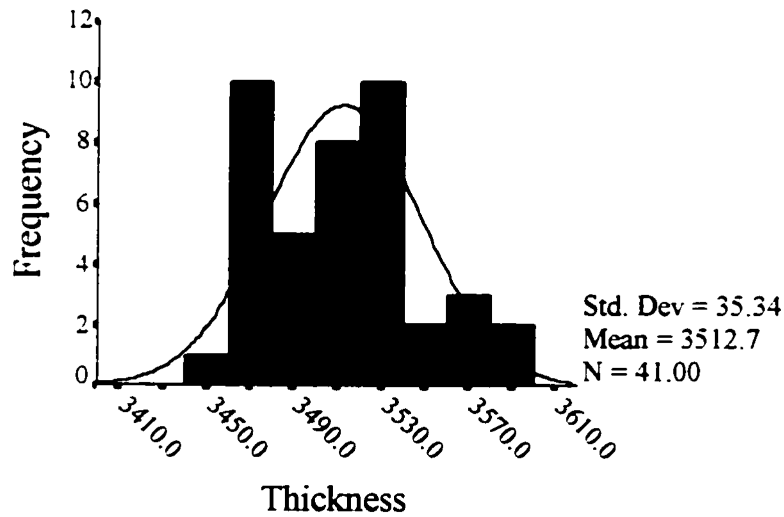

Figure 5.2: Histogram of Batch Mean Thickness Data (Control Data)

5.1.1 Within Subgroup Correlation

Because of the nature of the measurements, the thickness measurements on each wafer will be correlated. Also, there exists some correlation among thickness measurements from different wafers taken from the same batch. Tests for correlation have been proposed by Johnson and Wichern (1992). Two variables are independent if there is zero correlation between the two variables. For p variates and n data points, the correlation matrix, which is a standardized version of a variance-covariance matrix, is:

$$r_{ik} = \frac{s_{ik}}{\sqrt{s_{ii}}\sqrt{s_{kk}}} = \frac{\sum_{j=1}^{n}(x_{ij}-\bar{x}_i)(x_{kj}-\bar{x}_k)}{\sqrt{\sum_{j=1}^{n}(x_{ij}-\bar{x}_i)^2}\sqrt{\sum_{j=1}^{n}(x_{kj}-\bar{x}_k)^2}} \quad (5.2)$$

for $i = 1$ to p and $k = 1$ to p. This standardized form of the covariance matrix provides for ease of interpretation because:

1. the magnitude of r_{ik} is bounded from -1 to +1
2. r measures the strength of the correlation (r=0 represents no correlation or independence between variables i and k, $r > 0$ represents a positive relationship between i and k so that if variable i is large, then variable k will tend to be large, $r < 0$ represents a negative correlation between i and k so that if variable i is large, then variable k will tend to be small.

It should be noted that only linear associations are conveyed by r_{ik}.

The correlation matrix for the historical data set indicates that, on a per wafer basis, the thickness measurements are highly correlated. The correlation matrix for the historical data set and for the control data can be found in Appendix IX.

5.1.2 Current Monitoring Scheme

Historically, process engineers and operators had monitored reactor performance using Shewart charts with runs rules by plotting the batch mean thickness and the batch standard deviation. These charts are often referred to as X-bar and s-charts. Runs rules were introduced by the Western Electric Company to provide a more sensitive detection of upsets in the process (Western Electric, 1956). Examples of the X-bar and s-chart used to monitor the LPCVD reactor are shown in Figures 5.3 and 5.4. Details of the calculation of control limits are found in Appendix IX. The batch mean deposition rate and standard deviation were also monitored using Shewart charts.

Figures 5.3 and 5.4 indicate that the process is in a state of statistical process control since none of the data points falls outside the 3σ control limits. If runs rules are employed, the chart signals an out-of-control signal after 20 batches for violation of rule

#4: "8 consecutive points on one side of the centre-line" (Western Electric Company, 1956).

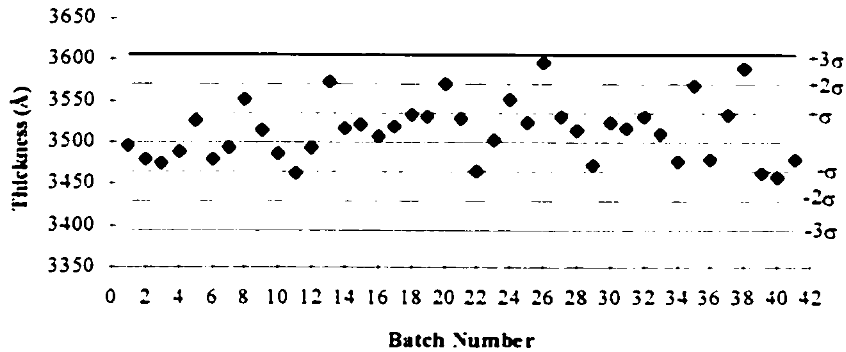

Figure 5.3: Shewart X-bar Chart for Thickness Data (Control Data)

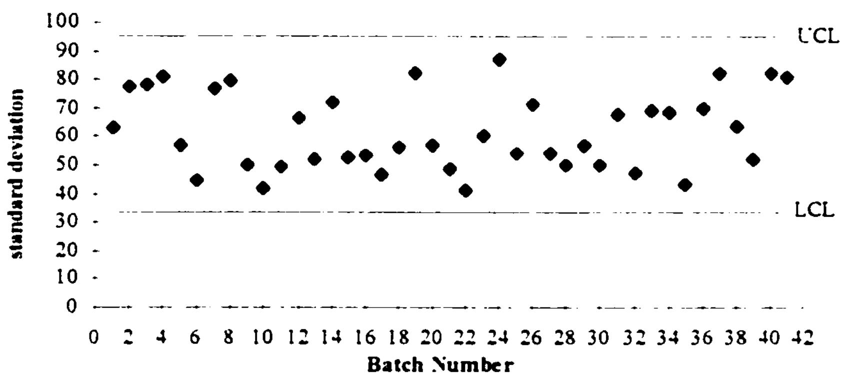

Figure 5.4: Shewart s-Chart for Thickness Data (Control Data)

The s-chart monitors the standard deviation of all the thickness measurements of a batch. Embedded in this value of standard deviation are within-wafer and cross-load standard deviations. It was felt that separate charts, shown in Figures 5.5 and 5.6, should be used to monitor within-wafer and cross-load variances since these variables are characteristic of interest, and they should therefore be monitored separately. It was also felt that greater sensitivity to shifts in the process would be achieved using two separate charts.

Figures 5.5 and 5.6 detect an out-of-control situation at batch number 37 (found by the within-wafer standard deviation chart). Investigation of Batch 37 shows a large range of thickness measurements across all four test wafers. The range of thickness measurements for C1 and C2 test wafers were particularly large indicating that these wafers may be spoiled. The s-chart failed to signal a problem with batch 37. This indicates that monitoring cross-load and within-wafer standard deviations separately provides greater sensitivity to changes in standard deviation and facilitates trouble-shooting of out-of-control signals.

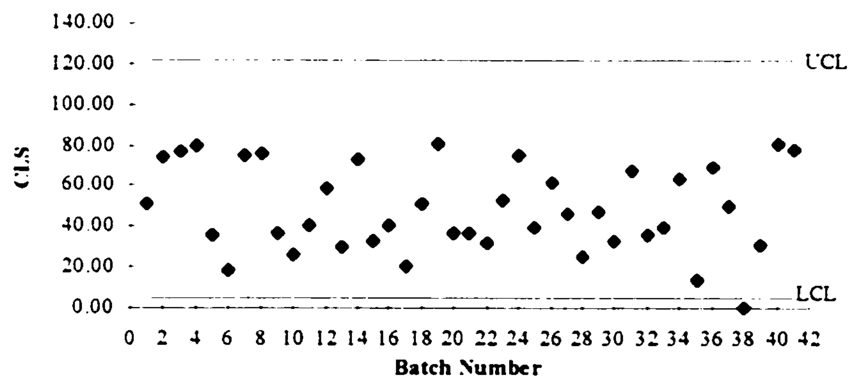

Figure 5.5: Cross-Load Standard Deviation Chart for Thickness Data (Control Data)

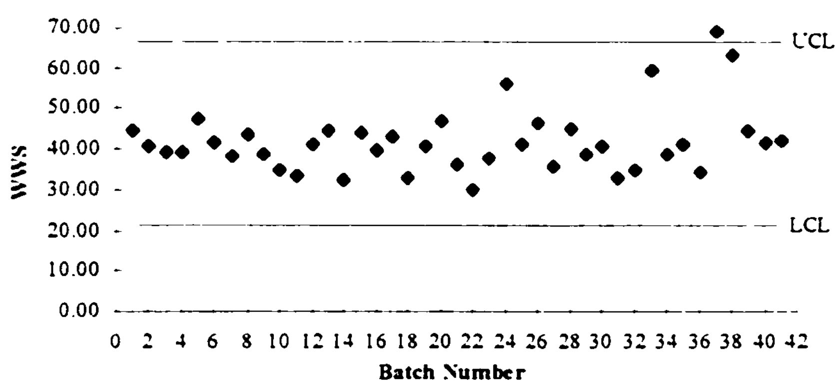

Figure 5.6: Within-Wafer Standard Deviation Chart (Control Data)

Due to effects of within subgroup correlation, care was taken to ensure the most appropriate estimate of process variance was determined. The estimate for variance used was the variance of the batch mean thickness measurements. Determining variance in this manner accounts directly for the effects of within subgroup correlation and ensures that the control limits are properly set. A complete discussion of the impact of within subgroup correlation is given by Neuhardt (1987).

5.2 Multivariate Control Charts

When there are several product quality variables coming from a process, the use of univariate control charts to monitor each variable can be confusing. Moreover, p control charts on p PQV fail to give information regarding interactions or correlation between PQV. This has led to the development of multivariate control charts.

In this section, four methods of monitoring multivariate data are discussed. These methods are: Hotelling's T^2 chart, Principal Components Analysis (PCA), Multivariate Cumulative Sum (CUSUM) charts, and Multivariate Exponentially Weighted Moving Average (MEWMA) charts. The data used to test these charting methods are the control or "tweak-free" data set introduced in Chapter 2.

5.2.1 Hotelling's T^2 Chart

Multivariate procedures for control charts are based on Hotelling's T^2 distribution (Hotelling, 1947). This is the multivariate analogue to the univariate t-distribution. Hotelling's T^2 statistic combines several cross-correlated variables into a single statistical score. The T^2 score is sensitive to shifts in the mean value of one or more variables. It is ideal for processes in which shifts in mean can occur in any direction. Hotelling's T^2 is defined as,

$$T^2 = n(\bar{\mathbf{x}} - \boldsymbol{\mu}_0)'\mathbf{S}^{-1}(\bar{\mathbf{x}} - \boldsymbol{\mu}_0) \qquad (5.3)$$

where

$$\bar{\mathbf{x}} = \begin{bmatrix} \bar{x}_1 \\ \bar{x}_2 \\ \vdots \\ \bar{x}_p \end{bmatrix} \quad \text{and} \quad \boldsymbol{\mu}_0 = \begin{bmatrix} \mu_1^0 \\ \mu_2^0 \\ \vdots \\ \mu_p^0 \end{bmatrix}. \qquad (5.4)$$

$\mathbf{S}^{-1}$ is the inverse of the sample variance-covariance matrix, $\mathbf{S}$, and n is the sample size of each $\bar{\mathbf{x}}_i, i = 1,2,\ldots,p$. It is desirable to test the hypothesis that $\mu = \mu_0$. When $\mu = \mu_0$, Hotelling's T^2 is distributed $\frac{p(n-1)}{n-p}F_{(p,n-p)}$, where $F_{(p,n-p)}$ refers to the F distribution with

p degrees of freedom in the numerator and n-p degrees of freedom in the denominator. The hypothesis $\mu = \mu_0$ is accepted whenever T^2 is smaller than $\frac{p(n-1)}{n-p} F_{\alpha(p,n-p)}$ for a given p-variate sample of size n and a suitable level of α. It has been suggested by Ryan (1989), that α be chosen such that $\alpha/2p$ = 0.00135 which is equivalent to the 3-sigma value for a univariate chart.

Since μ_0 is the true but unknown vector of means, μ_0 is estimated by

$$\bar{\bar{\mathbf{x}}} = \begin{bmatrix} \bar{\bar{x}}_1 \\ \bar{\bar{x}}_2 \\ \vdots \\ \bar{\bar{x}}_p \end{bmatrix}. \quad (5.5)$$

Each $\bar{\bar{\mathbf{x}}}$ is computed by averaging the means of all the subgroups. Thus, for subgroup j, one would plot

$$T_j^2 = n(\bar{\mathbf{x}}^{(j)} - \bar{\bar{\mathbf{x}}})' S_p^{-1} (\bar{\mathbf{x}}^{(j)} - \bar{\bar{\mathbf{x}}}) \quad (5.6)$$

for the jth subgroup (j = 1,2,...,k), where $\bar{\mathbf{x}}^{(j)}$ denotes a vector with p elements that contains the subgroup averages for each of the p characteristics for the jth subgroup. S_p is obtained by pooling the subgroup variance-covariance matrices over the k groups. Each of the k values from Equation 5.4 would be plotted with the following upper control limit (UCL). The lower control limit (LCL) is commonly set to zero because any shift in the mean will lead to an increase in the T^2 statistic. However, T^2 is also sensitive to changes in the covariance matrix of the data. To detect changes in the covariance matrix that would lead to abnormally low T^2 values, the LCL should calculated such that

$$\mathrm{LCL} = \chi^2(1 - \alpha/2; p) \quad (5.7)$$

(Tracy, 1992).

The upper control limit, as defined by Alt (1985), is,

$$\mathrm{UCL} = \left(\frac{p(m-1)(n-1)}{m(mn-n-p+1)} \right) F_{\alpha/2(p,mn-n-p+1)} \quad (5.8)$$

where p represents the number of variates; m represents the sample size; n represents the number of samples.

Tracy (1992), presented a multivariate control chart for individual observations. The T^2 statistic is essentially the same but the subgroup averages are replaced by the observed value. The upper and lower control limits are given by,

$$\mathrm{LCL} = \left(\frac{p(n-1)(n+1)}{n(n-p)}\right) F_{1-\alpha/2(p,n-p)} \tag{5.9}$$

$$\mathrm{UCL} = \left(\frac{p(n-1)(n+1)}{n(n-p)}\right) F_{\alpha/2(p,n-p)} \tag{5.10}$$

Values of T^2 outside the control limits require investigation.

The data from the Tylan/Tytan LPCVD reactor used in this research can be viewed in two ways. First, each of the twenty thickness measurements can be viewed as separate PQV such that $p = 20$ and $m = 1$. The second case reduces the data to $p = 4$ variates representing the mean of thickness measurements from the four test wafers in a batch (m = 5 measurements per test wafer). Although the matrix manipulations are less cumbersome in the second case, important information regarding within-wafer variance is lost in the averaging process. To compensate for this, a second chart monitoring within-wafer variance would have to be created. In the first case, shifts in the mean vector and changes in both cross-load and within-wafer variance are detected on the same chart. For this reason, the first case scenario will be used as the framework for multivariate control charts.

A T^2 chart for the control data is shown in Figure 5.7. It indicates that the process is out of control. Note that the Shewart charts for this data set showed that the process was in a state of statistical process control. It was expected that the T^2, and multivariate charts in general, would be more sensitive than the univariate X-bar and s-charts, since multivariate charts monitor changes in the correlation structure of the data. Sample calculations are given in Appendix IX.

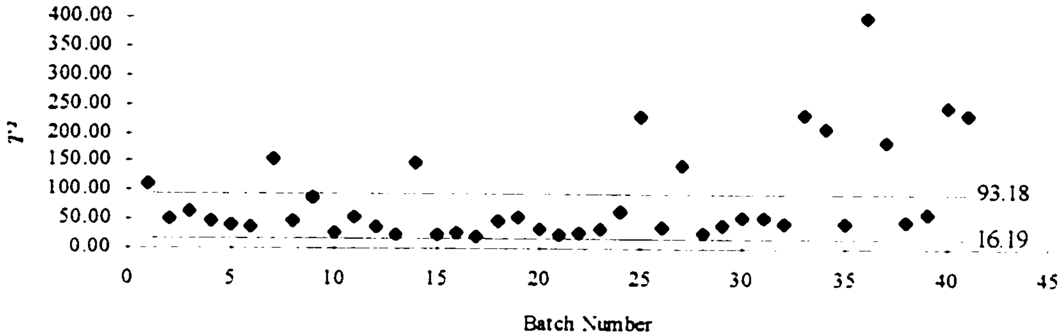

Figure 5.7: T^2 Chart of Control Data

Investigation of the data from batches which yielded an out-of-control signal showed large deviations from the target values for all batches, as indicated in Table 5.1.

Table 5.1: Out-of-Control Batches Detected by T^2 Chart - Deviations from Target

No.	L-C	L-T	L-R	L-F	L-L	C1-C	C1-T	C1-R	C1-F	C1-L	C2-C	C2-T	C2-R	C2-F	C2-L	P-C	P-T	P-R	P-F	P-L	T^2
1	63	57	30	123	29	5	-7	-44	70	32	-76	-94	-129	-4.	-39	-27	-38	-85	38	8	110
7	-92	-93	-140	-41	-57	-61	-56	-121	-14	-9	10	9	-42	69	47	82	87	57	123	87	155
14	50	56	36	87	57	105	63	101	87	138	-61	-56	-117	-23	-7	-47	-44	-94	-4	-12	148
25	-10	-13	-64	24	34	-20	11	-65	-32	55	14	-7	-29	102	50	78	72	54	116	97	229
27	102	34	37	48	39	-46	-45	-41	-37	-34	36	49	104	64	99	99	43	65	41	-57	145
33	63	45	75	59	55	41	-52	36	40	118	-48	-99	-17	59	-113	-46	-71	-10	111	-65	234
34	44	127	52	51	62	-33	-6	-4	7	-75	29	-87	-87	-78	-108	-83	-89	-60	-42	-112	210
36	100	-1	16	18	24	56	25	59	47	52	-109	-81	-80	-59	-157	-73	-73	-69	3	-99	399
37	128	95	97	153	60	60	28	86	131	-50	-48	-63	118	120	-91	-52	-74	43	0	-67	186
40	-118	-135	-163	-48	-96	-25	-28	-81	14	25	-105	-134	-164	-34	-67	58	54	43	107	63	244
41	-107	-150	-93	-41	-104	-5	-6	-61	24	47	-74	-89	-145	-4	-25	75	73	44	121	97	233

L-C = Load Centre, L-T = Load Top, L-R= Load Right, L-F= Load Flat L-L = Load Left
C1-C = C1 Centre C1-T = C1 Top, C1-R = C1 Right, C1-F = C1 Flat, C1-L = C1 Left
C2-C = C2 Centre C2-T = C2 Top, C2-R = C2 Right, C2-F = C2 Flat, C2-L = C2 Left
P-C = Pump Centre, P-T = Pump Top, P-R = Pump Right, P-F = Pump Flat, P-L = Pump Left

In all batches, the batch-mean thickness was reasonable, however, the within-wafer standard deviation for batches 33 and 37 is large and the cross-load standard deviation for batches 7, 14, 34, 36, 40 and 41 are also quite large, as shown in Table 5.2. Batches 1, 25 and 27 are exceptional because the batch-mean thickness, within-wafer standard deviation and cross-load standard deviation for these batches are reasonable values, yet the T^2 values clearly indicated that there is a problem with these batches. Looking back to Table 5.1, the deviations from target for locations load-flat, C2-top, C2-right and pump-right in batch 1 were unusually large. Moreover, the within-wafer ranges for the C1 and pump wafers were also large (144 Å and 123 Å, respectively). Also, data for the C1 and C2 wafers were not available and the missing data were replaced with the mean of the thickness measurements for following two batches. In batch 25, the deviations from target for the C2-Flat and the Pump-Flat location are large. Furthermore, the load, C1 and C2 wafers have unacceptably large within-wafer ranges of 98Å, 120 Å and 131 Å, respectively. In batch 27, the deviation from target for the load-centre, C2-right, pump-centre locations are large. Also, the within-wafer range for the wafer in the pump zone is 156 Å, which is unacceptably large.

Table 5.2: Out-of-Control Batches Detected by T^2 Chart - with Batch-Mean Thickness, Within-Wafer Standard Deviation and Cross-Load Standard Deviation

Batch Number	Batch-Mean Thickness	Within-Wafer Standard Deviation	Cross-Load Standard Deviation	T^2
[redacted]	[redacted]	[redacted]	[redacted]	[redacted]
7	3492.3	38.25	74.64	155
14	3515.8	32.25	72.62	148
[redacted]	[redacted]	[redacted]	[redacted]	[redacted]
[redacted]	[redacted]	[redacted]	[redacted]	[redacted]
33	3509.0	59.49	39.07	234
34	3475.4	38.50	63.35	210
36	3480.0	34.07	69.00	399
37	3533.7	68.96	50.07	186
40	3458.3	41.52	80.22	244
41	3478.9	42.08	77.92	233

5.2.2 Principal Components Analysis

Principal Components Analysis is a multivariate statistical method that can explain the variance-covariance structure of multivariate data through a few linear combinations of the original variables for the purposes of data reduction and ease of interpretation (Johnson and Wichern, 1992). PCA decomposes an p x n matrix $\mathbf{X}$ of p variates and n observations into a series of p principal components such that $\mathbf{X} = \sum_{i=1}^{p} \mathbf{Y}_i \mathbf{e}_i^T$, with each component characterized by a loading vector ($\mathbf{e}_i$) and a score vector ($\mathbf{Y}_i$). The loading vectors, $\mathbf{e}_i$, are the eigenvectors of the variance-covariance matrix of $\mathbf{X}$, and provide the directions with maximum variability. The scores, Y_i, are the coordinates for the objects in the reduced space. Scores are uncorrelated so that they measure different underlying information in the data.

The first principal component, Y_1, represents the selection of a new coordination system obtained by rotating the original variables to the direction of greatest variability. The second principal component, Y_2, represents the second largest amount of variation in the data and so on. With highly correlated variables, only a few principal components are needed to explain most of the significant variation in the data.

For $\mathbf{X}_{pxn}$ with variance-covariance matrix Σ the eigenvalue-eigenvector pairs of Σ are $(\lambda_1, \mathbf{e}_1), (\lambda_2, \mathbf{e}_2),\ldots, (\lambda_p, \mathbf{e}_p)$ such that $\lambda_1 > \lambda_2 \ldots > \lambda_p > 0$. The i'th principal component is given by:

$$Y_i = \mathbf{e}_i^T\mathbf{X} = e_{1i}X_1 + e_{2i}X_2 + \ldots + e_{pi}X_p \quad (i = 1, 2, \ldots, p). \qquad (5.9)$$

Also,

$$\mathrm{Var}(Y_i) = \lambda_i \text{ and } \mathrm{Cov}(Y_i, Y_k) = 0.\ i \neq k.$$

The total sample variance is given by

$$\sum_{i=1}^{p} s_{ii} = \lambda_1 + \lambda_2 + \ldots + \lambda_p .$$

The portion of the total variance represented by the *kth* principal component is thus,

$$\begin{pmatrix}\text{Portion of total} \\ \text{variance due to } k\text{th} \\ \text{principal component}\end{pmatrix} = \frac{\lambda_k}{\lambda_1 + \lambda_2 + \ldots + \lambda_p} \quad k = 1, 2, \ldots, p. \qquad (5.10)$$

According to Johnson and Wichern (1992), if 80 to 90% of the total population variance for large p can be described by the first few principal components, then these components can essentially replace the p variables without loss of much information. More traditional control charts can then be established using the scores from the first few principal components. Furthermore, plotting the scores of one principal component versus those of another clearly demonstrates which batches have similarities in their measurements and form clusters and which are isolated from the others and therefore represent an out-of-control situation or an outlier.

The results of the PCA applied to the historical data set used in the exploratory data analysis found in Chapter Two and to the control data are given in Appendix IX. For both the historical data and the control data, over 80% of the variability in the data was described by the first three principal components and the first two principal components represented the same phenomenon in both data sets. The first principal component, Y_1, was the sum of all twenty thickness measurements in a batch and reflects the batch mean thickness. The second principal component, Y_2, represented the difference between the thickness measurements on the first two test wafers and the last two test wafers (Y_2= (Load + C1) - (C2 + Pump)) reflecting cross-load variance. The third principal component, Y_3, was more difficult to interpret.

For the historical data set, the third principal component represented the difference between the end wafers and the middle wafers, such that $Y_{3,historical}$ = (Load + Pump) - (C1 + C2). This difference between the end wafers and the middle wafers was first noted during a preliminary data analysis exercise. It was found that the variance associated with the middle wafers was significantly higher than the variance of the end wafers. Through discussions with operators and engineers, it was discovered that lower quality test wafers were typically used in the C1 and C2 (middle) test wafer positions. The quality of the measurements taken from these wafers was often called to question and the data deemed unacceptable. Evidence of this was found in the historical data set, which showed numerous cases of missing data for test wafers in the C1 and C2 positions. Upon further investigation of these points, it was found that in most cases the data were not entered into the data storage system because it was believed to be erroneous.

The third principal component for the control data, $Y_{3,control}$, essentially represented the difference between the Right and Left thickness measurements on each of the test wafers. This can be viewed as within-wafer variance. Furthermore, the fourth principal component for the historical data represented the difference between the top and the flat positions on each of the test wafers. This, too, is a measure of the within-wafer variance. Because the range of thickness measurements on a wafer does not always come from the difference between the same measured locations, it is better to monitor the within-wafer standard deviation as shown in Figure 5.5. A summary of the PCA performance on the historical data and the control data is found in Table 5.3.

Table 5.3: Principal Component Analysis of the Control Data

	Percent Contribution		Representation	
	Historical Data	Control Data	Historical Data	Control Data
PC_1	67.80	41.27	Mean	Mean
PC_2	17.66	32.68	Cross-Load Range	Cross-Load Range
PC_3	3.81	8.61	Middle - End	Right-Left
Cumulative Percent	89.27	82.57		

The PCA found that most of the variation in the data stems from variables that were identified as requiring control, namely, batch mean thickness, cross-load variance and within-wafer variance. Note the subtle difference between the cross-load variance and the cross-load range identified by the PCA. The cross-load range may be more sensitive to a non-uniform thickness profile along the reactor than cross-load variance chart. The cross-load range is a measure of the difference in thickness measurements between wafers, whereas the cross-load variance is a measure of the difference between the measured values and the mean of all the measured values.

The serial plots of the scores from the first three principal components are given in Figures 5.8, 5.9 and 5.10 using the control data. The 3σ upper and lower control limits are indicated by the dashed lines. In Figure 5.10, one batch falls outside 3σ control limits indicating that the process is not in control. Serial plots of the first two principal components show no sign of an out-of-control situation.

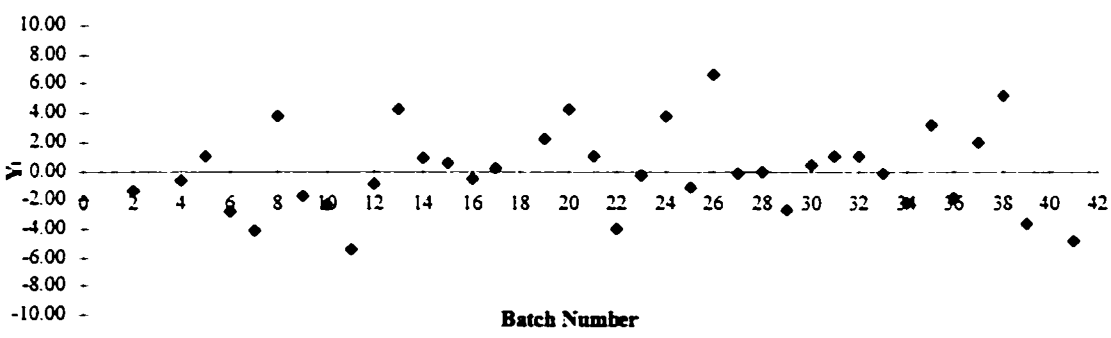

Figure 5.8: Serial Plot of the First Principal Component - Control Data

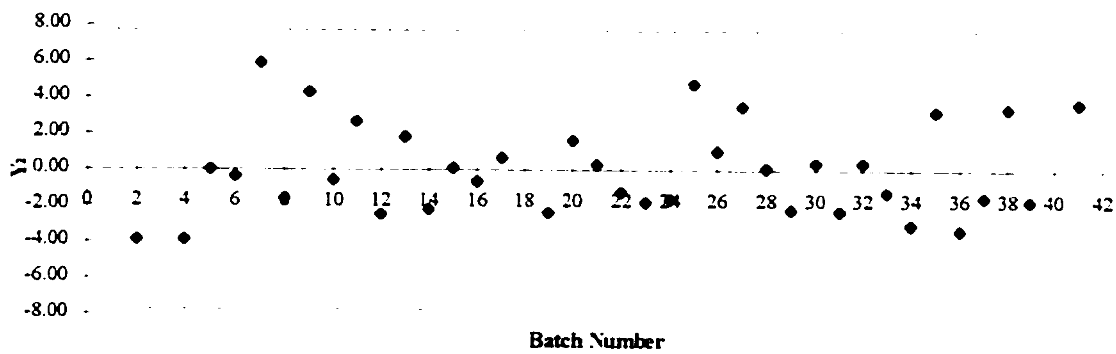

Figure 5.9: Serial Plot of the Second Principal Component - Control Data

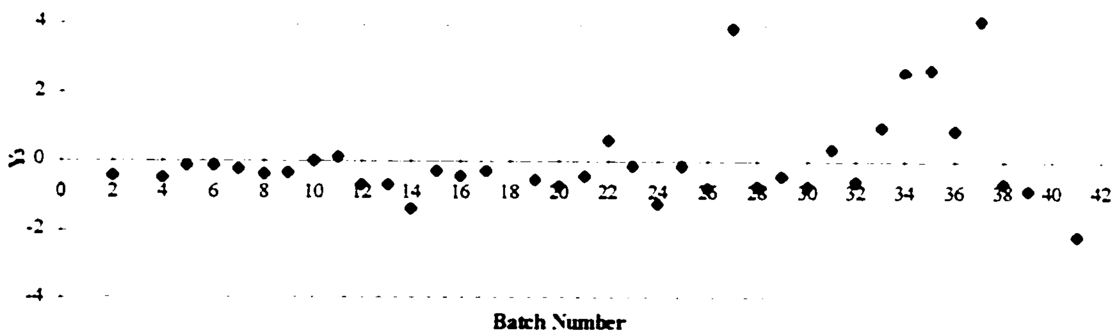

Figure 5.10: Serial Plot of the Third Principal Component - Control Data

A control chart based on cross-load range is depicted in Figure 5.11. It failed to signal any out-of-control batches, and therefore it is difficult to assess its sensitivity relative to the cross-load standard deviation chart.

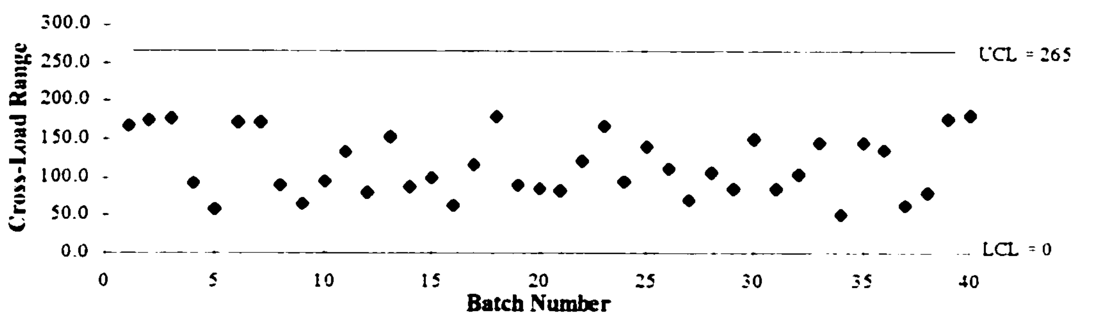

Figure 5.11: Cross-Load Range Chart

The power of the PCA is illustrated in this example. The control data set consisted of 20 variables. Plots of every possible combination of one variable versus another would have resulted in $\binom{20}{2} = 190$ graphs - an infeasible number of graphs to interpret! PCA reduced the number of variables to three principal components. This reduced number of variables requires $\binom{3}{2} = 3$ combinations of principal component plots. These plots, shown in Figures 5.12, 5.13. 5.14, reveal patterns in the data which were not identifiable in the three serial plots. The patterns are manifested in clusters of acceptable behaviour. Batches not in the region of the clusters indicate a change in the process. It is encouraging that many of the batches flagged as being "different" by Figures 5.12, 5.13 and 5.14 were also flagged by the Hotelling's T^2 chart.

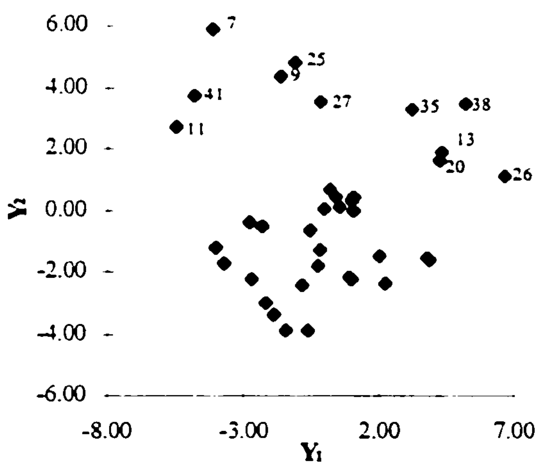

Figure 5.12: The Second PC vs. the First PC - Control Data

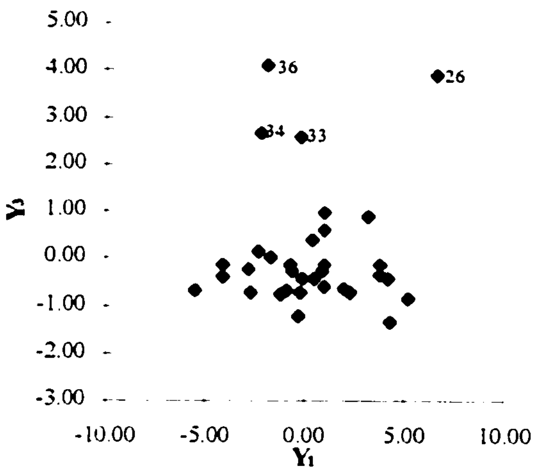

Figure 5.13: The Third PC vs. the First PC - Control Data

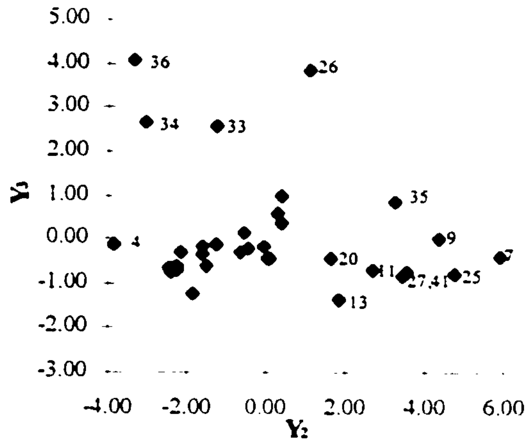

Figure 5.14: The Third PC vs. the Second PC - Control Data

5.2.3 Multivariate CUmulative SUM Charts

Multivariate CUmulative SUM charts or MCUSUM charts are the multivariate variation of the univariate CUSUM charts. The univariate CUSUM charts are constructed by plotting the statistic

$$S_t = \sum_{j=1}^{t} (\overline{X}_j - \tau), \qquad (5.11)$$

where τ can either be a target value or the overall process mean. If the process is in control, the CUSUM should fluctuate about the target value. The process mean $\overline{X}_t$ can be scaled into units of standard deviation such that,

$$z_t = \frac{\overline{X}_t - \tau}{\hat{\sigma}_{\bar{X}}}. \qquad (5.12)$$

Such scaling is advantageous since CUSUM charts are typically designed to detect shifts in the process mean of size n-sigma. The statistic that is plotted is then,

$$S_t = S_{t-1} + z_t. \qquad (5.13)$$

CUSUM charts are restarted at zero once the cause of an out-of-control signal has been removed from the process.

The MCUSUM chart proposed by Crosier (1988) involves calculating the following statistic,

$$C_n = [\mathbf{s}_{n-1} + \mathbf{x}_n - \mathbf{a}]'\Sigma^{-1}[\mathbf{s}_{n-1} + \mathbf{x}_n - \mathbf{a}]^{1/2} \quad (5.14)$$

where **a** is the target or mean value.

The vector of MCUSUM is,

$$\mathbf{s}_n = \mathbf{0} \quad \text{if } C_n \le k$$
$$\mathbf{s}_n = (\mathbf{s}_{n-1} + \mathbf{x}_n - \mathbf{a})(1 - k/C_n) \quad \text{if } C_n > k \quad (5.15)$$

where $\mathbf{s}_0 = \mathbf{0}$ and $k > 0$. The MCUSUM scheme signals an out-of-control situation whenever,

$$Y_n = [\mathbf{s}_n'\Sigma^{-1}\mathbf{s}_n]^{1/2} > h \quad (5.16)$$

and $h > 0$. The chart parameters h and k are chosen to yield optimal Average Run Length (ARL) performance. ARL(0) represents the average of the distribution of number of runs, for a process that is in control, until a false alarm occurs. Crosier (1988) determined the values *h and k* necessary to obtain on-target ARL's of 200 for a multivariate process with p=20 variates. These values of h and k, set at 24.7 and 0.5, respectively, were used to create of the MCUSUM chart for the thickness data depicted in Figure 5.15.

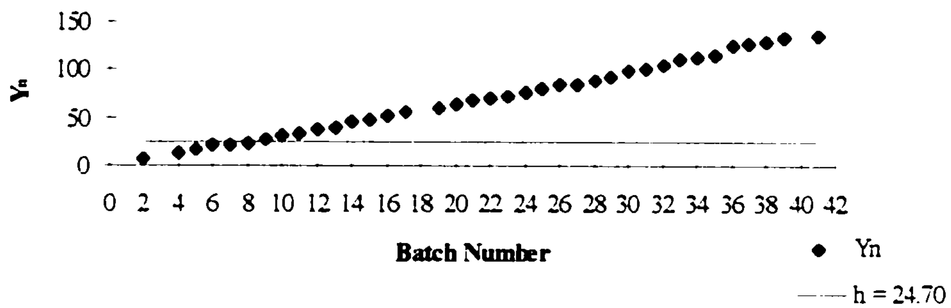

Figure 5.15: MCUSUM Chart for Control Data - Thickness (Å)

The MCUSUM chart very quickly indicates that the process is out-of-control. The advantage of this chart is that the vector of CUSUM's, found in Appendix IX, indicates the direction and location of the shift. The first five elements of the CUSUM vector were large as were the last five elements of the CUSUM. This corresponds to large deviations from the target thickness of 3500Å for thickness measured on the load and pump zone wafer, thus pointing to the location of the problem. The value of the elements of the CUSUM vector were positive in the load zone indicating that the deviation from target is positive. In other words, the wafers in the load zone are too thick. The value of the elements of the CUSUM were negative in the pump zone indicating that the deviation from target is negative and that the thickness of the deposited film on the pump zone wafers is too thin. A factor that might cause the thickness of the deposited film to be large in the load zone and thin in the pump zone is temperature. These results indicate that the temperature may not have been adequately ramped to compensate for depletion of reactant. Another factor that may have caused the problem is silane flowrate. These results could also indicate a problem with the gas flow meter. Although the data from the first few batches indicated that the load and pump zone thickness measurements were the cause of the problem, after ~20 batches, all variables are out-of-control.

5.2.4 Multivariate Exponentially Weighted Moving Average Chart

Multivariate Exponentially Weighted Moving Average charts or MEMWA charts are the multivariate version of the univariate EWMA chart. EWMA charts are known for their ability to rapidly detect small shifts in a process mean. EWMA charts involve calculating and plotting a statistic based on measured values of the characteristic of interest. This statistic, z_i, is given by:

$$z_i = (1-\lambda)z_{i-1} + \lambda y_i \tag{5.17}$$

where λ is a constant with values ranging from 0 to 1, and it is used to determine the relative weightings applied to current and previous values of the characteristic of interest, y. Upper and lower control limits for EWMA schemes are given by

$$LCL = \text{Target} - L_1\sigma_z \quad \text{and} \quad UCL = \text{Target} + L_2\sigma_z. \tag{5.18}$$

L_1 and L_2 are determined to provide the desired sensitivity for shift detection. For control limits that are symmetrical about the target, $L_1 = L_2 = L$. σ_z represents the standard deviation of the EWMA and is determined by

$$\sigma_z = \sqrt{\frac{\lambda}{2-\lambda}\sigma_a^2} \tag{5.19}$$

where σ_a^2 is the variance of the characteristic of interest, y, assuming the process is operating under IID conditions. Values for λ and L have been tabulated by Lucas and Sacucci (1990) for a desired ARL.

Lowry et al. (1992) proposed a multivariate EWMA, an extension of the EWMA chart, denoted as MEWMA. For a vector of observed variables **x**, this procedure involves calculating the statistic $\mathbf{Z}_i$, the ith vector of EWMAs such that

$$\mathbf{Z}_i = \mathbf{R}\mathbf{X}_i + (\mathbf{I} - \mathbf{R})\mathbf{Z}_{i-1}. \qquad (5.20)$$

where $\mathbf{Z}_0 = \mathbf{0}$ and $\mathbf{R} = \text{diag}(r_1, r_2, \ldots, r_p)$ such that $0 < r_j \Leftrightarrow 1$, $j = 1,2,\ldots,p$. The multivariate MEWMA parameter r_j is analogous to the univariate EWMA parameter λ. The MEWMA chart gives an out-of-control signal when

$$T_i^2 = \mathbf{Z}_i^T \Sigma_{Z_i}^{-1} \mathbf{Z}_i > h_4 \qquad (5.21)$$

where $h_4 > 0$ is chosen to achieve a desired in-control ARL performance. Σ_{Z_i} is the variance-covariance matrix of $\mathbf{Z}_i$. If there is no reason to weight past observations differently for the p variables, then the weighting coefficients can be equated to each other.

$$r_1 = r_2 = \ldots = r_p = r.$$

The MEWMA becomes

$$\mathbf{Z}_i = r\mathbf{X}_i + (1 - r)\mathbf{Z}_{i-1} \qquad (5.22)$$

The variance-covariance matrix of the MEWMA is,

$$\Sigma_{Z_i} = \frac{r\left[1 - (1 - r)^{2i}\right]}{2 - r}\Sigma. \qquad (5.23)$$

As i becomes large, Lowry et al. (1992) showed that Σ_{Z_i} approaches

$$\Sigma_{Z_i} = \frac{r}{2 - r}\Sigma. \qquad (5.24)$$

A MEWMA chart, using the control data, is depicted in Figure 5.16. The control limit, h_4, is indicated by the solid line. The control limit was set to the value reported by Lowry for p=20 variates, in order to achieve an average in-control run length of 200.

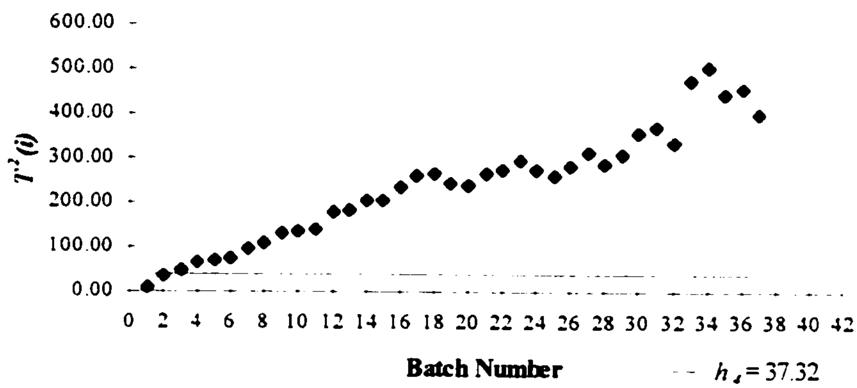

Figure 5.16: MEWMA Chart for "Control" Thickness Data

As with the MCUSUM chart, the MEWMA chart very quickly indicated that the process in out-of-control. A MEWMA chart based on the sample mean rather than target indicates that the process is in control. This demonstrates that a likely cause of the loss of control is that the mean is not on target.

There is some indication that the data are not distributed multivariate normal. Further work in the area of simulations is required to determine the sensitivity of these charts to the multivariate normal assumption.

5.2.5 Recommended Monitoring Scheme

The data from this process are highly correlated. For this reason, multivariate control charts appear to have potential. It is noteworthy that the principal component analysis identified the mean, the difference between the front wafers and the back wafers, and a form of within-wafer standard deviation as factors contributing over 80% of the variation in the data. Since these factors were not only identified as being important process parameters but also represent over 80% of the variation in the data, it is recommended that these factors be monitored by control charts. It is further recommended that the process be monitored using an X-bar chart for the batch mean thickness, a within-wafer standard deviation chart, and a cross-load standard deviation chart. This method of monitoring is advantageous since it is very similar to the current method of monitoring the process, and it involves theory that is already understood by the operations staff.

Furthermore, X-bar charts are robust to data in which the marginal distributions do not perfectly follow a normal distribution.

Although there appears to be potential for the use of multivariate charts to monitor this process, more work is required before a definite recommendation can be made. Simulated data from a multivariate normal distribution with p = 20 and a correlation structure similar to that found in the historical data set should be used to compare the effectiveness of the three types of multivariate control charts presented. Shifts in process mean, cross-load standard deviation and within-wafer standard deviation can be introduced to the data in order to determine how shifts in these parameters will manifest themselves in the multivariate control charts. Furthermore, simulations can be used to determine the sensitivity of the charts to non-normal data.

5.3 Dealing with out of control signals

When an out-of-control signal is identified, the production should cease in the reactor. Some possible causes of out-of-control signals from an X-bar chart are discussed:

- If one point falls beyond the 3σ control limits then: determine if the CLS and WWS charts were also effected by the signal. If the CLS and WWS do not indicate a problem, then inspect to determine if the recipe was altered. Specifically, determine if the deposition time had been altered, as the modeling work that was done in Chapter Three showed that deposition time has a large effect on batch-mean thickness, only a minor effect on within-wafer standard deviation, and no effect on cross-load standard deviation.

  If the CLS and WWS charts also indicate an out-of-control situation then this could indicate a problem with the centre temperature, reactor pressure or silane flowrate or any combination of the three. Tube plots for temperature, pressure and silane flowrate reveal irregularities with respect to these process input variables.

- If the control chart signals are due to a trending problem, this indicates that the problem is occurring over time. It is likely that a specific piece of operating equipment (mass-flow controller, pump, reactor door seal, thermocouples) is degrading. Also, ensure that the recipe had not been altered of the batches in question - the trend may coincide with adjustment made to the process input variables during the period in question.

- The cross-load standard deviation chart will signal out-of control when the thickness of the deposited film on one or more of the test wafers is significantly thicker or thinner than the other wafers. Once again, the tube plots should be examined to determine if one of the temperature zones was running hotter or cooler than desired. An unwanted increase in the silane flowrate will also cause an increase in cross-load standard deviation.
- An out-of-control signal on the within-wafer standard deviation chart will likely be due to an error in the thickness measuring tool, a data entry error or a misalignment of the cantilever arm. For the first two cases, the thickness of the test wafers should be remeasured. Knowing the locations of minimum and maximum thickness measurements will assist in realigning the cantilever.

If the cause of the out-of-control signal has not been determined, re-measure the test wafers to ensure the signal was not caused by a data entry error. Also, determine whether spectrophotometer (thickness measuring device) is due for scheduled servicing or calibration. The signal may be due to inaccurate thickness measurements.

In all cases, the log book should be reviewed to ensure that the proper recipe was run, and to determine if there were any unusual circumstances associated with the batch(es) in question.

Once all irregularities have been identified and remedied, execute two test batches to ensure that the problems have been resolved. If no irregularities are found, a test batch should be executed to determine if the signal was a false alarm. The test batches should meet the requirements for reactor qualification, which are "two consecutive test batches must fall between 3430 and 3570". As well, the within-wafer and cross-load standard deviations should fall within the control limits of the WWS and CLS control charts. Production can resume once these requirements are met. A detailed description of the problem and the steps taken to solve it should be documented to facilitate future problem-solving.

This chapter reviewed several different tools for monitoring a process with many measured variables. A preferred approach was recommended and a procedure for dealing with out-of-control signals was proposed. In the following and final chapter, the conclusions and recommendations for future work are presented.

Chapter Six

Conclusions and Recommendations

The objectives at the start of this work were: (i) to gain a better understanding of process behaviour through the development of an empirical model, (ii) to reduce process variability, and (iii) to implement an improved control scheme. The efforts made to achieve theses objectives followed by recommendations for future work will be discussed in this chapter.

6.1 Conclusions

Response surface methodologies were successfully applied for the purpose of building emipirical models to describe the LPCVD reactor. None of the models fitted in Chapter Three showed a significant lack of fit. These models provided a better understanding of how the operating variables affect the process thereby fullfilling objective (i). Process engineers now have a quantitative means of estimating the effects of temperature, temperature ramps, pressure, silane flowrate, and deposition time on film thickness, deposition rate, within-wafer variance, and cross-load variance.

A Components of Variance Analysis on the historical data set showed that the largest contributor to process variation was batch-to-batch variation. The batch-to-batch variation was 48.5 Å representing 42.8% of the total variation in the process. The within-wafer variance was 47.9 Å, which represented 42.3% of the total process variability. The cross-load variability was 28.4 Å, which represented 14.9% of the total process variability. Changes made to the process operating variables from batch to batch inflated process variance and caused serial correlation in the process data. This led to the early recommendation that an SPC approach be applied to the process. It was further shown that a 52% reduction in batch-to-batch variability can be achieved by not making any changes to the process operating variables from batch to batch. This result was the first step towards achieving objective (ii).

The optimal operating conditions for the Tylan/Tytan LPCVD reactor used in the deposition of polycrystalline silicon were found to be: Centre Temperature (T_c) = 619°C, Front Temperature Ramp (R_1) = 3°C, Back Temperature Ramp (R_2) = 7°C, Pressure (P) = 239 mTorr, Silane Flowrate (F_{SiH_4}) = 223 cm^3/min at standard temperature and pressure, and deposition time (t_{dep}) = 38 min. Operating at the optimal operating conditions, one can expect the within-wafer standard deviation to decrease from 41.4 Å to 20.6 Å. This represents an expected 50% reduction in within-wafer standard deviation. Also, a 5.2% increase in deposition rate from 88.3 Å/min to 93.1 Å/min can be expected if the reactor were run at the optimal operating conditions. This result further fullfills the attainment of objective (ii).

The proposed control scheme is: (i) operate the reactor at the optimal operating conditions,which were determined in Chapter Four, (ii) monitored the reactor using an X-bar chart, a cross-load standard deviation chart, and a within-wafer standard deviation chart. (iii) do not make changes to the process input variables from batch to batch, and (iv) follow the guidelines given in Chapter Five for dealing with out-of-control situations signalled by the control charts. This procedure was not tested as it is partially dependent on the models built in Chapter Three. Due to fundamental changes in the reactor, these models may no longer be characteristic of the process. However, the proposed procedure could be applied to the system after reformulating the models to compensate for the changes made to the reactor. Thus, objective (iii) was partially achieved.

6.2 Recommendations for Future Work

1. Repeat the experimental design to account for the change in reactor heating coil and for changes due to improved control system.
2. Simulation work on the various types of multivariate control charts is needed to assess their relative merits.
3. Simulation work on the sensitivity of multivariate charts to data that are not perfectly multivariate normal is needed.

References

Alt, F.B., "Multivariate Quality Control", The Encyclopedia of Statistical Sciences, **6**, 110-122 (1985).

Azzaro, C., P. Duverneuil and J.P. Couderc, "Thermal and Kinetic Modelling of Low-Pressure Chemical Vapour Deposition Hot-Wall Tubular Reactors", Chemical Engineering Science, **47**, 3827-3838 (1992).

Bowman, R., G. Fry, J. Griffin, D. Potter and R. Skinner, Practical VLSI Fabrication for the 90s, Integrated Circuit Engineering Corporation, 9.1-9.22 (1990).

Box, G.E.P. and D.R. Cox, "An Analysis of Transformations", Journal of the Royal Statistical Society, **B26**, 211-252 (1964).

Box, G.E.P. and N.R. Draper, Empirical Model Building and Response Surfaces, John Wiley & Sons, Inc., New York, NY (1987).

Box, G.E.P., W.G. Hunter and J.S. Hunter, Statistics for Experimenters, John Wiley & Sons Inc., Inc., New York, NY (1978).

Box, G.E.P. and G.M. Jenkins, Time Series Analysis: Forecasting and Control, Prentice Hall, Englewood Cliffs, NJ (1976).

Crosier, R.B., "Multivariate Generalizations of Cumulative Sum Quality Control Schemes", Technometrics, **30**, 291-303 (1988).

Deming, W.E., Out of the Crisis, MIT Center for Advanced Engineering Study, Cambridge, MA (1986).

Draper, N.R. and H. Smith, Applied Regression Analysis, John Wiley & Sons, Inc., New York, NY (1981).

Hotelling, H., "Techniques of Statistical Analysis", C. Eisenhart, M.W. Hastay and W.A. Wallis, Eds., McGraw-Hill, New York, NY, 111-184 (1947).

Johnson, R.A. and D. Wichern, Applied Multivariate Statistical Analysis, Prentice Hall, Englewood Cliffs, NJ (1992).

Kamins, T., Polycrystalline Silicon for Integrated Circuit Applications, Kluwer Academic Publishers, Boston, MA (1988).

Lowry, C. A., W.H. Woodhall, C.W. Champ and S.E. Rigdon, "A Multivariate Exponentially Weighted Moving Average Control Chart", Technometrics, **34**, 46-53 (1992).

Lucus, J.M. and M.S. Sacucci, "Exponentially Weighted Moving Average Control Schemes: Properties and Enhancements", Technometrics, **32**, 1-20 (1990).

Matlab 3.5m, Mathworks Inc., Sherbon, MA (1992).

Neuhardt, J.B. "Effects of Correlated Sub-Samples in Statistical Process Control", IIE Transactions, **19**, 208-214 (1987).

Nomikos, P. and J.F. MacGregor, "Multivariate SPC Charts for Monitoring Batch Processes", McMaster University, Hamilton, ON (1993).

RS/1 Statistical Software, BBN Software Products Corporation, Cambridge, MA (1988).

Ryan, T.P., Statistical Methods for Quality Improvement, John Wiley and Sons Inc., New York, NY (1989).

Sherman, A., Chemical Vapour Deposition for Microelectronics, Noyes Publications, Park Ridge, NJ (1987).

Shewart, W.A., Economic Control of Quality of Manufacturing Product, Nostrand-Reinhold, New York, NY (1931).

STATGRAPHICS 5.0 Statistical Graphic System, Rockville, MD (1991).

Tracy, N.D., J.C. Young and R.L. Mason, "Multivariate Control Charts for Individual Observations", Journal of Quality Technology, 24, 88-95 (1992).

Tucker, W.T., F.W. Faltin and S.A. Vander Wiel, "Algorithmic Statistical Process Control: An Elaboration", Technometrics, **35**, 363-375 (1993).

Western Electric Company, Statistical Quality Handbook, New York, NY (1956).

Woodall, W.H. and N.M. Ncube, "Multivariate CUSUM Quality Control Procedures", Technometrics, **27**, 285-292 (1985).

Wolf, S. and R.N. Tauber, Silicon Processing for the VLSI Era Volume 1 - Processs Technology, Lattice Price, CA (1986).

Appendix I

Spectrophotometer Repeatability Analysis

Table AI.1: Repeatability Data from the Spectrophotometer

Date	Time	Mean Thickness (Å)	Date	Time	Mean Thickness (Å)
02-Oct-94	07:23:50	3585.0	11-Nov-94	08:16:06	3583.0
03-Oct-94	08:19:36	3583.0	12-Nov-94	07:28:28	3584.0
04-Oct-94	10:55:32	3581.0	13-Nov-94	07:41:03	3583.0
05-Oct-94	07:38:02	3578.5	14-Nov-94	11:08:42	3584.0
06-Oct-94	07:55:21	3584.0	15-Nov-94	07:48:41	3578.0
07-Oct-94	11:09:45	3585.0	16-Nov-94	14:59:22	3584.0
09-Oct-94	08:10:50	3578.0	18-Nov-94	07:37:15	3581.0
10-Oct-94	11:11:54	3578.0	19-Nov-94	08:03:42	3580.0
12-Oct-94	08:13:48	3578.0	20-Nov-94	12:43:10	3578.0
13-Oct-94	07:37:50	3579.0	20-Nov-94	11:25:56	3578.0
14-Oct-94	07:44:34	3578.0	20-Nov-94	09:02:04	3578.0
15-Oct-94	07:26:33	3578.0	20-Nov-94	07:52:54	3578.0
16-Oct-94	08:25:09	3579.0	21-Nov-94	22:15:34	3578.0
17-Oct-94	08:59:18	3585.0	21-Nov-94	07:35:10	3583.0
18-Oct-94	14:29:29	3578.0	22-Nov-94	07:27:47	3578.0
19-Oct-94	15:46:41	3578.0	25-Nov-94	15:03:15	3577.0
20-Oct-94	08:38:05	3579.5	27-Nov-94	11:29:10	3576.0
21-Oct-94	07:32:34	3581.0	28-Nov-94	09:19:05	3579.0
22-Oct-94	08:57:07	3578.0	29-Nov-94	08:19:28	3578.0
24-Oct-94	07:49:26	3583.0	30-Nov-94	07:46:47	3577.0
25-Oct-94	08:07:13	3578.0	01-Dec-94	07:25:48	3576.0
27-Oct-94	08:23:00	3580.0	02-Dec-94	11:18:35	3580.0
28-Oct-94	10:44:08	3584.0	04-Dec-94	10:00:07	3578.0
31-Oct-94	07:57:35	3584.0	07-Dec-94	12:19:53	3578.0
01-Nov-94	10:59:38	3586.0	08-Dec-94	13:36:06	3582.0
02-Nov-94	14:32:08	3584.0	09-Dec-94	07:38:00	3581.0
02-Nov-94	12:25:58	3584.0	10-Dec-94	15:37:30	3580.0
03-Nov-94	10:14:49	3577.0	12-Dec-94	18:36:25	3580.0
03-Nov-94	05:49:55	3580.0	13-Dec-94	07:49:21	3582.0
04-Nov-94	02:30:10	3577.0	14-Dec-94	10:59:43	3580.0
05-Nov-94	16:43:00	3579.0	16-Dec-94	08:38:05	3582.0
05-Nov-94	12:40:39	3578.0	17-Dec-94	12:32:24	3582.0
06-Nov-94	07:47:12	3583.0	18-Dec-94	12:26:48	3581.5
07-Nov-94	16:36:59	3580.1	19-Dec-94	07:23:02	3580.0
08-Nov-94	15:25:59	3580.0	20-Dec-94	07:26:41	3580.0
09-Nov-94	08:17:06	3581.0	21-Dec-94	09:17:56	3582.0
10-Nov-94	07:57:42	3583.0			

Sample Calculations

Average of mean thickness data, $\overline{\overline{X}}$: 3580.3 Å

Variance of mean thickness data, $s_{\overline{X}}^2$: 6.6

Standard Deviation of mean thickness data, $s_{\overline{X}}$: 2.6

Number of observations, n 73

t-value for $\alpha = 0.05$ and n=73 1.99

95% confidence interval for mean is,

$$\left[3580.3 - (t_{n-1,\alpha/2} \times s_{\overline{X}}),\quad 3580.3 + (t_{n-1,\alpha/2} \times s_{\overline{X}})\right] \qquad \text{(AI.1)}$$

$$= \left[3580.3 - (1.99 \times 2.6),\quad 3580.3 + (1.99 \times 2.6)\right]$$

95% confidence interval for mean = (3575.2 Å, 3585.5 Å)

Appendix II

Data Sets Used in Exploratory Data Analysis

Table AII.1: Historical Thickness Data from Tylan/Tytan LPCVD Reactor - First 41 Batches are the "Tweak-Free" or Control Data

batch #	Load Centre	Load Top	Load Right	Load Flat	Load Left	C1 Centre	C1 Top	C1 Right	C1 Flat	C1 Left	C2 Centre	C2 Top	C2 Right	C2 Flat	C2 Left	Pump Centre	Pump Top	Pump Right	Pump Flat	Pump Left	t_{dep}	T_{load}	T_{pump}	PM
1	3563	3557	3530	3623	3529											3473	3462	3415	3538	3508	39.66	617	626	1
2	3569	3572	3547	3609	3568	3502	3490	3453	3568	3528	3423	3408	3368	3496	3459	3398	3391	3351	3469	3417	39.66	617	626	1
3	3556	3574	3536	3597	3555											3380	3397	3331	3431	3413	39.66	617	626	1
4	3582	3585	3570	3622	3587	3515	3503	3465	3575	3546	3429	3400	3379	3495	3469	3405	3393	3364	3473	3432	39.66	617	626	1
5	3574	3563	3571	3636	3575	3520	3482	3483	3607	3544	3482	3492	3432	3576	3515	3484	3461	3443	3576	3501	39.66	617	626	1
6	3510	3513	3487	3552	3524	3461	3435	3422	3535	3497	3491	3416	3391	3514	3485	3465	3450	3427	3524	3485	39.66	617	626	1
7	3408	3407	3360	3459	3443	3439	3444	3379	3486	3491	3510	3509	3458	3569	3547	3582	3587	3557	3623	3587	39.66	617	626	1
8	3635	3623	3630	3680	3638	3580	3559	3536	3653	3607	3497	3471	3443	3577	3539	3462	3440	3420	3540	3486	39.66	617	626	1
9	3473	3467	3424	3525	3505	3482	3489	3423	3527	3531	3510	3506	3458	3569	3550	3561	3559	3538	3611	3575	39.75	617	626	1
10	3522	3515	3519	3562	3535	3465	3443	3442	3528	3499	3459	3443	3407	3520	3501	3464	3473	3420	3497	3494	39.66	617	626	1
11	3428	3452	3391	3437	3464	3415	3408	3361	3478	3462	3465	3485	3414	3498	3503	3513	3528	3498	3539	3522	39.66	617	626	1
12	3562	3562	3541	3612	3571	3503	3504	3451	3563	3545	3440	3436	3381	3506	3491	3429	3419	3382	3492	3461	39.66	617	626	1
13	3608	3604	3586	3675	3613	3571	3566	3517	3643	3617	3541	3538	3473	3600	3596	3530	3525	3478	3583	3568	39.66	617	626	1
14	3550	3556	3536	3587	3557	3605	3563	3601	3587	3638	3439	3444	3383	3477	3493	3453	3456	3406	3496	3488	39.66	617	626	1
15	3566	3560	3560	3616	3567	3516	3504	3467	3599	3543	3475	3469	3410	3565	3512	3491	3474	3474	3566	3501	39.66	617	626	1
16	3560	3560	3548	3607	3566	3493	3488	3449	3560	3532	3462	3455	3402	3524	3507	3475	3471	3424	3534	3501	39.66	617	626	1
17	3547	3547	3543	3601	3547	3513	3500	3466	3589	3538	3485	3467	3427	3569	3518	3500	3488	3458	3574	3511	39.66	617	626	1
18	3596	3602	3589	3603	3601	3549	3563	3512	3542	3599	3495	3519	3451	3482	3559						39.66	617	626	1
19	3629	3623	3604	3677	3638	3549	3537	3504	3614	3586	3466	3454	3407	3530	3515	3448	3439	3406	3510	3476	39.66	617	626	1
20	3621	3611	3589	3684	3637	3567	3562	3508	3623	3617	3532	3526	3464	3597	3585	3534	3518	3472	3608	3562	39.66	617	626	1
21	3576	3578	3553	3613	3596	3520	3524	3472	3570	3566	3488	3492	3430	3537	3540	3495	3500	3450	3529	3533	39.66	617	626	1
22	3506	3496	3510	3530	3517	3448	3423	3426	3500	3481	3423	3398	3383	3478	3463	3458	3434	3502	3479	3458	39.66	617	626	1
23	3571	3555	3573	3599	3579	3511	3482	3481	3572	3545	3459	3429	3413	3526	3504	3449	3420	3419	3508	3475	39.66	617	626	1
24	3637	3622	3628	3694	3642	3561	3532	3512	3649	3693	3489	3461	3428	3577	3530	3469	3443	3429	3552	3490	39.66	617	626	1
25	3490	3487	3436	3524	3534	3480	3511	3435	3468	3555	3514	3493	3471	3602	3550	3578	3572	3554	3616	3597	39.66	617	626	1
26	3672	3660	3643	3744	3683	3605	3598	3543	3671	3653	3546	3539	3477	3607	3600	3534	3524	3479	3580	3579	39.66	617	626	1
27	3602	3534	3537	3548	3539	3454	3455	3459	3463	3466	3536	3549	3604	3564	3599	3599	3543	3565	3541	3443	39.66	617	626	1
28	3548	3539	3525	3611	3557	3514	3495	3453	3585	3548	3482	3474	3419	3541	3535	3479	3472	3425	3536	3520	39.66	617	626	1
29	3542	3535	3520	3570	3540	3470	3473	3412	3528	3504	3430	3438	3365	3486	3470	3429	3434	3376	3483	3450	39.66	617	626	1
30	3568	3560	3544	3629	3580	3512	3521	3464	3522	3579	3485	3497	3429	3494	3555	3496	3488	3441	3547	3537	39.66	617	626	1
31	3600	3579	3618	3621	3604	3534	3496	3525	3588	3555	3465	3426	3439	3531	3500	3448	3449	3413	3498	3460	39.66	617	626	1
32	3573	3569	3548	3621	3587	3535	3550	3491	3533	3592	3488	3506	3438	3490	3551	3498	3500	3452	3530	3541	39.66	617	626	1
33	3563	3545	3575	3559	3555	3541	3448	3536	3540	3618	3452	3401	3483	3559	3387	3454	3429	3490	3611	3435	39.66	617	626	1
34	3544	3627	3552	3551	3562	3467	3494	3496	3507	3425	3529	3413	3413	3422	3392	3417	3411	3440	3458	3388	39.66	617	626	1
35	3587	3589	3606	3598	3616	3555	3598	3556	3559	3502	3530	3591	3537	3563	3522	3675	3590	3542	3563	3490	39.66	617	626	1
36	3600	3499	3516	3518	3524	3556	3525	3559	3547	3552	3391	3419	3420	3441	3343	3427	3427	3431	3503	3401	39.66	617	626	1
37	3628	3595	3597	3653	3560	3560	3528	3586	3631	3450	3452	3437	3618	3620	3409	3448	3426	3543	3500	3433	39.66	617	626	1
38	3595	3576	3579	3674	3600	3552	3758	3549	3655	3586	3540	3540	3482	3644	3581	3568	3538	3520	3664	3585	39.66	617	626	1
39	3506	3496	3480	3575	3516	3455	3450	3400	3504	3503	3427	3415	3359	3497	3479	3432	3427	3380	3483	3474	39.66	617	626	1
40	3382	3365	3337	3452	3404						3395	3366	3336	3466	3433	3558	3554	3543	3607	3563	39.66	617	626	1
41	3393	3350	3407	3459	3396	3495	3494	3439	3524	3547	3426	3411	3355	3496	3475	3575	3573	3544	3621	3597	39.66	617	626	1

Table AII.1 (continued): Historical Thickness Data from Tylan/Tytan LPCVD Reactor

batch #	Load Centre	Load Top	Load Right	Load Flat	Load Left	C1 Centre	C1 Top	C1 Right	C1 Flat	C1 Left	C2 Centre	C2 Top	C2 Right	C2 Flat	C2 Left	Pump Centre	Pump Top	Pump Right	Pump Flat	Pump Left	t_{dep}	T_{load}	T_{pump}	PM
42						3392	3369	3357	3456	3480	3371	3339	3329	3437	3413						38.66	617	626	1
43	3486	3479	3456	3550	3497	3451	3429	3393	3545	3487	3445	3416	3376	3376	3540	3486	3468	3457	3406	3537	38.66	617	626	1
44	3487	3477	3459	3559	3499	3449	3434	3391	3537	3484	3433	3421	3361	3506	3481	3458	3449	3400	3510	3498	38.66	617	626	1
45	3555	3551	3528	3593	3579	3526	3519	3468	3590	3528	3485	3488	3422	3519	3544	3471	3464	3415	3533	3506	38.66	617	626	1
46	3479	3464	3474	3530	3488	3441	3403	3412	3515	3467	3430	3392	3382	3507	3465	3450	3424	3418	3517	3466	38.66	617	626	1
47	3473	3459	3431	3432	3486	3434	3397	3395	3496	3464	3390	3361	3352	3452	3415	3314	3297	3302	3352	3314	38.66	617	626	1
48	3399	3403	3362	3438	3418	3483	3486	3426	3522	3528	3521	3528	3458	3559	3576	3575	3579	3528	3616	3615	38.66	617	626	1
49	3429	3432	3390	3466	3449	3475	3475	3418	3518	3520	3498	3509	3435	3518	3553	3523	3532	3480	3538	3566	38.66	618	625	2
50	3496	3503	3457	3524	3514	3517	3521	3460	3548	3560	3478	3484	3414	3509	3532	3467	3464	3420	3519	3504	38.66	618	635	2
51	3462	3467	3424	3488	3483	3492	3494	3435	3532	3537	3407	3516	3445	3517	3562	3511	3510	3462	3546	3549	38.66	618	635	2
52	3456	3459	3420	3494	3478	3513	3541	3478	3495	3575	3547	3552	3483	3573	3601	3550	3552	3504	3571	3594	38.66	618	635	2
53	3512	3503	3467	3572	3533	3561	3544	3495	3629	3606	3593	3597	3524	3608	3663	3597	3586	3537	3650	3640	38.66	618	635	2
54	3489	3487	3448	3536	3511	3535	3529	3475	3587	3580	3544	3541	3474	3591	3600	3547	3540	3494	3597	3593	38.66	618	635	2
55	3557	3558	3512	3594	3599	3546	3539	3477	3595	3599	3512	3504	3459	3564	3556	3444	3446	3406	3486	3464	38.66	618	635	2
56	3443	3445	3405	3487	3465	3505	3498	3450	3562	3550	3537	3536	3474	3576	3591	3552	3549	3501	3597	3586	39.75	618	635	2
57	3424	3425	3388	3460	3445	3497	3505	3447	3516	3546	3506	3491	3441	3567	3554	3517	3518	3470	3545	3554	39.75	618	625	2
58	3442	3432	3411	3499	3451	3516	3503	3459	3585	3563	3543	3536	3477	3603	3597	3557	3548	3503	3610	3593	39.75	618	625	2
59	3486	3477	3449	3550	3499	3539	3477	3449	3550	3499	3539	3531	3504	3617	3632	3594	3582	3533	3649	3630	39.75	618		2
60	3496	3482	3457	3451	3518	3556	3548	3493	3612	3611	3566	3558	3493	3610	3629	3556	3545	3491	3593	3605	39.75	618	624	2
61	3514	3502	3471	3586	3522	3562	3534	3497	3652	3598	3552	3539	3478	3611	3608	3520	3502	3458	3591	3554	39.75	618	624	2
62	3482	3477	3450	3543	3495	3544	3536	3492	3610	3589	3550	3537	3488	3607	3602	3560	3558	3508	3597	3595	39.75	618	624	2
63	3424	3417	3392	3486	3435	3485	3478	3429	3533	3536	3532	3534	3467	3558	3588	3530	3533	3480	3569	3571	39.75	618	624	2
64	3478	3461	3471	3513	3400	3537	3537	3480	3570	3587	3547	3565	3494	3553	3613	3531	3494	3506	3587	3543	39.75	618	624	2
65	3461	3456	3428	3513	3476	3523	3522	3464	3557	3571	3540	3540	3473	3573	3597	3529	3522	3471	3574	3561	39.75	618	624	2
66	3589	3573	3542	3657	3600	3663	3647	3590	3736	3712	3660	3644	3583	3746	3715	3621	3602	3558	3706	3655	39.75	618	624	2
67	3448	3432	3435	3511	3457	3519	3479	3494	3590	3547	3546	3508	3495	3625	3585	3538	3507	3499	3606	3556	39.75	618	624	2
68	3490	3473	3463	3573	3497	3554	3522	3503	3652	3588	3577	3540	3519	3673	3613	3580	3549	3523	3672	3599	39.75	618	624	2
69	3566	3532	3511	3660	3581	3572	3535	3506	3679	3611	3554	3520	3504	3659	3585	3484	3467	3460	3561	3481	39.75	618	624	2
70	3524	3517	3488	3582	3532	3620	3624	3575	3726	3690	3623	3629	3568	3740	3709	3580	3568	3523	3636	3612	39.75	618	624	2
71	3488	3478	3453	3548	3496	3544	3526	3488	3626	3585	3547	3524	3482	3629	3622	3542	3525	3489	3616	3569	39.75	618	624	2
72	3451	3446	3419	3514	3449	3521	3509	3463	3604	3547	3550	3533	3482	3633	3583	3566	3561	3510	3646	3576	39.75	618	624	2
73	3543	3550	3517	3578	3549	3709	3711	3632	3775	3783	3755	3732	3691	3846	3791	3688	3678	3618	3730	3728	39.75	618	624	2
74	3376	3374	3411	3411	3363	3573	3538	3544	3615	3423	3621	3523	3578	3625	3476	3537	3514	3559	3566	3458	39.75	618	624	2
75	3463	3461	3429	3512	3485	3560	3565	3520	3655	3628	3595	3599	3526	3652	3658	3568	3573	3518	3617	3605	39.75	618	624	2
76	3477	3455	3474	3526	3486	3567	3543	3557	3669	3617	3592	3565	3567	3701	3653	3564	3569	3516	3584	3610	39.75	618	624	2
77	3492	3480	3461	3561	3503	3583	3569	3525	3662	3629	3628	3607	3555	3708	3682	3602	3590	3545	3675	3632	39.75	618	624	2
78	3458	3442	3446	3512	3466	3549	3526	3543	3658	3599	3578	3544	3544	3670	3630	3548	3521	3510	3616	3565	39.75	618	624	2
79	3503	3509	3465	3534	3521	3553	3562	3499	3613	3609	3519	3539	3460	3535	3584	3427	3427	3371	3464	3456	39.75	618	622	2
80	3508	3500	3468	3563	3531											3524	3528	3476	3525	3590	39.75	618	622	2
81	3533	3523	3490	3593	3554	3617	3606	3551	3673	3672	3619	3604	3539	3689	3677	3549	3543	3491	3591	3598	39.75	618	622	2
82	3557	3534	3528	3630	3556	3636	3591	3594	3736	3659	3628	3746	3555	3732	3798	3560	3529	3510	3659	3575	39.75	618	622	2

Table AII.1 (continued): Historical Thickness Data from Tylan/Tytan LPCVD Reactor

batch #	Load Centre	Load Top	Load Right	Load Flat	Load Left	C1 Centre	C1 Top	C1 Right	C1 Flat	C1 Left	C2 Centre	C2 Top	C2 Right	C2 Flat	C2 Left	Pump Centre	Pump Top	Pump Right	Pump Flat	Pump Left	t_{dep}	T_{load}	T_{pump}	PM
83	3363	3372	3330	3394	3376	3402	3418	3353	3427	3447	3414	3440	3360	3410	3466	3399	3411	3347	3429	3427	39.75	618	622	2
84						3461	3425	3567	3522	3479	3450	3401	3565	3526	3526									2
85	3378	3393	3335	3368	3430	3380	3394	3314	3401	3435	3378	3363	3324	3447	3407	3348	3357	3317	3374	3363	38.75	619	623	2
86	3391	3386	3352	3453	3407											3391	3421	3392	3515	3502	38.75	619	623	2
87	3415	3435	3383	3445	3422	3467	3490	3412	3498	3504	3484	3510	3420	3497	3532	3478	3503	3426	3489	3511	38.75	619	623	2
88	3476	3480	3427	3543	3483	3527	3581	3468	3607	3704	3546	3695	3466	3633	3721	3599	3532	3472	3626	3565	40.00	619	623	2
89	3530	3517	3473	3609	3554	3553	3555	3497	3654	3608	3545	3544	3504	3645	3593	3499	3506	3460	3561	3507	40.00	619	623	2
90	3553	3542	3497	3618	3580	3561	3541	3488	3635	3612	3576	3560	3526	3647	3614	3537	3544	3491	3580	3544	40.00	619	623	2
91	3532	3513	3477	3597	3568	3560	3532	3496	3632	3617	3573	3551	3523	3640	3617	3533	3536	3501	3581	3542	40.00	619	623	2
92	3567	3542	3507	3664	3600	3603	3562	3533	3696	3649	3599	3564	3552	3687	3664	3540	3527	3508	3612	3550	40.00	619	623	2
93	3512	3516	3473	3560	3534	3572	3573	3513	3620	3624	3592	3582	3511	3642	3652	3554	3553	3494	3605	3601	40.00	619	623	2
94	3463	3479	3434	3484	3477	3505	3498	3455	3563	3551	3520	3538	3447	3556	3570	3508	3539	3489	3472	3568	40.00	619	623	2
95	3522	3526	3484	3562	3542	3586	3582	3525	3631	3627	3606	3603	3769	3659	3663	3528	3582	3520	3634	3620	40.00	619	623	2
96	3525	3538	3486	3545	3524	3487	3501	3422	3502	3824	3452	3469	3385	3475	3500	3447	3463	3391	3469	3486	40.00	619	623	2
97	3589	3607	3562	3599	3573	3512	3533	3454	3526	3552	3448	3470	3384	3469	3496	3427	3453	3381	3431	3467	40.00	619	623	3
98	3716	3725	3676	3756	3726	3620	3627	3548	3667	3667	3497	3500	3427	3527	3554	3429	3433	3365	3466	3476	40.00	618	623	3
99	3585	3581	3551	3639	3600	3587	3587	3523	3626	3645	3533	3531	3464	3575	3597	3497	3489	3435	3543	3548	40.00	615	623	3
100	3517	3469	3488	3602	3536	3528	3511	3450	3610	3587	3556	3541	3486	3632	3606	3547	3543	3510	3586	3571	40.00	615	623	3
101	3548	3508	3500	3616	3601	3529	3504	3498	3598	3548	3547	3517	3509	3612	3576	3510	3484	3481	3575	3523	40.00	615	623	3
102	3503	3510	3462	3561	3517	3551	3545	3481	3633	3594	3553	3550	3472	3636	3606	3552	3552	3483	3608	3590	40.00	615	623	3
103	3665	3659	3628	3741	3677	3693	3823	3624	3783	3741	3628	3607	3553	3720	3686	3585	3566	3521	3674	3622	40.00	615	623	3
104	3568	3551	3540	3642	3580	3589	3553	3539	3687	3623	3576	3536	3510	3682	3616	3558	3527	3495	3655	3584	40.00	615	623	3
105	3433	3459	3400	3416	3480	3429	3462	3381	3413	3486	3429	3455	3388	3430	3478	3403	3421	3380	3415	3425	39.17	615	623	3
106	3475	3471	3449	3520	3493	3479	3454	3431	3542	3518	3458	3437	3390	3529	3509	3444	3427	3390	3511	3480	39.17	615	623	3
107	3437	3404	3382	3534	3465											3546	3531	3513	3616	3558	39.17	615	623	3
108	3572	3585	3543	3590	3599	3675	3689	3614	3640	3712	3619	3659	3593	3607	3695	3502	3526	3461	3496	3561	39.17	615	623	3
109	3564	3562	3518	3635	3582	3590	3578	3514	3670	3640	3559	3544	3477	3638	3618	3522	3516	3454	3595	3571	39.17	615	623	3
110	3571	3574	3531	3627	3592	3574	3564	3504	3639	3621	3591	3565	3492	3614	3618	3450	3439	3387	3528	3498	39.17	615	623	3
111	3474	3477	3441	3515	3490	3564	3521	3490	3583	3562	3418	3390	3357	3493	3462	3384	3362	3342	3460	3415	39.17	615	623	3
112	3439	3462	3385	3467	3476	3438	3452	3364	3468	3488	3526	3539	3471	3520	3540	3400	3425	3368	3434	3428	39.17	615	623	3
113	3452	3460	3416	3504	3466	3476	3463	3425	3549	3579	3463	3450	3545	3545	3512	3459	3452	3397	3541	3490	39.17	615	623	3
114	3481	3454	3503	3516	3485	3479	3489	3410	3488	3545	3487	3526	3466	3430	3568	3480	3421	3497	3544	3485	39.17	615	623	3
115	3432	3462	3397	3417	3483	3414	3436	3354	3425	3482	3422	3441	3369	3449	3427	3418	3432	3395	3447	3431	39.17	615	623	3
116	3436	3428	3411	3485	3443	3439	3437	3376	3530	3486	3432	3414	3352	3521	3472	3438	3424	3375	3524	3464	39.17	615	623	3
117	3442	3457	3413	3478	3453	3439	3450	3377	3486	3483	3433	3447	3366	3473	3487	3437	3451	3375	3482	3472	39.17	615	623	3
118	3482	3473	3454	3532	3494	3558	3599	3623	3683	3666	3466	3518	3634	3674	3658	3457	3458	3396	3498	3500	39.17	615	623	3
119	3518	3537	3505	3530	3526	3566	3522	3566	3623	3589	3564	3521	3531	3634	3606	3567	3582	3522	3561	3619	39.17	615	623	3
120	3501	3479	3467	3580	3510	3524	3486	3465	3624	3558	3510	3480	3428	3606	3560	3486	3459	3417	3583	3519	39.17	615	623	3
121	3589	3544	3616	3658	3556	3609	3552	3578	3724	3643	3597	3662	3522	3721	3657	3564	3564	3549	3496	3611	39.17	615	623	3
122	3432	3438	3392	3481	3438	3485	3506	3423	3518	3535	3445	3441	3364	3522	3489	3457	3463	3389	3507	3493	39.17	615	623	3
123	3441	3444	3421	3471	3442	3455	3443	3383	3534	3511	3471	3453	3412	3553	3515	3482	3480	3415	3501	3539	39.17	615	623	3

Table AII.1 (continued): Historical Thickness Data from Tylan/Tytan LPCVD Reactor

batch #	Load Centre	Load Top	Load Right	Load Flat	Load Left	C1 Centre	C1 Top	C1 Right	C1 Flat	C1 Left	C2 Centre	C2 Top	C2 Right	C2 Flat	C2 Left	Pump Centre	Pump Top	Pump Right	Pump Flat	Pump Left	t_{dep}	T_{load}	T_{pump}	PM
124	3484	3491	3456	3524	3496	3504	3510	3449	3532	3561	3483	3492	3419	3512	3547	3468	3473	3409	3506	3517	39.17	615	623	3
125	3396	3411	3365	3428	3410	3392	3417	3333	3423	3434	3373	3399	3314	3394	3425	3386	3408	3332	3407	3423	39.17	615	623	3
126	3480	3478	3444	3525	3504	3467	3449	3406	3549	3573	3438	3423	3363	3516	3494	3425	3417	3361	3494	3465	39.17	615	623	3
127	3476	3447	3487	3513	3482	3483	3437	3464	3553	3507	3451	3419	3386	3532	3495	3430	3403	3377	3506	3457	39.17	615	623	3
128	3442	3436	3427	3479	3458	3464	3446	3424	3528	3507	3456	3429	3405	3528	3508	3448	3459	3396	3466	3492	39.17	615	623	3
129	3442	3436	3427	3479	3458	3464	3446	3424	3528	3507	3456	3429	3405	3528	3508	3448	3459	3396	3466	3492	39.17	615	623	3
130	3450	3459	3411	3483	3467	3470	3469	3413	3519	3515	3454	3448	3383	3509	3509	3423	3423	3367	3470	3464	39.17	615	623	3
131	3480	3404	3441	3502	3504	3534	3548	3476	3545	3593	3534	3548	3476	3545	3593	3503	3510	3448	3523	3559	39.17	615	623	3
132	3354	3378	3338	3369	3356	3388	3414	3340	3446	3418	3381	3413	3320	3403	3422	3362	3391	3310	3399	3387	39.17	615	623	3
133	3284	3298	3260	3298	3276	3345	3368	3336	3314	3375	3369	3401	3368	3317	3404	3377	3400	3378	3339	3406	39.17	615	623	3
134	3344	3345	3337	3377	3340	3380	3370	3352	3436	3402	3390	3375	3348	3448	3419	3387	3376	3353	3440	3402	39.17	615	623	4
135	3446	3475	3408	3462	3466	3453	3484	3402	3471	3483	3461	3487	3420	3490	3484	3449	3471	3433	3476	3446	40.17	616	623	4
136	3543	3550	3535	3570	3547	3553	3559	3516	3599	3593	3540	3539	3486	3582	3574	3519	3518	3474	3556	3539	40.66	616	623	4
137	3493	3512	3486	3513	3489	3497	3527	3490	3479	3525	3485	3523	3466	3453	3517	3473	3505	3459	3461	3497	40.66	616	623	4
138	3515	3524	3507	3540	3523	3554	3576	3523	3562	3586	3557	3589	3523	3543	3598	3544	3511	3540	3577	3562	40.66	616	623	4
139	3498	3505	3495	3517	3504	3517	3539	3487	3519	3547	3510	3540	3469	3505	3546	3501	3523	3475	3493	3534	40.66	616	623	4
140	3522	3530	3510	3546	3527	3538	3557	3506	3553	3573	3554	3595	3538	3520	3598	3543	3567	3512	3533	3572	40.66	616	623	4
141	3586	3581	3576	3629	3578	3607	3588	3579	3677	3630	3608	3588	3569	3684	3639	3583	3567	3544	3649	3597	40.66	616	623	4
142	3505	3503	3479	3565	3501	3551	3535	3513	3628	3571	3557	3541	3502	3639	3586	3550	3540	3501	3626	3561	40.17	616	623	4
143	3442	3447	3460	3460	3442	3458	3480	3418	3482	3484	3465	3495	3435	3447	3502	3472	3498	3531	3455	3500	40.17	616	623	4
144	3571	3565	3554	3601	3589	3573	3614	3581	3538	3630	3553	3570	3506	3555	3605	3549	3557	3513	3550	3598	40.17	616	623	4
145	3522	3539	3492	3515	3559	3529	3561	3510	3497	3579	3539	3554	3505	3550	3573	3522	3526	3510	3556	3521	40.66	616	623	4
146	3530	3524	3522	3566	3525	3488	3496	3452	3524	3510	3469	3456	3440	3502	3502	3497	3478	3467	3525	3524	40.66	616	623	4
147	3627	3603	3648	3661	3609	3578	3558	3547	3650	3595	3552	3529	3517	3618	3572	3542	3517	3506	3606	3559	40.66	616	623	4
148	3491	3504	3442	3507	3525	3506	3525	3459	3530	3549	3528	3537	3484	3548	3562	3518	3516	3508	3547	3521	40.17	616	623	4
149	3531	3515	3539	3573	3522	3531	3498	3534	3592	3545	3512	3480	3483	3582	3534	3501	3475	3468	3567	3513	41.17	616	623	4
150	3540	3534	3544	3561	3541	3525	3543	3492	3537	3560	3487	3510	3436	3504	3521	3452	3440	3420	3495	3476	40.17	616	623	4
151	3522	3512	3529	3549	3519	3526	3518	3490	3584	3553	3520	3502	3478	3578	3555	3524	3514	3479	3573	3544	40.17	616	623	4
152	3561	3555	3548	3616	3557	3562	3552	3515	3632	3586	3551	3558	3486	3609	3585	3555	3538	3508	3616	3569	40.66	616	623	4
153	3576	3570	3563	3616	3570	3580	3572	3573	3639	3605	3571	3549	3531	3626	3602	3563	3560	3511	3620	3583	40.66	616	623	4
154	3543	3538	3540	3560	3531	3544	3568	3522	3533	3585	3541	3573	3507	3529	3581	3545	3567	3506	3544	3575	40.66	616	623	4
155	3571	3576	3552	3623	3569	3567	3583	3523	3610	3604	3599	3608	3546	3611	3607	3516	3531	3466	3551	3544	40.17	616	623	4
156	3525	3514	3537	3543	3525	3532	3508	3521	3573	3554	3528	3484	3526	3571	3553	3542	3526	3513	3583	3567	40.17	616	623	4
157	3550	3544	3536	3584	3551	3546	3553	3499	3602	3583	3528	3540	3471	3572	3570	3520	3531	3473	3539	3560	40.17	616	623	4
158	3527	3519	3509	3576	3532	3541	3502	3546	3590	3551	3550	3521	3507	3621	3580	3556	3564	3493	3599	3589	40.17	616	623	4
159	3530	3527	3528	3570	3523	3548	3531	3516	3612	3571	3556	3538	3506	3627	3589	3557	3535	3514	3617	3576	40.17	616	623	4
160	3509	3503	3505	3540	3509	3505	3533	3524	3659	3547	3483	3473	3432	3535	3523	3486	3467	3452	3530	3509	40.17	616	623	4
161	3479	3482	3460	3517	3479	3483	3477	3471	3528	3508	3477	3455	3450	3625	3576	3494	3519	3448	3589	3522	40.17	616	623	4
162	3522	3524	3508	3538	3532	3505	3522	3469	3522	3544	3485	3518	3450	3472	3529	3489	3510	3454	3486	3523	40.17	616	623	4
163	3492	3492	3476	3517	3503	3499	3509	3451	3549	3537	3508	3525	3450	3539	3552	3518	3538	3480	3519	3555	40.17	616	623	4
164	3528	3511	3517	3591	3520						3532	3504	3477	3612	3559	3527	3501	3487	3595	3539	40.17	616	623	4

Table AII.1 (continued): Historical Thickness Data from Tylan/Tytan LPCVD Reactor

batch #	Load Centre	Load Top	Load Right	Load Flat	Load Left	C1 Centre	C1 Top	C1 Right	C1 Flat	C1 Left	C2 Centre	C2 Top	C2 Right	C2 Flat	C2 Left	Pump Centre	Pump Top	Pump Right	Pump Flat	Pump Left	t_{dep}	T_{load}	T_{pump}	PM
165	3569	3545	3479	3615	3561	3567	3641	3602	3744	3598	3551	3545	3487	3641	3588	3548	3496	3550	3599	3554	40.17	616	623	4
166	3562	3566	3540	3589	3560	3567	3587	3521	3592	3601	3508	3557	3555	3563	3551	3469	3490	3440	3462	3506	40.17	616	623	4
167	3463	3475	3442	3494	3461	3562	3540	3470	3542	3536	3479	3510	3427	3492	3512	3504	3530	3454	3522	3525	40.17	616	623	4
168	3485	3494	3461	3513	3480	3483	3508	3438	3514	3516	3468	3501	3417	3490	3509	3475	3501	3433	3482	3501	40.17	616	623	4
169	3444	3447	3426	3460	3444	3465	3492	3428	3477	3501	3484	3522	3441	3488	3525	3513	3542	3470	3519	3537	40.17	616	623	4
170	3522	3510	3541	3538	3526	3514	3484	3511	3553	3536	3478	3445	3470	3524	3512	3469	3439	3455	3507	3492	40.17	616	623	4
171	3472	3474	3457	3508	3478	3495	3507	3452	3535	3534	3515	3547	3463	3536	3559	3514	3533	3469	3527	3545	40.17	616	623	4
172	3527	3530	3524	3547	3532	3539	3536	3501	3580	3571	3536	3542	3480	3579	3576	3536	3537	3485	3569	3560	40.66	616	623	4
173	3563	3560	3552	3570	3579	3570	3596	3567	3525	3626	3548	3576	3495	3555	3588	3528	3551	3552	3472	3563	40.66	616	623	4
174	3579	3581	3559	3622	3582	3591	3608	3550	3608	3633	3574	3552	3533	3636	3611	3564	3578	3517	3585	3602	40.66	616	623	4
175	3502	3486	3528	3516	3503	3523	3511	3483	3568	3547	3519	3492	3494	3565	3552	3523	3495	3504	3562	3549	40.17	616	623	4
176	3583	3578	3558	3634	3586	3587	3592	3534	3649	3628	3582	3592	3516	3641	3630	3565	3569	3507	3607	3597	40.17	616	623	4
177	3517	3527	3465	3543	3552	3519	3533	3456	3555	3566	3525	3531	3471	3574	3564	3526	3518	3496	3574	3526	40.17	616	623	4
178	3541	3528	3539	3595	3535	3557	3529	3525	3631	3577	3565	3542	3515	3650	3601	3592	3597	3531	3645	3623	40.17	616	623	4
179	3543	3532	3513	3602	3545	3549	3555	3496	3612	3592	3548	3553	3481	3607	3594	3558	3562	3495	3629	3586	40.17	616	623	4
180	3541	3535	3520	3573	3555	3552	3565	3503	3596	3592	3554	3565	3493	3582	3598	3540	3553	3486	3575	3572	40.17	616	623	4
181	3555	3544	3530	3596	3578	3560	3520	3567	3626	3571	3576	3591	3523	3565	3636	3580	3590	3520	3600	3625	40.17	616	623	4
182	3554	3546	3531	3592	3575	3607	3600	3551	3646	3637	3611	3630	3565	3597	3662	3572	3580	3518	3598	3615	40.17	616	623	4
183	3574	3564	3545	3628	3592	3618	3625	3584	3610	3677	3611	3628	3555	3612	3663	3561	3565	3500	3588	3598	40.17	616	623	4
184	3588	3576	3580	3639	3583	3608	3614	3552	3657	3647	3609	3625	3549	3629	3660	3614	3635	3621	3552	3674	40.66	616	623	4
185	3623	3625	3602	3661	3628	3682	3701	3641	3688	3728	3665	3693	3615	3668	3720	3620	3644	3590	3606	3671	40.66	616	623	4
186	3662	3659	3649	3673	3685	3655	3679	3631	3631	3713	3599	3628	3559	3582	3657	3551	3571	3531	3521	3607	40.66	616	623	4
187	3453	3459	3437	3490	3458	3514	3521	3473	3531	3534	3526	3538	3466	3505	3550	3479	3501	3430	3510	3509	39.5	616	623	4
188	3439	3440	3421	3482	3437	3455	3429	3447	3501	3477	3454	3441	3407	3508	3494	3461	3483	3427	3448	3499	39.5	616	623	4
189	3559	3528	3592	3577	3547	3563	3518	3565	3621	3573	3521	3468	3514	3586	3541	3509	3463	3499	3562	3516	39.5	616	623	4
190	3647	3640	3612	3694	3655	3648	3654	3586	3691	3689	3583	3600	3522	3608	3636	3549	3559	3503	3558	3600	40.66	616	623	4
191	3620	3615	3600	3646	3646	3627	3627	3578	3651	3675	3596	3615	3538	3617	3648	3534	3538	3504	3539	3577	40.66	616	623	4
192	3586	3590	3566	3615	3584	3614	3634	3572	3626	3649	3594	3621	3544	3604	3639	3576	3572	3534	3621	3602	40.66	616	623	4
193	3813	3809	3806	3834	3821	3834	3868	3818	3799	3886	3821	3792	3787	3875	3860	3822	3846	3782	3826	3862	44.66	615	623	4
194	3462	3474	3440	3486	3462	3491	3515	3444	3511	3520	3480	3510	3428	3496	3517	3479	3505	3436	3493	3504	40.66	615	623	5
195	3444	3449	3420	3479	3454	3476	3489	3431	3505	3517	3493	3510	3438	3517	3540	3521	3533	3473	3544	3557	40.66	615	623	5
196	3423	3435	3399	3459	3430						3493	3517	3443	3506	3539	3505	3535	3526	3461	3526	40.66	615	623	5
197	3457	3470	3442	3490	3470	3502	3516	3454	3552	3540	3516	3539	3459	3549	3562	3522	3541	3471	3554	3554	40.66	615	623	5
198	3430	3438	3402	3483	3440	3476	3487	3426	3519	3516	3492	3507	3429	3537	3537	3517	3530	3464	3553	3550	40.66	615	623	5
199	3468	3481	3445	3509	3482	3512	3529	3467	3548	3552	3518	3540	3460	3555	3563	3519	3539	3468	3546	3551	40.66	615	623	5
200	3532	3530	3502	3565	3553	3557	3566	3511	3594	3609	3543	3572	3500	3543	3614	3539	3555	3497	3562	3598	40.66	615	623	5
201	3542	3549	3501	3559	3510	3551	3562	3512	3556	3599	3527	3549	3469	3555	3573	3547	3566	3499	3565	3582	40.66	615	623	5
202	3470	3478	3436	3517	3474	3513	3523	3454	3568	3542	3519	3535	3451	3572	3558	3549	3563	3499	3563	3582	40.66	615	623	5
203	3533	3535	3502	3596	3539	3592	3575	3546	3678	3617	3589	3595	3518	3653	3641	3589	3597	3541	3599	3643	40.66	615	623	5
204	3487	3487	3457	3531	3500	3539	3548	3487	3579	3585	3543	3558	3483	3573	3597	3537	3512	3506	3605	3552	40.66	615	623	5
205	3460	3471	3438	3491	3472	3493	3513	3445	3528	3531	3495	3520	3442	3516	3541	3495	3516	3454	3502	3529	40.66	615	623	5

Table AII.1 (continued): Historical Thickness Data from Tylan/Tytan LPCVD Reactor

batch #	Load Centre	Load Top	Load Right	Load Flat	Load Left	C1 Centre	C1 Top	C1 Right	C1 Flat	C1 Left	C2 Centre	C2 Top	C2 Right	C2 Flat	C2 Left	Pump Centre	Pump Top	Pump Right	Pump Flat	Pump Left	t_{dep}	T_{load}	T_{pump}	PM
206	3568	3558	3549	3630	3568	3617	3623	3564	3638	3677	3634	3637	3560	3687	3687	3633	3637	3576	3647	3691	40.66	615	623	5
207	3545	3541	3524	3574	3549	3625		3578	3686	3653	3606	3603	3539	3678	3650	3574	3559	3530	3642	3596	40.66	615	623	5
208	3393	3391	3360	3457	3480	3416	3418	3355	3479	3452	3421	3427	3348	3494	3460	3418	3419	3354	3492	3441	39.00	615	623	5
209	3480	3501	3458	3503	3482	3505	3531	3452	3535	3535	3512	3535	3445	3556	3577	3514	3542	3472	3521	3539	40.83	616	623	5
210	3581	3580	3526	3669	3603	3585	3579	3513	3672	3622	3570	3558	3514	3652	3598	3515	3515	3484	3573	3516	40.83	616	623	5
211	3493	3511	3473	3522	3490	3519	3542	3474	3474	3533	3513	3540	3465	3538	3551	3518	3540	3463	3547	3539	40.83	616	623	5
212	3537	3567	3545	3571	3581	3586	3604	3538	3603	3625	3570	3598	3525	3523	3626	3555	3572	3527	3539	3608	40.83	616	623	5
213	3448	3448	3425	3486	3467	3507	3511	3459	3538	3554	3561	3577	3505	3569	3621	3604	3612	3547	3625	3646	40.66	615	623	5
214	3472	3480	3464	3474	3492	3505	3525	3466	3517	3545	3506	3533	3460	3510	3555	3511	3499	3472	3564	3534	40.66	615	623	5
215	3447	3453	3422	3472	3457	3522	3536	3482	3529	3566	3537	3558	3486	3544	3590	3539	3554	3498	3545	3584	40.66	615	623	5
216	3529	3527	3513	3557	3541	3564	3582	3525	3573	3603	3586	3616	3535	3596	3627	3531	3552	3489	3550	3568	40.83	616	623	5
217	3558	3560	3530	3598	3583	3583	3594	3541	3598	3644	3588	3599	3523	3620	3647	3585	3550	3575	3650	3594	40.83	616	623	5
218	3482	3475	3484	3517	3488	3564	3542	3530	3620	3578	3576	3504	3595	3611	3582	3531	3528	3475	3598	3543	40.83	616	623	5
219	3460	3457	3455	3470	3470	3508	3504	3467	3544	3537	3548	3538	3508	3597	3600	3537	3509	3526	3572	3563	40.83	616	623	5
220	3494	3492	3473	3523	3504	3556	3540	3493	3559	3672	3524	3536	3472	3590	3573	3531	3512	3497	3584	3554	40.83	616	623	5
221	3465	3474	3460	3457	3483	3500	3521	3462	3504	3536	3487	3521	3453	3465	3535	3485	3505	3446	3486	3521	40.66	615	623	5
222	3445	3455	3434	3445	3463	3501	3525	3470	3497	3540	3509	3539	3466	3498	3555	3515	3537	3483	3505	3553	40.66	615	623	5
223	3515	3514	3494	3523	3554	3582	3591	3535	3598	3639	3599	3620	3546	3594	3671	3592	3605	3568	3552	3671	40.66	615	623	5
224	3501	3505	3473	3557	3528	3551	3564	3512	3601	3594	3551	3569	3489	3581	3606	3586	3593	3523	3647	3616	40.83	616	623	5
225	3546	3525	3561	3577	3548	3581	3565	3536	3667	3608	3596	3564	3546	3684	3628	3600	3551	3592	3660	3607	40.83	616	623	5
226	3476	3494	3450	3512	3490	3526	3547	3482	3562	3565	3550	3581	3494	3570	3600	3564	3580	3508	3599	3598	40.83	616	623	5
227	3657	3631	3618	3742	3666	3567	3565	3514	3634	3607	3510	3498	3509	3558	3515	3510	3498	3509	3558	3515	40.83	616	623	5
228	3562	3562	3538	3619	3572	3603	3644	3557	3721	3686	3606	3594	3542	3726	3688	3599	3587	3539	3691	3622	40.83	616	623	5
229	3536	3559	3512	3578	3552	3600	3603	3541	3657	3628	3586	3597	3520	3657	3688	3562	3569	3514	3639	3603	40.83	616	623	5
230	3581	3580	3557	3599	3611	3619	3603	3571	3709	3643	3634	3585	3613	3716	3657	3631	3633	3567	3659	3681	40.83	616	623	5
231	3491	3507	3467	3517	3504	3536	3536	3493	3588	3569	3552	3545	3490	3616	3596	3563	3538	3541	3615	3591	40.83	616	623	5
232	3537	3535	3518	3584	3547	3599	3576	3568	3668	3622	3617	3597	3568	3710	3656	3619	3586	3568	3684	3628	40.83	616	623	5
233	3477	3493	3455	3510	3489	3519	3535	3467	3626	3553	3544	3539	3479	3609	3587	3568	3576	3507	3600	3597	40.83	616	623	5
234	3502	3514	3477	3533	3515	3592	3608	3540	3634	3629	3594	3604	3524	3646	3645	3543	3553	3491	3570	3584	40.83	616	623	5
235	3633	3633	3593	3699	3639	3694	3688	3624	3783	3727	3666	3664	3590	3757	3721	3591	3585	3520	3675	3623	40.83	616	623	5
236	3478	3475	3444	3514	3497	3541	3544	3488	3560	3593	3564	3579	3505	3564	3631	3578	3578	3511	3622	3618	40.66	615	623	5
237	3456	3468	3435	3477	3468	3527	3542	3480	3556	3563	3552	3575	3492	3581	3602	3555	3574	3504	3578	3593	40.66	615	623	5
238	3569	3569	3538	3611	3584	3631	3635	3574	3683	3674	3649	3659	3577	3690	3705	3640	3646	3580	3669	3688	40.66	615	623	5
239	3524	3532	3490	3576	3537	3609	3609	3549	3680	3642	3615	3626	3539	3682	3663	3576	3568	3519	3646	3594	40.66	615	623	5
240	3578	3579	3509	3611	3605	3620	3607	3557	3689	3664	3611	3605	3560	3674	3641	3532	3542	3506	3569	3544	40.83	616	623	5
241	3482	3489	3461	3498	3504	3547	3562	3503	3562	3591	3564	3591	3515	3550	3624	3559	3573	3506	3569	3609	40.83	616	623	5
242	3465	3476	3442	3478	3475	3539	3559	3499	3541	3575	3540	3564	3484	3538	3588	3514	3531	3466	3526	3554	40.66	615	623	5
243	3498	3511	3474	3524	3513	3572	3588	3518	3603	3606	3583	3605	3511	3613	3629	3554	3569	3493	3594	3587	40.83	616	623	5

Table AII.2: Thickness Data from Tylan/Tytan LPCVD Reactor - No Changes in Process Operating Variables from Batch to Batch

batch #	Load Centre	Load Top	Load Right	Load Flat	Load Left	C1 Centre	C1 Top	C1 Right	C1 Flat	C1 Left	C2 Centre	C2 Top	C2 Right	C2 Flat	C2 Left	Pump Centre	Pump Top	Pump Right	Pump Flat	Pump Left	t_{dep}	T_{load}	T_{pump}
1*	3658	3656	3618	3696	3671	3535	3541	3488	3572	3581	3429	3442	3368	3449	3491	3371	3381	3323	3366	3436	37.58	618	622
2*	3588	3595	3560	3636	3611	3543	3547	3496	3594	3588	3482	3490	3415	3532	3535	3426	3428	3363	3479	3465	37.58	618	622
3*	3600	3610	3585	3612	3623	3539	3552	3503	3555	3582	3472	3491	3420	3484	3527	3421	3434	3377	3426	3468	37.58	618	622
4*	3617	3624	3588	3672	3629	3612	3598	3569	3683	3643	3518	3501	3460	3597	3560	3425	3423	3381	3521	3466	37.58	617	623
5*	3515	3532	3492	3539	3532	3489	3502	3447	3521	3525	3444	3463	3386	3457	3495	3412	3429	3371	3410	3460	37.58	617	623
6*	3443	3463	3433	3443	3466	3426	3447	3392	3434	3464	3404	3431	3353	3398	3457	3412	3406	3354	3476	3440	37.58	617	624
7*	3344	3350	3333	3360	3363	3354	3375	3326	3359	3402	3362	3388	3320	3354	3421	3374	3392	3337	3370	3425	37.58	617	624
8*	3526	3534	3507	3548	3545	3533	3557	3517	3497	3599	3513	3542	3473	3487	3583	3517	3534	3483	3494	3580	39.00	618	624
9*	3528	3538	3505	3553	3543	3515	3532	3464	3545	3554	3493	3515	3434	3499	3549	3495	3510	3439	3514	3539	39.00	618	624
10	3564	3574	3542	3597	3571	3559	3541	3536	3616	3586	3543	3530	3483	3615	3584	3534	3549	3481	3551	3574	39.00	618	624
11	3453	3476	3439	3472	3463	3472	3497	3423	3494	3498	3461	3496	3408	3464	3504	3465	3491	3418	3465	3498	39.00	618	624
12	3518	3517	3507	3553	3528	3527	3500	3586	3550	3522	3487	3472	3589	3550	3525	3491	3502	3585	3541	3541	39.00	618	624
13	3562	3557	3557	3596	3574	3563	3546	3530	3630	3589	3541	3511	3496	3611	3575	3550	3527	3511	3612	3569	39.00	618	624
14	3577	3566	3558	3612	3578	3588	3566	3552	3659	3611	3552	3527	3503	3634	3586	3549	3514	3518	3617	3560	39.00	618	624
15	3573	3579	3555	3582	3605	3584	3566	3538	3649	3605	3566	3533	3522	3641	3596	3559	3565	3511	3558	3613	39.00	618	624
16	3537	3554	3511	3573	3551	3543	3538	3500	3592	3575	3524	3513	3456	3584	3567	3527	3546	3487	3519	3568	39.00	618	624
17	3553	3559	3528	3597	3572	3544	3552	3496	3596	3586	3520	3535	3462	3556	3576	3517	3522	3457	3560	3554	39.00	618	624
18	3529	3528	3523	3560	3540	3531	3522	3496	3586	3564	3535	3516	3487	3594	3574	3541	3535	3487	3591	3567	39.00	618	624
19	3600	3603	3580	3643	3610	3575	3565	3535	3641	3603	3552	3539	3494	3623	3586	3482	3468	3431	3552	3504	39.00	618	624
20	3548	3551	3527	3576	3569	3549	3558	3503	3580	3594	3530	3547	3474	3557	3591	3522	3531	3471	3533	3569	39.00	618	624
21	3507	3528	3489	3534	3514	3559	3555	3521	3603	3584	3515	3508	3450	3570	3554	3505	3532	3458	3509	3538	39.00	618	624
22	3554	3545	3544	3573	3568	3557	3554	3524	3610	3596	3513	3493	3461	3568	3554	3506	3491	3459	3559	3533	39.00	618	624
23	3634	3620	3610	3692	3641	3642	3610	3617	3721	3663	3632	3593	3584	3723	3660	3623	3598	3567	3707	3633	39.00	618	624
24	3519	3522	3502	3528	3536	3552	3572	3509	3568	3601	3556	3597	3530	3545	3636	3586	3598	3554	3550	3647	39.00	618	624
25	3524	3537	3505	3554	3538	3542	3527	3501	3596	3569	3527	3514	3464	3595	3566	3533	3549	3484	3543	3579	39.00	618	624
26	3610	3619	3589	3640	3623	3608	3600	3561	3670	3640	3533	3526	3487	3621	3585	3496	3480	3450	3562	3521	39.00	618	624
27	3575	3559	3580	3607	3580	3610	3596	3587	3705	3645	3624	3604	3570	3720	3667	3614	3583	3573	3686	3630	39.00	618	624
28	3613	3609	3578	3664	3608	3647	3661	3688	3695	3693	3596	3617	3532	3647	3661	3546	3529	3490	3626	3565	39.00	618	624
29	3519	3544	3495	3536	3525	3511	3540	3472	3518	3543	3473	3504	3417	3483	3519	3471	3501	3426	3482	3509	39.00	618	624
30	3531	3523	3519	3565	3542	3548	3531	3515	3613	3579	3558	3541	3499	3639	3599	3574	3551	3530	3638	3592	39.00	618	624

*Qualifying or Test Batches

Table AII.2 (continued): Thickness Data fromTylan/Tytan LPCVD Reactor - No Changes in Process Operating Variables from Batch to Batch

Batch #	Load Centre	Load Top	Load Right	Load Flat	Load Left	C1 Centre	C1 Top	C1 Right	C1 Flat	C1 Left	C2 Centre	C2 Top	C2 Right	C2 Flat	C2 Left	Pump Centre	Pump Top	Pump Right	Pump Flat	Pump Left	t_{dep}	T_{load}	T_{pump}
31	3557	3565	3529	3597	3582	3592	3594	3539	3633	3637	3584	3593	3515	3621	3645	3607	3613	3538	3654	3647	39.00	618	624
32	3541	3531	3523	3578	3552	3561	3540	3527	3627	3588	3572	3543	3520	3646	3605	3575	3546	3539	3642	3593	39.00	618	624
33	3557	3562	3531	3579	3573	3559	3698	3523	3628	3730	3538	3555	3473	3704	3840	3538	3530	3479	3587	3565	39.00	618	624
34	3543	3537	3518	3602	3558	3581	3561	3538	3661	3710	3602	3571	3537	3687	3631	3589	3564	3537	3665	3606	39.00	618	624
35	3511	3517	3482	3563	3533	3560	3561	3501	3614	3593	3567	3577	3497	3592	3617	3567	3575	3514	3580	3622	39.00	618	624
36	3531	3544	3523	3522	3568	3578	3590	3541	3564	3630	3588	3597	3524	3606	3642	3581	3590	3535	3578	3639	39.00	618	624
37	3562	3564	3517	3624	3568											3602	3595	3526	3688	3622	39.00	618	624
38	3515	3522	3477	3567	3533	3555	3559	3500	3608	3588	3574	3565	3493	3645	3615	3575	3565	3511	3644	3603	39.00	618	624
39	3507	3508	3479	3558	3527	3528	3495	3507	3598	3548	3549	3505	3510	3629	3575	3579	3553	3534	3662	3598	39.00	618	624
40	3574	3602	3553	3599	3577	3623	3644	3679	3584	3629	3671	3627	3656	3581	3604	3690	3633	3648	3577	3646	39.00	618	624
41	3511	3527	3486	3533	3515											3525	3538	3470	3538	3569	39.00	618	624
42	3591	3605	3562	3616	3603	3642	3649	3584	3694	3678	3622	3644	3558	3639	3674	3594	3608	3541	3606	3633	39.00	618	624
43	3543	3541	3514	3586	3554	3570	3581	3522	3598	3612	3557	3573	3493	3597	3613	3562	3573	3509	3582	3608	39.00	618	624
44	3478	3508	3455	3490	3489	3509	3542	3468	3529	3542	3498	3539	3441	3517	3546	3505	3533	3458	3515	3542	39.00	618	624
45	3504	3518	3476	3532	3524	3544	3557	3489	3578	3582	3563	3583	3490	3604	3616	3577	3588	3522	3573	3625	39.00	618	624
46	3449	3467	3415	3480	3459	3507	3529	3458	3538	3543	3559	3582	3585	3597	3608	3567	3584	3502	3618	3599	39.00	618	624
47	3537	3543	3504	3588	3562	3582	3582	3523	3641	3619	3607	3613	3532	3658	3662	3613	3618	3548	3663	3657	39.00	618	624
48	3645	3659	3627	3646	3678	3688	3709	3652	3675	3751	3665	3690	3607	3653	3736	3642	3655	3591	3632	3706	39.00	618	624
49	3546	3566	3507	3544	3590	3560	3595	3514	3569	3612	3565	3591	3532	3580	3650	3521	3543	3521	3504	3545	39.00	618	624
50	3585	3604	3554	3600	3600	3580	3604	3542	3596	3616	3523	3552	3471	3534	3576	3486	3502	3440	3492	3529	39.00	618	624
51	3513	3534	3496	3513	3537	3544	3567	3506	3569	3584	3542	3571	3493	3547	3598	3536	3555	3492	3537	3581	39.00	618	624
52	3514	3528	3492	3528	3544	3554	3569	3511	3592	3599	3573	3555	3506	3658	3615	3563	3577	3515	3565	3616	39.00	618	624
53	3576	3587	3552	3595	3596	3612	3635	3579	3623	3659	3607	3628	3542	3644	3665	3573	3586	3523	3588	3618	39.00	618	624
54	3554	3570	3498	3588	3591											3619	3640	3584	3640	3620	39.00	618	624
55	3539	3531	3514	3589	3556	3579	3560	3547	3660	3605	3594	3576	3529	3691	3630	3593	3572	3537	3682	3608	39.00	618	624
56	3466	3491	3447	3482	3481	3517	3544	3478	3538	3551	3542	3581	3495	3539	3593	3576	3602	3517	3590	3605	39.00	618	624
57	3588	3594	3564	3599	3621	3611	3619	3563	3616	3670	3601	3620	3545	3577	3682	3587	3593	3542	3573	3660	39.00	618	624
58	3527	3549	3521	3521	3546	3549	3572	3516	3552	3584	3539	3577	3513	3501	3591	3533	3560	3512	3505	3582	39.00	618	624
59						3619	3737	3562	3704	3776	3637	3636	3561	3692	3695						39.00	618	624
60	3522	3539	3514	3516	3541	3539	3558	3504	3542	3571	3520	3544	3470	3512	3572	3514	3533	3483	3503	3556	39.00	618	624

Note that blank spaces indicate missing data.

Appendix III

Components of Variance - Sample Calculations

The results of a components of variance analysis on the historical for $B = 243$ batches; $C = 4$ test wafers per batch and $W = 5$ thickness measurements per wafer.

$$V_W = \frac{\sum_{b=1}^{243}\sum_{c=1}^{4}\sum_{w=1}^{5}(y_{bcw} - \bar{y}_{bc})^2}{243 * 4(5-1)} = 2289.62 \text{ which estimates } \sigma^2_W$$

$$V_C = \frac{\sum_{b=1}^{243}\sum_{c=1}^{4}(\bar{y}_{bc} - \bar{y}_b)^2}{243(4-1)} = 1262.21 \text{ which estimates } \sigma^2_C + (\sigma^2_W/5)$$

$$V_B = \frac{\sum_{b=1}^{243}(\bar{y}_b - \bar{y})^2}{243-1} = 2633.98 \text{ which estimates } \sigma^2_B + (\sigma^2_C/4) + (\sigma^2_W/20)$$

The component variances that are estimated are then:

$\sigma^2_W = 2298.62$; $\sigma^2_C = 804.29$; $\sigma^2_B = 2318.42$

Appendix IV

Experimental Design - Phase I

Table AIV.1: Minimum Attainable Reactor Pressure for Various Flowrates of Silane and Temperature

T_c = 580°C	T_c = 610°C	T_c =640°C
Min. Pressure (mTorr)	Min. Pressure (mTorr)	Min. Pressure (mTorr)
104	121	125
160	175	183
211	222	234
250	262	276
290	299	314

Table AIV.2: Raw Data from 2^{6-2} Experimental Design - Phase I

Batch Number	Block Number	Load Centre	Load Top	Load Right	Load Flat	Load Left	C1 Centre	C1 Top	C1 Right	C1 Flat	C1 Left	C2 Centre	C2 Top	C2 Right	C2 Flat	C2 Left	Pump Centre	Pump Top	Pump Right	Pump Flat	Pump Left
1	1	4248	4255	4222	4257	4296	4794	4806	4751	4821	4885	5210	5226	5145	5241	5309	5535	5539	5492	5576	5619
2	1	2601	2610	2600	2618	2630	2646	2654	2633	2667	2678	2695	2705	2658	2693	2737	2707	2713	2681	2685	2746
3	1	2691	2706	2695	2691	2707	2864	2872	2841	2853	2876	3028	3059	2997	3021	3070	3154	3180	3146	3131	3196
4	1	2733	2746	2726	2727	2750	2892	2902	2867	2886	2911	3074	3099	3040	3070	3115	3220	3238	3203	3214	3252
5	1	2701	2713	2694	2702	2721	2868	2870	2844	2875	2891	3018	3036	2978	3023	3065	3161	3178	3134	3170	3198
6	1	177	182	175	152	163	2016	2024	2005	2021	2030	2119	2126	2095	2115	2132	2223	2222	2198	2210	2223
7	1	4004	4034	4009	4001	4042	4180	4209	4160	4184	4223	4224	4257	4187	4227	4274	4181	4208	4159	4181	4222
8	1	3159	3169	3150	3161	3195	3255	3263	3225	3273	3301	3344	3356	3301	3366	3400	3466	3473	3438	3493	3516
9	1	3387	3408	3381	3378	3415	3735	3762	3708	3739	3774	3875	3912	3832	3870	3929	3833	3863	3815	3825	3878
10	1	2025	2032	2022	2026	2039	2183	2192	2184	2209	2211	2309	2316	2287	2298	2326	2548	2566	2536	2551	2576
11	1	873	875	868	871	869	988	995	982	991	999	1957	1968	1936	1952	1974	1977	1975	1951	1962	1974
12	2	4027	4029	4020	4054	4020	4566	4592	4534	4565	4602	4955	5003	4916	4936	5013	5330	5370	5292	5327	5382
13	2	1768	927	925	1780	926	1816	1820	1793	1830	1833	1813	1812	1794	1824	1823	1836	1839	1812	1859	1853
14	2	2579	2581	2580	2585	2575	2737	2754	2717	2732	2755	2960	2985	2924	2952	2989	3156	3179	3128	3149	3181
15	2	2574	2569	2569	2594	2582	2754	2756	2722	2764	2791	3009	3016	2959	3020	3057	3225	3230	3182	3233	3271
16	2	2575	2574	2574	2581	2573	2732	2748	2712	2729	2756	2960	2984	2926	2952	2994	3166	3187	3138	3159	3195
17	2	2716	2718	2720	2734	2722	3022	3040	3005	3029	3052	3263	3295	3241	3263	3307	3507	3538	3493	3512	3550
18	2	3697	3678	3678	3734	3713	4201	4201	4139	4224	4254	4458	4476	4385	4474	4539	4550	4563	4495	4562	4626
19	2	1798	1800	1799	1806	1798	1988	1996	1980	1987	1999	2121	2128	2105	2114	2130	2277	2292	2258	2275	2295
20	2	4237	4243	4249	4254	4231	4450	4483	4432	4449	4482	4745	4794	4714	4730	4794	5115	5156	5084	5112	5155
21	2	3543	3552	3555	3564	3552	3628	3658	3620	3630	3666	3685	3728	3664	3678	3735	3715	3754	3699	3708	3756
22	2	2265	2274	2272	2288	2271	3366	3379	2440	2466	2466	2525	2548	2483	2553	2576	2621	2641	2580	2619	2639
23	2	2172	2180	2188	2197	2184	2199	2205	2201	2211	2214	2279	2292	2261	2283	2298	2517	2533	2488	2514	2537

Table AIV.3: Operating Conditions from Phase I Experiment

1	625	15	15	260	250	42.5	4961.4	116.7	2210.3	312830.4
2	595	5	5	260	250	42.5	2667.9	62.8	486.5	1790.3
3	610	10	10	220	200	40.0	2938.9	73.5	457.5	40845.7
4	610	10	10	220	200	40.0	2983.3	74.6	403.4	45670.8
5	610	10	10	220	200	40.0	2942.0	73.6	486.9	39480.6
6	595	5	15	185	150	42.5	1630.4	38.4	139.6	954531.4
7	625	5	5	235	250	37.5	4158.3	110.9	677.1	9026.0
8	625	5	15	200	150	37.5	3315.2	88.4	802.1	17309.3
9	625	15	5	185	150	42.5	3716.0	87.4	772.4	49426.4
10	595	15	15	235	250	37.5	2271.8	60.6	176.2	48800.5
11	595	15	5	200	150	37.5	1446.9	38.6	98.0	357035.3
12	625	15	15	260	250	42.5	4726.7	111.2	797.0	313961.8
13	595	5	5	185	150	37.5	1684.2	44.9	43295.7	69481.9
14	610	10	10	220	200	40.0	2859.9	71.5	291.5	64144.0
15	610	10	10	220	200	40.0	2893.9	72.4	590.7	81358.3
16	610	10	10	220	200	40.0	2860.8	71.5	309.8	67488.5
17	625	15	15	185	150	37.5	3136.4	83.6	326.0	116321.9
18	625	15	5	260	250	37.5	4232.3	112.9	1512.6	148304.8
19	595	15	15	200	150	42.5	2047.3	48.2	79.3	41130.6
20	625	5	15	235	250	42.5	4645.5	109.3	580.4	145983.3
21	625	5	5	200	150	42.5	3654.5	86.0	436.1	5753.6
22	595	15	5	235	250	42.5	2563.6	60.3	50661.2	41618.7
23	595	5	15	260	250	37.5	2297.7	61.3	140.8	23292.9

Appendix V

Sample Calculations:
Determining the Variance of $\hat{y}_k$ and $\hat{\beta}$ for Various Levels of α in a Central Composite Design

Variance of $\hat{y}_k$

In general, the predicted response at a vector of input conditions, $\mathbf{x}_k$, is

$$\hat{y}_k = \mathbf{x}_k^T \hat{\beta}$$

$$\mathrm{Var}(\hat{y}_k) = \mathrm{Var}(\mathbf{x}_k^T \hat{\beta})$$

$$\mathrm{Var}(\hat{y}_k) = \mathbf{x}_k^T \, \mathrm{Var}(\hat{\beta}) \, \mathbf{x}_k$$

$$\mathrm{Var}(\hat{\beta}) = \mathrm{Var}(\mathbf{X}^T\mathbf{X})^{-1}\mathbf{X}^T\mathbf{y}$$

$$\mathrm{Var}((\mathbf{X}^T\mathbf{X})^{-1}\mathbf{X}^T\mathbf{y}) = ((\mathbf{X}^T\mathbf{X})^{-1}\mathbf{X}^T)\mathrm{Var}(\mathbf{y})\,((\mathbf{X}^T\mathbf{X})^{-1}\mathbf{X}^T)^T$$

where Var(y) = σ^2 is the true but unknown value of the pure error variance of the response variable, y. This value, estimated by $\hat{\sigma}^2$, can be determined by the sum of squares of residuals (SSR) divided by the degrees of freedom of SSR or by the variance of the centre point replicates.

$$\mathrm{Var}((\mathbf{X}^T\mathbf{X})^{-1}\mathbf{X}^T\mathbf{y}) = ((\mathbf{X}^T\mathbf{X})^{-1}\mathbf{X}^T)\sigma^2(\mathbf{X}\,(\mathbf{X}^T\mathbf{X})^{-1})$$

$$\mathrm{Var}(\hat{\beta}) = (\mathbf{X}^T\mathbf{X})^{-1}\,\mathbf{X}^T\,\mathbf{X}\,(\mathbf{X}^T\,\mathbf{X})^{-1}\,\sigma^2$$

$$\mathrm{Var}(\hat{\beta}) = (\mathbf{X}^T\,\mathbf{X})^{-1}\,\sigma^2$$

$$\mathrm{Var}(\hat{y}_k) = \mathbf{x}_k^T\,(\mathbf{X}^T\mathbf{X})^{-1}\,\mathbf{x}_k\,\sigma^2$$

The values in Table 3.3 were determined by computing the ratios $\mathrm{Var}(\hat{\beta})/\sigma^2$ and $\mathrm{Var}(\hat{y}_k)/\sigma^2$ for various values of α in the **X** matrix.

<u>Example</u>

$\alpha = 1$

X Matrix

1	1	1	1	1	1	1	1	1	1	1	1	1	1	1	1	1	1	1	1	1	1	1	1	1	1	1	1
1	-1	1	1	1	1	1	-1	-1	-1	-1	-1	1	1	1	1	1	1	1	1	1	1	1	1	1	1	1	1
1	1	-1	1	1	1	-1	-1	1	1	1	-1	-1	-1	-1	1	1	1	-1	1	-1	-1	1	1	1	1	1	1
1	-1	-1	1	1	1	-1	1	-1	-1	-1	1	-1	-1	-1	1	1	1	-1	1	-1	-1	1	1	1	1	1	1
1	1	1	-1	1	1	-1	1	-1	1	1	-1	-1	1	1	-1	-1	-1	1	1	-1	-1	1	1	1	1	1	1
1	-1	1	-1	1	1	-1	-1	1	-1	-1	1	-1	1	1	-1	-1	-1	1	1	-1	-1	1	1	1	1	1	1
1	1	-1	-1	1	1	1	-1	-1	1	1	1	1	-1	-1	-1	-1	-1	-1	1	1	1	1	1	1	1	1	1
1	-1	-1	-1	1	1	1	1	1	-1	-1	-1	1	-1	-1	-1	-1	-1	-1	1	1	1	1	1	1	1	1	1
1	1	1	1	-1	1	-1	1	1	-1	1	-1	1	-1	1	-1	-1	1	-1	-1	1	-1	1	1	1	1	1	1
1	-1	1	1	-1	1	-1	-1	-1	1	-1	1	1	-1	1	-1	-1	1	-1	-1	1	-1	1	1	1	1	1	1
1	1	-1	1	-1	1	1	-1	1	-1	1	1	-1	1	-1	-1	-1	1	1	-1	-1	1	1	1	1	1	1	1
1	-1	-1	1	-1	1	1	1	-1	1	-1	-1	-1	1	-1	-1	-1	1	1	-1	-1	1	1	1	1	1	1	1
1	1	1	-1	-1	1	1	1	-1	-1	1	1	-1	-1	1	1	1	-1	-1	-1	-1	1	1	1	1	1	1	1
1	-1	1	-1	-1	1	1	-1	1	1	-1	-1	-1	-1	1	1	1	-1	-1	-1	-1	1	1	1	1	1	1	1
1	1	-1	-1	-1	1	-1	-1	-1	-1	1	-1	1	1	-1	1	1	-1	1	-1	1	-1	1	1	1	1	1	1
1	-1	-1	-1	-1	1	-1	1	1	1	-1	1	1	1	-1	1	1	-1	1	-1	1	-1	1	1	1	1	1	1
1	1	1	1	1	-1	-1	1	1	1	-1	-1	1	1	-1	-1	1	-1	-1	-1	-1	1	1	1	1	1	1	1
1	-1	1	1	1	-1	-1	-1	-1	-1	1	1	1	1	-1	-1	1	-1	-1	-1	-1	1	1	1	1	1	1	1
1	1	-1	1	1	-1	1	-1	1	1	-1	1	-1	-1	1	-1	1	-1	1	-1	1	-1	1	1	1	1	1	1
1	-1	-1	1	1	-1	1	1	-1	-1	1	-1	-1	-1	1	-1	1	-1	1	-1	1	-1	1	1	1	1	1	1
1	1	1	-1	1	-1	1	1	-1	1	-1	1	-1	1	-1	1	-1	1	-1	-1	1	-1	1	1	1	1	1	1
1	-1	1	-1	1	-1	1	-1	1	-1	1	-1	-1	1	-1	1	-1	1	-1	-1	1	-1	1	1	1	1	1	1
1	1	-1	-1	1	-1	-1	-1	-1	1	-1	-1	1	-1	1	1	-1	1	1	-1	-1	1	1	1	1	1	1	1
1	-1	-1	-1	1	-1	-1	1	1	-1	1	1	1	-1	1	1	-1	1	1	-1	-1	1	1	1	1	1	1	1
1	1	1	1	-1	-1	1	1	1	-1	-1	1	1	-1	-1	1	-1	-1	1	1	-1	-1	1	1	1	1	1	1
1	-1	1	1	-1	-1	1	-1	-1	1	1	-1	1	-1	-1	1	-1	-1	1	1	-1	-1	1	1	1	1	1	1
1	1	-1	1	-1	-1	-1	-1	1	-1	-1	-1	-1	1	1	1	-1	-1	-1	1	1	1	1	1	1	1	1	1
1	-1	-1	1	-1	-1	-1	1	-1	1	1	1	-1	1	1	1	-1	-1	-1	1	1	1	1	1	1	1	1	1
1	1	1	-1	-1	-1	-1	1	-1	-1	-1	-1	-1	-1	-1	-1	1	1	1	1	1	1	1	1	1	1	1	1
1	-1	1	-1	-1	-1	-1	-1	1	1	1	1	-1	-1	-1	-1	1	1	1	1	1	1	1	1	1	1	1	1
1	1	-1	-1	-1	-1	1	-1	-1	-1	-1	1	1	1	1	-1	1	1	-1	1	-1	-1	1	1	1	1	1	1
1	-1	-1	-1	-1	-1	1	1	1	1	1	-1	1	1	1	-1	1	1	-1	1	-1	-1	1	1	1	1	1	1
1	1	0	0	0	0	0	0	0	0	0	0	0	0	0	0	0	0	0	0	0	0	1	0	0	0	0	0
1	-1	0	0	0	0	0	0	0	0	0	0	0	0	0	0	0	0	0	0	0	0	1	0	0	0	0	0
1	0	1	0	0	0	0	0	0	0	0	0	0	0	0	0	0	0	0	0	0	0	0	1	0	0	0	0
1	0	-1	0	0	0	0	0	0	0	0	0	0	0	0	0	0	0	0	0	0	0	0	1	0	0	0	0
1	0	0	1	0	0	0	0	0	0	0	0	0	0	0	0	0	0	0	0	0	0	0	0	1	0	0	0
1	0	0	-1	0	0	0	0	0	0	0	0	0	0	0	0	0	0	0	0	0	0	0	0	1	0	0	0
1	0	0	0	1	0	0	0	0	0	0	0	0	0	0	0	0	0	0	0	0	0	0	0	0	1	0	0
1	0	0	0	-1	0	0	0	0	0	0	0	0	0	0	0	0	0	0	0	0	0	0	0	0	1	0	0
1	0	0	0	0	1	0	0	0	0	0	0	0	0	0	0	0	0	0	0	0	0	0	0	0	0	1	0
1	0	0	0	0	-1	0	0	0	0	0	0	0	0	0	0	0	0	0	0	0	0	0	0	0	0	1	0
1	0	0	0	0	0	1	0	0	0	0	0	0	0	0	0	0	0	0	0	0	0	0	0	0	0	0	1
1	0	0	0	0	0	-1	0	0	0	0	0	0	0	0	0	0	0	0	0	0	0	0	0	0	0	0	1
1	0	0	0	0	0	0	0	0	0	0	0	0	0	0	0	0	0	0	0	0	0	0	0	0	0	0	0

Appendix V: Sample Calculations: Determining the Variance of $\hat{y}_k$ and $\hat{\beta}$ for Various Levels of α in a Central Composite Design

$(X^TX)^{-1}$

0.055	0	0	0	0	0	0	0	0	0	0	0	0	0	0	0	0	0	0	0	0	0	-0.01	-0.01	-0.01	-0.01	-0.01	-0.01
0	0.029	0	0	0	0	0	0	0	0	0	0	0	0	0	0	0	0	0	0	0	0	0	0	0	0	0	0
0	0	0.029	0	0	0	0	0	0	0	0	0	0	0	0	0	0	0	0	0	0	0	0	0	0	0	0	0
0	0	0	0.029	0	0	0	0	0	0	0	0	0	0	0	0	0	0	0	0	0	0	0	0	0	0	0	0
0	0	0	0	0.029	0	0	0	0	0	0	0	0	0	0	0	0	0	0	0	0	0	0	0	0	0	0	0
0	0	0	0	0	0.029	0	0	0	0	0	0	0	0	0	0	0	0	0	0	0	0	0	0	0	0	0	0
0	0	0	0	0	0	0.029	0	0	0	0	0	0	0	0	0	0	0	0	0	0	0	0	0	0	0	0	0
0	0	0	0	0	0	0	0.031	0	0	0	0	0	0	0	0	0	0	0	0	0	0	0	0	0	0	0	0
0	0	0	0	0	0	0	0	0.031	0	0	0	0	0	0	0	0	0	0	0	0	0	0	0	0	0	0	0
0	0	0	0	0	0	0	0	0	0.031	0	0	0	0	0	0	0	0	0	0	0	0	0	0	0	0	0	0
0	0	0	0	0	0	0	0	0	0	0.031	0	0	0	0	0	0	0	0	0	0	0	0	0	0	0	0	0
0	0	0	0	0	0	0	0	0	0	0	0.031	0	0	0	0	0	0	0	0	0	0	0	0	0	0	0	0
0	0	0	0	0	0	0	0	0	0	0	0	0.031	0	0	0	0	0	0	0	0	0	0	0	0	0	0	0
0	0	0	0	0	0	0	0	0	0	0	0	0	0.031	0	0	0	0	0	0	0	0	0	0	0	0	0	0
0	0	0	0	0	0	0	0	0	0	0	0	0	0	0.031	0	0	0	0	0	0	0	0	0	0	0	0	0
0	0	0	0	0	0	0	0	0	0	0	0	0	0	0	0.031	0	0	0	0	0	0	0	0	0	0	0	0
0	0	0	0	0	0	0	0	0	0	0	0	0	0	0	0	0.031	0	0	0	0	0	0	0	0	0	0	0
0	0	0	0	0	0	0	0	0	0	0	0	0	0	0	0	0	0.031	0	0	0	0	0	0	0	0	0	0
0	0	0	0	0	0	0	0	0	0	0	0	0	0	0	0	0	0	0.031	0	0	0	0	0	0	0	0	0
0	0	0	0	0	0	0	0	0	0	0	0	0	0	0	0	0	0	0	0.031	0	0	0	0	0	0	0	0
0	0	0	0	0	0	0	0	0	0	0	0	0	0	0	0	0	0	0	0	0.031	0	0	0	0	0	0	0
0	0	0	0	0	0	0	0	0	0	0	0	0	0	0	0	0	0	0	0	0	0.031	0	0	0	0	0	0
-0.01	0	0	0	0	0	0	0	0	0	0	0	0	0	0	0	0	0	0	0	0	0	0.42	-0.081	-0.081	-0.081	-0.081	-0.081
-0.01	0	0	0	0	0	0	0	0	0	0	0	0	0	0	0	0	0	0	0	0	0	-0.081	0.42	-0.081	-0.081	-0.081	-0.081
-0.01	0	0	0	0	0	0	0	0	0	0	0	0	0	0	0	0	0	0	0	0	0	-0.081	-0.081	0.42	-0.081	-0.081	-0.081
-0.01	0	0	0	0	0	0	0	0	0	0	0	0	0	0	0	0	0	0	0	0	0	-0.081	-0.081	-0.081	0.42	-0.081	-0.081
-0.01	0	0	0	0	0	0	0	0	0	0	0	0	0	0	0	0	0	0	0	0	0	-0.081	-0.081	-0.081	-0.081	0.42	-0.081
-0.01	0	0	0	0	0	0	0	0	0	0	0	0	0	0	0	0	0	0	0	0	0	-0.08	-0.081	-0.081	-0.081	-0.081	0.42

The values on the diagonal represent the $Var(\hat{\beta})/\sigma^2$ for $\hat{\beta}_0$ to $\hat{\beta}_6$, $\hat{\beta}_{12}$ to $\hat{\beta}_{56}$, and $\hat{\beta}_{11}$ to $\hat{\beta}_{66}$.

The values of $Var(\hat{y}_k)/\sigma^2 = \mathbf{x}_k^T (\mathbf{X}^T\mathbf{X})^{-1} \mathbf{x}_k$ for k = 1 to 54 are listed in Table AV.1. Conditions for k = 1 to 32 represent factorial locations, k=33 to 44 represent axial locations, and k=45 to 54 represent centre point locations.

Table AV.1: $Var(\hat{y}_k)/\sigma^2$ **for k = 1 to 54**

k	$Var(\hat{y}_k)/\sigma^2$	Location	k	$Var(\hat{y}_k)/\sigma^2$	Location
1	0.676	Factorial	28	0.676	Factorial
2	0.676	Factorial	29	0.676	Factorial
3	0.676	Factorial	30	0.676	Factorial
4	0.676	Factorial	31	0.676	Factorial
5	0.676	Factorial	32	0.676	Factorial
6	0.676	Factorial	33	0.484	axial
7	0.676	Factorial	34	0.484	axial
8	0.676	Factorial	35	0.484	axial
9	0.676	Factorial	36	0.484	axial
10	0.676	Factorial	37	0.484	axial
11	0.676	Factorial	38	0.484	axial
12	0.676	Factorial	39	0.484	axial
13	0.676	Factorial	40	0.484	axial
14	0.676	Factorial	41	0.484	axial
15	0.676	Factorial	42	0.484	axial
16	0.676	Factorial	43	0.484	axial
17	0.676	Factorial	44	0.484	axial
18	0.676	Factorial	45	0.055	centre point
19	0.676	Factorial	46	0.055	centre point
20	0.676	Factorial	47	0.055	centre point
21	0.676	Factorial	48	0.055	centre point
22	0.676	Factorial	49	0.055	centre point
23	0.676	Factorial	50	0.055	centre point
24	0.676	Factorial	51	0.055	centre point
25	0.676	Factorial	52	0.055	centre point
26	0.676	Factorial	53	0.055	centre point
27	0.676	Factorial	54	0.055	centre point

Appendix VI

Experimental Design - Phase II

Table AVI.1: Raw Data From 2^{6-1} Experimental Design - Phase II

Test Number	Load Centre	Load Top	Load Right	Load Flat	Load Left	C1 Centre	C1 Top	C1 Right	C1 Flat	C1 Left	C2 Centre	C2 Top	C2 Right	C2 Flat	C2 Left	Pump Centre	Pump Top	Pump Right	Pump Flat	Pump Left
1	3188	3194	3178	3199	3195	3319	3333	3290	3318	3350	3354	3374	3310	3357	3390	3302	3318	3362	3307	3332
2	4023	4014	4007	4052	4039	4090	4090	4048	4112	4140	4038	4047	3981	4062	4097	3881	3884	3830	3919	3932
3	3526	3537	3527	3531	3524	3540	3562	3521	3538	3560	3500	3527	3478	3493	3526	3418	3439	3397	3416	3441
4	3360	3369	3362	3363	3355	3508	3527	3486	3509	3526	3587	3615	3552	3590	3614	3608	3634	3584	3606	3633
5	4247	4262	4250	4256	4248	4102	4125	4085	4104	4131	3918	3947	3894	3927	3958	3735	3758	3719	3761	3770
6	4056	4076	4062	4066	4053	3916	3947	3899	3918	3944	3728	3761	3700	3730	3759	3494	3521	3474	3497	3521
7	2947	2961	2951	2948	2946	2930	2955	2912	2928	2948	2873	2903	2847	2866	2896	2776	2802	2758	2773	2795
8	3516	3522	3517	3513	3518	3516	3534	3498	3514	3537	3463	3487	3434	3460	3488	3372	3393	3352	3368	3397
9	2748	2752	2747	2753	2748	2728	2741	2710	2728	2747	2712	2728	2684	2716	2735	2703	2713	2680	2702	2726
10	3835	3845	3833	3840	3836	3897	3914	3873	3894	3922	3862	3888	3836	3851	3895	3776	3795	3755	3773	3805
11	3378	3387	3378	3379	3379	3419	3436	3399	3410	3442	3428	3450	3396	3424	3457	3427	3446	3386	3449	3445
12	2851	2866	2842	2866	2851	2945	2964	2922	2952	2965	2968	2991	2942	2967	2996	2951	2970	2930	2944	2975
13	3616	3632	3613	3626	3622	3636	3659	3608	3644	3665	3579	3603	3544	3582	3613	3473	3491	3448	3474	3503
14	2776	2785	2779	2778	2790	2888	2906	2880	2875	2922	2886	2918	2882	2864	2932	2811	2836	2800	2798	2847
15	3565	3581	3558	3572	3562	3571	3591	3551	3565	3593	3520	3546	3495	3507	3550	3422	3445	3399	3413	3448
16	4193	4203	4217	4180	4194	4081	4102	4120	4038	4121	3962	3993	3990	3918	4010	3841	3869	3836	3829	3873
17	3992	4016	3982	4006	3985	3903	3929	3869	3919	3924	3764	3790	3719	3792	3791	3595	3623	3560	3630	3616
18	3603	3602	3583	3625	3625	3629	3632	3592	3630	3682	3582	3591	3538	3584	3642	3491	3496	3465	3475	3559
19	4110	4124	4126	4074	4138	4102	4107	4119	4066	4140	4009	4032	4041	3965	4034	3840	3871	3857	3810	3866
20	3930	3956	3917	3945	3925	3952	3975	3926	3956	3974	3873	3899	3833	3888	3905	3748	3773	3727	3763	3782
21	4848	4852	4843	4852	4878	4754	4767	4708	4778	4797	4555	4575	4505	4565	4610	4310	4325	4272	4338	4338
22	4225	4230	4222	4234	4241	4185	4197	4137	4192	4224	4098	4118	4056	4108	4170	4020	4033	3981	4044	4066
23	3522	3539	3528	3518	3513	3556	3581	3542	3545	3568	3523	3554	3495	3518	3544	3441	3469	3425	3435	3461
24	3217	3237	3203	3227	3210	3320	3341	3283	3334	3335	3313	3339	3265	3335	3341	3225	3252	3188	3245	3246
25	3618	3632	3623	3625	3619	3628	3647	3603	3644	3649	3557	3580	3525	3569	3587	3443	3462	3419	3469	3471
26	3027	3048	3035	3017	3021	3059	3082	3045	3050	3071	3041	3071	3029	3020	3064	2971	2996	2961	2955	2990
27	3042	3065	3023	3062	3041	3146	3167	3108	3172	3162	3176	3196	3130	3204	3200	3163	3185	3124	3196	3182
28	3514	3523	3509	3510	3509	3558	3574	3527	3553	3572	3531	3551	3492	3520	3556	3450	3468	3415	3460	3468
29	3161	3175	3167	3160	3155	3191	3214	3178	3188	3206	3201	3231	3177	3193	3224	3184	3210	3163	3184	3205
30	3725	3718	3703	3745	3752	3791	3778	3745	3834	3835	3685	3673	3627	3730	3742	3470	3460	3429	3520	3516
31	3313	3330	3309	3314	3323	3382	3403	3354	3386	3406	3370	3398	3334	3364	3406	3301	3324	3280	3296	3331
32	3441	3465	3413	3434	3457	3526	3558	3475	3536	3547	3567	3595	3528	3577	3576	3533	3562	3512	3538	3527
33	3774	3773	3742	3824	3790	3820	3816	3765	3862	3864	3788	3792	3723	3819	3850	3703	3704	3648	3759	3749
34	3681	3686	3635	3716	3728	3794	3806	3736	3811	3857	3847	3849	3799	3877	3895	3804	3813	3775	3858	3818
35	3567	3584	3555	3579	3572	3652	3671	3615	3665	3675	3638	3661	3592	3636	3671	3534	3554	3494	3556	3555
36	3512	3515	3515	3506	3532	3552	3562	3519	3562	3582	3553	3576	3542	3516	3619	3514	3529	3477	3535	3546
37	4015	4026	4028	3994	4036	4003	4027	3982	3995	4032	3920	3951	3884	3913	3960	3802	3828	3798	3779	3846
38	3481	3493	3479	3473	3488	3515	3533	3487	3517	3533	3477	3506	3454	3456	3510	3386	3407	3367	3378	3414
39	3521	3542	3529	3524	3522	3533	3558	3515	3532	3549	3486	3520	3456	3477	3511	3377	3406	3351	3378	3398

Table AVI.1 (continued): Raw Data From 2^{6-1} Experimental Design - Phase II

Test Number	Load Centre	Load Top	Load Right	Load Flat	Load Left	C1 Centre	C1 Top	C1 Right	C1 Flat	C1 Left	C2 Centre	C2 Top	C2 Right	C2 Flat	C2 Left	Pump Centre	Pump Top	Pump Right	Pump Flat	Pump Left
40	3666	3694	3654	3681	3665	3709	3737	3671	3734	3729	3657	3687	3603	3682	3691	3520	3550	3483	3539	3542
41	3719	3742	3716	3732	3723	3752	3777	3720	3772	3775	3712	3741	3665	3724	3745	3603	3629	3567	3619	3626
42	3773	3785	3769	3767	3784	3803	3823	3787	3784	3834	3757	3785	3718	3748	3795	3655	3678	3630	3651	3685
43*	3669	3671	3597	3721	3717	3711	3712	3662	3733	3763	3684	3685	3651	3729	3699	3574	3575	3527	3585	3626
44	3620	3631	3612	3628	3628	3699	3709	3665	3713	3725	3667	3685	3627	3666	3713	3562	3572	3535	3574	3596
45	3896	3914	3885	3897	3914	3819	3832	3783	3830	3847	3629	3648	3590	3639	3671	3393	3401	3376	3418	3423
46	4309	4321	4303	4317	4318	4398	4412	4369	4407	4431	4351	4373	4313	4362	4398	4216	4226	4195	4228	4248
47	3586	3601	3587	3581	3591	3664	3682	3639	3671	3686	3650	3675	3615	3649	3690	3556	3572	3539	3569	3584
48	4578	4592	4573	4577	4589	4657	4676	4631	4668	4688	4617	4643	4578	4625	4666	4499	4517	4487	4511	4534
49	3649	3644	3634	3661	3674	3560	3556	3528	3587	3595	3448	3450	3409	3475	3497	3326	3321	3303	3363	3370
50	3574	3595	3562	3592	3577	3634	3650	3604	3663	3655	3619	3636	3572	3647	3655	3531	3546	3498	3569	3547
51	3178	3195	3201	3160	3185	3195	3220	3202	3181	3213	3167	3202	3163	3148	3195	3079	3099	3081	3068	3098
52	2868	2882	2868	2858	2869	3025	3041	3008	3021	3038	3112	3133	3083	3110	3136	3132	3145	3128	3122	3150
53	3584	3605	3577	3583	3588	3635	3655	3616	3642	3653	3616	3647	3588	3623	3649	3518	3539	3506	3532	3537
54	3065	3065	3059	3058	3080	3212	3212	3186	3216	3241	3266	3277	3229	3277	3311	3227	3226	3208	3236	3261
55	3293	3301	3317	3273	3308	3311	3323	3335	3283	3345	3305	3332	3308	3280	3344	3285	3292	3302	3263	3318
56	4321	4333	4338	4293	4347	4217	4220	4229	4196	4251	4155	4167	4182	4108	4183	4059	4083	4082	4027	4098
57	4311	4321	4333	4276	4334	4183	4189	4199	4160	4217	4102	4125	4136	4044	4126	4010	4039	4038	3978	4038

* Start of Runs from Second PM Cycle

Table AVI.2: Operating Conditions and Derived Data from Phase II Experiments - First Block

Test	Tc	R_1	R_2	P	F	tdep	TH	DR	WWV	CLV	LTH	C1TH	C2TH	PTH	LDR	C1DR	C2DR	PDR	LWWV	C1WWV	C2WWV	PWWV
1	614	7	3	200	225	42	3298.5	78.54	508	5310	75.97	79.10	79.93	79.15	75.97	79.10	79.93	79.15	67	489	899	579
2	626	7	3	240	225	38	4014.3	105.64	1211	7567	105.97	107.79	106.45	102.35	105.97	107.79	106.45	102.35	339	1142	1786	1580
3	620	5	5	220	200	40	3500.1	87.50	276	2902	88.23	88.61	87.62	85.56	88.23	88.61	87.62	85.56	27	290	456	332
4	614	7	7	240	225	42	3519.4	83.80	351	12889	80.04	83.60	85.51	86.02	80.04	83.60	85.51	86.02	26	280	660	439
5	626	3	7	240	175	42	4194.5	99.87	637	11538	103.01	100.54	99.02	96.90	103.01	100.54	99.02	96.90	437	398	947	767
6	626	3	3	200	175	42	3806.1	90.62	383	59155	96.73	93.45	88.94	83.37	96.73	93.45	88.94	83.37	82	413	637	398
7	614	3	7	200	175	38	2725.1	71.71	220	338	72.36	71.86	71.45	71.18	72.36	71.86	71.45	71.18	7	204	385	286
8	620	5	5	220	200	40	3470.0	86.75	228	4448	87.93	88.00	86.66	84.41	87.93	88.00	86.66	84.41	11	255	498	346
9	614	3	3	240	175	38	2885.8	75.94	291	5837	77.65	77.23	75.71	73.18	77.65	77.23	75.71	73.18	37	293	519	314
10	626	7	7	200	225	38	3846.3	101.22	347	2481	100.99	102.63	101.75	99.49	100.99	102.63	101.75	99.49	23	364	616	384
11	614	3	7	200	225	42	3415.8	81.33	402	502	80.48	81.46	81.69	81.68	80.48	81.46	81.69	81.68	15	319	580	696
12	614	7	7	240	175	38	2932.9	77.18	308	2723	75.14	77.62	78.23	77.74	75.14	77.62	78.23	77.74	111	308	469	346
13	620	5	5	220	200	40	3581.6	89.54	426	5279	90.55	91.06	89.61	86.95	90.55	91.06	89.61	86.95	58	503	708	434
14	614	7	3	200	175	38	2847.7	74.94	418	3170	73.20	76.16	76.22	74.17	73.20	76.16	76.22	74.17	33	380	775	484
15	614	3	3	240	225	42	3522.7	83.87	354	4641	84.94	85.10	83.90	81.56	84.94	85.10	83.90	81.56	82	317	576	439
16	626	3	7	240	225	38	4028.5	106.01	769	22353	110.46	107.69	104.59	101.31	110.46	107.69	104.59	101.31	187	1190	1298	402
17	626	3	3	200	225	38	3820.3	100.53	646	29079	105.16	102.86	99.24	94.86	105.16	102.86	99.24	94.86	208	590	989	799
18	620	5	5	220	200	40	3581.3	89.53	1015	3289	90.19	90.83	89.69	87.43	90.19	90.83	89.69	87.43	316	1027	1369	1347
19	626	7	3	240	175	42	4021.6	95.75	729	15107	97.96	97.78	95.62	91.64	97.96	97.78	95.62	91.64	609	735	964	610
20	626	7	7	200	175	42	3882.4	92.44	486	7758	93.68	94.20	92.37	89.49	93.68	94.20	92.37	89.49	247	400	827	471
21	626	3	3	240	225	42	4623.5	110.08	876	56568	115.59	113.35	108.62	102.78	115.59	113.35	108.62	102.78	185	1120	1445	755
22	626	3	7	200	225	42	4139.1	98.55	934	7694	100.72	99.69	97.86	95.92	100.72	99.69	97.86	95.92	56	1000	1682	999
23	620	5	5	220	200	40	3513.9	87.85	309	2216	88.10	88.96	88.17	86.16	88.10	88.96	88.17	86.16	101	264	535	335
24	614	7	3	240	175	42	3272.8	77.92	610	2953	76.64	79.11	79.01	76.93	76.64	79.11	79.01	76.93	182	549	1023	689
25	626	7	7	240	175	38	3568.5	93.91	370	6840	95.35	95.64	93.78	90.86	95.35	95.64	93.78	90.86	31	373	595	479
26	614	3	3	200	225	38	3027.7	79.68	296	1360	79.73	80.56	80.13	78.28	79.73	80.56	80.13	78.28	152	230	484	319
27	614	7	7	200	175	42	3137.2	74.70	677	3668	72.54	75.02	75.74	75.48	72.54	75.02	75.74	75.48	296	673	935	803
28	620	5	5	220	200	40	3513.0	87.83	386	1891	87.83	88.92	88.25	86.31	87.83	88.92	88.25	86.31	36	358	666	487
29	614	3	7	240	225	38	3188.4	83.90	280	260	83.25	84.09	84.35	83.93	83.25	84.09	84.35	83.93	59	209	495	356
30	626	7	3	200	175	38	3673.9	96.68	1380	18504	98.12	99.91	97.14	91.55	98.12	99.91	97.14	91.55	399	1478	2144	1498
31	615.5	5	5	220	200	40	3346.2	83.66	443	1507	82.95	84.66	84.36	82.66	82.95	84.66	84.36	82.66	73	432	829	437
32	620	5	5	205	200	40	3518.4	87.96	600	2784	86.05	88.21	89.22	88.36	86.05	88.21	89.22	88.36	415	1034	618	333
33	620	5	5	220	200	41.5	3778.3	91.04	1676	1931	91.10	92.18	91.43	89.46	91.10	92.18	91.43	89.46	891	1649	2210	1954
34	620	5	5	235	200	40	3789.3	94.73	1353	4680	95.34	96.34	95.02	92.23	95.34	96.34	95.02	92.23	840	1327	1884	1310
35	620	6.5	5	220	200	40	3601.3	90.03	588	2963	89.29	91.39	90.99	88.47	89.29	91.39	90.99	88.47	126	591	931	705
36	620	5	6.5	220	200	40	3538.2	88.46	713	405	87.90	88.89	89.03	88.01	87.90	88.89	89.03	88.01	94	533	1510	717
37	624.5	5	5	220	200	40	3941.0	98.52	588	9187	100.50	100.20	98.14	95.27	100.50	100.20	98.14	95.27	264	452	937	697
38	620	5	5	220	200	38.5	3467.7	90.07	378	2858	90.46	91.35	90.41	88.06	90.46	91.35	90.41	88.06	61	354	709	388
39	620	5	5	220	181.3	40	3484.3	87.11	370	4990	88.19	88.44	87.25	84.55	88.19	88.44	87.25	84.55	74	277	671	459
40	620	5	3.5	220	200	40	3644.7	91.12	764	6548	91.80	92.90	91.60	88.17	91.80	92.90	91.60	88.17	244	752	1338	721
41	620	3.5	5	220	200	40	3703.0	92.57	593	4144	93.16	93.98	92.94	90.22	93.16	93.98	92.94	90.22	112	580	1034	647
42	620	5	5	220	218.8	40	3750.6	93.76	496	3921	94.39	95.16	94.02	91.50	94.39	95.16	94.02	91.50	71	482	941	489

Table AVI.2: Operating Conditions and Derived Data from Phase II Experiments - Second Block

Test	T_c	R_1	R_2	P	$F_{S,H4}$	t_{dep}	TH	DR	WWV	CLV	LTH	C1TH	C2TH	PTH	LDR	C1DR	C2DR	PDR	LWWV	C1WWV	C2WWV	PWWV
43	620	5	5	220	200	40	3641.4	91.03	513	3342	3623.8	3702.2	3671.6	3567.8	90.60	92.56	91.79	89.20	60	519	984	490
44	626	3	3	240	175	38	3690.3	97.11	497	49198	3901.2	3822.2	3635.4	3402.2	102.66	100.58	95.67	89.53	159	580	885	364
45	626	7	3	200	225	42	4324.8	102.97	480	5886	4313.6	4403.1	4359.4	4222.6	102.70	104.84	103.80	100.54	55	515	976	373
46	620	5	5	220	200	40	3619.4	90.48	379	2493	3589.2	3668.4	3655.8	3564.0	89.73	91.71	91.40	89.10	56	346	821	295
47	626	7	7	240	225	42	4595.3	109.41	481	4296	4581.8	4664.0	4625.8	4509.6	109.09	111.05	110.14	107.37	68	469	1069	319
48	626	3	7	200	175	38	3502.5	92.17	717	18558	3652.4	3565.2	3455.8	3336.6	96.12	93.82	90.94	87.81	240	715	1088	824
49	620	5	5	220	200	40	3596.3	89.91	626	2051	3580.0	3641.2	3625.8	3538.2	89.50	91.03	90.65	88.46	185	545	1087	689
50	614	3	3	200	175	42	3161.5	75.27	296	2670	3183.8	3202.2	3175.0	3085.0	75.80	76.24	75.60	73.45	256	234	517	177
51	614	7	7	200	225	38	3036.5	79.91	211	14646	2869.0	3026.6	3114.8	3135.4	75.50	79.65	81.97	82.51	73	179	456	138
52	620	5	5	220	200	40	3594.7	89.87	297	2501	3587.4	3640.2	3624.6	3526.4	89.69	88.43	89.50	91.71	112	250	628	197
53	614	7	3	240	225	38	3195.6	84.09	424	8049	3065.4	3213.4	3272.0	3231.6	80.67	84.56	86.11	85.04	77	381	864	373
54	614	3	7	240	175	42	3305.9	78.71	474	70	3298.4	3319.4	3313.8	3292.0	78.53	79.03	78.90	78.38	280	577	624	417
55	626	3	7	240	175	42	4158.0	99.00	364	15568	4315.0	4189.6	4106.6	4020.6	102.74	99.75	97.78	95.73	565	440	1380	718

Appendix VII:

Individual Wafer Models

This appendix deals with the models obtained from fitting thickness, deposition rate, and within-wafer variance data on a per wafer basis. These models were used to better understand how the operating variables affect the process, and to verify results of optimization runs in Chapter Four. In Chapter Four, the overall models were used to determine the optimal operating conditions. An alternative to using the four overall models in the optimization routine would be to use the twelve individual models to determine the optimal operating conditions. Using the four overall models greatly simplifies the optimization problem. The individual wafer models were then used to check if the results obtained using the overall models compare well with those predicted by the individual models.

For the sake of brevity, the models are presented with a brief summary of the results. As was the case with the overall models, all models were tested for lack of fit using standard lack of fit tests. The significance of the F-value is indicated in parentheses. Also noted are the R^2 values. Residual plots are presented following the discussion of the individual models.

AVII.1: Thickness Models of Load, C1, C2 and Pump Zones

$$\begin{aligned} LTH = (&0.000278 - 0.000039X1 + 0.000005X2 + 0.000002X3 \\ &-0.000008X4 - 0.000010X5 - 0.000015X6 \\ &+0.000003X1X6 + 0.000007X3^2)^{-1} \end{aligned} \qquad \text{(AVII. 1)}$$

No significant lack of fit (0.08)

R^2 = 0.98

Centre temperature, X1, has the strongest influence on the Load thickness. It is interesting to note that the relationship between Load zone thickness and the process operating variables is not linear. Also, X3, back-end temperature ramp, strongly affects the film thickness in the Load zone. At low back-end temperature ramps, there is an increase in Load zone thickness and an increase when the back-end temperature ramp is steep. This is a surprising result since the reactants enter via the front end of the tube. When the back-end temperature ramp is large, the Pump zone temperature is high compared to the Load and centre zone temperatures. At high Pump zone temperatures, the reaction rate is high thereby causing an increase in pressure (due to stoichiometry). High pressures also increase the reaction rate. Because the pressure is maintained using a pressure controller, the pump will have to pump the reactants out at a faster rate in order to maintain pressure. This will cause increased movement of the reactant to the Pump end of the tube where the temperatures are high thereby depositing thicker films.

As with the overall thickness model, X4, X5 and X6, (pressure, silane flowrate and deposition time, respectively), all have significant effects on the Load zone thickness for the same reasons laid out in section 3.4.1.

$$\begin{aligned} C1TH = 3631.7 + 442.7X1 - 28.7X3 + 96.6X4 + 151.5X5 \\ +194.6X6 + 36.7X1X5 - 26.9X2X4 + 26.5X4X6 \end{aligned} \qquad \text{(AVII. 2)}$$

No significant lack of fit (0.15)

$R^2 = 0.97$

The interesting aspect of this model is that the front-end temperature ramp does not affect the thickness in zone C1, but the back-end temperature does influence the thickness in zone C1. It is likely that the reasons for the significance of the back-end temperature ramp are the same as for the Load thickness. The reason the front-end temperature ramp does *not* effect C1 thickness may be because the front-end temperature zone is too far from the C1 wafer to have an effect.

The other factors that influence C1 thickness (X1, X4, X5 and X6) are important for the same reasons stated in the explanation of the overall thickness model.

$$\begin{aligned} C2TH = 3593.1 + 389.6X1 + 29.3X2 + 92.9X4 \\ +164.2X5 + 196.4X6 + 33.0X1X5 + 28.9X4X6 \end{aligned} \qquad \text{(AVII.3)}$$

No significant lack of fit (0.24)

$R^2 = 0.96$

The interesting aspect of this model is that the front-end temperature ramp, X2, has an effect on C2 zone thickness, and the back-end temperature ramp, X3, has no effect. It should be noted at this time that the models and the model building process were thoroughly checked to ensure that the data were not switched. The effect of X2 on C2 thickness was expected, since X2 dictates the temperature in the Load zone. A higher temperature in the Load zone will cause more depletion of reactant in the Load zone leaving less reactant to react in the end zones of the reactor. This is why X2 has a positive effect on C2 thickness. When X2 is large, the difference between the centre and Load zone temperatures will be large. Therefore T_{load} will be small compared to T_{centre} so that the depletion of reactant in the front end of the reactor will be relatively small. The reason X3 does not have an effect on C2 thickness is likely due the fact that the back-end temperature zone is too far from the C2 wafer to have a significant effect.

$$\begin{aligned} PTH &= 3500.7 + 336.5X1 + 39.1X2 + 36.6X3 \\ &+ 87.3X4 + 174.3X5 + 198.1X6 + 30.9X1X5 + 29.6X4X6 \end{aligned} \quad \text{(AVII.4)}$$

No significant lack of fit (0.17)

$R^2 = 0.96$

Like the Load zone thickness model, all the operating parameters have a significant effect on the Pump zone thickness. The X1, X4, X5 and X6 were expected to have an effect on Pump zone thickness, since these parameters are global parameters in the sense that they effect the entire reactor. As was the case with C2 zone thickness, X2 has an effect on Pump zone thickness for the same reasons it effects C2 zone thickness. X3 also effects the Pump zone thickness because it dictates the temperature in the Pump zone. It is interesting to note that the front temperature ramp has a greater effect on Pump thickness than does the back-end temperature ramp. This may be because the Pump zone thermocouple is 20 cm away from the Pump zone wafer (cf. Figure 2.3). This would indicate that the concentration of reactant in the Pump zone (controlled in part by the front-end temperature ramp) has a greater effect on the Pump thickness than the back-end temperature ramp.

The effect of silane flowrate, X5, increases with position along the tube. This agrees with the literature (Kamins, 1988). At the front of the reactor, the concentration of reactant is high regardless of the flowrate. However, towards the back of the reactor, the concentration of reactant decreases, therefore a higher flowrate is needed to achieve the same deposition rate as in the front of the tube. Thus, X5 has a more significant impact on thickness and deposition rate as position from gas inlet increases.

AVII.2: Deposition Rate Models of Load, C1, C2 and Pump Zones

$$LDR = 90.0 + 12.3X1 - 1.6X2 - 0.7X3 + 2.6X4 + 3.3X5 + 0.9X1X5 - 0.7X2X4 + 0.6X4X5 \quad \text{(AVII. 5)}$$

Moderately significant lack of fit (0.04)

$R^2 = 0.98$

$$C1DR = 90.7 + 11.1X1 - 0.7X3 + 2.4X4 + 3.8X5 + 0.9X1X5 - 0.7X2X4 \quad \text{(AVII.6)}$$

No significant lack of fit (0.21)

$R^2 = 0.97$

$$C2DR = 89.8 + 9.8X1 + 0.7X2 + 2.3X4 + 4.1X5 + 0.8X1X5 \quad \text{(AVII.7)}$$

No significant lack of fit (0.21)

$R^2 = 0.96$

$$PDR = 88.3 + 8.4X1 + 1.0X2 + 0.9X3 + 2.2X4 + 4.3X5 + 0.7X1X5 - 1.2X5^2 \quad \text{(AVII.8)}$$

No significant lack of fit (0.61)

$R^2 = 0.95$

There is significant lack of fit in the Load deposition rate model (LDR) at the 95% level but not at the 99% level indicating only moderate lack of fit. This is odd because there is no sign of lack of fit in the deposition rate models for the C1, C2 and Pump zones. It is interesting to note that the Load thickness model shows very slight signs of lack of fit. It may be more difficult to model thickness and deposition rate in the Load zone since the reactant enters the tube from the Load zone thus causing a disturbance. Since the lack of fit is moderate, it was not investigated further.

Like the overall deposition rate model, the zone deposition rate models are all independent of deposition time. The explanation of the effects of the X1, X2, X3, X4 and X5 are analogous to those given for the zone thickness models.

AVII.3: Within Wafer Variance Models of Load, C1, C2 and Pump Zones

$$\log(LWWV) = 4.7 + 0.4X1 - 0.5X5X6 - 1.9X4^2 - 1.9X5^2 \qquad \text{(AVII.9)}$$

No significant lack of fit (0.53)

$R^2 = 0.31$

$$C1WWV = (0.05 - 0.008X1 + 0.004X1X6 + 0.004X2X3 - 0.020X4^2 + 0.022X5^2)^{-1/2} \qquad \text{(AVII.10)}$$

No significant lack of fit (0.67)

$R^2 = 0.44$

$$C2WWV = (0.035 - 0.005X1 + 0.003X2X3)^{-1/2} \qquad \text{(AVII.11)}$$

No significant lack of fit (0.64)

$R^2 = 0.34$

$$PWWV = (0.046 - 0.005X1 + 0.004X1X6 + 0.005X2X3 + 0.004X2X5 - 0.004X3X6)^{1/2} \qquad \text{(AVII.12)}$$

No significant lack of fit (0.86)

$R^2 = 0.43$

As was the case with the overall within-wafer variance model, the R^2 values are quite low for within-wafer models for the Load, C1, C2 and Pump zones. Unlike the overall within-wafer variance model, the Load and C1 zone models have quadratic terms. Also, X4, pressure, effects the within-wafer variance only at the front end of the tube. Silane flowrate, X5, also has a very significant effect on the front end of the tube arising as a quadratic term in both the Load and C1 within-wafer variance models. Although X5 appears in the Pump zone model, it acts as an interaction term.

Within-wafer variance in the back end of the tube (zones C2 and Pump) is controlled largely by temperature, evidenced by the frequent appearance of the temperature terms X1, X2 and X3.

In all four models, (AVII.9), (AVII.10), (AVII.11) and (AVII.12), within-wafer variance is minimized at low X1. This is consistent with the overall within-wafer variance model. Equations (AVII.10), (AVII.11) and (AVII.12) all contain an X2X3 interaction term. In all three models, within-wafer variance is reduced when either both X2 and X3 are low or when both are high. This also agrees with the overall within-wafer variance model.

Residual Plots from Individual Wafer Models

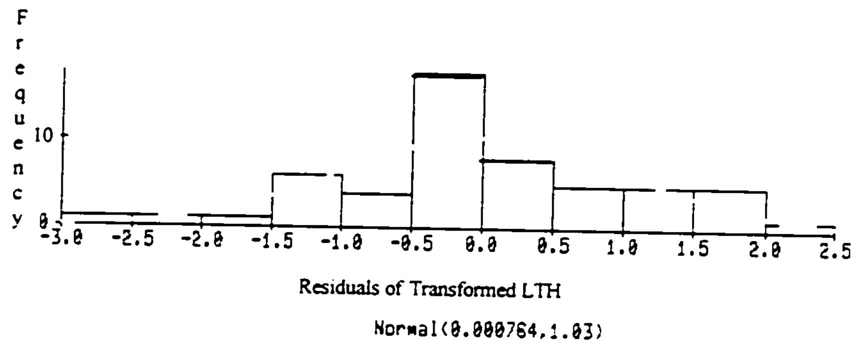

Figure AVII.1: Histogram of Residuals from Load Thickness (LTH) Model

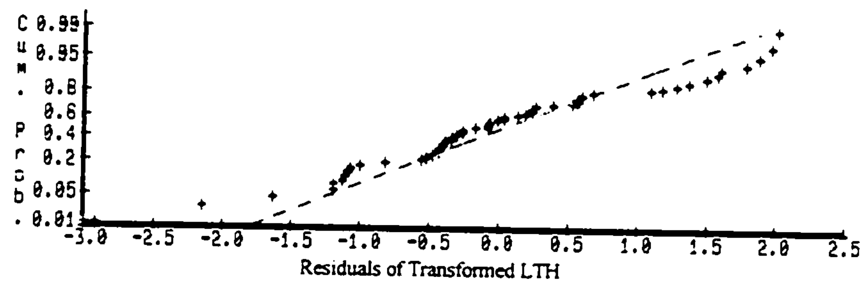

Figure AVII.2: Cumulative Probability Plot of Residuals from Load Thickness (LTH) Model

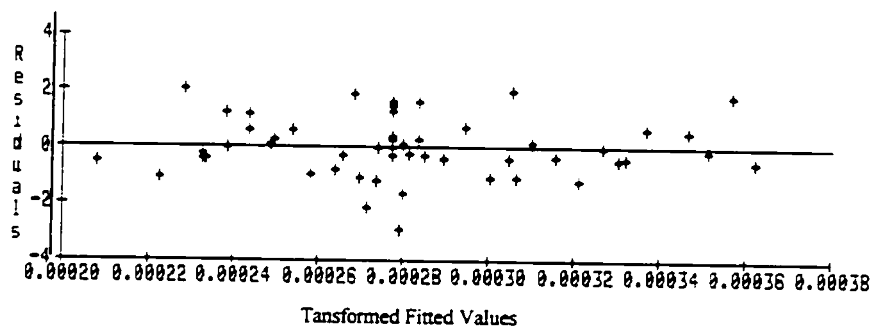

Figure AVII.3: Residuals versus Fitted Values for Load Thickness (LTH) Model

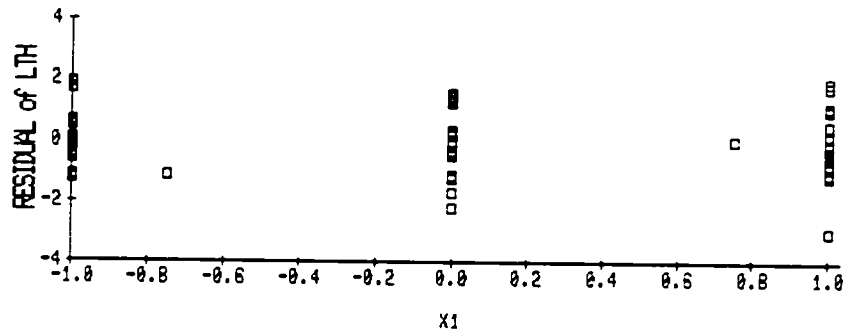

Figure AVII.4: Residuals versus X1 for Load Thickness (LTH) Model

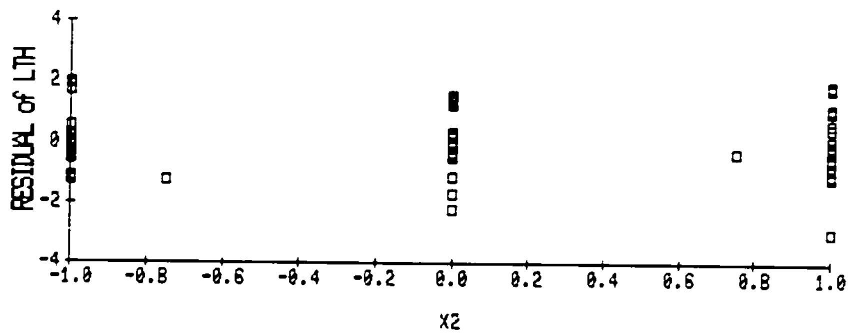

Figure AVII.5: Residuals versus X2 for Load Thickness (LTH) Model

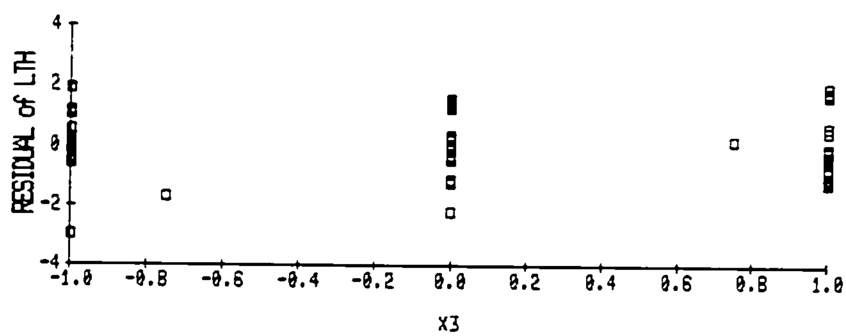

Figure AVII.6: Residuals versus X3 for Load Thickness (LTH) Model

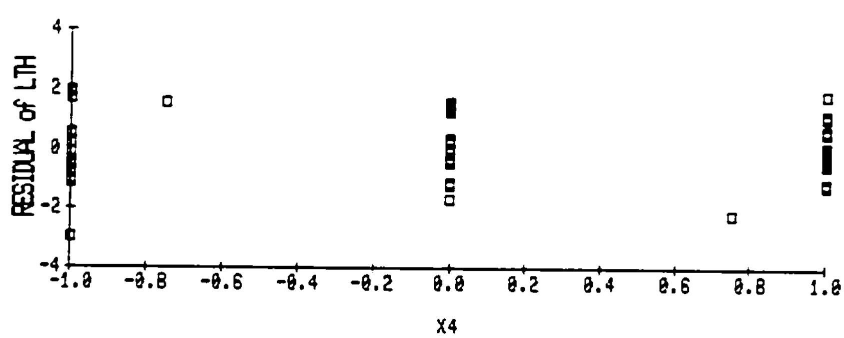

Figure AVII.7: Residuals versus X4 for Load Thickness (LTH) Model

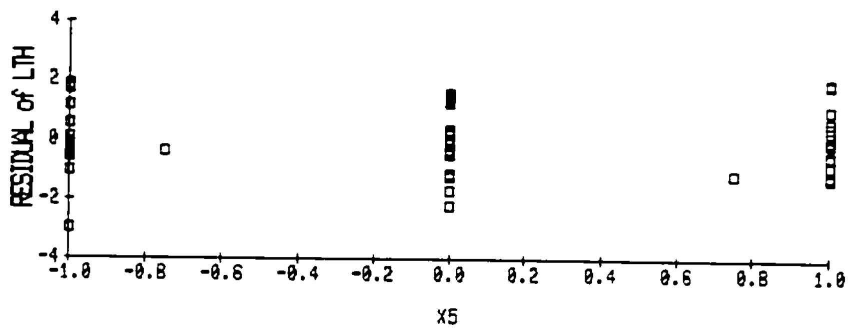

Figure AVII.8: Residuals versus X5 for Load Thickness (LTH) Model

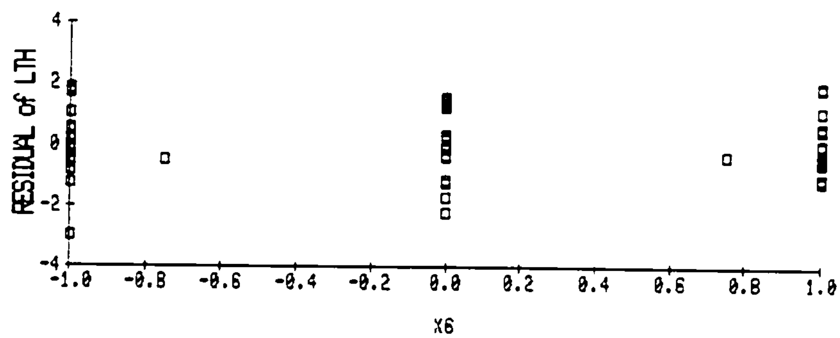

Figure AVII.9: Residuals versus X6 for Load Thickness (LTH) Model

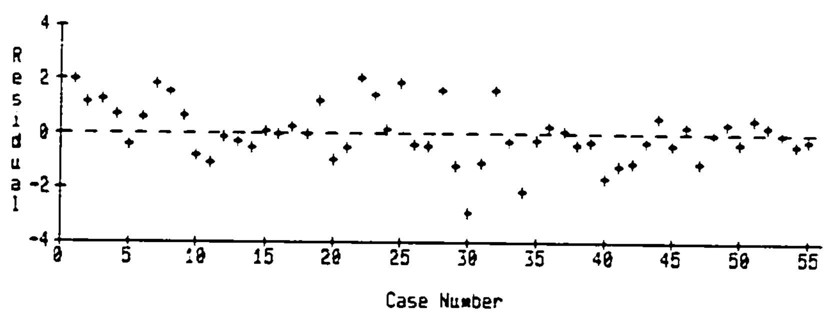

Figure AVII.10: Time Series Plot of Residuals from Load Thickness (LTH) Model

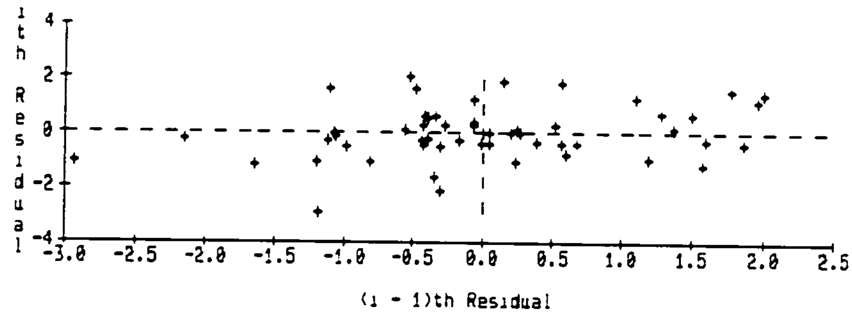

Figure AVII.11: Lag-1 Plot of Residuals from Load Thickness (LTH) Model

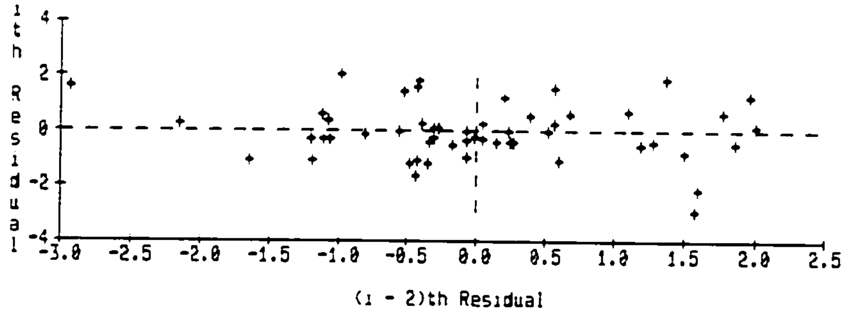

Figure AVII.12: Lag-2 Plot of Residuals from Load Thickness (LTH) Model

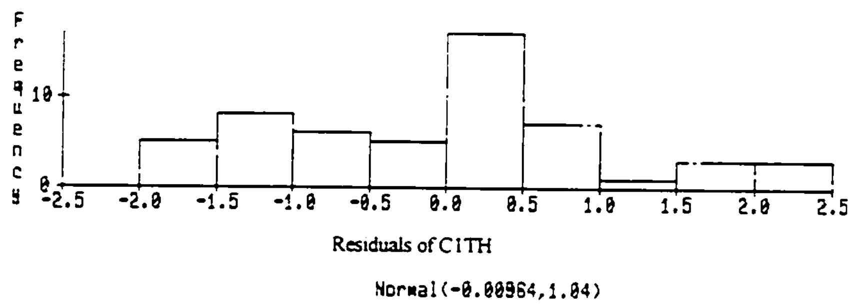

Figure AVII.13: Histogram of Residuals from C1 Thickness (C1TH) Model

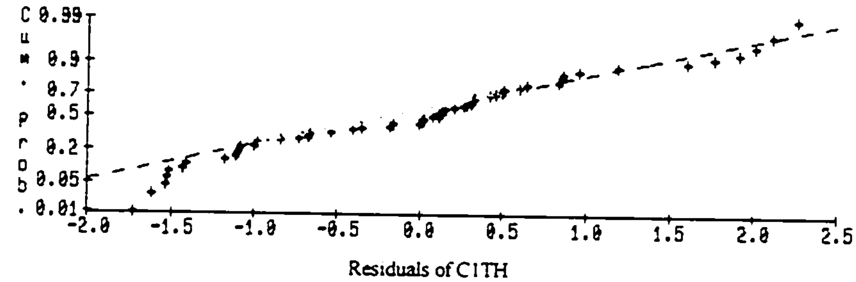

Figure AVII.14: Cumulative Probability Plot of Residuals from C1 Thickness (C1TH) Model

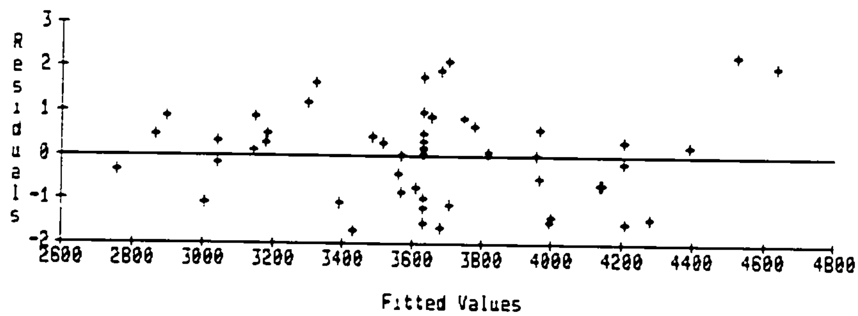

Figure AVII.15: Residuals versus Fitted Values for C1 Thickness (C1TH) Model

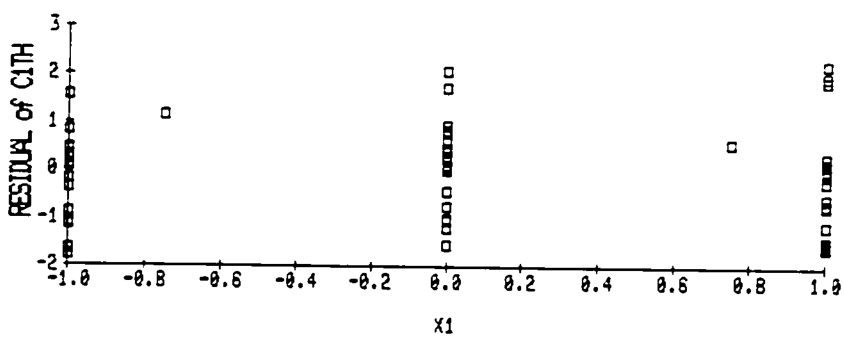

Figure AVII.16: Residuals versus X1 for C1 Thickness (C1TH) Model

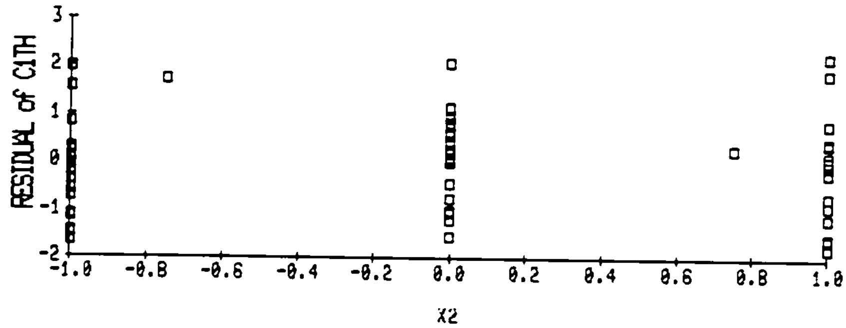

Figure AVII.17: Residuals versus X2 for C1 Thickness (C1TH) Model

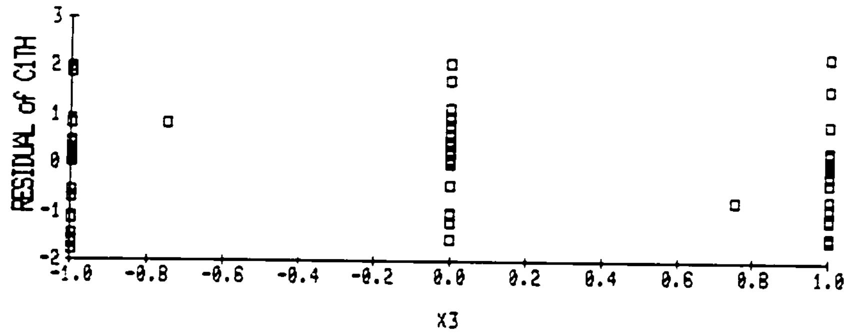

Figure AVII.18: Residuals versus X3 for C1 Thickness (C1TH) Model

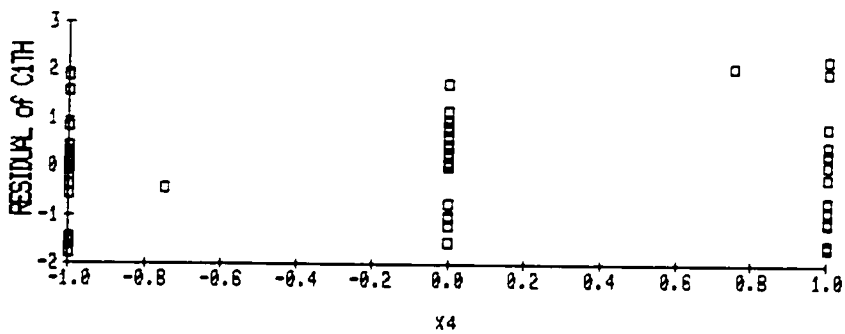

Figure AVII.19: Residuals versus X4 for C1 Thickness (C1TH) Model

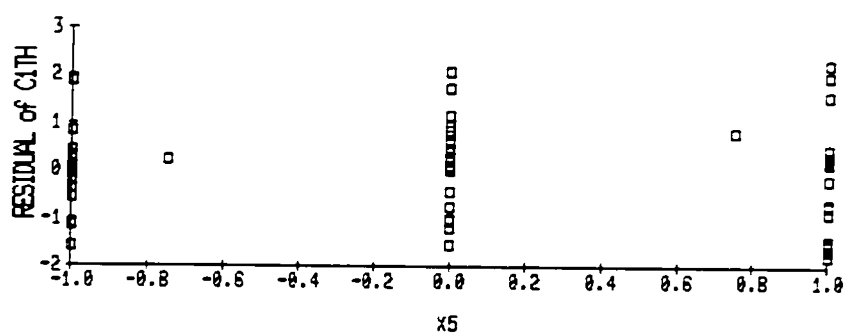

Figure AVII.20: Residuals versus X5 for C1 Thickness (C1TH) Model

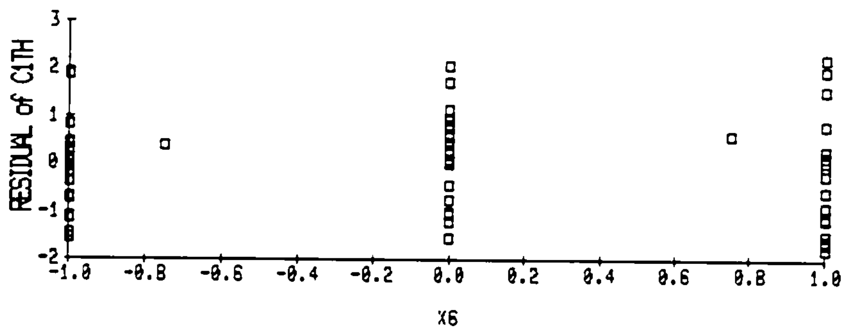

Figure AVII.21: Residuals versus X6 for C1 Thickness (C1TH) Model

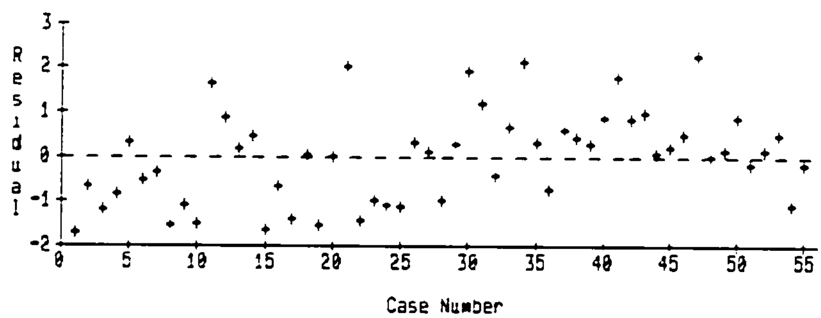

Figure AVII.22: Time Series Plot of Residuals from C1 Thickness (C1TH) Model

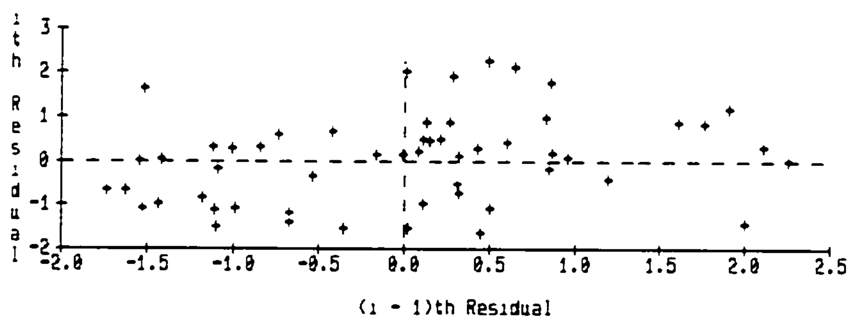

Figure AVII.23: Lag-1 Serial Plot of Residuals from C1 Thickness (C1TH) Model

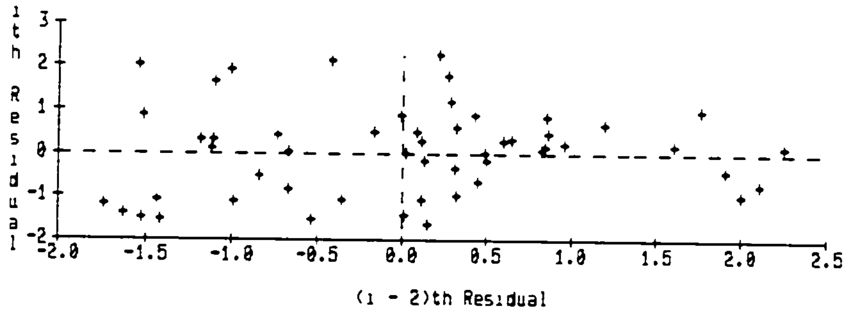

Figure AVII.24: Lag-2 Serial Plot of Residuals from C1 Thickness (C1TH) Model

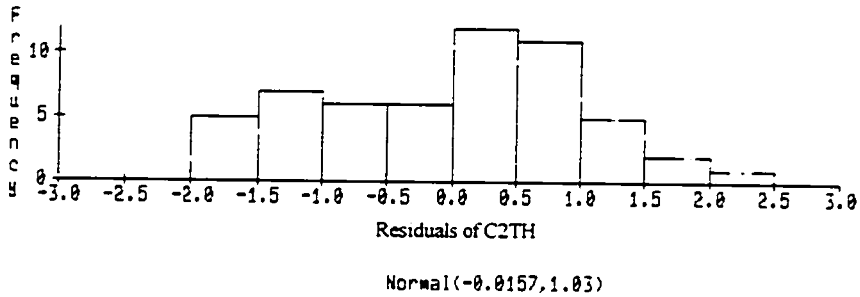

Figure AVII.25: Histogram of Residuals from C2 Thickness (C2TH) Model

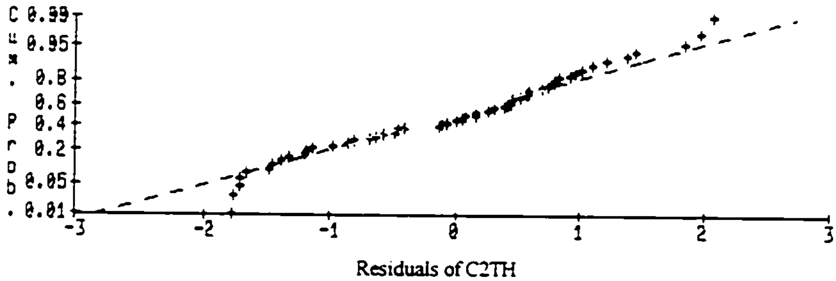

Figure AVII.26: Cumulative Probability Plot of Residuals from C2 Thickness (C2TH) Model

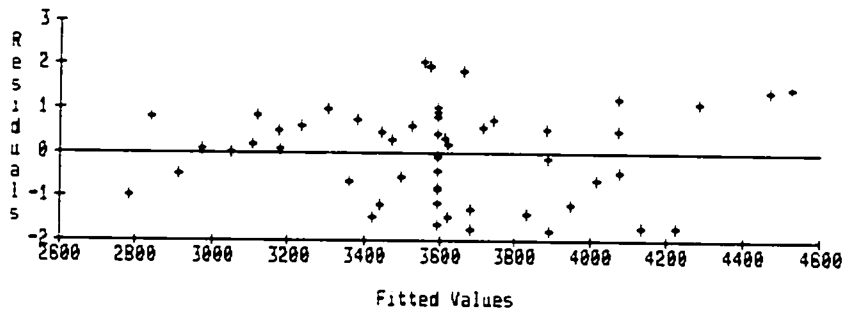

Figure AVII.27: Residuals versus Fitted Values for C2 Thickness (C2TH) Model

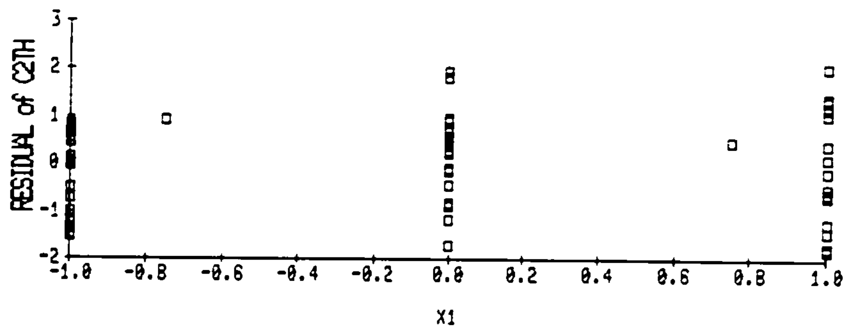

Figure AVII.28: Residuals versus X1 for C2 Thickness (C2TH) Model

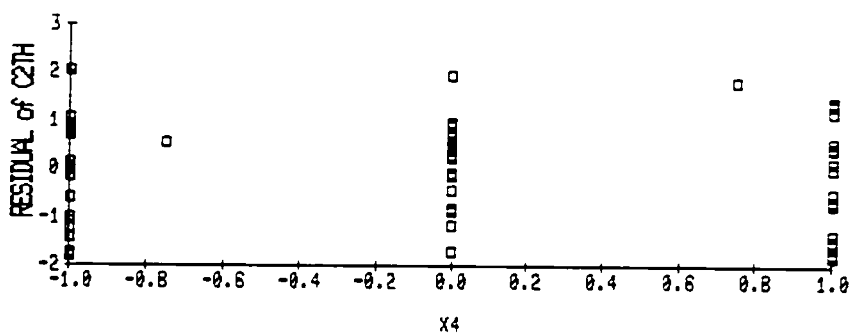

Figure AVII.29: Residuals versus X4 for C2 Thickness (C2TH) Model

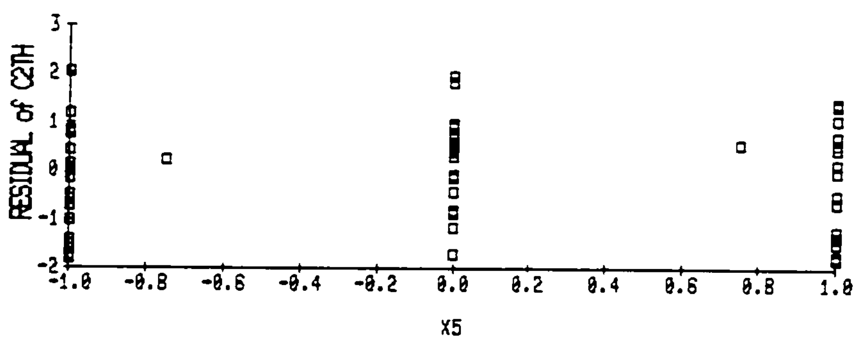

Figure AVII.30: Residuals versus X5 for C2 Thickness (C2TH) Model

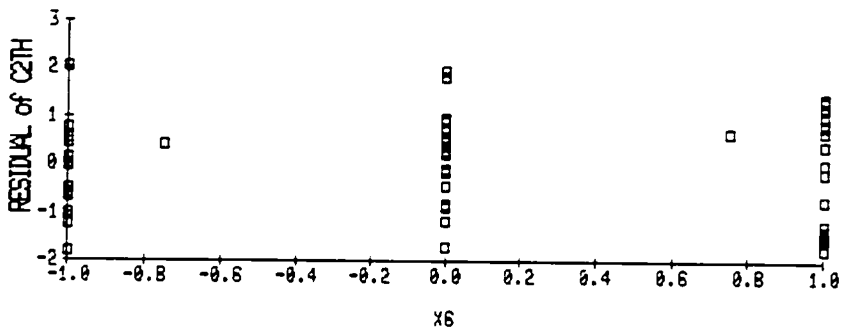

Figure AVII.31: Residuals versus X6 for C2 Thickness (C2TH) Model

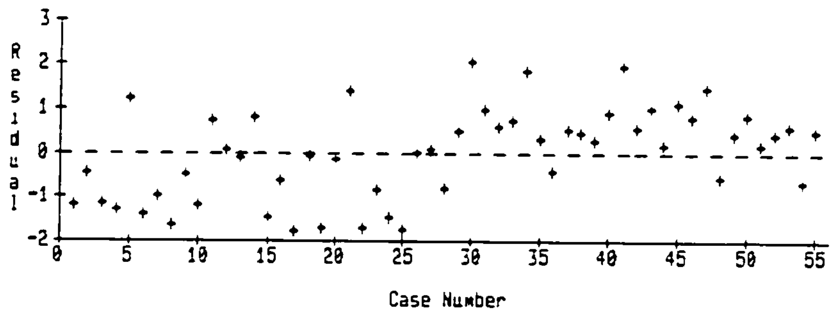

Figure AVII.32: Time Series Plot of Residuals from C2 Thickness (C2TH) Model

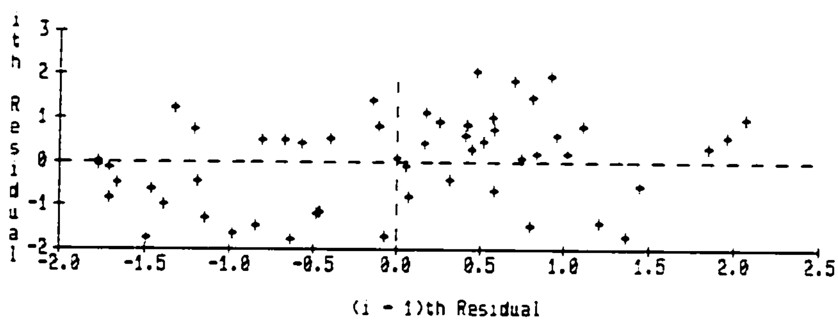

Figure AVII.33: Lag-1 Serial Plot of Residuals from C2 Thickness (C2TH) Model

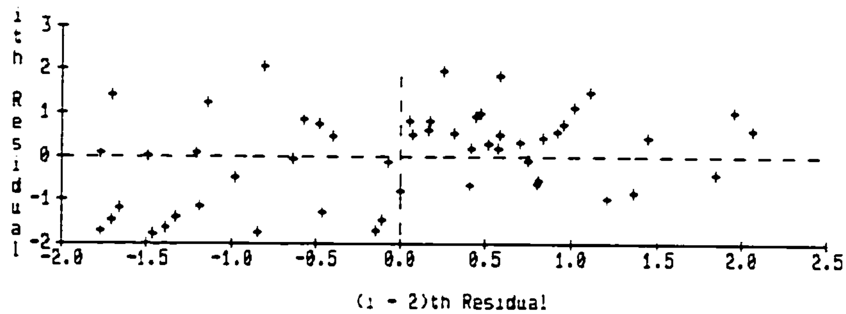

Figure AVII.34: Lag-2 Serial Plot of Residuals from C2 Thickness (C2TH) Model

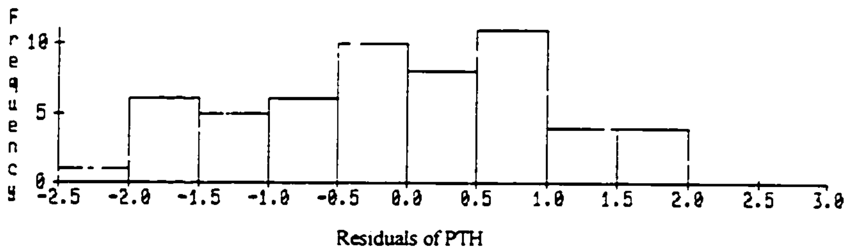

Figure AVII.35: Histogram of Residuals from Pump Thickness (PTH) Model

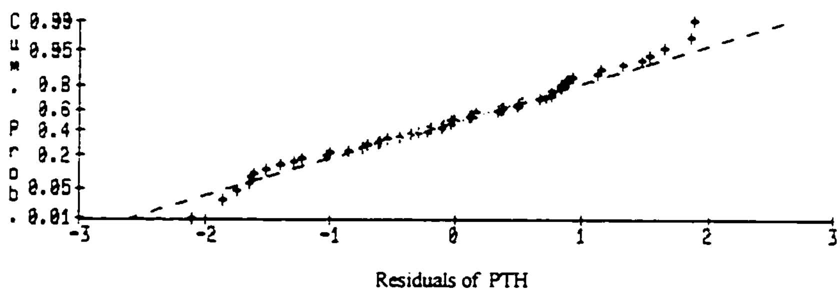

Figure AVII.36: Cumulative Probability Plot of Residuals from Pump Thickness (PTH) Model

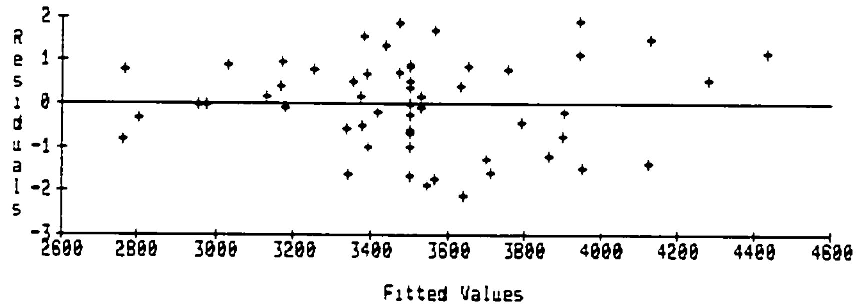

Figure AVII.37: Residuals versus Fitted Values for Pump Thickness (PTH) Model

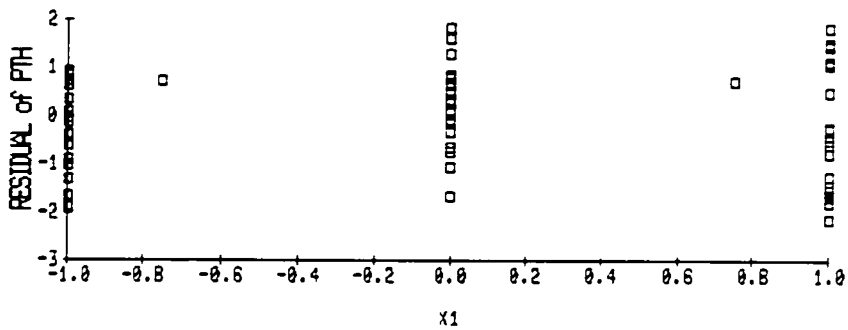

Figure AVII.38: Residuals versus X1 for Pump Thickness (PTH) Model

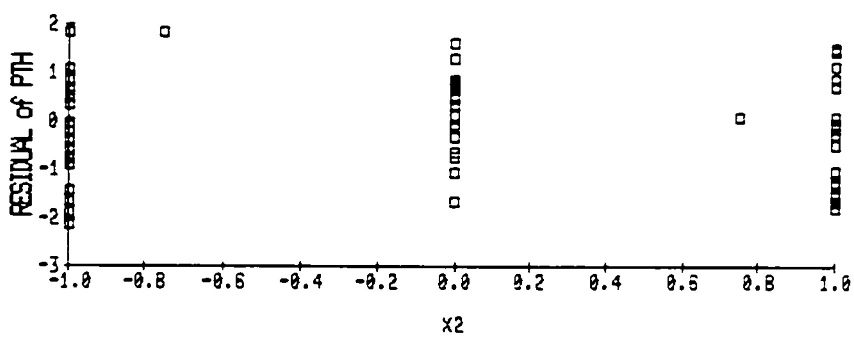

Figure AVII.39: Residuals versus X2 for Pump Thickness (PTH) Model

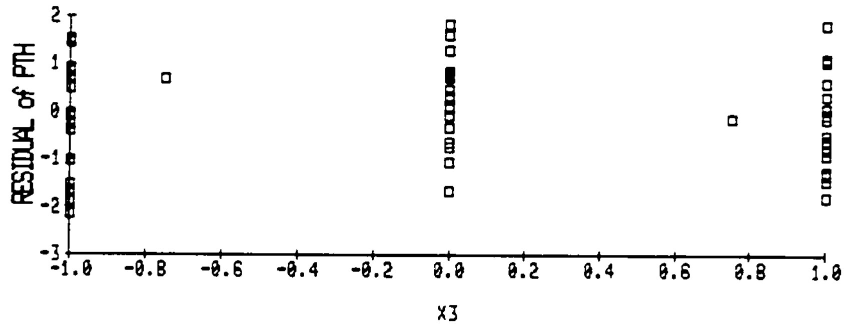

Figure AVII.40: Residuals versus X3 for Pump Thickness (PTH) Model

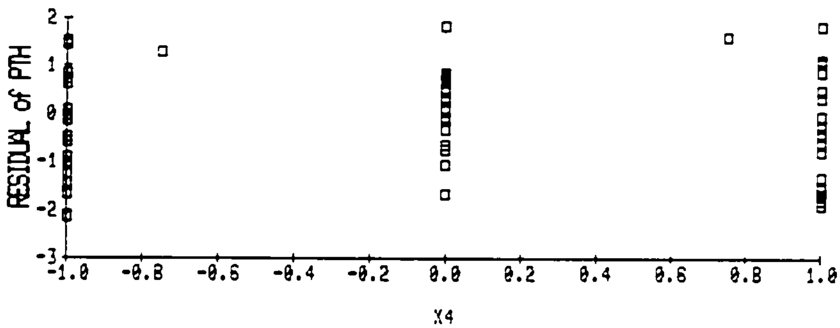

Figure AVII.41: Residuals versus X4 for Pump Thickness (PTH) Model

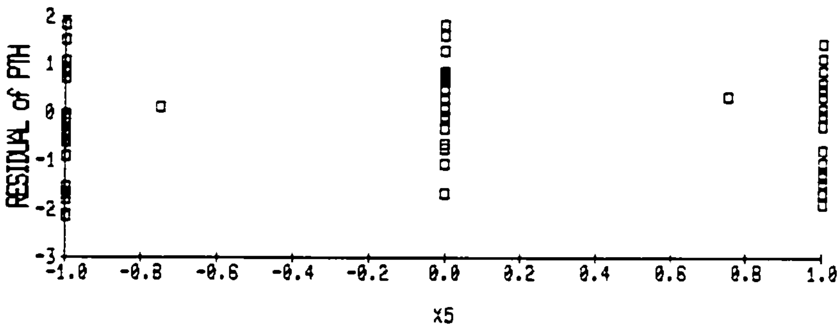

Figure AVII.42: Residuals versus X5 for Pump Thickness (PTH) Model

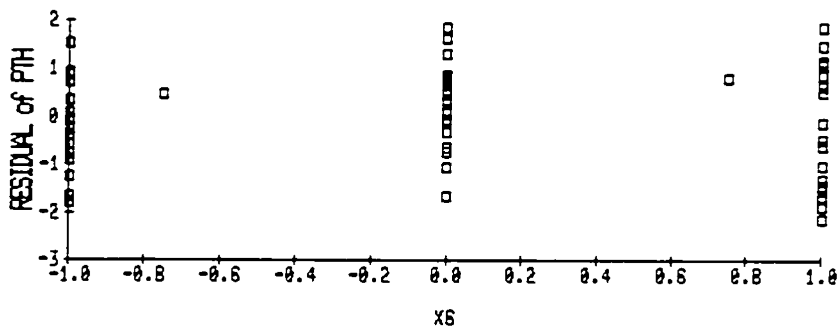

Figure AVII.43: Residuals versus X6 for Pump Thickness (PTH) Model

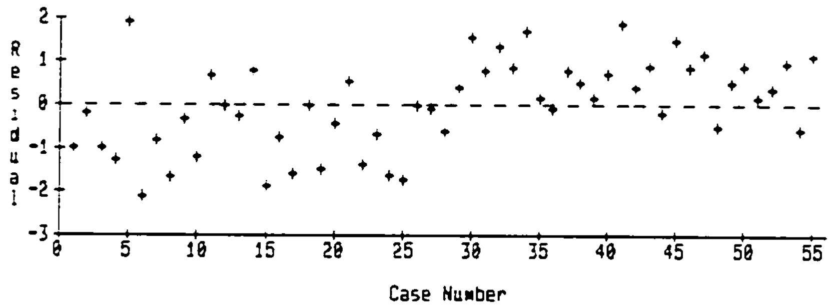

Figure AVII.44: Time Series Plot of Residuals from Pump Thickness (PTH) Model

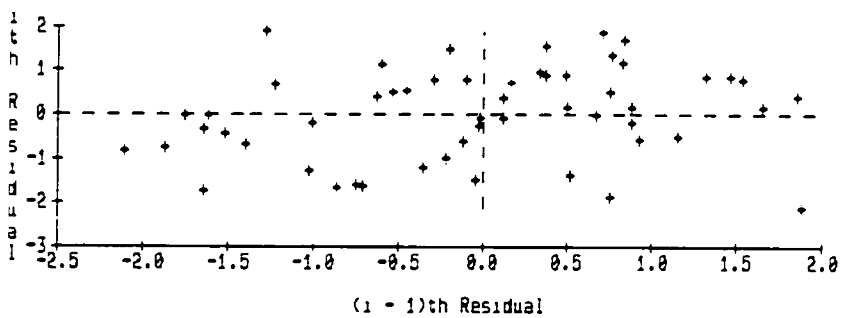

Figure AVII.45: Lag-1 Serial Plot of Residuals from Pump Thickness (PTH) Model

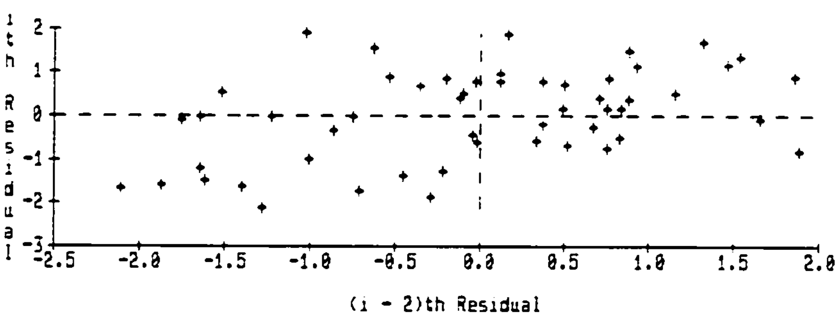

Figure AVII.46: Lag-2 Serial Plot of Residuals from Pump Thickness (PTH) Model

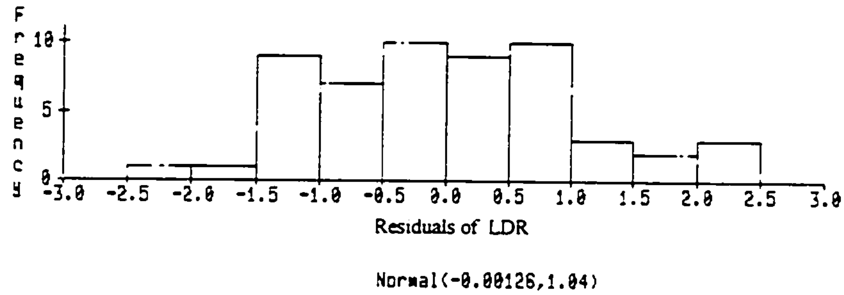

Figure AVII.47: Histogram of Residuals from Load Deposition Rate (LDR) Model

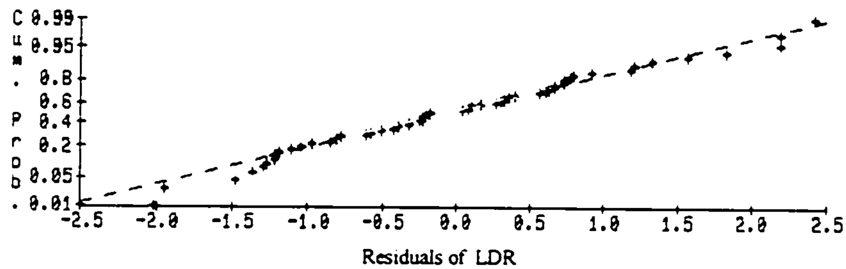

Figure AVII.48: Cumulative Probability Plot of Residuals from Load Deposition Rate (LDR) Model

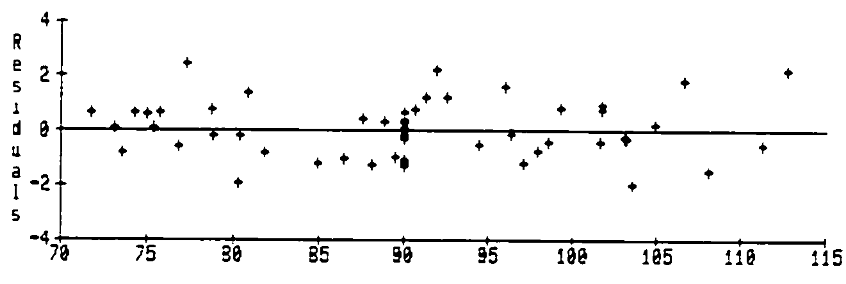

Figure AVII.49: Residuals versus Fitted Values for Load Deposition Rate (LDR) Model

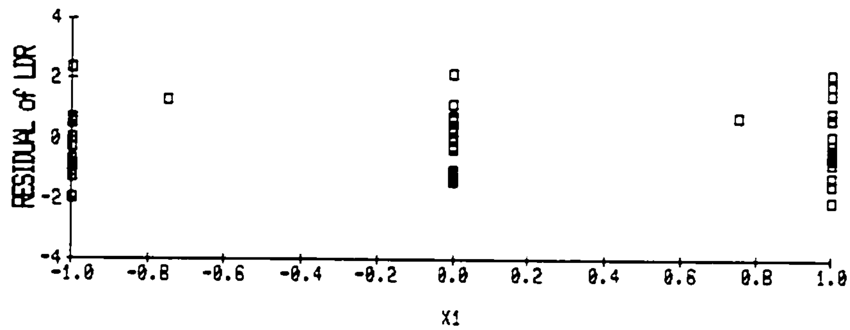

Figure AVII.50: Residuals versus X1 Values for Load Deposition Rate (LDR) Model

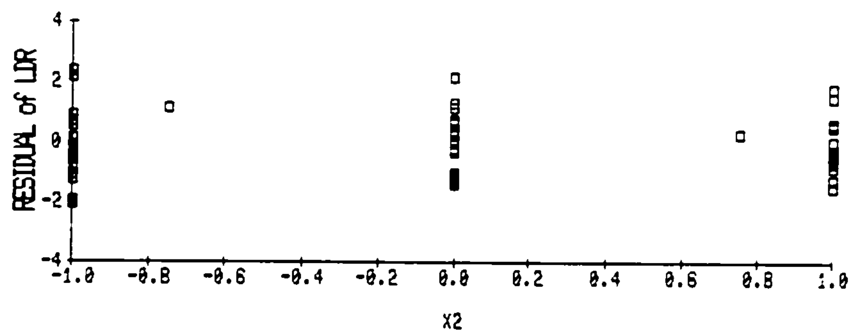

Figure AVII.51: Residuals versus X2 Values for Load Deposition Rate (LDR) Model

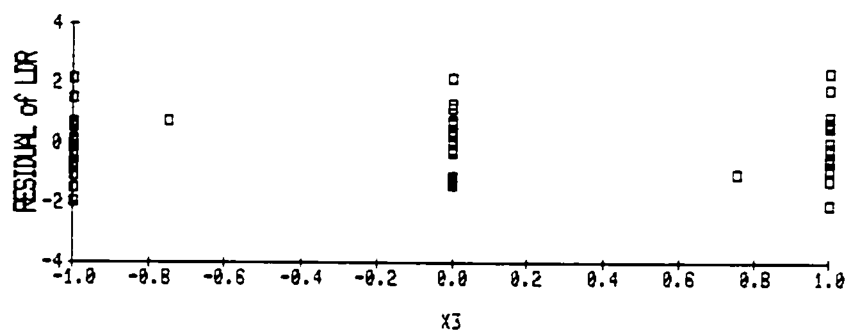

Figure AVII.52: Residuals versus X3 Values for Load Deposition Rate (LDR) Model

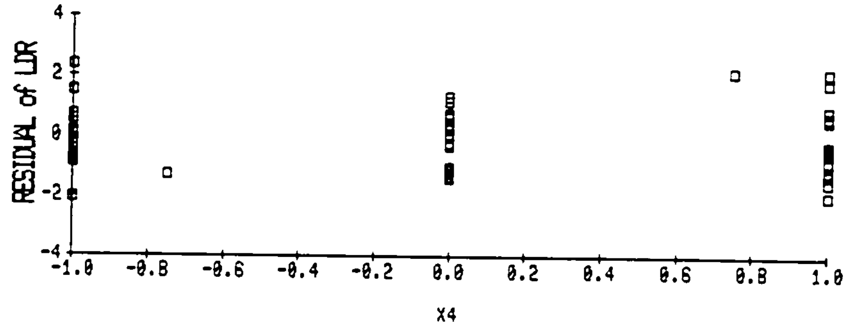

Figure AVII.53: Residuals versus X4 Values for Load Deposition Rate (LDR) Model

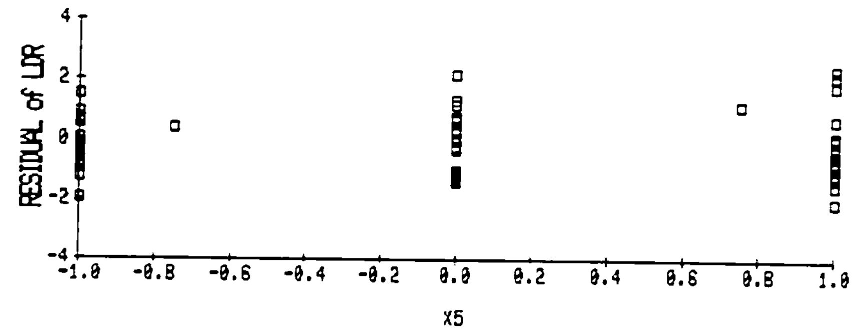

Figure AVII.54: Residuals versus X5 Values for Load Deposition Rate (LDR) Model

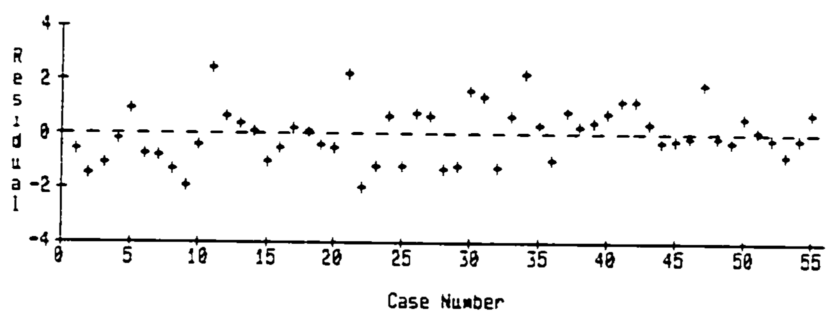

Figure AVII.55: Time Series of Residuals from Load Deposition Rate (LDR) Model

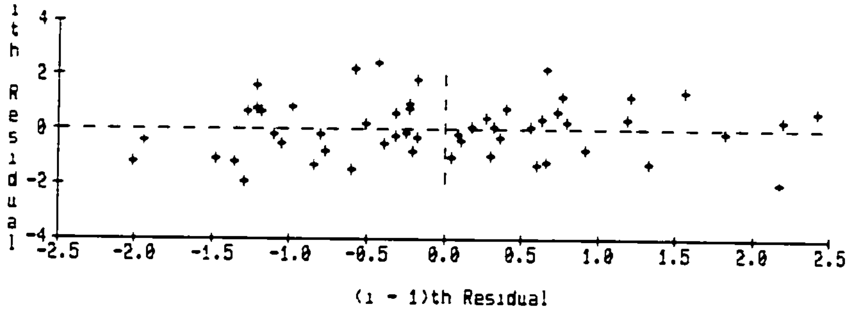

Figure AVII.56: Lag-1 Serial Plot of Residuals from Load Deposition Rate (LDR) Model

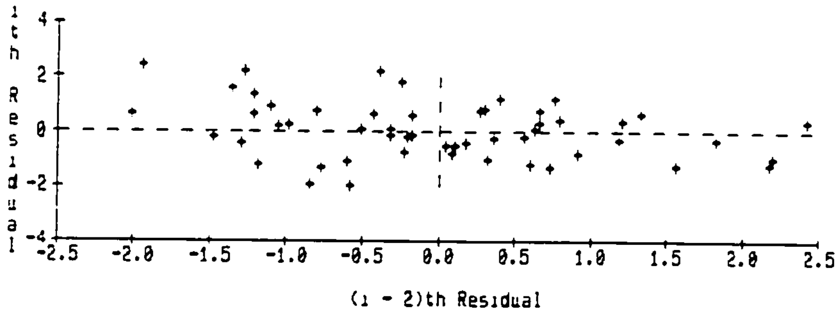

Figure AVII.57: Lag-2 Serial Plot of Residuals from Load Deposition Rate (LDR) Model

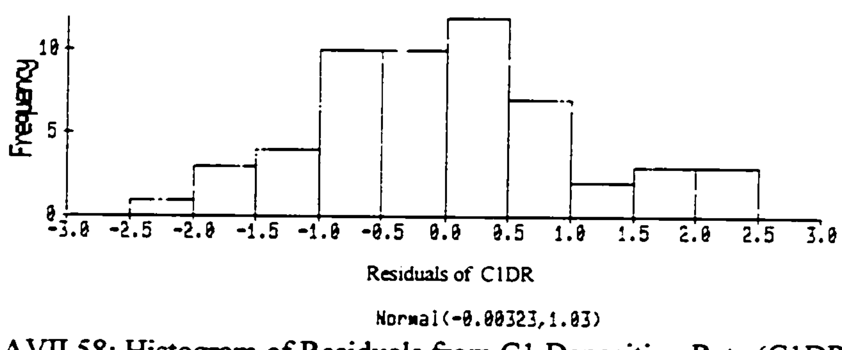

Figure AVII.58: Histogram of Residuals from C1 Deposition Rate (C1DR) Model

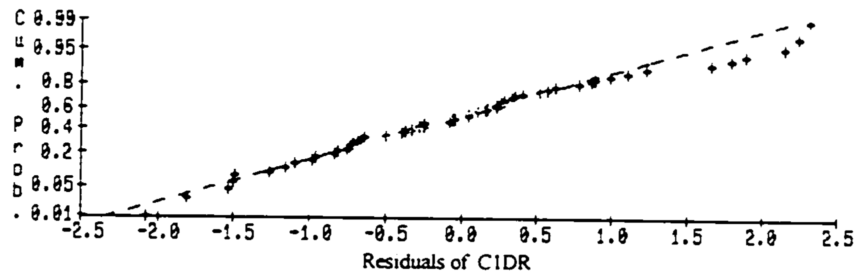

Figure AVII.59: Cumulative Probability Plot of Residuals from C1 Deposition Rate (C1DR) Model

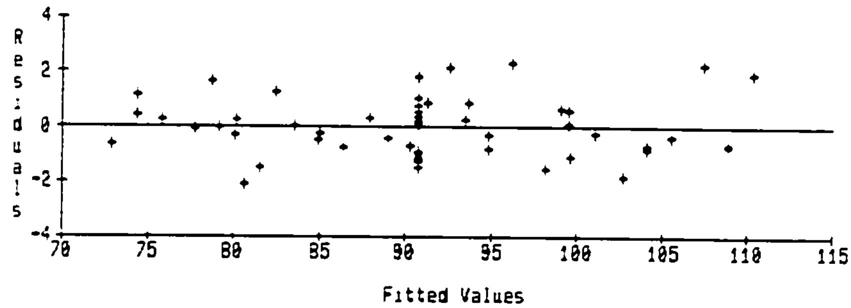

Figure AVII.60: Residuals versus Fitted Values for C1 Deposition Rate (C1DR) Model

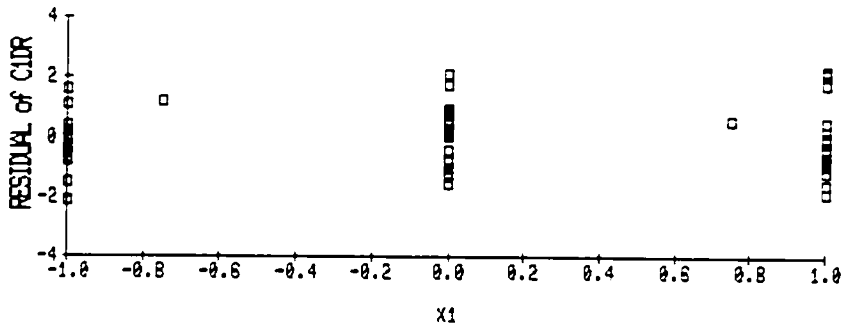

Figure AVII.61: Residuals versus X1 for C1 Deposition Rate (C1DR) Model

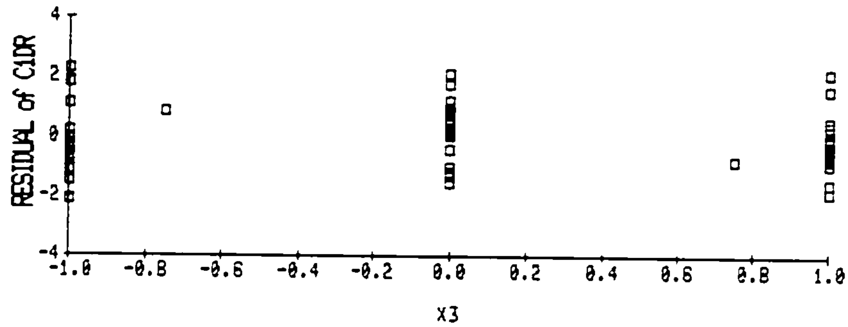

Figure AVII.62: Residuals versus X3 for C1 Deposition Rate (C1DR) Model

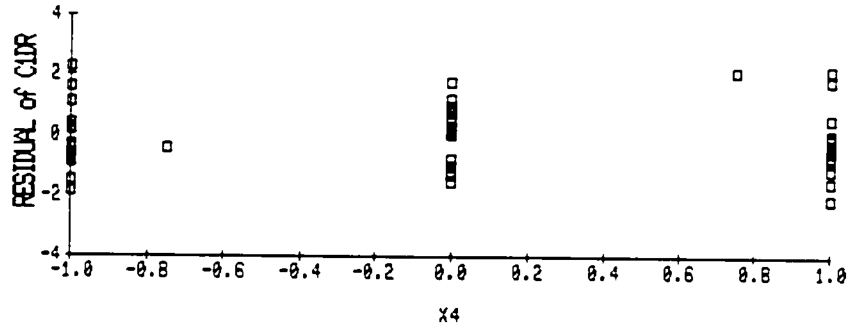

Figure AVII.63: Residuals versus X4 for C1 Deposition Rate (C1DR) Model

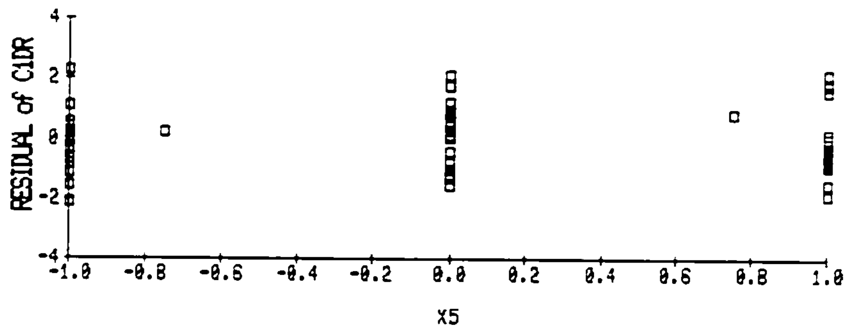

Figure AVII.64: Residuals versus X5 for C1 Deposition Rate (C1DR) Model

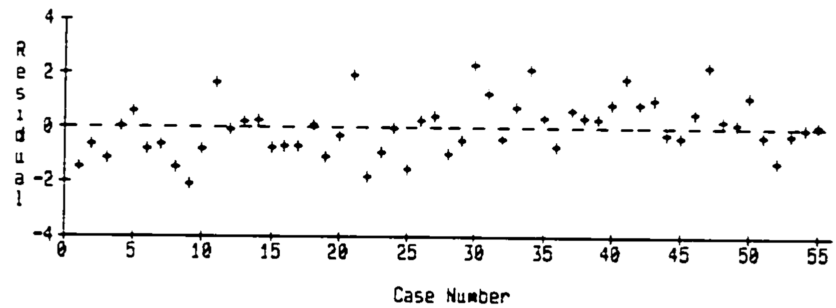

Figure AVII.65: Serial Plot of Residuals from C1 Deposition Rate (C1DR) Model

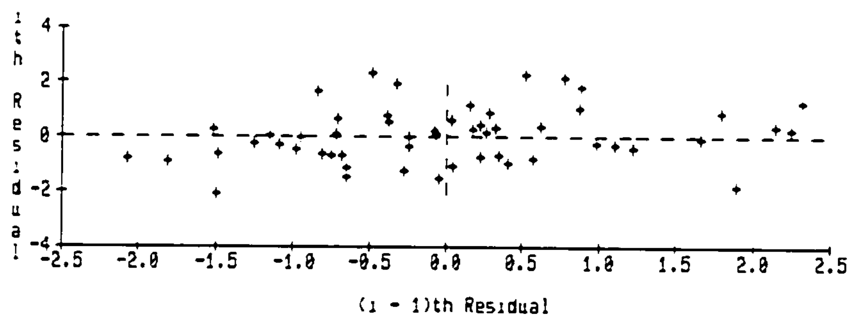

Figure AVII.66: Lag-1 Serial Plot of Residuals from C1 Deposition Rate (C1DR) Model

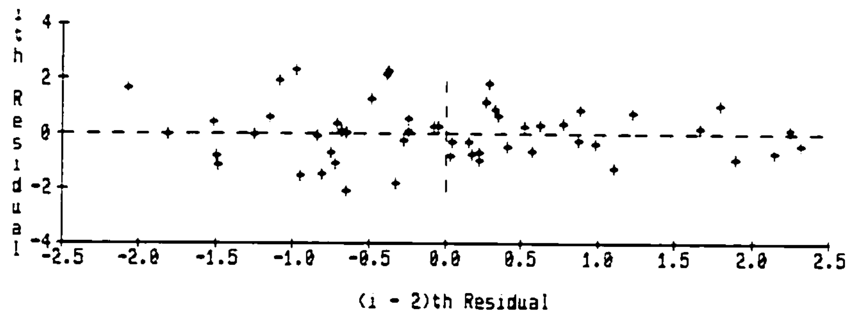

Figure AVII.67: Lag-2 Serial Plot of Residuals from C1 Deposition Rate (C1DR) Model

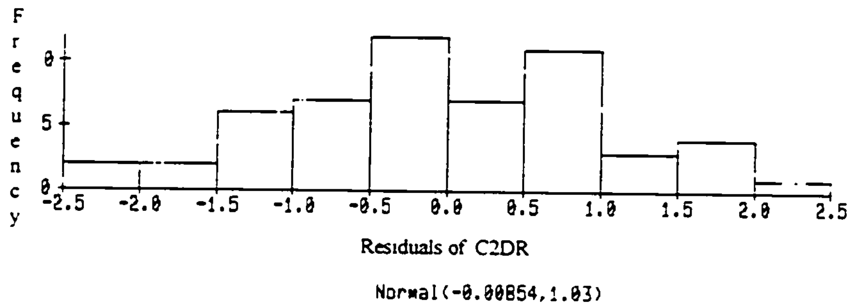

Figure AVII.68: Histogram of Residuals from C2 Deposition Rate (C2DR) Model

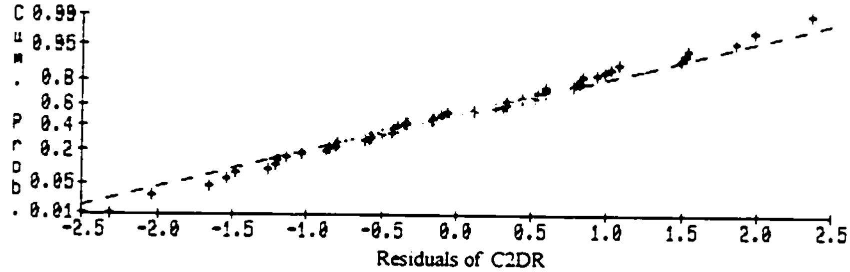

Figure AVII.69: Cumulative Probability Plot of Residuals from C2 Deposition Rate (C2DR) Model

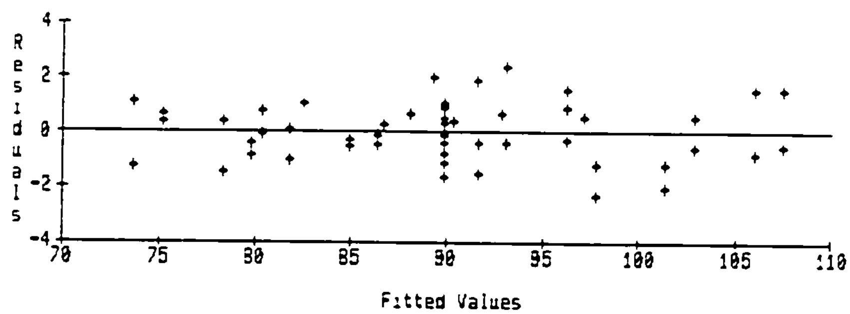

Figure AVII.70: Residuals versus Fitted Values for C2 Deposition Rate (C2DR) Model

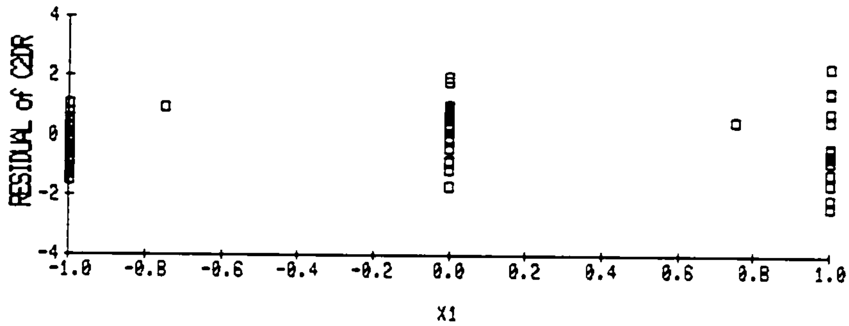

Figure AVII.71: Residuals versus X1 for C2 Deposition Rate (C2DR) Model

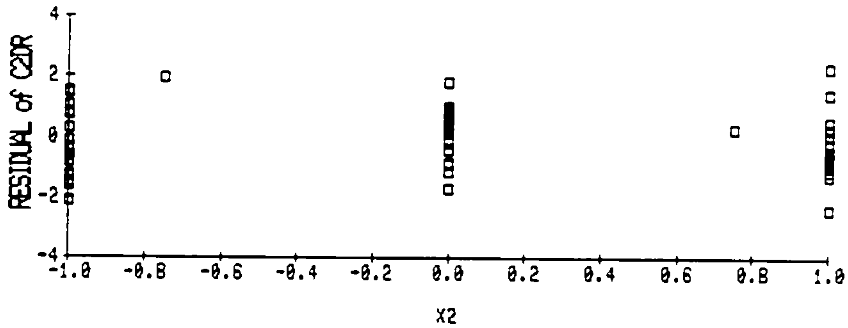

Figure AVII.72: Residuals versus X2 for C2 Deposition Rate (C2DR) Model

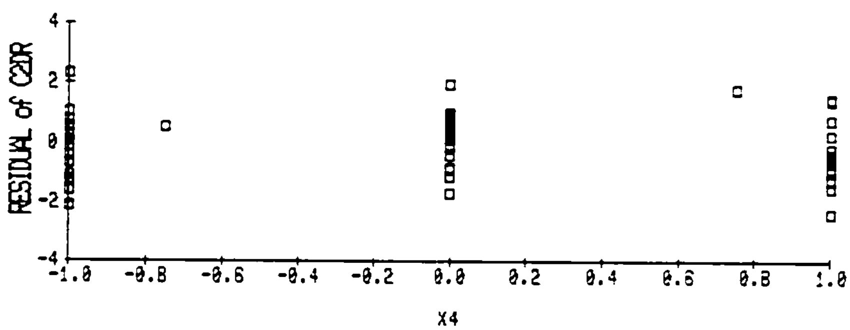

Figure AVII.73: Residuals versus X4 for C2 Deposition Rate (C2DR) Model

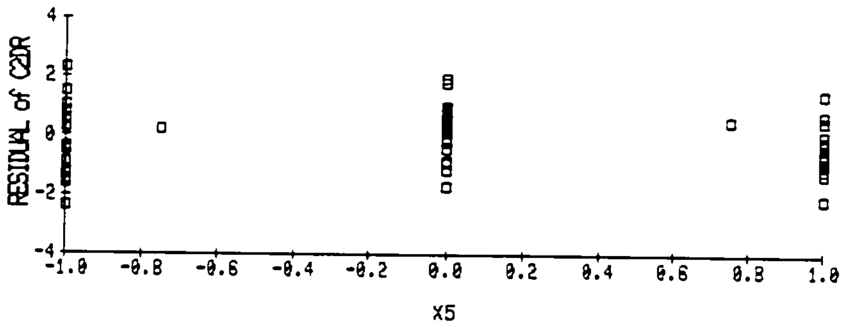

Figure AVII.74: Residuals versus X5 for C2 Deposition Rate (C2DR) Model

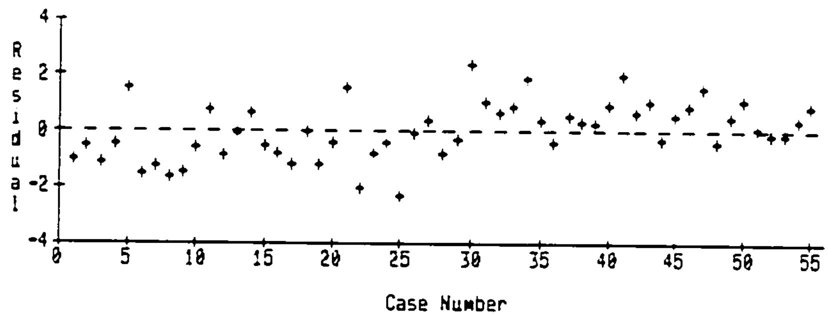

Figure AVII.75: Serial Plot of Residuals from C2 Deposition Rate (C2DR) Model

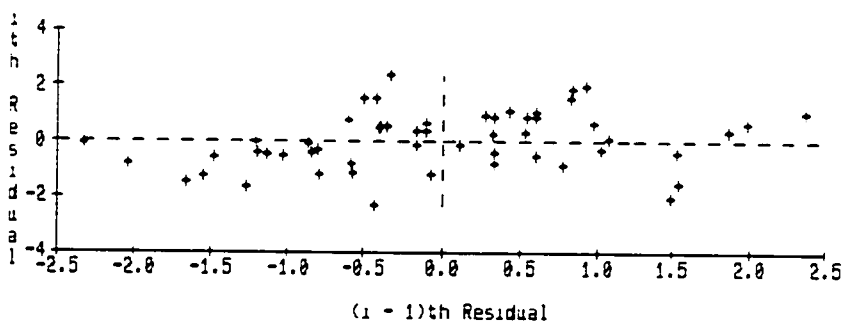

Figure AVII.76: Lag-1Serial Plot of Residuals from C2 Deposition Rate (C2DR) Model

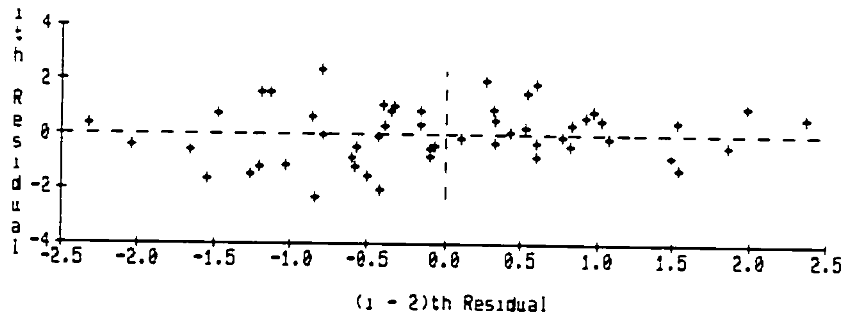

Figure AVII.77: Lag-2 Serial Plot of Residuals from C2 Deposition Rate (C2DR) Model

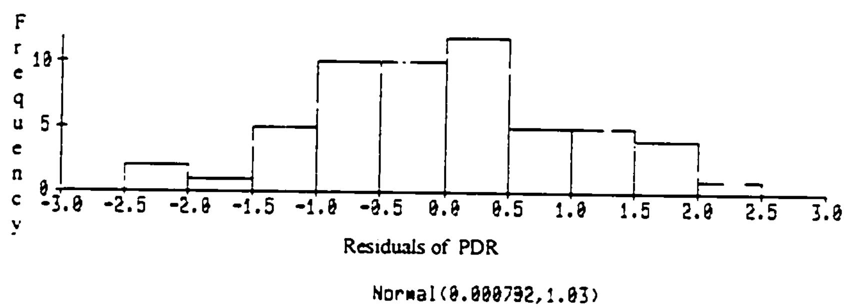

Figure AVII.78: Histogram of Residuals from Pump Deposition Rate (PDR) Model

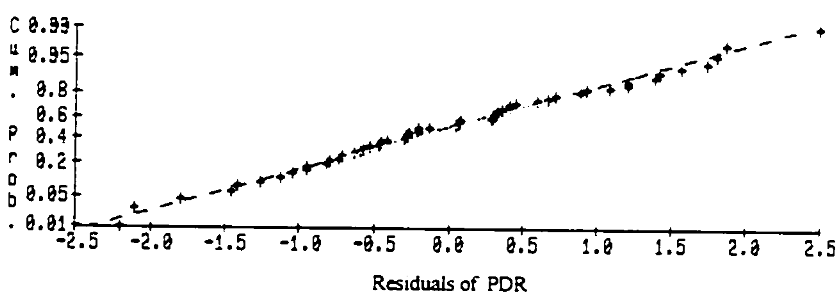

Figure AVII.79: Cumulative Probability Plot of Residuals from Pump Deposition Rate (PDR) Model

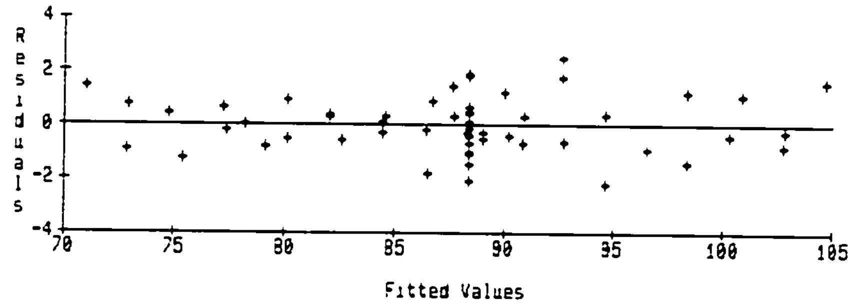

Figure AVII.80: Residuals versus Fitted Values for Pump Deposition Rate (PDR) Model

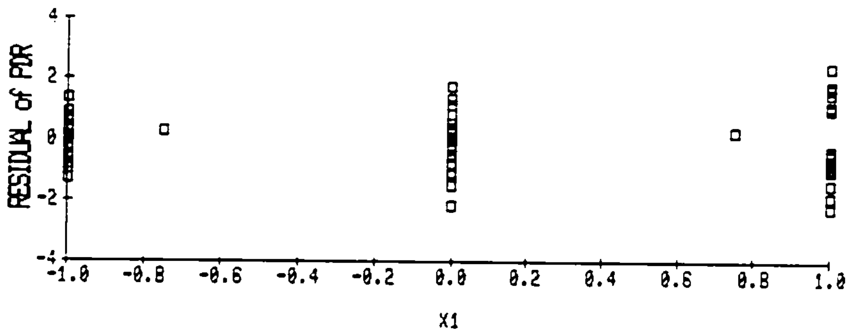

Figure AVII.81: Residuals versus X1 for Pump Deposition Rate (PDR) Model

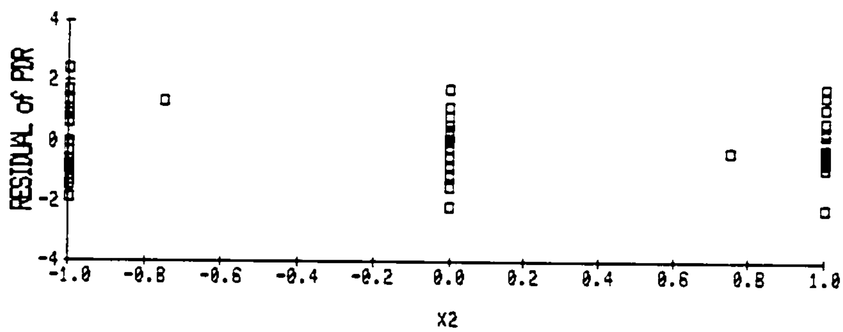

Figure AVII.82: Residuals versus X2 for Pump Deposition Rate (PDR) Model

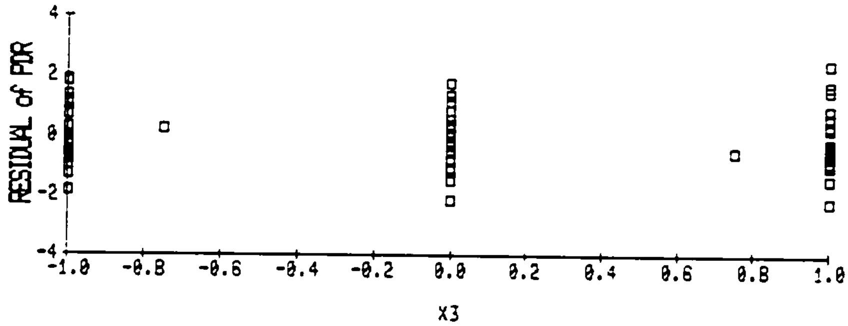

Figure AVII.83: Residuals versus X3 for Pump Deposition Rate (PDR) Model

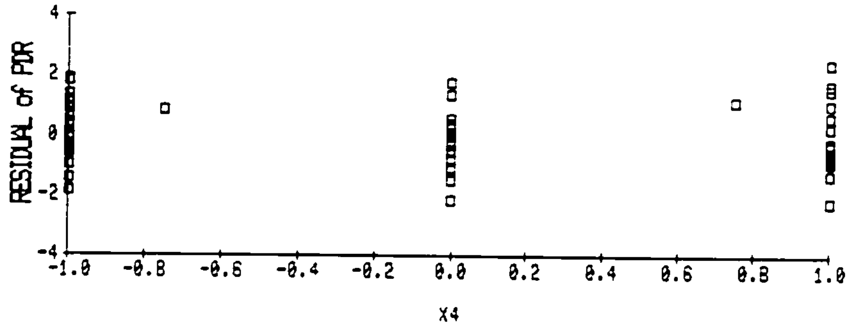

Figure AVII.84: Residuals versus X4 for Pump Deposition Rate (PDR) Model

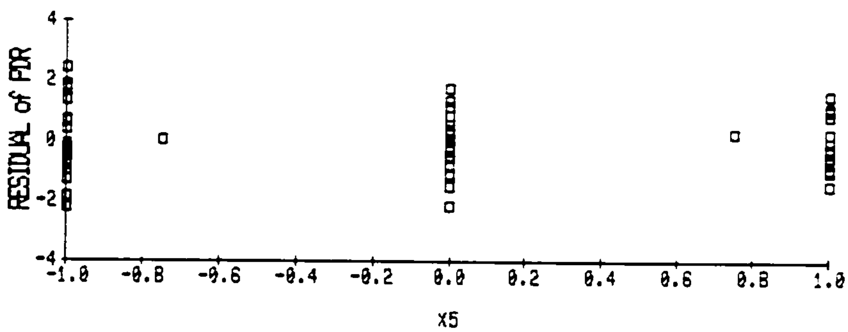

Figure AVII.85: Residuals versus X5 for Pump Deposition Rate (PDR) Model

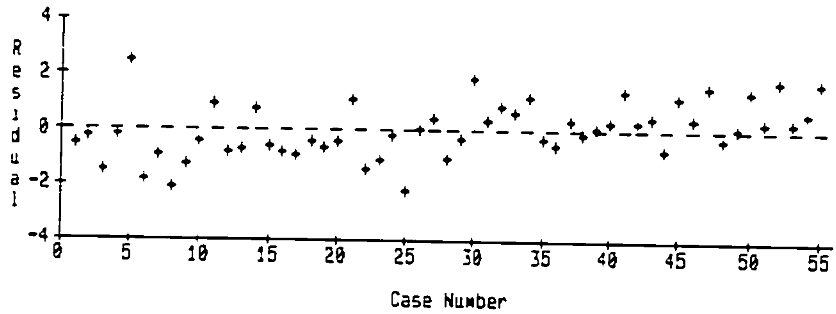

Figure AVII.86: Serial Plot of Residuals from Pump Deposition Rate (PDR) Model

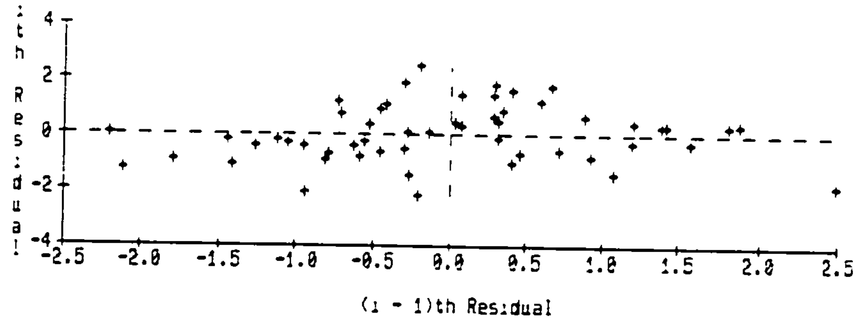

Figure AVII.87: Lag-1Serial Plot of Residuals from Pump Deposition Rate (PDR) Model

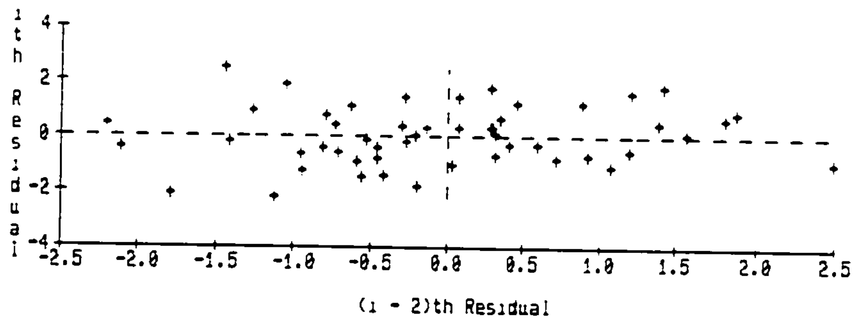

Figure AVII.88: Lag-2 Serial Plot of Residuals from Pump Deposition Rate (PDR) Model

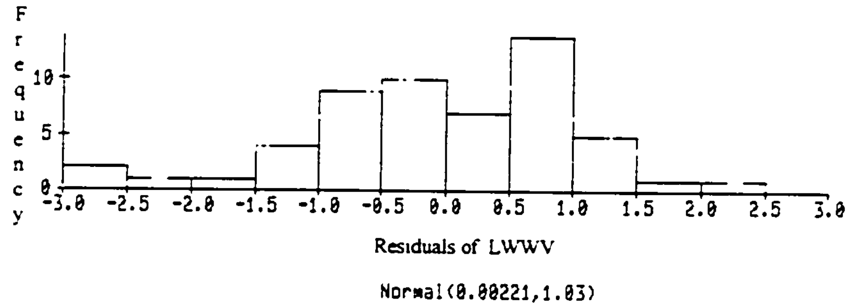

Figure AVII.89: Histogram of Residuals from Load Within-Wafer Variance (LWWV) Model

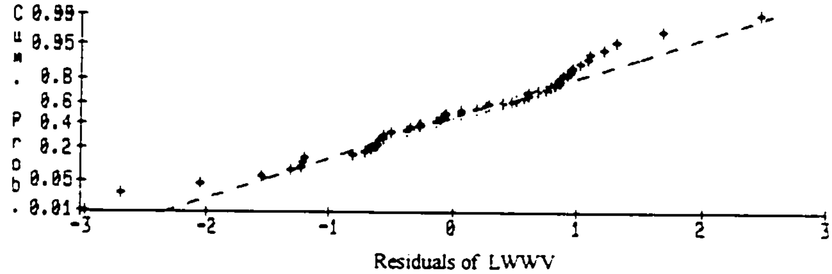

Figure AVII.90: Cumulative Probability Plot of Residuals from Load Within-Wafer Variance (LWWV) Model

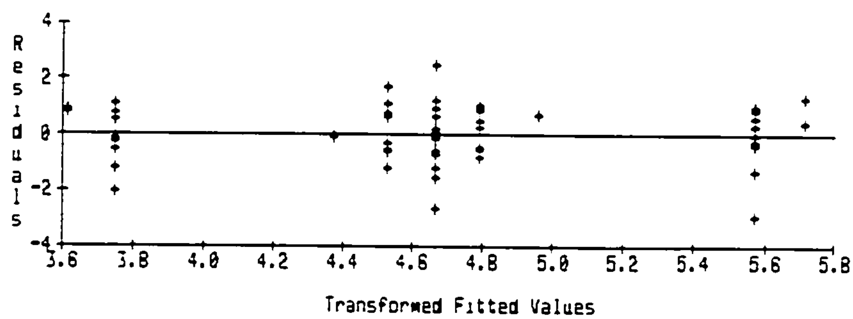

Figure AVII.91: Residuals versus Transformed Fitted Values for Load Within-Wafer Variance (LWWV) Model

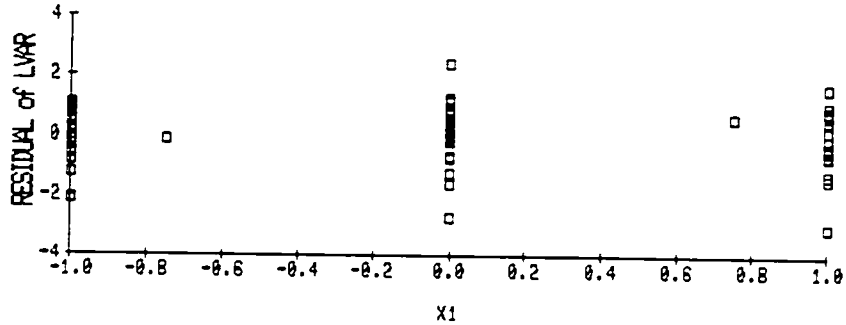

Figure AVII.92: Residuals versus X1 for Load Within-Wafer Variance (LWWV) Model

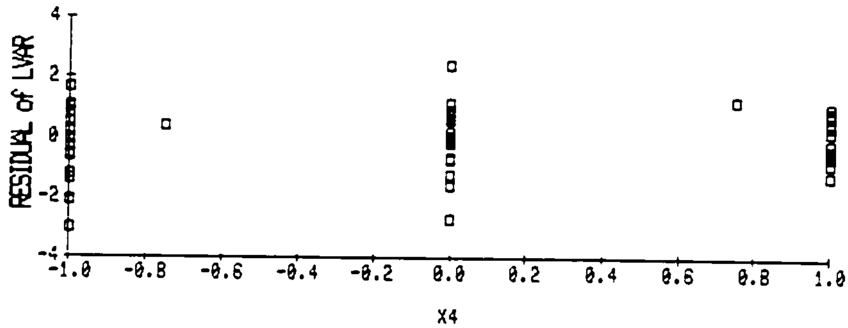

Figure AVII.93: Residuals versus X4 for Load Within-Wafer Variance (LWWV) Model

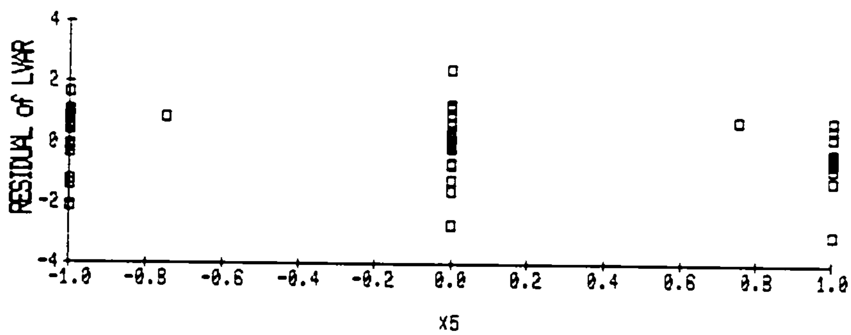

Figure AVII.94: Residuals versus X5 for Load Within-Wafer Variance (LWWV) Model

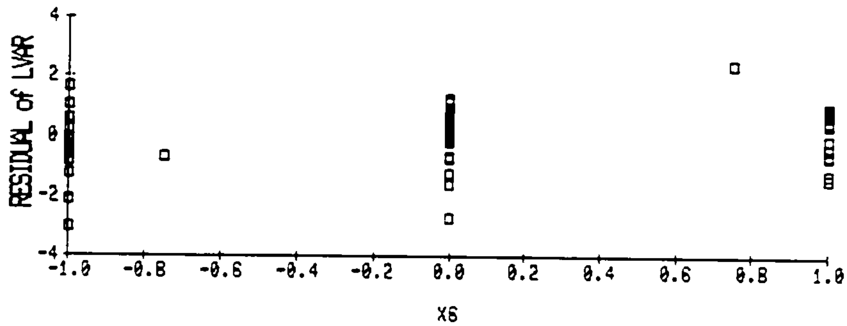

Figure AVII.95: Residuals versus X6 for Load Within-Wafer Variance (LWWV) Model

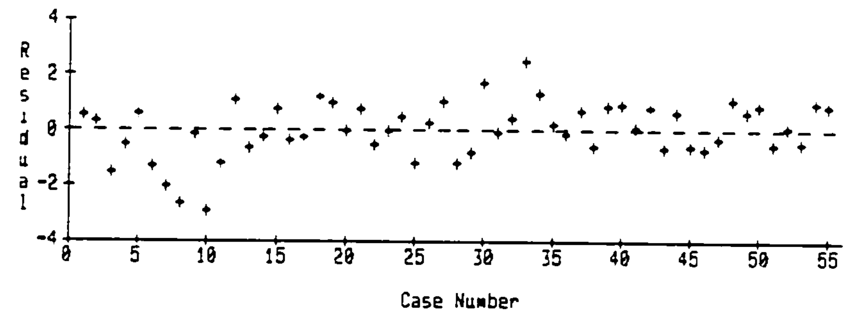

Figure AVII.96: Serial Plot of Residuals from Load Within-Wafer Variance (LWWV) Model

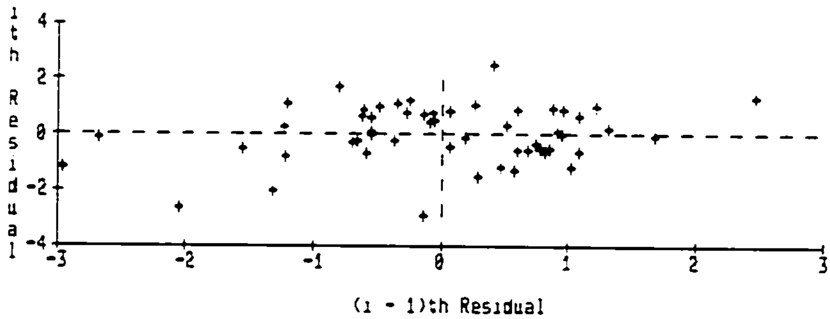

Figure AVII.97: Lag-1 Serial Plot of Residuals from Load Within-Wafer Variance (LWWV) Model

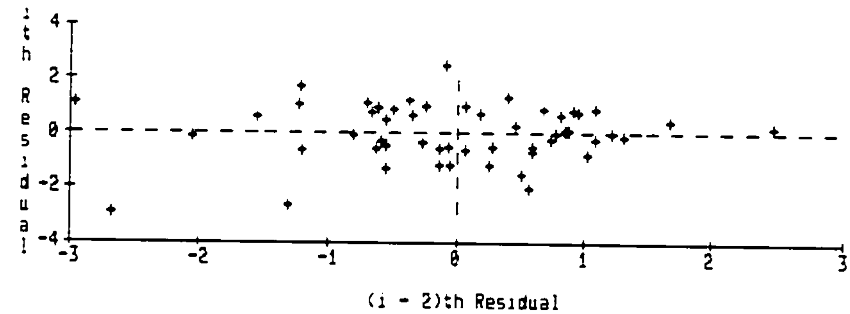

Figure AVII.98: Lag-2 Serial Plot of Residuals from Load Within-Wafer Variance (LWWV) Model

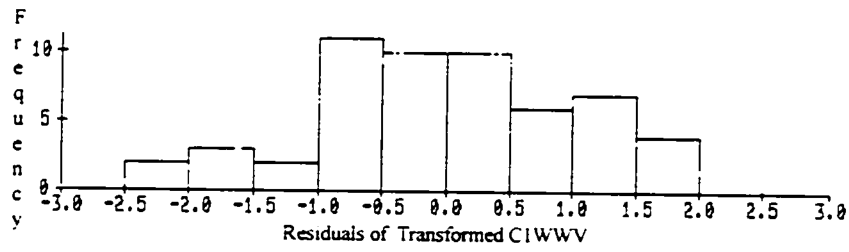

Figure AVII.99: Histogram of Residuals from C1 Within-Wafer Variance (C1WWV) Model

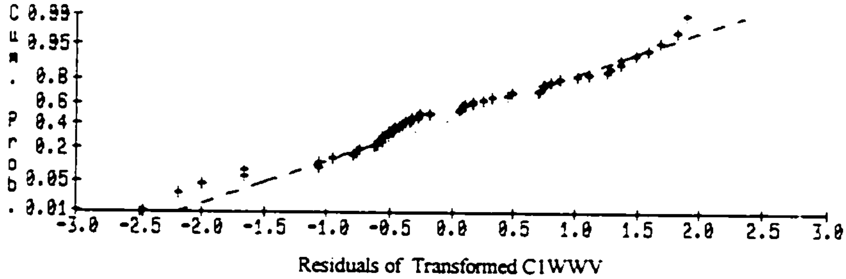

Figure AVII.100: Cumulative Probability Plot of Residuals from C1 Within-Wafer Variance (C1WWV) Model

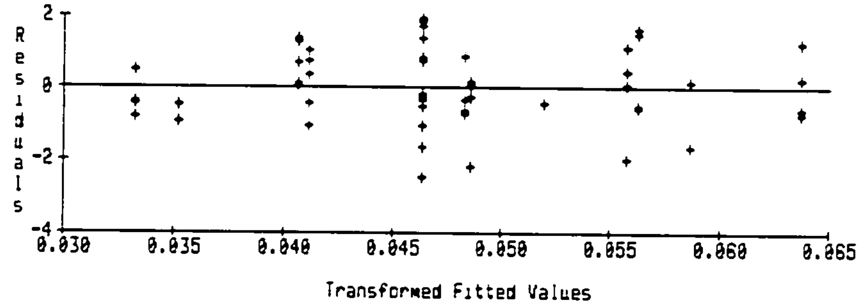

Figure AVII.101: Residuals versus Transformed Fitted Values for C1 Within-Wafer Variance (C1WWV) Model

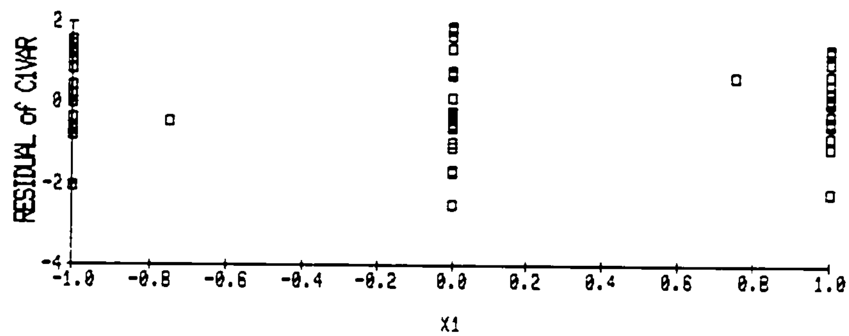

Figure AVII.102: Residuals versus X1 for C1 Within-Wafer Variance (C1WWV) Model

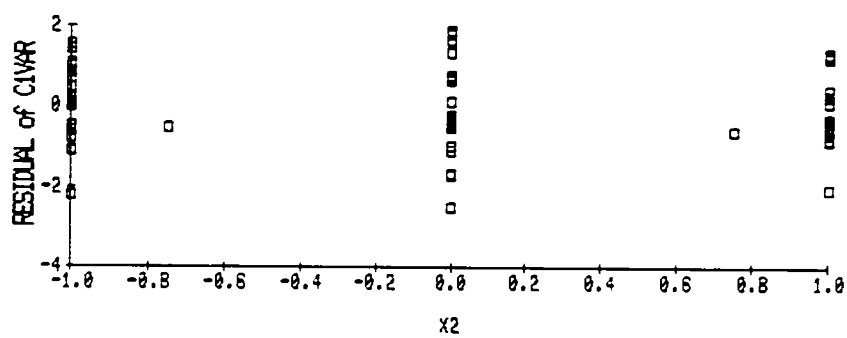

Figure AVII.103: Residuals versus X2 for C1 Within-Wafer Variance (C1WWV) Model

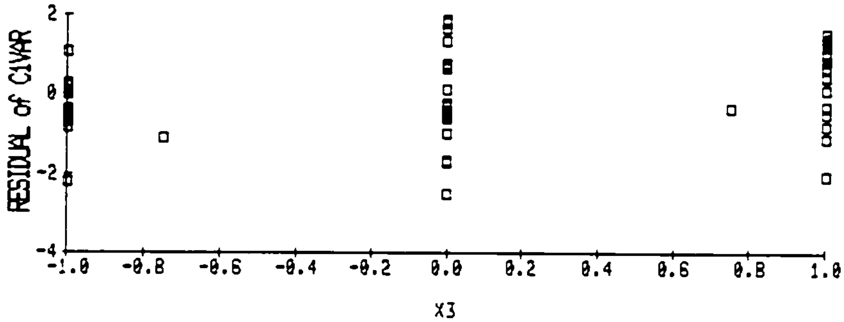

Figure AVII.104: Residuals versus X3 for C1 Within-Wafer Variance (C1WWV) Model

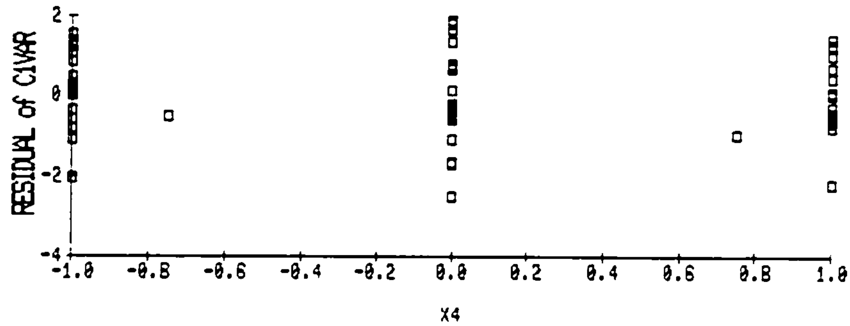

Figure AVII.105: Residuals versus X4 for C1 Within-Wafer Variance (C1WWV) Model

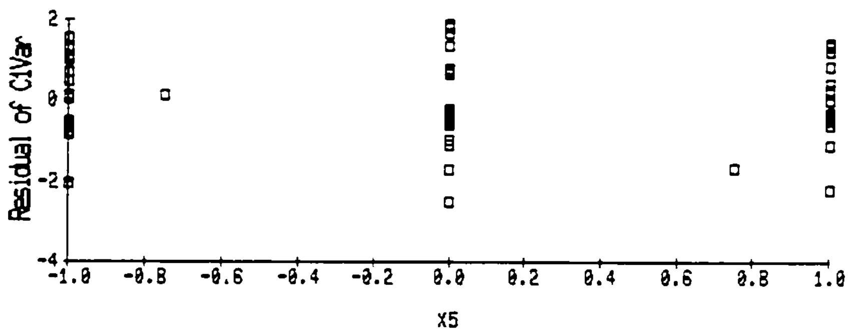

Figure AVII.106: Residuals versus X5 for C1 Within-Wafer Variance (C1WWV) Model

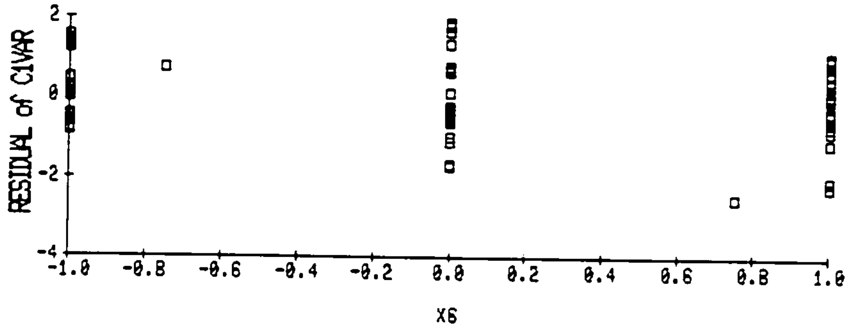

Figure AVII.107: Residuals versus X6 for C1 Within-Wafer Variance (C1WWV) Model

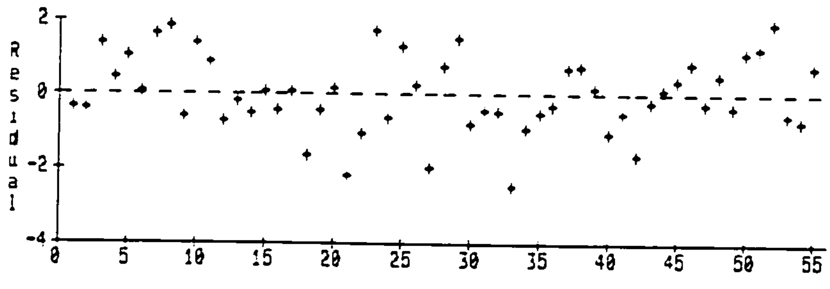

Figure AVII.108: Serial Plot of Residuals from C1 Within-Wafer Variance (C1WWV) Model

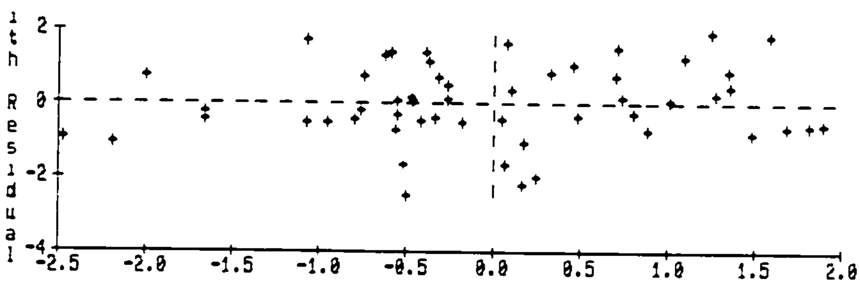

Figure AVII.109: Lag-1 Serial Plot of Residuals from C1 Within-Wafer Variance (C1WWV) Model

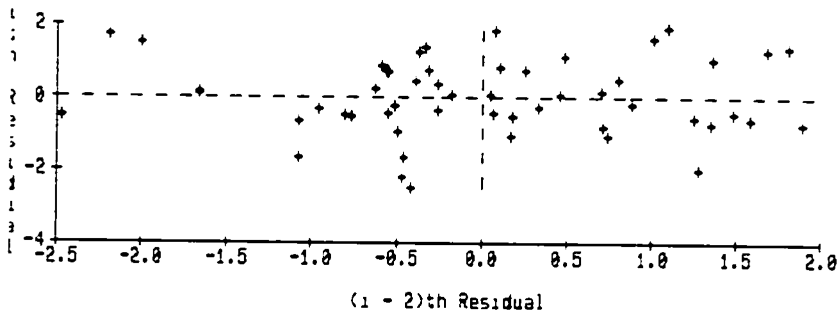

Figure AVII.110: Lag-2 Serial Plot of Residuals from C1 Within-Wafer Variance (C1WWV) Model

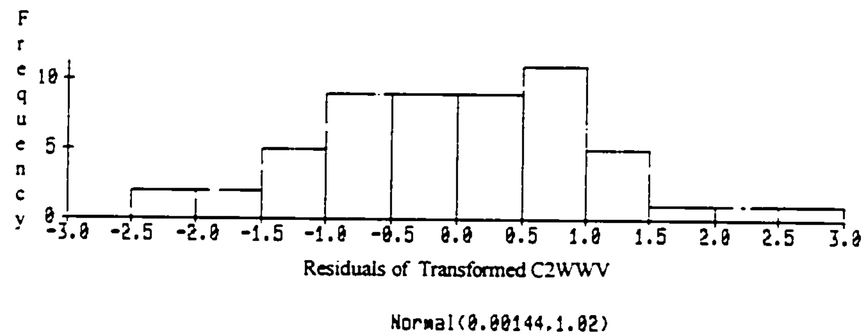

Figure AVII.111: Histogram of Residuals from C2 Within-Wafer Variance (C2WWV) Model

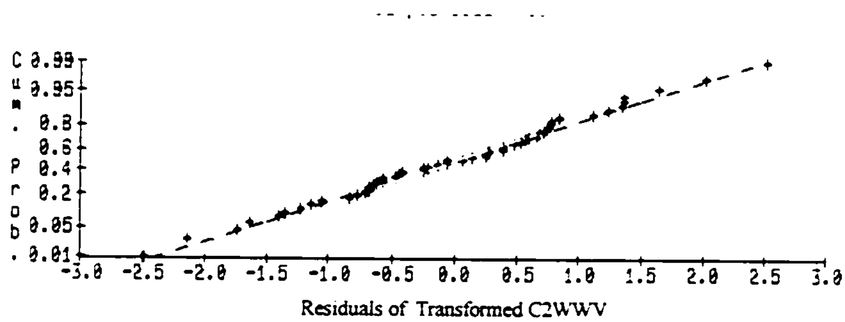

Figure AVII.112: Cumulative Probability Plot of Residuals from C2 Within-Wafer Variance (C2WWV) Model

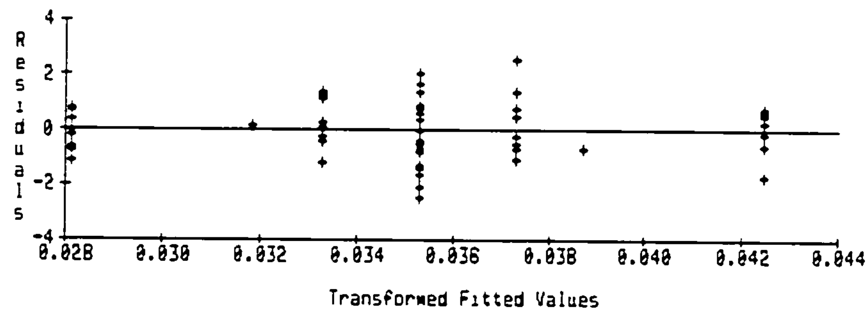

Figure AVII.113: Residuals versus Transformed Fitted Values for C2 Within-Wafer Variance (C2WWV) Model

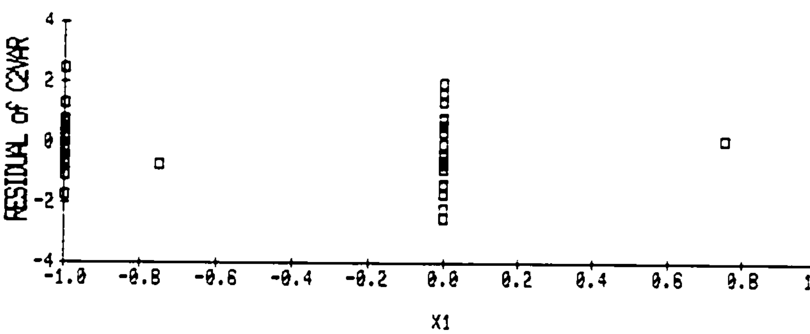

Figure AVII.114: Residuals versus X1 for C2 Within-Wafer Variance (C2WWV) Model

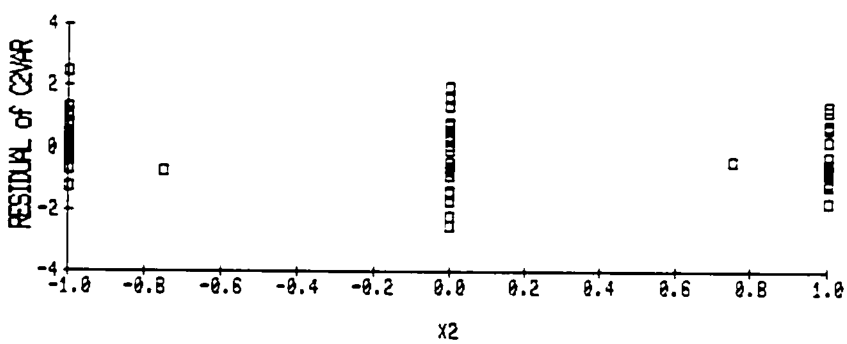

Figure AVII.115: Residuals versus X2 for C2 Within-Wafer Variance (C2WWV) Model

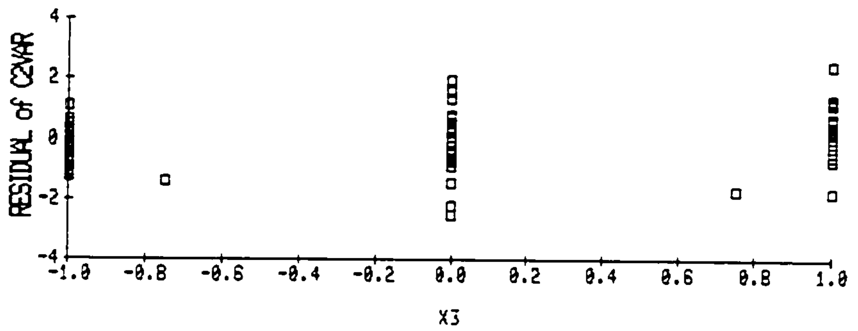

Figure AVII.116: Residuals versus X3 for C2 Within-Wafer Variance (C2WWV) Model

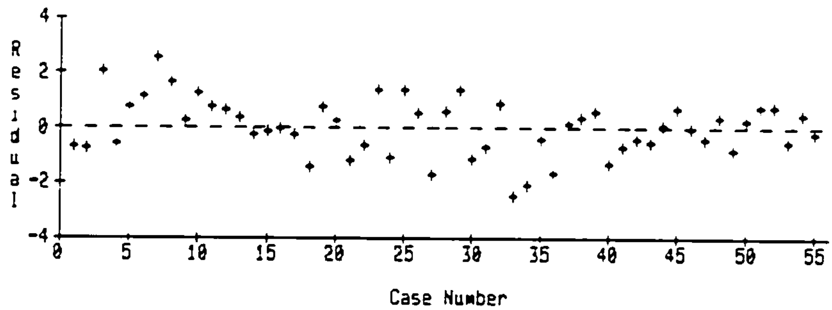

Figure AVII.117: Serial Plot of Residuals from C2 Within-Wafer Variance (C2WWV) Model

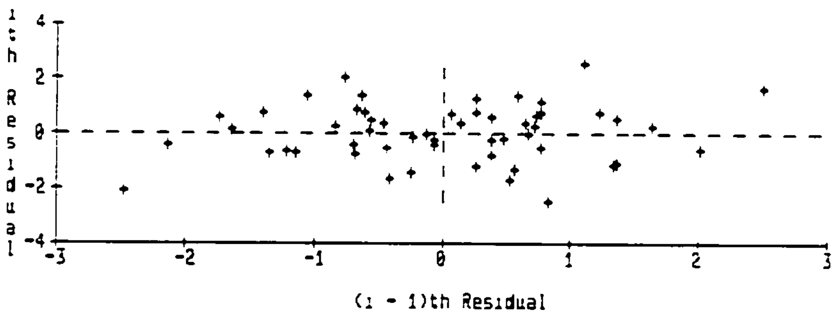

Figure AVII.118: Lag-1 Serial Plot of Residuals from C2 Within-Wafer Variance (C2WWV) Model

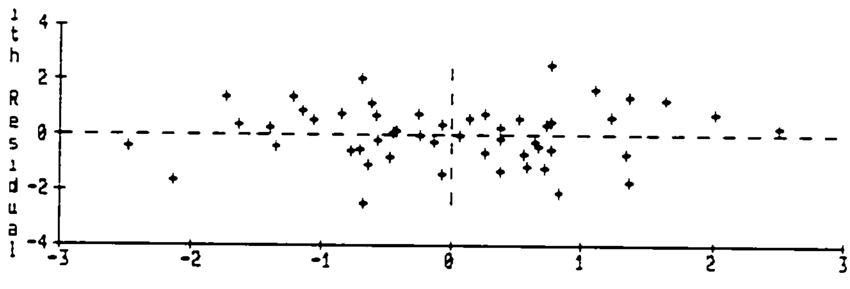

Figure AVII.119: Lag-2 Serial Plot of Residuals from C2 Within-Wafer Variance (C2WWV) Model

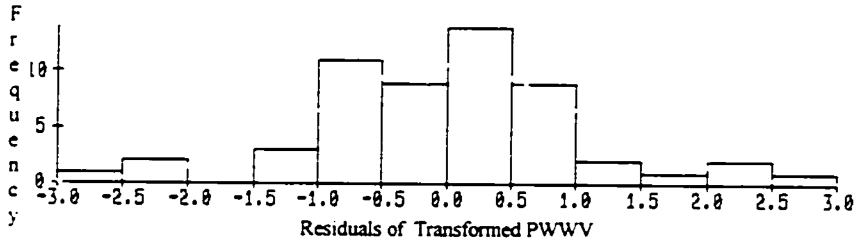

Figure AVII.120: Histogram of Residuals from Pump Within-Wafer Variance (PWWV) Model

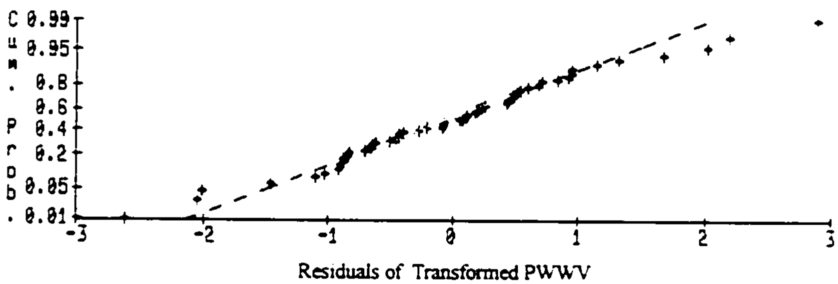

Figure AVII.121: Cumulative Probability Plot of Residuals from Pump Within-Wafer Variance (PWWV) Model

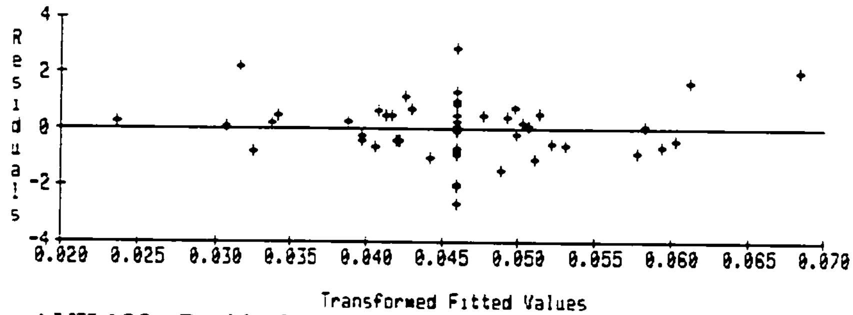

Figure AVII.122: Residuals versus Fitted Values for Pump Within-Wafer Variance (PWWV) Model

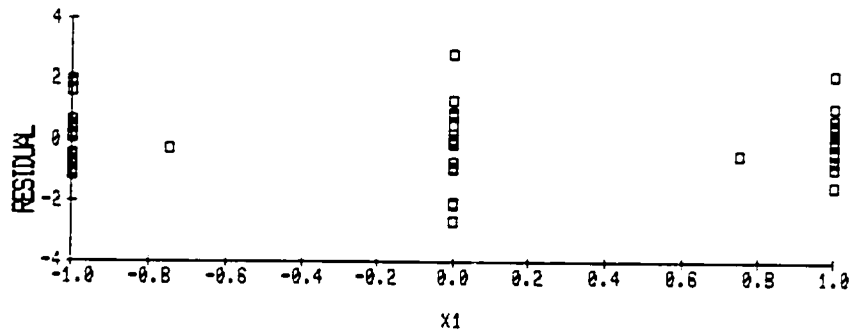

Figure AVII.123: Residuals versus X1 for Pump Within-Wafer Variance (PWWV) Model

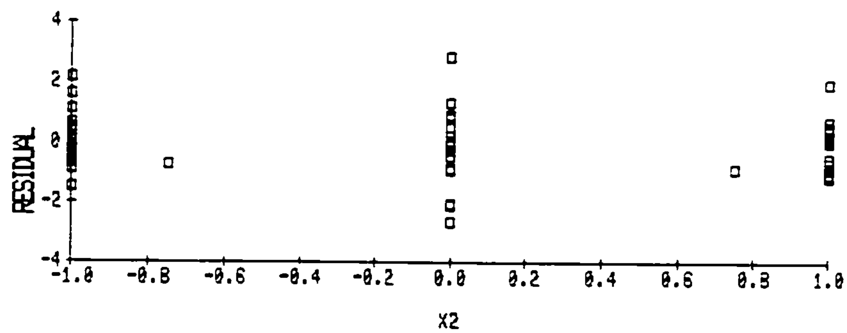

Figure AVII.124: Residuals versus X2 for Pump Within-Wafer Variance (PWWV) Model

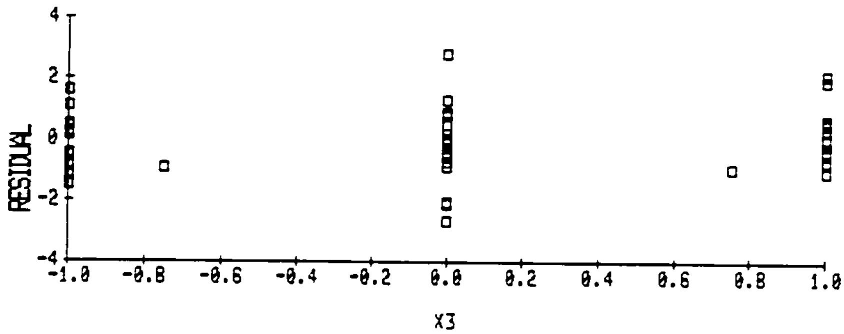

Figure AVII.125: Residuals versus X3 for Pump Within-Wafer Variance (PWWV) Model

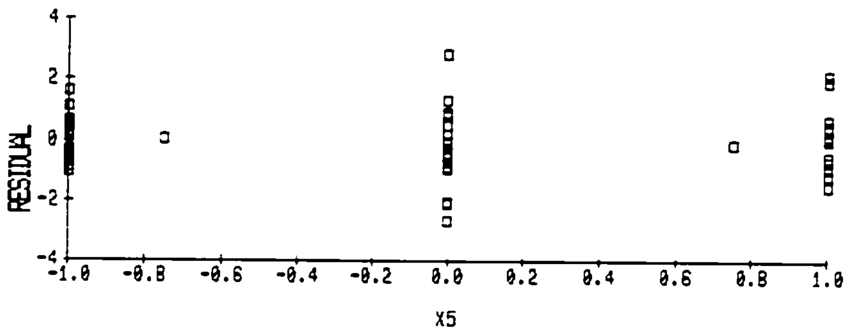

Figure AVII.126: Residuals versus X5 for Pump Within-Wafer Variance (PWWV) Model

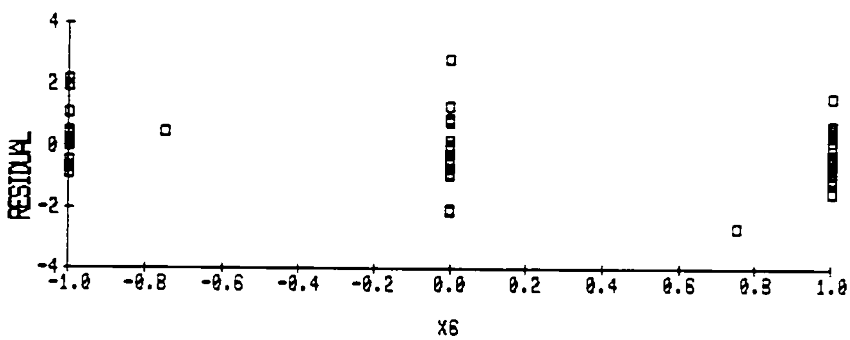

Figure AVII.127: Residuals versus X6 for Pump Within-Wafer Variance (PWWV) Model

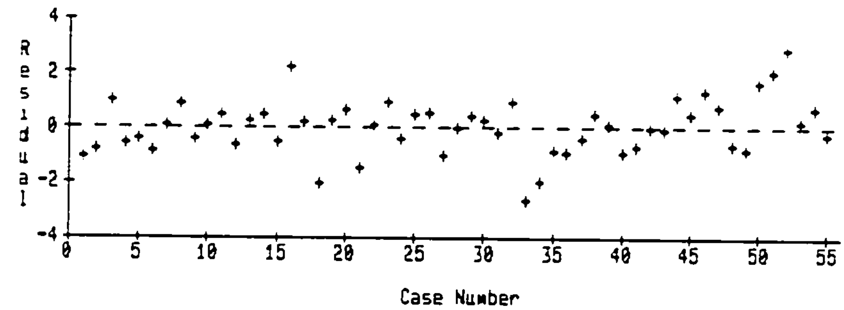

Figure AVII.128: Serial Plot of Residuals from Pump Within-Wafer Variance (PWWV) Model

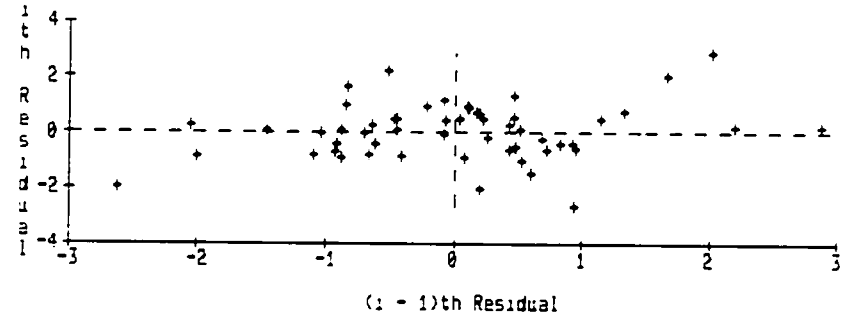

Figure AVII.129: Lag-1 Serial Plot of Residuals from Pump Within-Wafer Variance (PWWV) Model

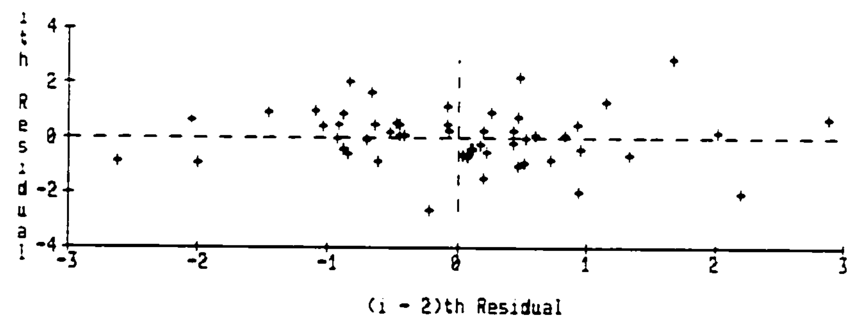

Figure AVII.130: Lag-2 Serial Plot of Residuals from Pump Within-Wafer Variance (PWWV) Model

Appendix VIII:

Determination of Confidence Intervals for Optima

The method for calculating the confidence intervals is based upon a method described by Bacon (1990). In this work, the optimum was a future prediction of the response based upon accepted models. The parameters in the models were determined by least-squares method. The variance of a future measured response is:

$$Var\left(y_k^f\right) = Var(\hat{y}_k) + \sigma^2 \qquad \text{(AVIII.1)}$$

Determination of $Var(\hat{y}_k)$ was given in Appendix V. Since σ^2 is the true but unknown variance, an estimate of σ^2 is needed. The variance was estimated using:

$$\hat{\sigma}^2 = \frac{SSR}{n-p} \qquad \text{(AVIII.2)}$$

where σ^2 is an estimate of pure error variance, SSR represents the Sum of Squares of the Residuals, n is the number of observations, p is the number of parameters. Equation (AVIII.2) was used rather than simply the variance of the centre point replicates since there are more degrees of freedom associated with (AVIII.2).

A 95% confidence interval for y_k^{future} is:

$$\hat{y}_k \pm t_{v,\alpha/2}(\text{estimated variance of } y_k^f)^{1/2} \qquad \text{(AVIII.3)}$$

For the case in which the responses were transformed, the confidence intervals were determined for the transformed version of the model, and the upper and lower limits were subsequently reverted back to their original form. The disadvantage of this method is that the resultant interval is no longer centered about the prediction.

An example follows for the determination of a 95% confidence interval for the predicted Within-Wafer Standard Deviation at the optimum.

$$1/WWS = 0.0464 - 0.0058X1 + 0.0034X2X3 + 0.0034X1X6 \qquad \text{(AVIII.4)}$$

At the optimum, X1 = -0.2368; X2 = -1.0000; X3 = 1.0000; X6 = -1.000, 1/WWS=0.045 and WWS = 20.6. The matrix manupulations involved are now introduced.

$\mathbf{x}^T_k$ = [-0.2368 -1.000 1.000 -1.000]

X =

X0	X1	X2X3	X1X6
1	-1.000	-1.000	-1.000
1	1.000	-1.000	-1.000
1	-1.000	1.000	-1.000
1	1.000	-1.000	1.000
1	1.000	1.000	1.000
1	-1.000	-1.000	1.000
1	-1.000	1.000	1.000
1	1.000	1.000	-1.000
1	-1.000	-1.000	-1.000
1	-1.000	1.000	1.000
1	-1.000	-1.000	1.000
1	-1.000	1.000	-1.000
1	1.000	-1.000	-1.000
1	1.000	1.000	-1.000
1	1.000	-1.000	1.000
1	1.000	1.000	1.000
1	1.000	1.000	1.000
1	1.000	-1.000	1.000
1	-1.000	-1.000	-1.000
1	1.000	1.000	1.000
1	-1.000	1.000	1.000
1	-1.000	1.000	-1.000
1	-1.000	-1.000	1.000
1	1.000	-1.000	-1.000
1	-0.750	0.000	0.000
1	0.000	0.000	0.000
1	0.000	0.000	0.000
1	0.000	0.000	0.000
1	0.000	0.000	0.000
1	0.000	0.000	0.000
1	0.750	0.000	0.000
1	0.000	0.000	0.000
1	0.000	0.000	0.000
1	0.000	0.000	0.000
1	0.000	0.000	0.000
1	0.000	0.000	0.000
1	1.000	1.000	-1.000
1	1.000	-1.000	1.000
1	1.000	1.000	1.000
1	1.000	-1.000	-1.000
1	-1.000	1.000	-1.000
1	-1.000	-1.000	1.000
1	-1.000	1.000	1.000
1	-1.000	-1.000	-1.000
1	0.000	0.000	0.000
1	0.000	0.000	0.000
1	0.000	0.000	0.000
1	0.000	0.000	0.000
1	0.000	0.000	0.000
1	0.000	0.000	0.000
1	0.000	0.000	0.000
1	0.000	0.000	0.000
1	0.000	0.000	0.000
1	0.000	0.000	0.000
1	1.000	-1.000	1.000

$\mathbf{X}^T\mathbf{X}$ =

55	1	-1	3
1	34.125	-1	3
-1	-1	33	1
3	3	1	33

$(\mathbf{X}^T\mathbf{X})^{-1}$ =

0.018	0.000	0.001	-0.002
0.000	0.030	0.001	-0.003
0.001	0.001	0.030	-0.001
-0.002	-0.003	-0.001	0.031

$\mathbf{x}^T{}_k (\mathbf{X}^T\mathbf{X})^{-1} \mathbf{x}_k = 0.0515$

The estimate of pure error variance, by Equation (AVIII.2), is $\hat{\sigma}^2 = 7.63\text{x}10^{-5}$. The degrees of freedom, ν, associated with this estimate is 51. Therefore,

$$Var(y_k^{futrue}) = 0.0515 * 7.63\ \text{x}10^{-5} + 7.63\text{x}10^{-5} = 8.02\ \text{x}10^{-5}. \qquad \text{(AVIII.5)}$$

A 95% confidence interval for 1/WWS is given by

$$\begin{aligned} 95\% \text{ Confidence Interval} &= 0.045 \pm t_{\nu,\alpha/2} * Var(y_k^{futrue})^{1/2} \qquad \text{(AVIII.6)} \\ &= 0.045 \pm 2.01 * 8.02 \text{ x } 10^{-5} \end{aligned}$$

The 95% Confidence Interval for 1/WWS is (0.027, 0.063). The 95% confidence interval for WWS = 1/0.045 = 20.2 is (1/0.027, 1/0.063). More clearly, the 95% confidence interval for Within-Wafer Standard Deviation at the optimum is (15.84, 36.82). Note that this does not yield a symmetrical confidence interval.

Appendix IX:

Creating Control Charts - Sample Calculations

AIX.1: Shewart X-bar Charts

The Shewart X-bar chart is created by sequentially plotting the batch mean thickness measurements. Also indicated on the chart is the process target and both the upper and lower control or action limits. These limits are set at plus or minus three standard deviations. One can expect, under normal conditions, that 3 out of every 1000 batches will fall outside the upper or lower control limits.

The mean of batch i,

$$\overline{X}_i = \frac{\sum_{j=1}^{20} X_{ij}}{20}. \qquad \text{(AIX.1)}$$

Control limits are set at $3500 \pm 3\sigma_{\bar{X}}$, where 3500 represents the target value and $\sigma_{\bar{X}}$ is the true but unknown standard deviation of the batch mean thicknesses. If the observations within a batch are independent then,

$$\sigma_{\bar{X}} = \frac{\sigma}{\sqrt{n}}. \qquad \text{(AIX.2)}$$

In order to set the control limits, an estimate of the process standard deviation, σ, is required. There are two methods that can be used to calculate an estimate of $\sigma_{\bar{X}}$. Method I, uses the following estimate of σ,

$$\hat{\sigma} = \frac{\bar{s}}{c_4} \qquad \text{(AIX.3)}$$

where

$$\bar{s} = \frac{\sum_{i=1}^{k} s_i}{k} \qquad \text{(AIX.4)}$$

and s_i is standard deviation of the data from each batch.

The estimator $\bar{s}$ is a biased estimator of σ. The constant c_4 compensates for the bias in $\bar{s}$. This constant has been widely tabulated and can be found in Ryan (1989). The control limits become,

$$3500 \pm \frac{3\bar{s}}{c_4\sqrt{n}}. \qquad \text{(AIX.5)}$$

An alternative approach, Method II, uses the standard deviation of the batch mean thicknesses as an estimate of $\sigma_{\bar{X}}$. Determining an estimate of $\sigma_{\bar{X}}$ by the first method yields an estimate with more degrees of freedom than by the second method. However, the first method has one major draw back. For cases in which there is a high degree of correlation between data within a sub-group, determining an estimate of $\sigma_{\bar{X}}$ by the first method will substantially underestimate the standard deviation. The second method avoids the effects of within sub-group correlation, because only the subgroup average is used to determine an estimate of $\sigma_{\bar{X}}$.

AIX.2: Standard Deviation Charts

Standard deviation charts, or s-charts, are created by sequentially plotting the standard deviation of a subgroup. An out-of-control situation is signaled whenever the variation within a subgroup exceded the control limits. Control limits are set such that 2 out of every 1000 observations can be expected to fall outside the control limits under normal process conditions. This corresponds to a probability of 0.001. The chi-square distribution is used to determine the probabilities. If $X \sim N(\mu,\sigma^2)$, then

$$\frac{(n-1)s^2}{\sigma^2} \sim \chi^2_{n-1}. \quad \text{(AIX.6)}$$

In this case n-1 degrees of freedom are associated with s^2, the estimate of σ^2. The control limits for the s-chart are,

$$\text{LCL} = \sigma\sqrt{\frac{\chi^2_{0.001}}{n-1}} \quad \text{(AIX.7)}$$

$$\text{UCL} = \sigma\sqrt{\frac{\chi^2_{0.999}}{n-1}}. \quad \text{(AIX.8)}$$

If the average standard deviation, $\bar{s}$, is used to estimate the population standard deviation, σ, then the control limits become

$$\text{LCL} = \frac{\bar{s}}{c_4}\sqrt{\frac{\chi^2_{0.001}}{n-1}} \quad \text{(AIX.9)}$$

$$\text{UCL} = \frac{\bar{s}}{c_4}\sqrt{\frac{\chi^2_{0.999}}{n-1}}. \quad \text{(AIX.10)}$$

This procedure was followed to create the X-bar and s-charts in Chapter 5. For the historical data set, the estimate of the standard deviation of the batch mean thicknesses, $s_{\bar{X}}$, is 35.34. The control limits were then set such that LCL = 3394 Å and UCL = 3606 Å with a target value of 3500Å. The estimate of variance for the s-chart was $\bar{s}/c_4 = 61.82/0.9869 = 62.64$. The lower and upper control limits are given by,

$$\mathrm{LCL} = \frac{\bar{s}}{c_4}\sqrt{\frac{\chi^2_{0.001}}{n-1}} = 62.64\sqrt{\frac{5.407}{20-1}} = 33.41 \quad \text{(AIX.11)}$$

$$\mathrm{UCL} = \frac{\bar{s}}{c_4}\sqrt{\frac{\chi^2_{0.999}}{n-1}} = 62.64\sqrt{\frac{43.82}{20-1}} = 95.12 \quad \text{(AIX.12)}$$

For the case of the CVD reactor used in this research, it has been proposed that two s-charts be used to monitor the within-subgroup correlation. The estimate of variance for the cross-load standard deviation chart is $\bar{s}_{cls}/c_4 = 48.30/0.9213 = 52.43$. The control limits are,

$$\mathrm{LCL} = \frac{\bar{s}_{cls}}{c_4}\sqrt{\frac{\chi^2_{0.001}}{n-1}} = 52.43\sqrt{\frac{0.024}{4-1}} = 4.82 \quad \text{(AIX.13)}$$

$$\mathrm{UCL} = \frac{\bar{s}_{cls}}{c_4}\sqrt{\frac{\chi^2_{0.999}}{n-1}} = 52.43\sqrt{\frac{16.266}{4-1}} = 122.07 \quad \text{(AIX.14)}$$

For this chart $n = 4$, since s_{cls} represents the variance between the four test wafer positions in the reactor.

The estimate of variance for the within-wafer standard deviation chart is $\bar{s}_{wws}/c_4 = 41.79/0.9832 = 42.50$.

$$\mathrm{LCL} = \frac{\bar{s}_{wws}}{c_4}\sqrt{\frac{\chi^2_{0.001}}{n-1}} = 42.50\sqrt{\frac{3.942}{16}} = 21.10 \quad \text{(AIX.15)}$$

$$\mathrm{UCL} = \frac{\bar{s}_{wws}}{c_4}\sqrt{\frac{\chi^2_{0.999}}{n-1}} = 42.50\sqrt{\frac{39.252}{16}} = 66.57 \quad \text{(AIX.16)}$$

There are 16 degrees of freedom associated with each calculation of s_{wws}, since it represents the pooled within-wafer variances of the thickness measurements from the four test wafers [$\nu = 4\times(5-1)=16$].

AIX.1: Sample Calculations for Multivariate Control Charts

Determination of the statistic plotted for multivariate control charts requires the calculation of either the variance-covariance matrix or the correlation matrix. The correlation matrix, **R**, for the "Tweak-Free" or Control Data is,

1.00	0.91	0.94	0.88	0.92	0.74	0.54	0.73	0.73	0.48	0.23	0.21	0.37	0.31	0.14	-0.21	-0.35	-0.29	-0.17	-0.30
0.91	1.00	0.92	0.88	0.95	0.65	0.50	0.63	0.69	0.40	0.34	0.19	0.24	0.24	0.16	-0.27	-0.39	-0.37	-0.24	-0.28
0.94	0.92	1.00	0.88	0.91	0.74	0.51	0.74	0.76	0.47	0.19	0.11	0.26	0.27	0.08	-0.24	-0.40	-0.33	-0.19	-0.32
0.88	0.88	0.88	1.00	0.92	0.75	0.63	0.59	0.86	0.60	0.32	0.27	0.20	0.46	0.36	-0.16	-0.25	-0.32	-0.01	0.02
0.92	0.95	0.91	0.92	1.00	0.72	0.58	0.61	0.73	0.57	0.39	0.32	0.23	0.36	0.33	-0.12	-0.24	-0.32	-0.08	-0.09
0.74	0.65	0.74	0.75	0.72	1.00	0.73	0.89	0.83	0.75	0.17	0.24	0.25	0.37	0.13	-0.01	-0.08	-0.11	0.16	0.07
0.54	0.50	0.51	0.63	0.58	0.73	1.00	0.67	0.66	0.52	0.44	0.51	0.29	0.46	0.37	0.30	0.24	0.11	0.38	0.33
0.73	0.63	0.74	0.59	0.61	0.89	0.67	1.00	0.66	0.48	0.14	0.15	0.42	0.26	-0.11	-0.03	-0.15	0.00	0.03	-0.19
0.73	0.69	0.76	0.86	0.73	0.83	0.66	0.66	1.00	0.63	0.21	0.18	0.13	0.51	0.22	-0.13	-0.19	-0.22	0.15	0.09
0.48	0.40	0.47	0.60	0.57	0.75	0.52	0.48	0.63	1.00	0.15	0.20	-0.08	0.33	0.36	0.01	0.02	-0.19	0.35	0.35
0.23	0.34	0.19	0.32	0.39	0.17	0.44	0.14	0.21	0.15	1.00	0.81	0.57	0.62	0.71	0.66	0.61	0.50	0.56	0.51
0.21	0.19	0.11	0.27	0.32	0.24	0.51	0.15	0.18	0.20	0.81	1.00	0.59	0.61	0.78	0.81	0.77	0.53	0.59	0.60
0.37	0.24	0.26	0.20	0.23	0.25	0.29	0.42	0.13	-0.08	0.57	0.59	1.00	0.64	0.25	0.53	0.40	0.68	0.36	0.08
0.31	0.24	0.27	0.46	0.36	0.37	0.46	0.26	0.51	0.33	0.62	0.61	0.64	1.00	0.59	0.53	0.46	0.50	0.70	0.53
0.14	0.16	0.08	0.36	0.33	0.13	0.37	-0.11	0.22	0.36	0.71	0.78	0.25	0.59	1.00	0.61	0.62	0.27	0.51	0.73
-0.21	-0.27	-0.24	-0.16	-0.12	-0.01	0.30	-0.03	-0.13	0.01	0.66	0.81	0.53	0.53	0.61	1.00	0.96	0.82	0.75	0.68
-0.35	-0.39	-0.40	-0.25	-0.24	-0.08	0.24	-0.15	-0.19	0.02	0.61	0.77	0.40	0.46	0.62	0.96	1.00	0.79	0.76	0.80
-0.29	-0.37	-0.33	-0.32	-0.32	-0.11	0.11	0.00	-0.22	-0.19	0.50	0.53	0.68	0.50	0.27	0.82	0.79	1.00	0.68	0.49
-0.17	-0.24	-0.19	-0.01	-0.08	0.16	0.38	0.03	0.15	0.35	0.56	0.59	0.36	0.70	0.51	0.75	0.76	0.68	1.00	0.78
-0.30	-0.28	-0.32	0.02	-0.09	0.07	0.33	-0.19	0.09	0.35	0.51	0.60	0.08	0.53	0.73	0.68	0.80	0.49	0.78	1.00

The variance-covariance matrix, S, for the control data is given in the sample calculation for the T^2 chart.

Hotelling's T^2 - Sample Calculations

$$T^2 = (\bar{\mathbf{x}} - \mu_0)^T \mathbf{S}^{-1} (\bar{\mathbf{x}} - \mu_0)$$

$$T^2 = \begin{bmatrix} x_{i1} - 3500 \\ x_{i2} - 3500 \\ x_{i3} - 3500 \\ x_{i4} - 3500 \\ x_{i5} - 3500 \\ x_{i6} - 3500 \\ x_{i7} - 3500 \\ x_{i8} - 3500 \\ x_{i9} - 3500 \\ x_{i10} - 3500 \\ x_{i11} - 3500 \\ x_{i12} - 3500 \\ x_{i13} - 3500 \\ x_{i14} - 3500 \\ x_{i15} - 3500 \\ x_{i16} - 3500 \\ x_{i17} - 3500 \\ x_{i18} - 3500 \\ x_{i19} - 3500 \\ x_{i20} - 3500 \end{bmatrix}^T \begin{bmatrix} 7349 & 6668 & 6436 & 9257 & 6932 & 3389 & 3448 & 3421 & 6368 & 5486 & 3157 & 4041 & 6108 & 4123 & 3971 & 3963 & 4000 & 4792 & 4250 & 3651 \\ 6668 & 6691 & 6139 & 8581 & 6632 & 2988 & 3019 & 3068 & 5719 & 5116 & 2843 & 3870 & 5812 & 3688 & 3444 & 3757 & 3830 & 4527 & 4203 & 3492 \\ 6436 & 6139 & 6366 & 7985 & 6216 & 3082 & 3175 & 3407 & 5416 & 4761 & 2654 & 3602 & 5331 & 3797 & 3266 & 3673 & 3763 & 4084 & 4305 & 3316 \\ 9257 & 8581 & 7985 & 13566 & 9348 & 4428 & 4841 & 4311 & 9236 & 7591 & 3930 & 5142 & 8125 & 5512 & 4723 & 4848 & 5079 & 6834 & 5420 & 4318 \\ 6932 & 6632 & 6216 & 9348 & 7093 & 3217 & 3438 & 3014 & 6300 & 5534 & 2836 & 3827 & 5714 & 3908 & 3482 & 3770 & 3783 & 4711 & 4181 & 3343 \\ 3389 & 2988 & 3082 & 4428 & 3217 & 2225 & 2278 & 2129 & 3076 & 2883 & 1525 & 1942 & 2876 & 2205 & 2040 & 1957 & 1945 & 2161 & 2015 & 1754 \\ 3448 & 3019 & 3175 & 4841 & 3438 & 2278 & 3695 & 2284 & 3349 & 2827 & 1591 & 2064 & 2720 & 2598 & 2197 & 2228 & 1954 & 1980 & 2789 & 1935 \\ 3421 & 3068 & 3407 & 4311 & 3014 & 2129 & 2284 & 3508 & 2779 & 2288 & 2312 & 2834 & 4600 & 2110 & 2076 & 2801 & 2860 & 3249 & 2629 & 2360 \\ 6368 & 5719 & 5416 & 9236 & 6300 & 3076 & 3349 & 2779 & 6806 & 5289 & 2566 & 3334 & 5103 & 4171 & 3250 & 3233 & 3379 & 4386 & 3751 & 2905 \\ 5486 & 5116 & 4761 & 7591 & 5534 & 2883 & 2827 & 2288 & 5289 & 5445 & 2145 & 2772 & 4201 & 3394 & 3222 & 2558 & 2811 & 3511 & 3370 & 2746 \\ 3157 & 2843 & 2654 & 3930 & 2836 & 1525 & 1591 & 2312 & 2566 & 2145 & 2478 & 2986 & 4175 & 1592 & 2076 & 2524 & 2564 & 3061 & 1984 & 2197 \\ 4041 & 3870 & 3602 & 5142 & 3827 & 1942 & 2064 & 2834 & 3334 & 2772 & 2986 & 4147 & 5386 & 2109 & 2559 & 3462 & 3510 & 4011 & 2578 & 2709 \\ 6108 & 5812 & 5331 & 8125 & 5714 & 2876 & 2720 & 4600 & 5103 & 4201 & 4175 & 5386 & 8666 & 2976 & 3375 & 4608 & 4895 & 6407 & 3680 & 3748 \\ 4123 & 3688 & 3797 & 5512 & 3908 & 2205 & 2598 & 2110 & 4171 & 3394 & 1592 & 2109 & 2976 & 3584 & 2845 & 2427 & 2353 & 2302 & 3232 & 2492 \\ 3971 & 3444 & 3266 & 4723 & 3482 & 2040 & 2197 & 2076 & 3250 & 3222 & 2076 & 2559 & 3375 & 2845 & 3420 & 2528 & 2469 & 2546 & 2821 & 2855 \\ 3963 & 3757 & 3673 & 4848 & 3770 & 1957 & 2228 & 2801 & 3233 & 2558 & 2524 & 3462 & 4608 & 2427 & 2528 & 3982 & 3617 & 3973 & 2867 & 2918 \\ 4000 & 3830 & 3763 & 5079 & 3783 & 1945 & 1954 & 2860 & 3379 & 2811 & 2564 & 3510 & 4895 & 2353 & 2469 & 3617 & 3703 & 4106 & 2745 & 2867 \\ 4792 & 4527 & 4084 & 6834 & 4711 & 2161 & 1980 & 3249 & 4386 & 3511 & 3061 & 4011 & 6407 & 2302 & 2546 & 3973 & 4106 & 5874 & 2719 & 2988 \\ 4250 & 4203 & 4305 & 5420 & 4181 & 2015 & 2789 & 2629 & 3751 & 3370 & 1984 & 2578 & 3680 & 3232 & 2821 & 2867 & 2745 & 2719 & 4448 & 2963 \\ 3651 & 3492 & 3316 & 4318 & 3343 & 1754 & 1935 & 2360 & 2905 & 2746 & 2197 & 2709 & 3748 & 2492 & 2855 & 2918 & 2867 & 2988 & 2963 & 3166 \end{bmatrix} \begin{bmatrix} x_{i1} - 3500 \\ x_{i2} - 3500 \\ x_{i3} - 3500 \\ x_{i4} - 3500 \\ x_{i5} - 3500 \\ x_{i6} - 3500 \\ x_{i7} - 3500 \\ x_{i8} - 3500 \\ x_{i9} - 3500 \\ x_{i10} - 3500 \\ x_{i11} - 3500 \\ x_{i12} - 3500 \\ x_{i13} - 3500 \\ x_{i14} - 3500 \\ x_{i15} - 3500 \\ x_{i16} - 3500 \\ x_{i17} - 3500 \\ x_{i18} - 3500 \\ x_{i19} - 3500 \\ x_{i20} - 3500 \end{bmatrix}$$

The upper and lower control limits are:

$$UCL = \left(\frac{p(n-1)(n+1)}{n(n-p)}\right)F_{\alpha/2(p,n-p)} = \left(\frac{20(42-1)(42+1)}{42(42-20)}\right)F_{0.05/2(20,42-20)} = 93.18$$

$$LCL = \left(\frac{p(n-1)(n+1)}{n(n-p)}\right)F_{1-\alpha/2(p,n-p)} = \left(\frac{20(42-1)(42+1)}{42(42-20)}\right)F_{(1-0.05/2)(20,42-20)} = 16.19$$

Table AIX.1: Data used to Create Hotelling's T^2 Chart

Batch Number	$(\mathbf{x}_i - \bar{\mathbf{x}})^T$																				T^2
1	63	57	30	123	29	5.25	-6.75	-44	70	33	-76	-94	-129	-4	-39	-27	-38	-85	38	8	109.9
2	69	72	47	109	68	2	-10	-47	68	28	-77	-92	-132	-4	-41	-102	-109	-149	-31	-83	51.3
3	56	74	36	97	55	8.5	-3.5	-41	72	37	-74	-96	-127	-5	-36	-120	-103	-169	-69	-87	63.2
4	82	85	70	122	87	15	3	-35	75	46	-71	-100	-121	-5	-31	-95	-107	-136	-27	-68	48.0
5	74	63	71	136	75	20	-18	-17	107	44	-18	-8	-68	76	15	-16	-39	-57	76	1	41.5
6	10	13	-13	52	24	-39	-65	-78	35	-3	-9	-84	-109	14	-15	-35	-50	-73	24	-15	38.4
7	-92	-93	-140	-41	-57	-61	-56	-121	-14	-9	10	9	-42	69	47	82	87	57	123	87	155.1
8	135	123	130	180	138	80	59	36	153	107	-3	-29	-57	77	39	-38	-60	-80	40	-14	45.5
9	-27	-33	-76	25	5	-18	-11	-77	27	31	10	6	-42	69	50	61	59	38	111	75	86.5
10	22	15	19	62	35	-35	-57	-58	28	-1	-41	-57	-93	20	1	-36	-27	-80	-3	-6	26.0
11	-72	-48	-109	-63	-36	-85	-92	-139	-22	-38	-35	-15	-86	-2	3	13	28	-2	39	22	52.8
12	62	62	41	112	71	3	4	-49	63	45	-60	-64	-119	6	-9	-71	-81	-118	-8	-39	37.1
13	108	104	86	175	113	71	66	17	143	117	41	38	-27	100	96	30	25	-22	83	68	22.2
14	50	56	36	87	57	105	63	101	87	138	-61	-56	-117	-23	-7	-47	-44	-94	-4	-12	148.0
15	66	60	60	116	67	16	4	-33	99	43	-25	-31	-90	65	12	-9	-26	-26	66	1	24.7
16	60	60	48	107	66	-7	-12	-51	60	32	-38	-45	-98	24	7	-25	-29	-76	34	1	27.2
17	47	47	43	101	47	13	0	-34	89	38	-15	-33	-73	69	18	0	-12	-42	74	11	19.8
18	96	102	89	103	101	49	63	12	42	99	-5	19	-49	-18	59	-26	-37	-68	42	-7	45.7
19	129	123	104	177	138	49	37	4	114	86	-34	-46	-93	30	15	-52	-61	-94	10	-24	55.2
20	121	111	89	184	137	67	62	8	123	117	32	26	-36	97	85	34	18	-28	108	62	34.3
21	76	78	53	113	96	20	24	-28	70	66	-12	-8	-70	37	40	-5	0	-50	29	33	22.7
22	6	-4	10	30	17	-52	-77	-74	0	-19	-77	-102	-117	-22	-37	-42	-66	2	-21	-42	25.4
23	71	55	73	99	79	11	-18	-19	72	45	-41	-71	-87	26	4	-51	-80	-81	8	-25	33.1
24	137	122	128	194	142	61	32	12	149	193	-11	-39	-72	77	30	-31	-57	-71	52	-10	63.5
25	-10	-13	-64	24	34	-20	11	-65	-32	55	14	-7	-29	102	50	78	72	54	116	97	228.5

Table AIX.1 (continued): Data used to Create Hotelling's T^2 Chart

Batch Number	$(\mathbf{x}_i - \bar{\mathbf{x}})^T$																				T^2
26	172	160	143	244	183	105	98	43	171	153	46	39	-23	107	100	34	24	-21	80	79	38.4
27	102	34	37	48	39	-46	-45	-41	-37	-34	36	49	104	64	99	99	43	65	41	-57	145.2
28	48	39	25	111	57	14	-5	-47	85	48	-18	-26	-81	41	35	-21	-28	-75	36	20	27.8
29	42	35	20	70	40	-30	-27	-88	28	4	-70	-62	-135	-14	-30	-71	-66	-124	-17	-50	41.3
30	68	60	44	129	80	12	21	-36	22	79	-15	-3	-71	-6	55	-4	-12	-59	47	37	54.5
31	100	79	118	121	104	34	-4	25	88	55	-35	-74	-61	31	0	-52	-51	-87	-2	-40	52.8
32	73	69	48	121	87	35	50	-9	33	92	-12	6	-62	-10	51	-2	0	-48	30	41	45.0
33	63	45	75	59	55	41	-52	36	40	118	-48	-99	-17	59	-113	-46	-71	-10	111	-65	233.5
34	44	127	52	51	62	-33	-6	-4	7	-75	29	-87	-87	-78	-108	-83	-89	-60	-42	-112	210.0
35	87	89	106	98	116	55	98	56	59	2	30	91	37	63	22	175	90	42	63	-10	44.1
36	100	-1	16	18	24	56	25	59	47	52	-109	-81	-80	-59	-157	-73	-73	-69	3	-99	399.3
37	128	95	97	153	60	60	28	86	131	-50	-48	-63	118	120	-91	-52	-74	43	0	-67	186.4
38	95	76	79	174	100	52	258	49	155	86	40	40	-18	144	81	68	38	20	164	85	47.1
39	6	-4	-20	75	16	-45	-50	-100	4	3	-73	-85	-141	-3	-21	-68	-73	-120	-17	-26	60.9
40	-118	-135	-163	-48	-96	-25	-28	-80.5	14	25	-105	-134	-164	-34	-67	58	54	43	107	63	244.4
41	-107	-150	-93	-41	-104	-5	-6	-61	24	47	-74	-89	-145	-4	-25	75	73	44	121	97	233.2

Principal Components

The eigenvalues of the correlation matrix, **R**, for the control data, are: 8.25, 6.54, 1.72, 1.33, 0.69, 0.41, 0.29, 0.18, 0.16, 0.13, 0.09, 0.07, 0.05, 0.03, 0.02, 0.02, 0.01, 0.01, 0.00 and 0.00. The percentages of the total variability explained by the associated principal components are: 41.27%, 32.68%, 8.61%, 6.66%, 3.43%, 2.03%,1.47%, 0.88%, 0.78%, 0.64%, 0.43%, 0.34%, 0.25%, 0.15%, 0.12%, 0.10%, 0.06%, 0.05%, 0.02% and 0.01%, respectively. Only the first three principal components should be retained since combined, these three account for (41.27 + 32.68 + 8.61)% = 82.56% of the variation in the data. The eigenvector associated with the first principal component is $\mathbf{e}^T$ = [0.29, 0.28, 0.28, 0.31, 0.31, 0.30, 0.28, 0.26, 0.29, 0.23, 0.19, 0.19, 0.16, 0.22, 0.17, 0.07, 0.03, 0.01, 0.10, 0.07]. The first principal component is,

$Y_1 = 0.29X_1 + 0.28X_2 + 0.28X_3 + 0.31X_4 + 0.31X_5 + 0.30X_6 + 0.28X_7 + 0.26X_8 + 0.29X_9 + 0.23X_{10} + 0.19X_{11} + 0.19X_{12} + 0.16X_{13} + 0.22X_{14} + 0.17X_{15} + 0.07X_{16} + 0.03X_{17} + 0.01X_{18} + 0.10X_{19} + 0.07X_{20}$, which is the weighted sum of the measurements and is similar to the batch mean thickness.

The eigenvector associated with the second principal component is e^T = [-0.17, -0.18, -0.19, -0.12, -0.13, -0.08, 0.05, -0.11, -0.10, -0.02, 0.24, 0.28, 0.17, 0.21, 0.24, 0.36, 0.38, 0.33, 0.32, 0.31]. The second principal component is,
$Y_2 = -0.17X_1 - 0.18X_2 - 0.19X_3 - 0.12X_4 - 0.13X_5 - 0.08X_6 + 0.05X_7 - 0.11X_8 - 0.10X_9 - 0.02X_{10} + 0.24X_{11} + 0.28X_{12} + 0.17X_{13} + 0.21X_{14} + 0.24X_{15} + 0.36X_{16} + 0.38X_{17} + 0.33X_{18} + 0.32X_{19} + 0.31X_{20}$, which is essentially a difference between measurements 1 to 10 and 11 to 20. This is a cross-load range and measures the variability across a batch. This measurement is similar to the cross-load standard deviation.

The eigenvector associated with the third principal component is e^T = [0.16, 0.13, 0.12, -0.09, 0.01, -0.09, -0.09, 0.19, -0.17, -0.45, 0.13, 0.08, 0.55, 0.05, -0.23, 0.10, -0.03, 0.30, -0.16, -0.39]. The third principal component is, $Y_3 = 0.16X_1 + 0.13X_2 + 0.12X_3 - 0.09X_4 + 0.01X_5 - 0.09X_6 - 0.09X_7 + 0.19X_8 - 0.17X_9 - 0.45X_{10} + 0.13X_{11} + 0.08X_{12} + 0.55X_{13} + 0.05X_{14} - 0.23X_{15} + 0.10X_{16} - 0.03X_{17} + 0.30X_{18} - 0.16X_{19} - 0.39X_{20}$, which is mainly the difference between the Left and Right positions on each wafer. This difference is similar to a within-wafer standard deviation measurement.

Table AIX.2: Scores for the First Three Principal Components of the Control Data (Based on Standarized Data)

Batch Number	Y_1	Y_2	Y_3	Batch Number	Y_1	Y_2	Y_3
1				22	-4.06	-1.23	0.59
2	-1.43	-3.91	-0.43	23	-0.27	-1.84	-0.13
3				24	3.76	-1.58	-1.22
4	-0.66	-3.87	-0.48	25	-1.18	4.77	-0.17
5	1.04	-0.03	-0.14	26	6.60	1.08	-0.78
6	-2.79	-0.43	-0.15	27	-0.23	3.54	3.87
7	-4.14	5.89	-0.23	28	-0.07	0.05	-0.75
8	3.81	-1.60	-0.39	29	-2.69	-2.23	-0.43
9	-1.69	4.33	-0.36	30	0.40	0.42	-0.72
10	-2.33	-0.54	-0.01	31	1.00	-2.24	0.36
11	-5.48	2.68	0.12	32	1.02	0.41	-0.60
12	-0.90	-2.45	-0.70	33	-0.21	-1.27	0.97
13	4.25	1.85	-0.67	34	-2.19	-3.03	2.56
14	0.89	-2.17	-1.36	35	3.18	3.26	2.66
15	0.52	0.11	-0.28	36	-1.86	-3.37	0.87
16	-0.57	-0.65	-0.43	37	2.00	-1.51	4.09
17	0.18	0.64	-0.29	38	5.19	3.43	-0.63
18				39	-3.71	-1.75	-0.85
19	2.26	-2.41	-0.53	40			
20	4.22	1.63	-0.74	41	-4.85	3.70	-2.17
21	0.98	0.31	-0.43				

Principal components can also be determined using statistical software. The principal components of the historic data, which were determined using RS/1 statistical software, are:

$Y_1 = 0.20X_1 + 0.19X_2 + 0.18X_3 + 0.20X_4 + 0.19X_5 + 0.26X_6 + 0.24X_7 + 0.24X_8 + 0.23X_9 + 0.23X_{10} + 0.25X_{11} + 0.23X_{12} + 0.23X_{13} + 0.24X_{14} + 0.24X_{15} + 0.23X_{16} + 0.21X_{17} + 0.21X_{18} + 0.22X_{19} + 0.22X_{20}$, which is a weighted sum of the measurements and is similar to the batch mean thickness. Y_1 accounts for 67.8% of the variability in the data.

$Y_2 = -0.36X_1 - 0.35X_2 - 0.35X_3 - 0.32X_4 - 0.34X_5 - 0.08X_6 + 0.05X_7 - 0.10X_8 - 0.08X_9 - 0.06X_{10} + 0.15X_{11} + 0.18X_{12} + 0.12X_{13} + 0.10X_{14} + 0.17X_{15} + 0.24X_{16} + 0.27X_{17} + 0.22X_{18} + 0.18X_{19} + 0.24X_{20}$, which is essentially a difference between measurements 1 to 10 and 11 to 20. This is a measurement of the cross-load range and measures the variability across a batch. This measurement is similar to the cross-load standard deviation. Y_2 accounts for 17.7 % of the variability in the data.

$Y_3 = -.17X_1 - 0.17X_2 - 0.25X_3 - 0.09X_4 - 0.14X_5 + 0.20X_6 + 0.16X_7 + 0.11X_8 + 0.33X_9 + 0.31X_{10} + 0.11X_{11} + 0.13X_{12} + 0.08X_{13} + 0245X_{14} + 0.22X_{15} - 0.31X_{16} - 0.30X_{17} - 0.43X_{18} - 0.14X_{19} - 0.19X_{20}$, which is the difference between the end wafers and the middle wafers (Load + Pump) - (C1 + C2). Y_3 accounts for 3.8% of the variability in the data.

Table AIX.3: Scores for the First Three Principal Components of the Historical Data (Based on Standarized Data)

Batch Number	Y_1	Y_2	Y_3
1			
2	3.50	4.27	0.26
3			
4	2.84	4.56	0.11
5	0.45	2.44	-0.60
6	3.38	1.24	-0.78
7	2.29	-4.11	-1.81
8	-1.13	4.53	0.18
9	0.96	-1.97	-1.47
10	3.01	1.52	-0.87
11	4.28	-2.12	-1.62
12	2.60	3.42	-0.04
13	-2.55	2.20	-0.49
14	0.88	3.19	0.72
15	0.69	2.15	-0.93
16	1.73	2.37	-0.92
17	0.80	1.55	-0.79
18			
19	0.20	4.71	-0.26
20	-2.48	2.53	-0.81
21	0.26	2.22	-0.90

Batch Number	Y_1	Y_2	Y_3
22	4.27	1.40	-1.61
23	1.89	3.19	-0.36
24	-1.16	4.58	0.13
25	0.38	-1.89	-1.98
26	-4.10	3.85	-0.72
27	0.08	-0.28	-2.52
28	1.23	1.83	-0.33
29	9.87	2.68	-0.44
30	0.62	1.99	-1.00
31	1.01	3.98	-0.43
32	0.11	2.10	-0.87
33	1.44	2.69	-0.80
34	3.63	3.64	-1.37
35	-2.48	0.96	-2.53
36	3.22	3.23	-0.22
37	-0.08	3.63	-0.91
38	-3.78	1.37	-0.59
39	4.48	1.86	-0.36
40			
41	3.09	-3.26	-1.58
42			

Table AIX.3 (con't): Scores for the First Three Principal Components of the Historical Thickness Data (Based on Standarized Data)

Batch Number	Y_1	Y_2	Y_3
43	4.31	0.63	-1.20
44	4.34	0.93	-0.57
45	1.12	2.14	-0.18
46	4.87	0.91	-0.72
47	8.43	2.97	-1.73
48	1.64	-4.21	-0.75
49	2.69	-2.34	-0.43
50	2.26	0.68	0.41
51	2.41	-1.07	-0.34
52	0.34	-2.37	-0.25
53	-2.76	-2.01	-0.36
54	-0.42	-1.38	-0.06
55	0.67	2.57	1.04
56	0.78	-2.64	-0.16
57	2.35	-2.26	0.24
58	0.39	-2.79	0.12
59	-0.68	-2.51	-1.40
60	-1.05	-1.82	0.54
61	-0.87	-0.17	0.94
62	-0.84	-1.68	0.04
63	1.85	-2.82	0.07
64	0.27	-1.80	0.57
65	0.66	-1.71	0.41
66	-7.21	-0.71	0.77
67	0.58	-2.10	0.39
68	-1.91	-1.93	0.15
69	-1.32	1.75	1.26
70	-4.90	-1.48-	1.85
71	-0.67	1.31	0.53
72	-0.03	-2.72	-0.04
73	-10.04	-3.53	1.72
74	1.24	-3.60	0.93
75	-2.12	-2.70	1.09
76	-2.42	-2.25	1.16
77	-3.70	-2.75	0.62
78	-1.24	-2.23	1.30
79	1.38	1.44	2.48
80			
81	-3.73	-0.60	1.62
82	-5.62	-0.81	2.26

Batch Number	Y_1	Y_2	Y_3
83	8.32	-1.34	0.87
84			
85	9.97	0.21	1.00
86			
87	3.98	-1.78	0.35
88	-1.91	-2.32	1.54
89	-1.02	0.54	1.18
90	-2.08	0.27	0.28
91	-1.72	-0.19	0.48
92	-3.64	0.53	1.02
93	-2.33	-1.14	0.64
94	1.44	-1.36	0.04
95	-3.91	-1.70	0.83
96	2.34	2.02	0.96
97	2.32	3.81	-0.37
98	-2.27	7.24	0.57
99	-1.68	2.29	0.62
100	-0.89	-0.83	-0.20
101	-0.54	0.82	-0.10
102	-1.24	-1.04	0.28
103	-8.38	2.54	1.12
104	-3.24	0.56	0.26
105	6.47	0.29	0.25
106	3.88	0.73	0.49
107			
108	-4.50	1.21	2.36
109	-2.40	1.11	0.82
110	-1.17	2.33	1.92
111	4.46	2.44	2.18
112	4.84	-0.35	1.34
113	3.06	-0.40	1.01
114	2.72	-0.16	-0.49
115	6.67	0.15	-0.33
116	5.55	-0.09	0.43
117	5.49	-0.02	0.06
118	-0.84	0.22	3.67
119	-2.02	-0.92	-0.32
120	1.18	0.38	0.86
121	-4.54	0.54	0.56
122	4.37	-0.49	0.77

Table AIX.3 (con't): Scores for the First Three Principal Components of the Historical Thickness Data (Based on Standarized Data)

Batch Number	Y_1	Y_2	Y_3	Batch Number	Y_1	Y_2	Y_3
123	3.96	-1.10	0.09	164			
124	2.44	0.30	0.45	165	-2.92	0.61	0.72
125	8.81	0.04	0.17	166	-0.59	1.92	0.80
126	4.36	1.34	0.86	167	1.96	-0.69	0.01
127	4.22	1.14	0.74	168	2.98	0.15	-3.2
128	4.49	-0.24	0.52	169	3.03	-1.83	-0.83
129	4.49	-0.24	0.52	170	1.89	1.49	-0.20
130	4.80	0.37	1.03	171	1.47	-1.15	-0.27
131	0.92	-1.27	0.92	172	-0.63	-0.04	-0.43
132	9.63	-0.68	1.19	173	-1.81	0.81	-0.70
133	11.65	-2.96	0.28	174	-3.46	0.59	-0.47
134	9.53	-1.38	0.75	175	0.53	-0.34	-0.50
135	4.57	-0.35	-0.12	176	-3.66	0.55	-0.19
136	-0.96	0.75	0.03	177	0.17	-0.15	-0.46
137	2.35	0.36	-0.52	178	-2.66	-0.89	-1.05
138	-1.26	-0.60	-0.31	179	-1.79	-0.23	-0.53
139	1.14	-0.11	-0.40	180	-1.49	0.03	-0.25
140	-1.04	-0.61	-0.65	181	-2.80	-0.41	-0.96
141	-4.74	0.22	-0.14	182	-3.95	-0.49	0.21
142	-1.23	-0.98	0.13	183	-4.29	0.35	0.50
143	3.88	-1.07	-1.12	184	-5.27	-0.45	-1.23
144	-2.55	0.77	-0.70	185	-8.11	0.14	0.07
145	-0.27	-0.09	-0.59	186	-5.94	2.83	-0.22
146	2.02	1.10	-1.27	187	2.16	-0.93	0.67
147	-3.07	2.37	-0.93	188	4.63	0.60	-0.15
148	0.86	-0.80	-0.41	189	-0.69	1.57	-0.16
149	0.36	0.94	-0.14	190	-5.24	2.62	0.14
150	1.60	2.09	0.24	191	-4.48	2.06	0.40
151	0.10	0.14	-0.44	192	-4.41	0.37	-0.26
152	-2.11	0.48	-0.56	193	-19.32	0.68	-2.36
153	-3.18	0.58	-0.43	194	2.97	-0.54	-0.00
154	-1.13	-0.06	-.093	195	2.50	-1.85	-0.63
155	-2.44	0.99	0.41	196			
156	-0.43	-0.14	-0.94	197	1.31	-1.58	-0.11
157	-0.80	0.79	-0.26	198	2.68	-2.06	-0.31
158	-1.24	-0.50	-0.68	199	1.01	-1.21	-0.01
159	-1.55	-0.43	-0.45	200	-1.50	-0.24	-0.23
160	1.21	0.95	0.43	201	-0.95	-0.21	-0.70
161	1.82	-0.75	-0.22	202	0.64	-1.74	-0.53
162	1.61	0.81	-0.70	203	-3.59	-1.12	-0.03
163	1.22	-0.65	-0.61	204	-0.33	-1.19	0.18

Table AIX.3 (con't): Scores for the First Three Principal Components of the Historical Thickness Data (Based on Standarized Data)

Batch Number	Y_1	Y_2	Y_3
205	2.32	-0.92	-0.03
206	-5.86	-1.36	-0.57
207			
208	6.85	-0.46	0.52
209	1.23	-0.94	-2.4
210	-2.61	1.65	0.63
211	1.06	-0.65	-0.66
212	-2.68	0.11	-0.46
213	-0.55	-3.66	-1.15
214	1.56	-0.94	-0.25
215	0.69	-2.37	0.03
216	-1.92	-0.46	0.35
217	3.68	-0.40	-0.61
218	-0.88	-1.17	0.82
219	0.60	-2.14	-0.13
220	-0.37	-0.73	0.45
221	2.57	-0.58	-0.09
222	1.96	-1.80	-0.25
223	-3.30	-1.91	-0.33
224	-1.89	-1.59	-0.69

Batch Number	Y_1	Y_2	Y_3
225	-3.75	-0.96	-0.57
226	-0.62	-2.06	-.46
227	-2.29	3.97	-1.33
228	-5.42	-0.62	0.61
229	-3.65	-0.69	0.52
230	-6.05	-.087	-0.54
231	-0.94	-1.60	-0.45
232	-4.60	-1.58	-0.14
233	-0.53	-1.90	-0.34
234	-2.44	-1.16	1.24
235	-2.14	1.06	1.45
236	-1.09	-2.39	-0.32
237	-0.12	-2.51	-0.07
238	-6.51	-1.55	-0.28
239	-3.95	-1.23	-0.99
240	-3.96	0.74	1.26
241	-1.02	-1.93	-0.09
242	0.60	-1.41	0.59
243	-1.93	-1.45	0.53

MCUSUM - Sample Calculations

For $k = 0.5$ and $h = 24.7$

$$C_t = [(\mathbf{s} + \mathbf{x}_i - \mathbf{a})^T \, S^{-1} \, (\mathbf{s} + \mathbf{x}_i - \mathbf{a})]^{1/2} \qquad \text{(AXI.17)}$$

The response vector was standardized such that

$$z_{ij} = \frac{x_{ij} - \tau}{\hat{\sigma}_j} \text{ for } i = 1, 2, \ldots 41 \text{ and } j = 1, 2, \ldots 20. \qquad \text{(AXI.18)}$$

This results in

$$C_t = [(\mathbf{s}_{t-1} + \mathbf{z}_i)^T \, R^{-1} \, (\mathbf{s}_{t-1} + \mathbf{z}_i)]^{1/2} \qquad \text{(AXI.19)}$$

where R is the correlation matrix of the non-standardized variables. The vector of multivariate CUSUM's is

$\mathbf{s}_t = \mathbf{0}$ if $C_t \leq 0.5$ (AXI.20)

$\mathbf{s}_t = (\mathbf{s}_{t-1} + \mathbf{z}_t)(1 - 0.5/C_t)$ if $C_t > 0.5$ (AXI.21)

and

$\mathbf{s}_0 = [0\ 0\ 0\ 0\ 0\ 0\ 0\ 0\ 0\ 0\ 0\ 0\ 0\ 0\ 0\ 0\ 0\ 0\ 0\ 0\ 0\ 0\ 0]^T$ (AXI.22)

Thus the statistic plotted,

$$Y_t = \left[\mathbf{s}_t^T \mathbf{R}^{-1} \mathbf{s}_t\right]^{1/2} \quad \text{(AXI.23)}$$

signals an out-of-control situation whenever $Y_t > 24.7$.

The data generated from this procedure is given in Table AIX.3.

MEWMA - Sample Calculations

For $r = 0.1$ and $h_4 = 37.32$

$\mathbf{Z}_i = r\mathbf{z}_i + (1\text{-}r)\mathbf{z}_{i-1}$ (AXI.24)

The covariance of $\mathbf{Z}_i$ is $\mathbf{R}_{Z_i} = r/(2\text{-}r)(1\text{-}(1\text{-}r)^{2t})\mathbf{R}$ (AXI.25)

An out-of-control situation is signalled if

$T_t^2 = \mathbf{Z}_t^T \mathbf{R}_{Z_t}^{-1} \mathbf{Z}_{t-1} > 37.32$. (AXI.26)

The data generated from this procedure is given in Table AIX.4.

Table AIX.4: Data Used to Create a MCUSUM Chart

i	S_{i1}	S_{i2}	S_{i3}	S_{i4}	S_{i5}	S_{i6}	S_{i7}	S_{i8}	S_{i9}	S_{i10}	S_{i11}	S_{i12}	S_{i13}	S_{i14}	S_{i15}	S_{i16}	S_{i17}	S_{i18}	S_{i19}	S_{i20}	Cn	Yn
0	0	0	0	0	0	0	0	0	0	0	0	0	0	0	0	0	0	0	0	0		
2	64	67	44	101	63	2	-9	-44	63	26	-72	-86	-123	-4	-38	-95	-101	-139	-29	-77		
4	141	146	109	215	145	16	-6	-76	133	69	-137	-179	-235	-8	-67	-183	-201	-264	-54	-140	7	7
5	208	203	175	341	213	35	-23	-90	233	110	-151	-181	-294	66	-50	-193	-233	-312	22	-135	13	13
6	213	211	158	383	231	-4	-86	-164	261	104	-156	-259	-393	78	-63	-222	-276	-375	44	-146	17	17
7	118	115	18	334	170	-63	-139	-278	242	93	-142	-244	-425	143	-16	-137	-184	-311	164	-58	20	20
8	248	233	145	503	302	16	-78	-237	386	196	-142	-267	-472	216	22	-171	-239	-383	199	-70	22	21
9	217	196	67	519	301	-2	-88	-308	406	223	-130	-256	-504	279	71	-108	-177	-339	305	5	24	23
10	235	208	85	571	331	-36	-142	-361	427	218	-168	-308	-588	295	71	-142	-200	-412	297	-1	28	27
11	161	158	-24	501	290	-119	-231	-492	399	178	-200	-318	-664	288	73	-127	-170	-408	331	20	31	30
12	220	217	17	605	357	-115	-224	-534	456	220	-257	-377	-772	290	63	-195	-248	-519	318	-18	34	34
13	324	317	102	770	464	-43	-156	-510	591	332	-213	-335	-789	385	157	-163	-220	-534	396	49	37	37
14	369	369	136	847	515	61	-92	-405	671	465	-271	-387	-896	358	148	-208	-261	-621	388	37	40	39
15	431	424	194	953	576	76	-87	-433	762	503	-293	-413	-976	419	159	-215	-284	-640	449	37	45	44
16	486	479	240	1050	636	69	-98	-480	814	530	-328	-454	-1063	439	164	-237	-310	-709	479	38	48	47
17	528	522	280	1141	677	81	-97	-509	895	563	-340	-483	-1126	503	180	-235	-319	-744	548	49	52	52
19	652	639	381	1307	808	129	-59	-501	1000	643	-370	-524	-1209	529	194	-285	-377	-831	553	24	55	55
20	767	745	467	1479	937	194	2	-489	1115	754	-336	-494	-1236	621	277	-249	-356	-853	656	86	60	60
21	837	817	516	1581	1026	213	26	-513	1176	814	-345	-499	-1296	653	314	-252	-353	-896	680	118	65	64
22	837	807	522	1599	1035	160	-50	-583	1167	790	-419	-596	-1403	627	275	-292	-416	-888	654	75	69	68
23	901	856	591	1686	1107	170	-68	-598	1231	829	-457	-663	-1480	648	277	-341	-493	-962	658	50	70	69
24	1032	971	714	1868	1241	229	-36	-582	1371	1015	-465	-697	-1541	720	305	-369	-546	-1026	705	40	72	72
25	1015	952	646	1880	1267	208	-24	-643	1331	1064	-448	-700	-1561	817	353	-289	-471	-966	816	136	77	76
26	1180	1106	784	2112	1441	311	73	-597	1493	1209	-400	-657	-1574	919	451	-254	-445	-982	891	214	80	80
27	1275	1133	817	2147	1471	263	28	-634	1447	1169	-362	-604	-1462	977	546	-154	-399	-911	926	156	85	84
28	1315	1166	837	2245	1520	276	23	-677	1524	1210	-378	-627	-1534	1012	578	-174	-425	-981	957	175	85	85
29	1350	1194	852	2303	1551	244	-4	-761	1543	1207	-445	-685	-1660	993	545	-244	-488	-1099	935	124	89	88
30	1411	1248	892	2420	1623	255	17	-793	1557	1280	-458	-685	-1722	982	597	-246	-498	-1152	977	160	93	93
31	1503	1320	1005	2528	1719	288	13	-764	1637	1328	-490	-755	-1774	1008	594	-297	-546	-1233	970	120	99	98
32	1569	1383	1048	2636	1797	321	62	-769	1662	1413	-500	-745	-1828	993	642	-298	-544	-1275	995	160	100	100
33	1624	1421	1118	2683	1844	361	10	-730	1694	1524	-546	-840	-1836	1047	527	-342	-612	-1279	1101	94	105	104
34	1661	1541	1165	2722	1897	326	4	-731	1694	1443	-514	-923	-1915	965	417	-423	-698	-1333	1055	-18	110	110
35	1741	1623	1265	2808	2005	379	102	-672	1745	1439	-482	-829	-1870	1024	437	-247	-605	-1285	1113	-27	114	114
36	1833	1616	1276	2815	2020	434	126	-610	1785	1485	-589	-906	-1942	961	279	-319	-675	-1349	1111	-126	115	115
37	1954	1704	1368	2956	2072	492	154	-522	1909	1429	-634	-965	-1817	1077	187	-369	-746	-1301	1107	-192	125	125
38	2041	1773	1441	3118	2164	542	410	-472	2056	1509	-592	-922	-1828	1216	267	-300	-706	-1276	1266	-107	128	128
39	2039	1763	1416	3181	2172	495	359	-569	2052	1507	-663	-1003	-1961	1208	245	-367	-776	-1391	1244	-132	129	129
41	1925	1607	1318	3129	2060	488	352	-628	2068	1548	-734	-1088	-2099	1200	219	-291	-700	-1342	1360	-35	135	134

Table AIX.5: Data Used to Create a MEWMA Chart

i	Z_{i1}	Z_{i2}	Z_{i3}	Z_{i4}	Z_{i5}	Z_{i6}	Z_{i7}	Z_{i8}	Z_{i9}	Z_{i10}	Z_{i11}	Z_{i12}	Z_{i13}	Z_{i14}	Z_{i15}	Z_{i16}	Z_{i17}	Z_{i18}	Z_{i19}	Z_{i20}	T^2
	0.00	0.00	0.00	0.00	0.00	0.00	0.00	0.00	0.00	0.00	0.00	0.00	0.00	0.00	0.00	0.00	0.00	0.00	0.00	0.00	
2	0.08	0.09	0.06	0.09	0.08	0.00	-0.02	-0.08	0.08	0.04	-0.15	-0.14	-0.14	-0.01	-0.07	-0.16	-0.18	-0.19	-0.05	-0.15	9.75
4	0.17	0.18	0.14	0.19	0.18	0.04	-0.01	-0.13	0.17	0.10	-0.28	-0.28	-0.26	-0.01	-0.12	-0.30	-0.34	-0.35	-0.08	-0.25	32.90
5	0.24	0.24	0.22	0.29	0.25	0.07	-0.04	-0.15	0.28	0.15	-0.29	-0.27	-0.30	0.11	-0.08	-0.29	-0.37	-0.39	0.04	-0.23	49.38
6	0.23	0.23	0.18	0.30	0.25	-0.02	-0.14	-0.26	0.29	0.13	-0.28	-0.37	-0.39	0.13	-0.10	-0.32	-0.41	-0.45	0.07	-0.23	63.06
7	0.10	0.10	-0.02	0.24	0.16	-0.14	-0.22	-0.44	0.25	0.10	-0.23	-0.32	-0.40	0.23	-0.01	-0.16	-0.23	-0.33	0.25	-0.05	70.17
8	0.24	0.24	0.15	0.37	0.31	0.04	-0.10	-0.34	0.41	0.24	-0.21	-0.33	-0.42	0.33	0.06	-0.20	-0.30	-0.40	0.28	-0.07	72.34
9	0.19	0.17	0.04	0.35	0.28	0.00	-0.11	-0.43	0.40	0.26	-0.17	-0.29	-0.42	0.42	0.14	-0.08	-0.18	-0.31	0.42	0.07	97.79
10	0.19	0.17	0.06	0.37	0.30	-0.08	-0.19	-0.49	0.39	0.23	-0.24	-0.35	-0.48	0.41	0.13	-0.13	-0.20	-0.38	0.38	0.05	108.00
11	0.09	0.10	-0.08	0.28	0.22	-0.25	-0.32	-0.67	0.33	0.15	-0.28	-0.34	-0.52	0.36	0.12	-0.10	-0.14	-0.35	0.40	0.08	129.03
12	0.15	0.16	-0.02	0.35	0.28	-0.22	-0.28	-0.69	0.37	0.20	-0.38	-0.40	-0.60	0.34	0.09	-0.20	-0.26	-0.47	0.34	0.01	134.77
13	0.26	0.27	0.09	0.46	0.39	-0.04	-0.15	-0.59	0.51	0.34	-0.26	-0.30	-0.57	0.47	0.25	-0.13	-0.19	-0.45	0.43	0.13	140.42
14	0.30	0.32	0.12	0.49	0.42	0.18	-0.03	-0.36	0.56	0.49	-0.35	-0.36	-0.64	0.39	0.21	-0.19	-0.24	-0.53	0.39	0.09	176.29
15	0.34	0.36	0.19	0.54	0.46	0.20	-0.02	-0.38	0.63	0.50	-0.37	-0.37	-0.67	0.46	0.21	-0.19	-0.26	-0.51	0.45	0.09	183.02
16	0.38	0.40	0.23	0.58	0.49	0.16	-0.04	-0.43	0.64	0.49	-0.41	-0.41	-0.71	0.45	0.20	-0.21	-0.28	-0.56	0.45	0.08	202.21
17	0.40	0.41	0.26	0.61	0.50	0.17	-0.03	-0.44	0.68	0.50	-0.40	-0.42	-0.72	0.52	0.21	-0.19	-0.27	-0.56	0.52	0.09	205.70
19	0.51	0.52	0.36	0.70	0.61	0.26	0.03	-0.39	0.75	0.56	-0.43	-0.45	-0.74	0.52	0.22	-0.25	-0.35	-0.62	0.48	0.04	236.14
20	0.60	0.61	0.44	0.79	0.71	0.38	0.13	-0.34	0.82	0.67	-0.32	-0.36	-0.71	0.63	0.34	-0.17	-0.28	-0.60	0.59	0.15	259.61
21	0.63	0.64	0.46	0.81	0.75	0.38	0.16	-0.35	0.83	0.69	-0.31	-0.34	-0.71	0.63	0.37	-0.16	-0.25	-0.60	0.58	0.19	266.84
22	0.57	0.57	0.43	0.75	0.70	0.23	0.01	-0.44	0.74	0.59	-0.43	-0.46	-0.77	0.53	0.27	-0.21	-0.34	-0.54	0.49	0.10	241.38
23	0.60	0.58	0.48	0.76	0.72	0.23	-0.02	-0.43	0.76	0.60	-0.47	-0.53	-0.78	0.52	0.25	-0.27	-0.44	-0.59	0.45	0.04	237.68
24	0.70	0.67	0.59	0.85	0.82	0.34	0.04	-0.37	0.86	0.80	-0.45	-0.53	-0.78	0.60	0.28	-0.30	-0.49	-0.62	0.49	0.02	265.83
25	0.62	0.59	0.45	0.79	0.78	0.26	0.05	-0.44	0.74	0.79	-0.38	-0.49	-0.74	0.71	0.34	-0.14	-0.32	-0.49	0.61	0.19	275.29
26	0.75	0.73	0.58	0.92	0.92	0.46	0.21	-0.32	0.87	0.92	-0.25	-0.38	-0.69	0.81	0.47	-0.07	-0.25	-0.47	0.67	0.31	294.56
27	0.80	0.70	0.57	0.87	0.87	0.32	0.11	-0.36	0.74	0.78	-0.15	-0.27	-0.51	0.84	0.60	0.09	-0.15	-0.34	0.66	0.18	273.94
28	0.77	0.67	0.55	0.88	0.85	0.31	0.09	-0.40	0.77	0.77	-0.17	-0.28	-0.54	0.82	0.60	0.05	-0.18	-0.40	0.65	0.20	261.28
29	0.75	0.65	0.52	0.85	0.81	0.22	0.04	-0.51	0.72	0.70	-0.29	-0.35	-0.63	0.72	0.49	-0.07	-0.27	-0.52	0.56	0.09	283.34
30	0.75	0.66	0.52	0.87	0.83	0.22	0.07	-0.52	0.68	0.73	-0.29	-0.32	-0.65	0.64	0.53	-0.07	-0.27	-0.55	0.58	0.15	314.17
31	0.79	0.69	0.62	0.89	0.87	0.27	0.06	-0.43	0.72	0.74	-0.34	-0.40	-0.65	0.62	0.48	-0.14	-0.32	-0.61	0.51	0.06	288.90
32	0.80	0.70	0.61	0.91	0.89	0.32	0.13	-0.40	0.69	0.79	-0.33	-0.35	-0.65	0.55	0.52	-0.13	-0.29	-0.61	0.51	0.13	310.21
33	0.79	0.69	0.65	0.87	0.86	0.37	0.03	-0.30	0.67	0.87	-0.39	-0.47	-0.60	0.59	0.27	-0.19	-0.38	-0.56	0.62	0.00	354.46
34	0.76	0.77	0.65	0.82	0.85	0.27	0.02	-0.28	0.61	0.68	-0.29	-0.56	-0.64	0.40	0.06	-0.30	-0.49	-0.58	0.50	-0.20	370.22
35	0.79	0.81	0.72	0.82	0.90	0.36	0.18	-0.15	0.62	0.61	-0.20	-0.36	-0.53	0.47	0.09	0.00	-0.29	-0.47	0.54	-0.20	333.62
36	0.83	0.72	0.66	0.76	0.84	0.44	0.20	-0.04	0.61	0.62	-0.40	-0.45	-0.57	0.32	-0.19	-0.11	-0.38	-0.51	0.49	-0.35	472.39
37	0.89	0.77	0.72	0.81	0.83	0.52	0.23	0.11	0.71	0.49	-0.46	-0.50	-0.38	0.49	-0.32	-0.18	-0.46	-0.41	0.44	-0.44	506.14
38	0.91	0.78	0.75	0.88	0.86	0.58	0.63	0.18	0.83	0.56	-0.33	-0.39	-0.36	0.68	-0.15	-0.06	-0.36	-0.34	0.65	-0.24	444.93
39	0.83	0.70	0.65	0.86	0.80	0.43	0.49	0.00	0.75	0.51	-0.45	-0.48	-0.48	0.61	-0.17	-0.16	-0.44	-0.46	0.56	-0.27	454.43
41	0.62	0.45	0.47	0.74	0.59	0.37	0.43	-0.11	0.70	0.52	-0.55	-0.57	-0.59	0.54	-0.20	-0.03	-0.28	-0.36	0.68	-0.07	398.23

TEST TARGET (QA-3)

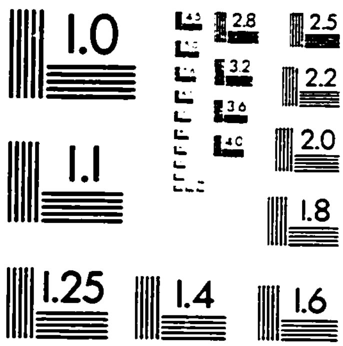

150mm

6"

APPLIED IMAGE . Inc

1653 East Main Street
Rochester, NY 14609 USA
Phone: 716/482-0300
Fax: 716/288-5989